

RICE UNIVERSITY

Evolutionary Dynamics Leading to Tigecycline Resistance in *Enterococcus faecalis*

by

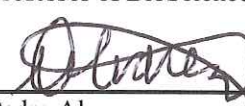
Kathryn Roberta Beabout

A THESIS SUBMITTED
IN PARTIAL FULFILLMENT OF THE
REQUIREMENTS FOR THE DEGREE

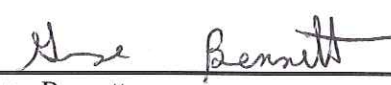
Doctor of Philosophy

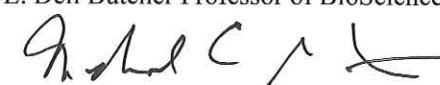
APPROVED, THESIS COMMITTEE


Yousif Shamoo, Thesis Advisor
Professor of BioSciences, Vice Provost for Research


Pedro Alvarez
George R. Brown Professor of Engineering, Chair of
the Civil and Environmental Engineering Department


Bonnie Bartel
Ralph and Dorothy Looney Professor of BioSciences


George Bennett
E. Dell Butcher Professor of BioSciences


Michael Gustin
Professor of BioSciences

HOUSTON, TEXAS
December 2016

Abstract

Evolutionary Dynamics Leading to Tigecycline Resistance in *Enterococcus faecalis*

By

Kathryn Beabout

The rising frequency of multidrug resistant pathogens poses an increasing threat to public health. There is a dire need for novel approaches to combat these deadly pathogens and maintain the efficacy of currently available antibiotics. In particular horizontal gene transfer threatens the therapeutic success of antibiotics by facilitating the rapid dissemination of resistance alleles among bacterial species. The conjugative mobile element Tn916 provides an excellent context for examining the role of adaptive parasexuality as it carries the tetracycline-resistance allele *tetM* and has been identified in a wide range of pathogens. For this thesis I used quantitative experimental evolution, a pipeline developed by our lab to identify clinically relevant resistance mechanisms, to study tigecycline resistance in a hospital strain of *Enterococcus faecalis*. Quantitative experimental evolution uses a combination of experimental evolution and allelic frequency measurements to gain insights into the adaptive trajectories leading to resistance and to predict what mechanisms of resistance are most likely to appear in the clinical setting. Here we show that antibiotic selection led to the near fixation of adaptive alleles that simultaneously altered TetM expression and produced remarkably increased levels of Tn916 horizontal gene transfer. In the absence of drug, approximately 1 in 120,000 of the non-adapted *Enterococcus faecalis* S613 cells had an excised copy of

Tn916, whereas nearly 1 in 50 cells had an excised copy of Tn916 upon selection for resistance resulting in a more than 1,000-fold increase in conjugation rates. We also show that tigecycline, a translation inhibitor, selected for a mutation in the ribosomal S10 protein in the *E. faecalis* adapting populations. Furthermore, we show that mutation of S10 is an important allele for a broad range of Gram-positive and Gram-negative pathogens to adapt to tigecycline. These results show the first example of mutations that concurrently confer resistance to an antibiotic and lead to constitutive conjugal transfer of the resistance allele. Selection created a highly parasexual phenotype and high frequency of Tn916 jumping demonstrating how the use of antibiotics can lead directly to the proliferation of resistance in, and potentially among, pathogens.

Acknowledgements

First I would like to thank my thesis advisor, Yousif Shamoo, for his advice, support, wisdom, and guidance. I am grateful that Shamoo made my training and career development a priority, took the time to help me navigate the challenges of my project, and, most importantly, fostered and encouraged my passion for science and research.

I would also like to thank my other lab members. Thank you Troy Hammerstrom for helping me troubleshoot the many problems I encountered while completing this project, for helping me run the bioreactor, and for teaching me to be a careful and thorough scientist. Thank you Gerda Saxer for your thoughtful guidance, for challenging me to think deeply and carefully about my experiments, for your continuous support, and for the many fun and engaging conversations (especially when those conversations included espressos or Swiss chocolate). Thank you Corwin Miller, Milya Davlieva, Anisha Perez, Xu Wang, Amy Prater, Heer Mehta, Meisam Nosrati, and Ramya Ganiga Prabhakar for your advice, helpfulness, kindness, and friendship. It has truly been a pleasure to work with each of you and you have all made my time at Rice enjoyable and fruitful.

Thank you to my undergraduate students, Tim Wang, Megan McCurry, and Maia Ogumbo. I am so grateful to have had such a talented and dedicated team of undergraduates and I look forward to seeing what each of you accomplishes in the future.

I would also like to thank my committee, Bonnie Bartel, Mike Gustin, George Bennett, and Pedro Alvarez, for their support and advice, which has been instrumental to my success.

Thank you to my parents for supporting me, believing in me, and moving mountains to ensure that I have the tools I need to succeed. I have not forgotten the hours spent helping me with my homework assignments and advocating for my education. I would never have achieved my dreams without your support and I am eternally grateful.

Last, but most certainly not least, thank you to my loving, kind, supportive, intelligent, and funny husband. Thank you for making me laugh during the hard times and for sharing in my excitement during the good times. I could not have done it without you.

Table of Contents

Abstract	ii
Acknowledgements	iv
Table of Contents	vi
List of Figures	xi
List of Tables	xiii
Nomenclature	xiv
Chapter 1: General Introduction	1
1.1 The increasing threat of antibiotic resistance.....	1
1.2 Dwindling development of new antibiotics.....	2
1.3 Antibiotic resistance in Healthcare Associated Infections.....	5
1.4 Vancomycin-resistant <i>Enterococcus</i> (VRE).....	6
1.5 The tetracycline class of antibiotics.....	8
1.5.1 Structure and mechanism of action of tetracycline.....	8
1.6 Mechanisms of tetracycline resistance.....	11
1.6.1. Efflux pumps.....	11
1.6.2 Ribosomal protection proteins.....	12
1.6.3 Mutations in the ribosome.....	13
1.6.4 Enzymatic degradation by TetX.....	13
1.7 Tigecycline: a third-generation tetracycline and drug of last resort.....	15
1.7.1 Resistance to tigecycline.....	16
1.8 Role of horizontal gene transfer in tetracycline resistance.....	17
1.8.1 The conjugative transposon Tn916.....	18
1.8.2 Genetic structure of Tn916.....	19
1.8.3 Regulation of <i>tetM</i> expression and Tn916 conjugation.....	19
1.9 Experimental evolution.....	22
1.9.1 Adaptation techniques of experimental evolution.....	22
1.9.2 Advantages of studying antibiotic resistance with experimental evolution.....	24
1.10 Goals of this study.....	25
1.10.1 Summary of approach.....	26
1.10.2 Workflow of quantitative experimental evolution.....	27
1.10.3 Relevance of quantitative experimental evolution.....	30

1.10.4 Using quantitative experimental evolution to study tigecycline resistance in VRE.....	31
Chapter 2: Materials and Methods.....	32
2.1 Bacterial strains and growth conditions.....	32
2.2 Serial transfer adaption of <i>E. faecalis</i> S613 to minocycline and tigecycline..	32
2.3 Bioreactor design, setup, and operation.....	33
2.3.1 Overview of bioreactor.....	33
2.3.2 Detection of CO ₂ and maintenance of population at a constant cell density.....	33
2.3.3 Selection regime and increases in antibiotic concentration.....	34
2.3.4 Collecting samples and sterility checks.....	34
2.4 Phenotypic characterization of bioreactor end-point strains.....	37
2.4.1 Minimal inhibitory concentrations (MICs) on agar.....	37
2.4.2 Flocculation assay.....	37
2.4.3 Colony size on chloramphenicol.....	37
2.5 Preparation of DNA samples for whole genome sequencing.....	39
2.6 Analysis of whole genome sequencing data.....	39
2.6.1 Clonal samples from the end of adaption.....	39
2.6.2 Meta-genomic samples from intermediate days of adaptation.....	39
2.6.3 Estimate of average Tn916 copy number in population samples...	40
2.7 Quantification of <i>tetM</i> gene expression and Tn916 copy number.....	41
2.7.1 Isolation of total RNA and preparation of cDNA for quantification of <i>tetM</i> gene expression.....	41
2.7.2 Isolation of total DNA for quantification of Tn916 copy number....	42
2.7.3 Quantitative real-time PCR.....	42
2.8 Conjugation assays.....	43
2.9 Competitive Fitness Assay.....	44
2.10 Measurement of spontaneous mutation rate of S613.....	44
2.11 Long-range PCR.....	45
2.12 Creation of Fisher-Muller diagrams outlining models for the role of conjugation during adaptation to TGC resistance.....	46
2.12.1 Copies of Tn916 located at the ancestral site lack deletions, while copies of Tn916 at newly acquired sites carry deletions upstream of <i>tetM</i>	46

2.12.2 Identical deletions were identified in different strains despite the fact that deletions of different sizes and locations can confer resistance.....	47
2.12.3 The spontaneous mutation rate of S613 is vastly lower than the conjugation of rate of the BTR87a and BTR22 strains.....	47
2.13 Serial transfer adaptation of <i>Enterococcus faecium</i> , <i>Staphylococcus aureus</i> , <i>Acinetobacter baumannii</i> and <i>Escherichia coli</i> to tigecycline.....	48
2.14 Measuring the growth rate of S613 and BTR0.....	49
2.15 Measuring the affinity of <i>tetM</i> leader RNA for tetracycline.....	49
2.15.1 Template DNA for T7 RNA polymerase <i>in vitro</i> transcription.....	49
2.15.2 Incorporation of template DNA into pUC19.....	50
2.15.3 T7 RNA polymerase <i>in vitro</i> transcription.....	51
2.15.4 Measuring the affinity of <i>tetM</i> leader RNA for tetracycline by detection of changes in fluorescence.....	52
2.16 Tracking the movement and conjugation of Tn916 in mice gastrointestinal tract.....	53
2.16.1 Animal care and treatment.....	53
2.16.2 Determination of CFUs and isolation of bacterial DNA from mouse feces.....	53
Chapter 3: Bioreactor adaptation of <i>Enterococcus faecalis</i> S613 to tigecycline resistance.....	54
3.1 Introduction.....	54
3.2 Advantages of our bioreactor adaptation technique.....	55
3.3 Serial transfer adaptation to minocycline and tigecycline.....	58
3.4 Growth phase and %CO ₂ of S613 in the bioreactor.....	60
3.5 Using %CO ₂ to maintain S613 in exponential growth.....	62
3.6 Bioreactor adaptation of S613 to tigecycline.....	64
3.7 Discussion.....	67
Chapter 4: Phenotypic characterization of bioreactor end-point adapted populations.....	69
4.1 Introduction.....	69
4.2 Phenotypic characterization of Run 1 bioreactor isolates.....	70
4.2.1 High-throughput MIC testing on agar.....	70
4.2.2 Flocculation phenotype.....	73

4.2.3 Colony sizes on chloramphenicol.....	75
4.2.4 Selection of Run 1 isolates for whole genome sequencing.....	77
4.3 Phenotypic characterization of bioreactor Run 2 isolates.....	80
4.4 Discussion.....	83
Chapter 5: Identification of the most important alleles leading to TGC resistance in <i>E. faecalis</i>.....	86
5.1 Introduction.....	86
5.2 Deletion of regulatory elements upstream of <i>tetM</i>	90
5.3 Mutation of the S10 protein may remodel the ribosome rendering TGC less effective.....	93
5.4 Mutations in hypothetical ATP-binding cassette-type transporters.....	95
5.5 Discussion.....	96
Chapter 6: The role of <i>tetM</i> overexpression and Tn916 conjugation in adaptation of S613 to TGC resistance.....	98
6.1 Introduction.....	98
6.2 Constitutive overexpression of <i>tetM</i> leads to TGC resistance.....	99
6.3 Rampant parasexuality evolves in the S613 bioreactor populations during TGC selection.....	100
6.3.1 Constitutive overexpression of TetM leads to hyperconjugation of Tn916.....	100
6.3.2 Increased chromosomal copy number of Tn916.....	105
6.3.3 Hyperconjugation of Tn916 contributed to a rapid spread of resistance within adapting populations.....	109
6.4 Fitness cost associated with TGC resistance.....	111
6.5 The expression of <i>tetM</i> might be regulated by a novel tetracycline-binding riboswitch.....	114
6.6 Movement of hyperconjugative Tn916 in mice intestinal flora.....	117
6.7 Discussion.....	121
Chapter 7: The role of S10 mutations in tigecycline resistance across many different species.....	123
7.1 Introduction.....	123
7.2 Flask adaptation of <i>Enterococcus faecium</i> , <i>Staphylococcus aureus</i> , <i>Acinetobacter baumannii</i> and <i>Escherichia coli</i> to tigecycline.....	124
7.3 Identification of S10 alleles in tigecycline adapted strains.....	124

7.3.1 Adaptation of <i>E. faecium</i> R499 to tigecycline.....	124
7.3.2 Adaptation of <i>E. faecium</i> 105 to tigecycline.....	125
7.3.3 Adaptation of <i>S. aureus</i> MRSA131 to tigecycline.....	125
7.3.4 Adaptation of <i>A. baumannii</i> AB210 to tigecycline.....	126
7.3.5 Adaptation of <i>E. coli</i> BW25113 to tigecycline.....	126
7.4 Validation of S10 mutation in conferring resistance.....	130
7.5 Mutations to S10 did not alter growth rates in the absence of antibiotic suggesting a low fitness cost.....	131
7.6 Discussion.....	133
Chapter 8: Discussion, conclusions, and future work.....	137
8.1 Discussion and conclusions.....	137
8.2 Future work.....	141
8.2.1 Does a tetracycline-binding riboswitch regulate <i>tetM</i> expression?.....	141
8.2.2 How readily could hyperconjugative Tn916 spread TGC-resistance inside the gastrointestinal tract of animals or within the hospital setting?.....	143
8.2.3 How stable are the <i>tetM</i> overexpressing and hyperconjugative alleles?.....	143
8.2.4 Do the S10 mutations reduce the affinity of TGC for the ribosome?.....	144
8.2.5 Is there synergistic epistasis between the S10 and <i>tetM</i> alleles?.	145
8.2.6 What alternative alleles play a role in TGC resistance?.....	146
8.2.7 Application of quantitative experimental evolution to study more pathogens and antibiotics.....	147
References.....	148
Appendix A.....	163
Appendix B.....	184
Appendix C.....	193

List of Figures

Figure 1.1: Number of novel antibiotics approved by the FDA over the corresponding five-year time intervals.....	4
Figure 1.2: Structures of three different antibiotics of last resort for treating <i>Enterococcus faecalis</i> infections.....	7
Figure 1.3: The structures of three different molecules representing the tetracycline family of antibiotics.....	10
Figure 1.4: Mechanisms of tetracycline resistance.....	14
Figure 1.5: A diagram outlining the genetic structure, transcriptional regulation, and movement of the conjugative transposon Tn916.....	21
Figure 1.6: Flow chart outlining the steps of quantitative experimental evolution.....	29
Figure 2.1: The bioreactor setup used for quantitative experimental evolution.....	35
Figure 3.1: Buildup of biofilm on the interior walls of the bioreactor.....	57
Figure 3.2: Batch culture adaptation of <i>E. faecalis</i> S613 to minocycline and TGC.....	59
Figure 3.3: Relationship between %CO ₂ and the growth phase of S613.....	61
Figure 3.4: Use of a control loop and %CO ₂ to maintain a population of S613 in growth phase.....	63
Figure 3.5: The concentrations of TGC and total LBHI media used over the course of two replicate bioreactor runs where S613 populations were adapted to TGC resistance.....	65
Figure 4.1: TGC MICs against 94 clones selected from the Run 1 end-point adapted population.....	72
Figure 4.2: Comparison of the propensity of 25 Run 1 end-point clones to flocculate.....	74
Figure 4.3: Colony sizes of 14 Run 1 end-point adapted clones on agar plates with 2 µg/mL CL.....	76
Figure 4.4: Summary of Run 1 end-point adapted isolates selected for whole genome sequencing.....	78
Figure 4.5: TGC MICs against 94 clones selected from the Run 2 end-point adapted population.....	81
Figure 5.1: Experimental evolution of pathogenic <i>E. faecalis</i> to TGC shows that deletion of <i>tetM</i> regulatory elements and mutation of the ribosomal protein S10 provides the successful evolutionary trajectories to TGC resistance.....	91

Figure 5.2: Deletion in S10 may decrease the binding affinity of TGC by remodeling the ribosome.....	94
Figure 6.1: Deletions upstream of <i>tetM</i> increase <i>tetM</i> expression and Tn916 conjugation.....	103
Figure 6.2: New Tn916 insertions emerged frequently in response to TGC selection.....	106
Figure 6.3: Fitness cost associated with <i>tetM</i> overexpression and increased Tn916 copy number.....	113
Figure 6.4: Preliminary binding studies investigating a potential tetracycline-binding riboswitch in the <i>tetM</i> leader RNA.....	116
Figure 6.5: Preliminary experiments evaluating the movement of a TGC-resistant hyperconjugative variant of Tn916 in mouse gastrointestinal flora.....	119
Figure 6.6: Tigecycline selection converts the population to a rampant parasexual phenotype.....	122
Figure 7.1: S10 mutations identified in strains that underwent TGC exposure.....	127
Figure 7.2: TGC selects for mutations on a loop of S10 that is in close proximity to the 16S rRNA that composes the TGC binding pocket.....	128
Figure 7.3. The S10 ^{R53Q-Δ54-57ATHK} mutation in <i>E. faecalis</i> confers improved growth in the presence of TGC.....	132

List of Tables

Table 2.1: Primers used for confirmatory Sanger sequencing.....	39
Table 2.2: Primers used for qPCR.....	43
Table 2.3: Primers used for long-range PCR.....	45
Table 2.4: Primers used for <i>rpsJ</i> colony PCR and Sanger sequencing.....	48
Table 5.1: Genotypes of bioreactor-adapted TGC resistant (BTR) clonal strains isolated from the end of adaptation.....	87
Table 5.2: List of all mutations identified from Run 1 and 2 that reached $\geq 5\%$ within the population, or were identified in sequenced isolates from the end of adaptation.....	88
Table 6.1: List of new Tn916 insertion sites identified in the population samples from Run 1 and 2.....	107
Table 7.1: MICs against four <i>E. faecalis</i> strains determined by CLSI agar dilution method.....	130

Nomenclature

5' UTR	5' Untranslated Region
ABC	ATP-Binding Cassette transporters
BEA	Bile Esculin Agar
BHI	Brain Heart Infusion media
BRIG	BLAST Ring Image Generator
BTR	Bioreactor-adapted TGC Resistant strains
CDC	Center for Disease Control and Prevention
CFU	Colony Forming Units
CL	Chloramphenicol
CLSI	Clinical Laboratory Standards Institute
DAP	Daptomycin
EF-G	Elongation Factor G
EUCAST	European Committee on Antimicrobial Susceptibility Testing
FDA	Food and Drug Administration
HAI	Healthcare Associated Infection
IACUC	Institutional Animal Care and Use Committee
LB	Lysogeny Broth
LBHI	80% Lysogeny Broth and 20% Brain Heart Infusion media
MATE	Multidrug and Toxin Extrusion pumps
MF	McFarland units
MIC	Minimal Inhibitory Concentration
MIN	Minocycline
OD	Optical Density

ORF	Open Reading Frame
qPCR	Quantitative real-time PCR
RND	Resistance Nodulation-cell Division pumps
RPP	Ribosomal Protection Proteins
SOC	Super Optimal broth with Catabolite repression
TET	Tetracycline
TGC	Tigecycline
VRE	Vancomycin-Resistant <i>Enterococcus</i>
YFP	Yellow Fluorescent Protein

Chapter 1: General Introduction.

Portions of this chapter are reproduced with permission from Beabout, et al. 2015 *Mol Biol Evol* and Beabout, et al. 2015 *Antimicrob Agents Chemother*.

1.1 The increasing threat of antibiotic resistance.

Antibiotics have become an essential component of modern medicine as they ensure that patients and individuals are safe from the threat of infection. However, an unavoidable consequence of antibiotic use is selection for resistance. Any bacterial cells harboring resistance are given an immense advantage over susceptible cells in the presence of the antibiotic. Thus the more an antibiotic is used the more likely resistance will emerge and disseminate, in turn undermining the efficacy of the antibiotic. Over the past few decades increased antibiotic usage has led to an increase in the prevalence of multi-drug resistant pathogens (Andersson and Hughes 2010). In 2013 the U.S. Center for Disease Control and Prevention (CDC) reported that at least two million infections and 23,000 deaths in the U.S. were the direct result of resistant pathogens (CDC 2013). Additionally, resistant infections were more likely to result in poor outcomes for patients, were associated with increased death rates, and resulted in an estimated \$20 billion dollars in additional health costs in the U.S. (CDC 2011; Cosgrove 2006). In response to this threat, efforts have been initiated to promote antibiotic stewardship, where healthcare professionals work together to limit and optimize antibiotic administration. These efforts have been successful at deterring resistance when appropriately implemented (Gould 2015; Kaki, et al. 2011). However, lack of incentives and enforcement has prevented widespread compliance with the goals of antibiotic stewardship and many healthcare professionals still do not prescribe antibiotics

appropriately (Spellberg, et al. 2016; Ventola 2015). Additionally, antibiotics continue to be widely used in agriculture, creating a reservoir of resistant cells and genes in livestock (Chang, et al. 2015; Ventola 2015), and in some countries antibiotics can be purchased over-the-counter without a prescription, leading to inefficient and unnecessary usage (Laxminarayan and Chaudhury 2016; Nagaraj, et al. 2015). Combined, these factors have contributed to the increasing prevalence and threat of resistance and some officials fear we may enter a so-called “post-antibiotic era,” wherein many infections that were once easily cured can no longer be treated by available antibiotics (Kahrstrom 2013).

1.2 Dwindling development of new antibiotics.

As bacterial pathogens increasingly become resistant to currently available antibiotics, fewer new antibiotics are being developed or approved by the US Food and Drug Administration (FDA) to address this threat (**Figure 1.1**). A combination of high cost of development and low profitability has discouraged many pharmaceutical companies from investing in novel antibiotic agents (Outterson, et al. 2015; Ventola 2015). There are several factors that prevent antibiotics from being profitable. They are normally administered for short durations and are usually curative, and thus not as profitable as therapies for chronic conditions. When new antibiotics become available on the market healthcare professionals usually advise the community to reserve the antibiotic for “last resort” scenarios when treating patients (Foster and Grundmann 2006; Outterson, et al. 2015). This practice has the advantage of preventing unnecessary selection for resistance and maintaining the long-term efficacy of the antibiotic, but conversely limits the agent’s profitability by discouraging the use of the drug. Additionally, it is impossible

to predict how long after an antibiotic reaches the market until the development of resistance renders it ineffective, which makes antibiotic development a risky investment (Ventola 2015). Aggressive and proactive measures must be taken to maintain the efficacy of approved antibiotics, develop novel antibiotics, and avoid a worst-case scenario where antibiotics are no longer available to treat common infections.

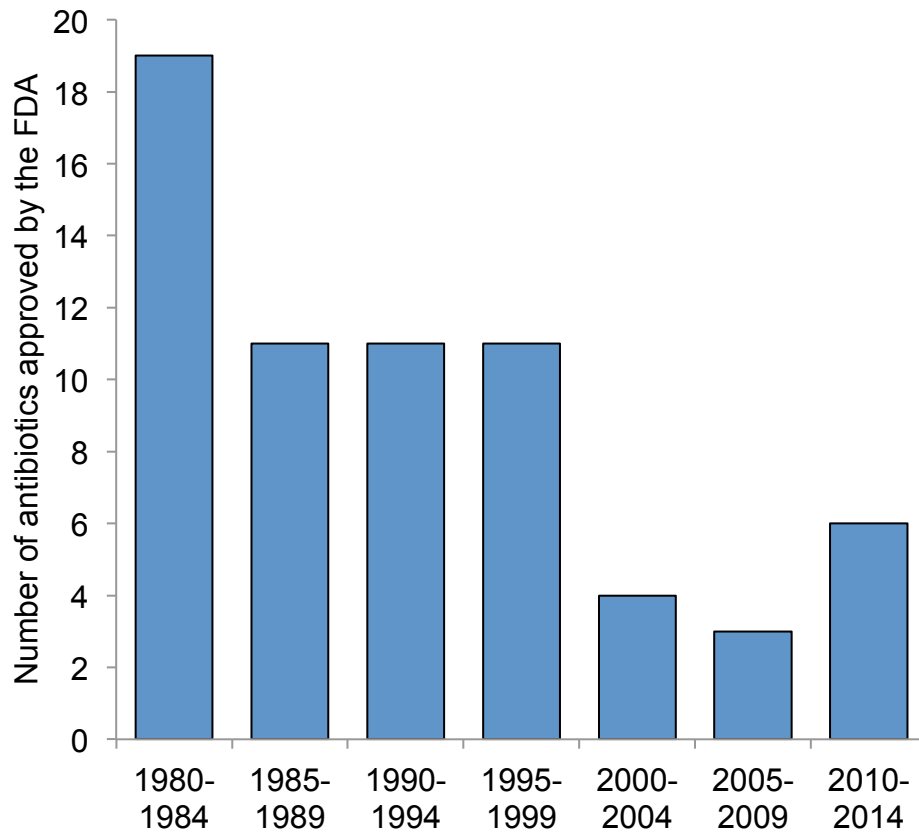


Figure 1.1: Number of novel antibiotics approved by the FDA over the corresponding five-year time intervals. During the early 1980s the FDA approved nearly twenty new antibiotics for clinical use. However in following years the number of new antibiotics undergoing development and FDA approval continued to decline until reaching a low of only three agents from 2005 to 2009. More recently six new antibiotics were approved from 2010 to 2014. While this modest increase is promising more antibiotic development will likely be needed to keep up with the increasing prevalence of multidrug resistant pathogens. This figure was adapted with permission from (Ventola 2015).

1.3 Antibiotic resistance in Healthcare Associated Infections.

Healthcare Associated Infections (HAIs), also known as nosocomial infections, are infections acquired while undergoing healthcare-related treatment. HAIs are often caused by opportunistic pathogens, which are pathogens that typically do not pose a threat to healthy individuals, but are capable of causing deadly infections in immunocompromised individuals, such as those with HIV or undergoing immunesuppressive therapies (Collins 2008). There are a variety of life-threatening HAIs, including endocarditis, bacteremia, pneumonia, wound and surgical infections, skin and skin structure infections, gastrointestinal infections, and catheter-associated urinary tract infections (Collins 2008). The U.S. Department of Health and Human Services reports that HAIs are the most common complication of a hospital stay and one of the top ten leading causes of death in the United States (Marcel, et al. 2008). Additionally, the CDC estimates that HAIs will cause approximately 90,000 deaths annually (CDC 2011). In some cases HAIs are associated with resistance because antibiotics are administered at high concentrations in the healthcare setting, which in turn selects for the evolution of resistance (Seigal, et al. 2016). The CDC estimates that nearly 70% of HAIs will be resistant to one or more clinically relevant antibiotic (CDC 2011). To address this issue, Rice *et al.* and the Infectious Disease Society of America have stressed the urgency of investigating antibiotic resistance in the most threatening hospital-associated pathogens also known as the no ‘ESKAPE’ (*Enterococcus faecium*, *Staphylococcus aureus*, *Klebsiella pneumoniae*, *Acinetobacter baumannii*, *Pseudomonas aeruginosa*, and *Enterobacter* species) pathogens, since infections caused by these species frequently escape antibiotic treatment (Rice 2008). By studying the ESKAPE pathogens the goal is to generate new paradigms for resistance that will in turn be used to help develop

strategies to keep patients safe from infection and resistance while undergoing healthcare related treatment.

1.4 Vancomycin-resistant *Enterococcus* (VRE).

Enterococcus faecium and *E. faecalis* are worrisome hospital-associated pathogens for several reasons; they have intrinsic resistance to many commonly used antibiotics, including cephalosporins, they are capable of causing life-threatening illnesses, including bacteremia and endocarditis, and they are the second leading cause of catheter-related infections in the blood, urinary track, skin and soft-tissue (Arias and Murray 2012; Collignon 2012). *Enterococcus* species are Gram-positive facultative anaerobes that commonly colonize the human gastrointestinal tract without causing illness in healthy individuals. However, *E. faecium* and *E. faecalis* can act as opportunistic pathogens in individuals with compromised immune systems. Most infections caused by *Enterococcus* species can be treated with vancomycin, but the prevalence of vancomycin-resistant *Enterococcus* (VRE) has been on the rise over the last decade (CDDEP 2010).

Vancomycin is a large glycopeptide molecule that specifically kills Gram-positive bacteria by inhibiting synthesis of the peptidoglycan layer (Reynolds 1989) (**Figure 1.2**). Vancomycin is often a drug of last resort, and individuals with VRE infections have limited therapies available, including the antibiotics daptomycin (DAP) and linezolid. DAP is a lipopeptide that disrupts the cell membrane in a calcium depended manner (Tran, et al. 2013), while linezolid is a translation inhibitor that blocks peptide bond formation (Ippolito, et al. 2008) (**Figure 1.2**). Unfortunately, resistance to both of these drugs has also been observed in VRE clinical isolates, increasing the probability that hospitalized individuals will contract infections without effective treatment (Arias and Murray 2009).

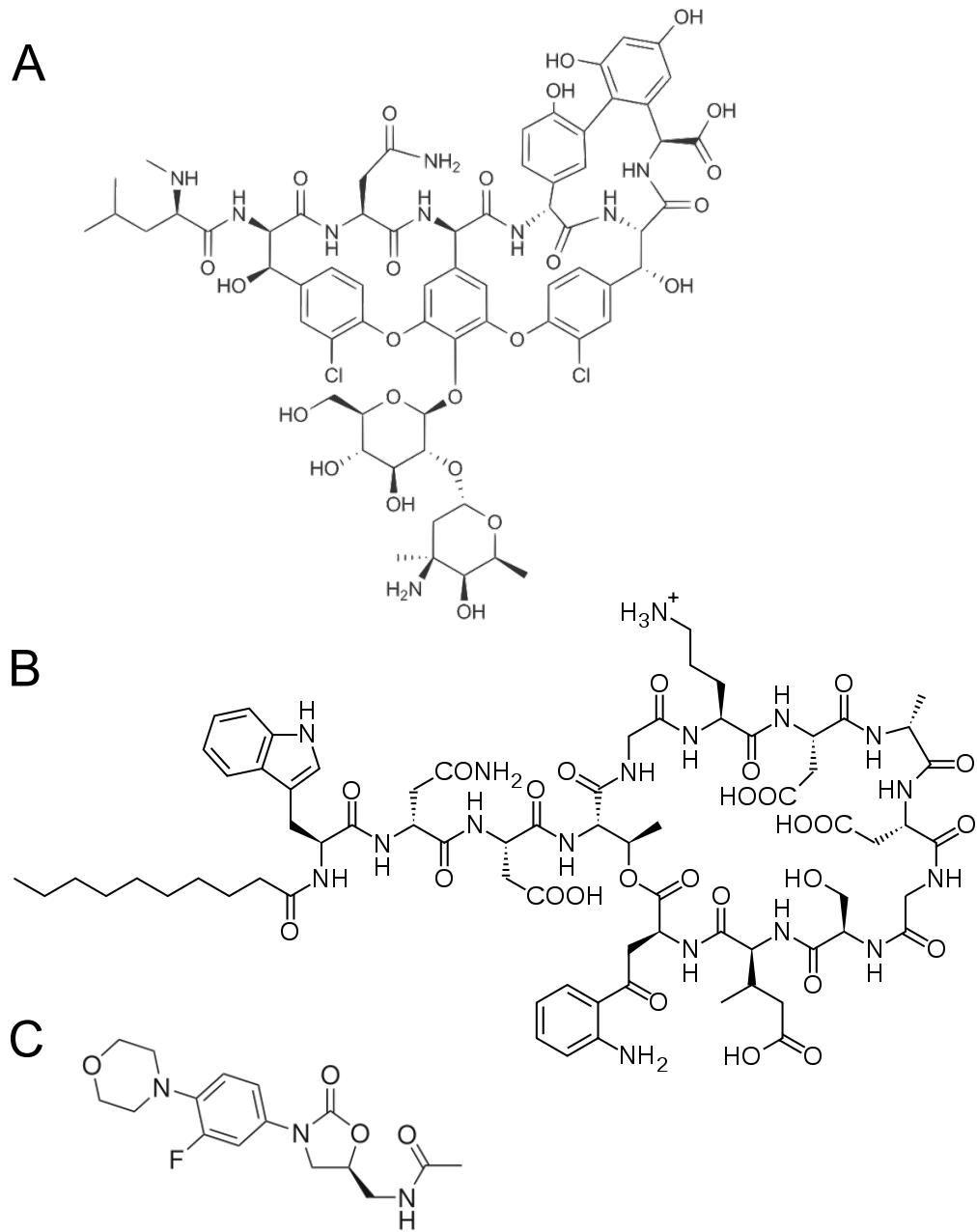


Figure 1.2: Structures of three different antibiotics of last resort for treating

***Enterococcus faecalis* infections.** Three antibiotics that are often used as drugs of last resort for treating *E. faecalis* infections include **A)** vancomycin, a glycopeptide that inhibits peptidoglycan synthesis, **B)** daptomycin, a lipopeptide that disrupts membrane function, and **C)** linezolid, an oxazolidinone that inhibits translation by blocking peptide bond formation.

1.5 The tetracycline class of antibiotics.

Tetracyclines are a broad-spectrum class of antibiotics that have been in use since their discovery in the 1940s. They are inexpensive and effective at treating infections caused by many Gram-positive, Gram-negative, and intracellular bacterial pathogens, including *Bacillus anthracis*, *Yersinia pestis*, *Mycoplasma pneumoniae*, *Francisella tularensis*, *Borrelia burgdorferi*, *Chlamydia* species, *Rickettsia* species and more (Eliopoulos, et al. 2003). The first molecules belonging to the tetracycline class were discovered as natural products produced by various *Streptomyces* species, such as chlortetracycline from *Streptomyces aureofaciens*, oxytetracycline from *Streptomyces rimosus*, and tetracycline from *S. aureofaciens* (Chopra and Roberts 2001). Later semisynthetic approaches were used to improve the efficacy and solubility of tetracyclines resulting in “second generation” derivatives, such as minocycline (MIN), doxycycline, and methacycline (Chopra and Roberts 2001). More recently, the semisynthetic glycylcycline family of tetracycline derivatives, including tigecycline (TGC), were developed and considered the “third generation” of tetracycline derivatives for their improved efficacy over first and second generation tetracyclines (Livermore 2005).

1.5.1 Structure and mechanism of action of tetracycline.

Structurally, tetracyclines are composed of a planer four-ringed core that includes a phenolic ring and several keto-enol systems (**Figure 1.3**). Attached to the core rings are different functional groups, which are typically hydrophilic along one side of the ring structure (**Figure 1.3**). Tetracyclines work by reversibly binding to the 30S subunit of the bacterial ribosome and inhibiting protein synthesis. The hydrophilic functional groups of tetracycline interact with several residues located on the 16S rRNA of the small 30S ribosomal subunit (Brodersen, et al. 2000). Several tetracycline-binding sites have been

identified on the 30S subunit, however the highest affinity site, which is located between helix 31 and helix 34 of the 16S rRNA, is thought to be the primary location through which tetracycline inhibits translation (Bauer, et al. 2004; Brodersen, et al. 2000; Pioletti, et al. 2001). The binding of tetracycline to the ribosome blocks aminoacyl-tRNAs from entering the acceptor, or A-site, of the ribosome, thus inhibiting peptide elongation (Brodersen, et al. 2000). Tetracyclines are strong chelating agents and metal ions are essential for their activity (Grenier, et al. 2000). Divalent magnesium facilitates the formation of salt bridges between the phosphate backbone of the 16S rRNA and the hydrophilic side chains of tetracycline (Brodersen, et al. 2000).

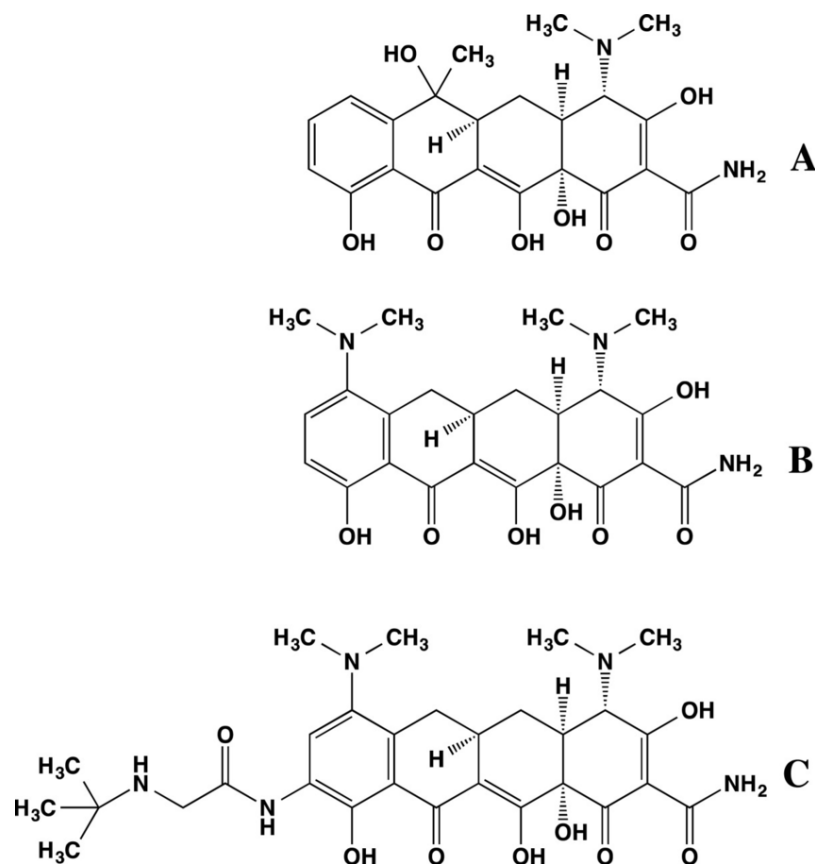


Figure 1.3: The structures of three different molecules representing the tetracycline family of antibiotics. Tetracyclines all share a core four-ringed structure with different functional groups attached. **A)** Tetracycline is a natural product of *Streptomyces* species and is considered a first generation tetracycline. **B)** MIN is a semisynthetic derivative of tetracycline with increased efficacy over tetracycline and is considered a second-generation tetracycline. **C)** TGC is a more recently developed tetracycline-derivative and has a structure identical to MIN, but with the addition of a t-butylglyclamido side group at position 9. TGC has improved efficacy over second-generation tetracyclines and is therefore considered a third generation tetracycline. This figure was originally published in (Sahu, et al. 2014). Copyright by Sahu *et al.* from <http://dx.doi.org/10.1186/1475-2875-13-414>, used under Creative Commons Attribution 4.0 International license: <http://creativecommons.org/licenses/by/4.0/>.

1.6 Mechanisms of tetracycline resistance.

The widespread prevalence of tetracycline resistance genes and alleles has limited the therapeutic success and usefulness of this class of antibiotics. To address this growing concern efforts have been focused on looking into the molecular mechanisms responsible for tetracycline resistance (Chopra and Roberts 2001). There are four different classes of mechanisms that are known to commonly confer resistance to tetracyclines: 1) efflux pumps, 2) ribosomal protection proteins, 3) mutation of ribosomal RNAs or ribosomal proteins, and 4) TetX facilitated enzymatic degradation (**Figure 1.4**).

1.6.1. Efflux pumps.

One of the most prevalent resistance mechanisms against tetracyclines are efflux pumps, which eject tetracyclines from the cytoplasm to reduce intracellular concentrations of tetracycline and prevent the antibiotic from accessing the ribosome.

One class of tetracycline-specific efflux pumps is typically found in Gram-negative bacteria. This class includes the efflux genes *tetA*, *tetB*, *tetC*, *tetD*, *tetE*, *tetG*, *tetJ*, *tetY*, *tetZ*, and *tet30*, which encode for proton antiporters with 12 transmembrane domains (Aminov, et al. 2002). TetA and related efflux pumps have high substrate specificity that reportedly can be altered by introducing mutations into a conserved interdomain loop (Sapunaric and Levy 2005). Interestingly, TetA pumps impose a fitness cost in the absence of tetracycline since as antiporters they eject important ions, such as K⁺, however cells can often acquire compensatory mutations to overcome this fitness disadvantage (Hellweger 2013; Hong, et al. 2014). Additionally, there are two tetracycline-specific efflux pumps (TetK and TetL) that are more often identified in Gram-positive bacteria (Markham and Neyfakh 2001). Like TetA-related effluxers, TetK and TetL are also antiporters that use energy to eject tetracyclines, however TetK and TetL

have 14 transmembrane domains and usually express relatively poorly in Gram-negative bacteria (Noguchi, et al. 1994). In addition to tetracycline-specific efflux pumps, there are multidrug efflux pumps with broad substrate specificity that can confer resistance to tetracyclines when overexpressed, such as the AcrAB efflux pump in *Klebsiella pneumonia* (Sun, et al. 2014).

1.6.2 Ribosomal protection proteins.

Ribosomal protection proteins (RPPs) work by displacing tetracycline from the ribosome and thus decreasing the apparent affinity of tetracycline for the ribosome (Connell, et al. 2003). The most common and well studied RPPs are TetM and TetO, however a variety of different RPPs have been identified including TetS, TetT, TetQ, TetP, TetW, and OtrA that presumably function the same as TetM and TetO (Connell, et al. 2003). RPPs have sequence similarity and homology to the ribosomal elongation factor G (EF-G) and bind to the ribosome at the same site as EF-G (Sanchez-Pescador, et al. 1988). While RPPs are related to EF-G they cannot perform the same role as EF-G in translation (Burdett 1996). Therefore RPPs likely evolved from EF-G in such a way as to lose their original function while acquiring the ability to confer tetracycline resistance (Burdett 1996). The ribosomal binding sites of RPPs and tetracyclines are overlapping (Li, et al. 2013). When an RPP binds to the ribosome it alters the conformation of several nucleotides on helix 34 of the 16S rRNA, which in turn results in a configuration favoring the release of tetracycline (Donhofer, et al. 2012). The presence of GTP is essential for the activity of RPPs (Burdett 1996). Once tetracycline is released from the ribosome the RPP then dissociates by hydrolyzing a bound GTP, which subsequently frees the ribosome to continue with translation (Connell, et al. 2003). While RPPs have been identified in both Gram-negative and Gram-positive bacteria, they are more frequently found in Gram-positive organisms (Eliopoulos, et al. 2003).

1.6.3 Mutations in the ribosome.

In some cases bacteria have acquired resistance to tetracyclines by mutating the ribosome. Several tetracycline-resistant propionibacteria clinical isolates were found to have a guanine to cytosine mutation in the 16S rRNA near the binding site of tetracycline (Ross, et al. 1998). Modifying the 16S rRNA may reduce the binding affinity of tetracycline to the ribosome or it may allow tRNAs to access the A-site despite the presence of tetracycline (Ross, et al. 1998). Similar 16S rRNA mutations have also been found to play a role in tetracycline resistance in *Helicobacter pylori* (Gerrits, et al. 2002; Nonaka, et al. 2005; Trieber and Taylor 2002). Additionally, *Bacillus subtilis*, *Neisseria gonorrhoeae*, and *Staphylococcus aureus* can achieve tetracycline resistance by acquiring mutations in the ribosomal *rpsJ* gene, which encodes the S10 protein (Akanuma, et al. 2013; Hu, et al. 2005; Wozniak, et al. 2012). While tetracyclines do not directly interact with S10, the mutations conferring resistance occur on a loop of S10 that is located near the tetracycline-binding pocket and could alter tetracycline binding.

1.6.4 Enzymatic degradation by TetX.

Tetracyclines can be enzymatically degraded by the TetX protein. The *tetX* gene was first identified in *Bacteroides fragilis* and encodes a flavoprotein that reduces the stability of tetracycline substrates by hydroxylating a carbon in the ring core (Yang, et al. 2004). While TetX can degrade most tetracyclines, the clinical significance of *tetX* is unclear as this gene has never been observed in pathogens and only confers a modest level of resistance (Speer, et al. 1992). Interestingly, our group showed that relatively small changes in the K_m of TetX for minocycline could increase the resistance of *E. coli* to relevant drug concentrations (Walkiewicza, et al. 2012). This suggests that *tetX* could potentially contribute to clinical resistance under the appropriate selection conditions.

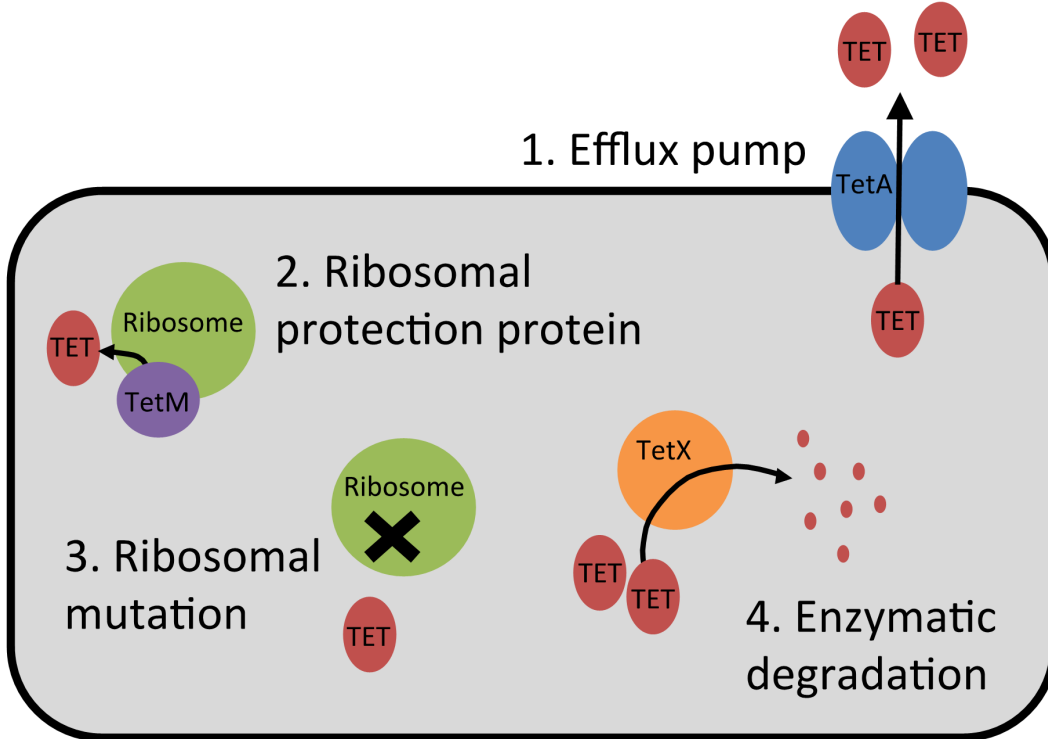


Figure 1.4: Mechanisms of tetracycline resistance. There are four different molecular mechanisms commonly found to protect cells from tetracycline (TET) antibiotics. **1)** Efflux pumps eject tetracyclines from the cytoplasm preventing the antibiotic from having access to the ribosome. For example, TetA-related effluxers are a common class of tetracycline-specific antiporters with 12 transmembrane domains. **2)** RPPs, such as TetM, mimic EF-G and bind to the ribosome at the same site as EF-G. However, instead of acting as elongation factors RPPs displace tetracyclines from the ribosome and free the ribosome to continue with translation. **3)** Certain mutations in the 16S rRNA or S10 protein of the ribosome protect cells from tetracyclines possibly by lowering the affinity of the tetracycline-ribosome interaction. **4)** TetX is a monooxygenase that covalently modifies tetracyclines to reduce the stability of the antibiotic causing the molecule to degrade. The clinical relevance of TetX is unclear as the protein only provides a modest level of protection against tetracyclines.

1.7 Tigecycline: a third-generation tetracycline and drug of last resort.

Tigecycline (TGC) is a semisynthetic third generation tetracycline belonging to the glycycycline family. TGC was approved by the FDA in 2005 for the treatment of complicated skin and intra-abdominal infections caused by *E. faecalis* (Livermore 2005). The mechanism of action for TGC is the same as other tetracyclines, where it inhibits translation by binding to the 16S rRNA and blocking the entry of transfer RNAs into the ribosome (Chopra 2001). The structure of TGC is identical to minocycline, but with the addition of a t-butylglyclamido side-group at position 9 (**Figure 1.3**). The position 9 side-group of TGC interacts with the C1054 nucleotide of the 16S rRNA, causing TGC to have a 20-fold increase over tetracycline in affinity for the ribosome (Bauer, et al. 2004; Jenner, et al. 2013; Olson, et al. 2006). The increased ribosomal binding affinity of TGC results in about a 100-fold increase in translation inhibition over tetracycline making TGC an important therapy (Olson, et al. 2006). Importantly, TGC stills maintains high efficacy against many pathogens that are resistant to other tetracyclines (Bauer, et al. 2004; Jenner, et al. 2013; Olson, et al. 2006). This is because the most common tetracycline-resistance genes, including RPPs and efflux pumps, are ineffective against TGC (Bergeron, et al. 1996). It has been hypothesized that steric-hindrance created by the 9-t-butylglyclamido side-group of TGC prevents it from being efficiently ejected by most efflux-pumps (Livermore 2005). RPPs, which dislodge tetracycline from the ribosome and allow for translation to continue, have limited efficacy against TGC at normal expression levels (Connell, et al. 2003). Donhofer *et al.* determined the structure of the RPP TetM bound to a bacterial ribosome using cryo-EM and observed that TetM must interact with, and alter the conformation of the C1054 nucleotide on the 16S rRNA to effectively dislodge tetracycline (Donhofer, et al. 2012). Since the 9-t-butylglyclamido

side-group of TGC interacts with C1054, TetM has limited access to this residue and is therefore less effective against TGC (Jenner, et al. 2013). Also, it is likely that the increased binding affinity of TGC for the ribosome plays a role in the ability of TGC to inhibit ribosomes that are protected by TetM and other RPPs (Donhofer, et al. 2012). Taken together, TGC has high efficacy against pathogens resistant to other antibiotics and thus is frequently used a drug of last resort when all other agents have failed (Huttner, et al. 2012; Rincon, et al. 2014).

1.7.1 Resistance to tigecycline.

Despite the promising *in vitro* activity of TGC, resistance to this drug has been observed in clinical strains due to chromosomal mutations that up-regulate efflux pumps, including the Resistance Nodulation-cell Division (RND) pumps, AcrAB-TolC pump, and the Multidrug and Toxin Extrusion (MATE) pumps in *Acinetobacter baumannii*, *Escherichia coli*, and *Staphylococcus aureus*, respectively (Coyne, et al. 2011; Keeney, et al. 2008; McAleese, et al. 2005). Infections caused by TGC-resistant *E. faecalis* have thus far been rare, but are often fatal, underlining the dangers of TGC-resistant VRE infections (Cordina, et al. 2012; Werner, et al. 2008). As TGC is used more over time, dissemination of resistance will likely become an increasing problem. At the start of these studies the mechanisms behind TGC-resistance in *E. faecalis* were poorly characterized. During the completion of these studies it was discovered that clinically isolated strains of *Enterococcus faecium* and *Klebsiella pneumoniae* could acquire mutations impacting the ribosomal S10 protein to achieve resistance to TGC (Cattoir, et al. 2014; Villa, et al. 2014). Also, TGC can be enzymatically degraded by the TetX protein, however since *tetX* has never been found to confer resistance in the clinical setting it is unclear if this mechanism poses a threat to the efficacy of TGC (Speer, et al. 1992). Interestingly, using error prone mutagenesis Dan Andersson's group found that

mutations in the C-terminal region of TetX could confer a high level of TGC resistance without losing the ability to confer resistance to first and second generation tetracyclines (Linkevicius, et al. 2015). This suggests that *tetX* could potentially play a worrisome role in conferring resistance to all classes of tetracyclines. Through error prone mutagenesis Andersson's group also identified mutations in the efflux pumps TetA and TetK, and in the RPP TetM that were capable of conferring TGC resistance. However, these mutations showed a trade-off as they reduced the ability of the protein to confer resistance to earlier generations of tetracyclines (Linkevicius, et al. 2015). These results show how the high prevalence of tetracycline resistance alleles could potentially undermine the efficacy of TGC.

1.8 Role of horizontal gene transfer in tetracycline resistance.

The therapeutic efficacies of tetracyclines have been greatly undermined by the high prevalence of tetracycline resistance genes. Horizontal gene transfer has played a major role in facilitating the dissemination of tetracycline resistance and many tetracycline resistance genes and determinants are located on mobile or conjugative elements (Chopra and Roberts 2001). The most common tetracycline efflux pumps, *tetA-E*, *tetG-H*, and *tetK-L*, are almost exclusively found on plasmids or transposons (Poole 2005; Roberts 1994). Additionally, the conjugative Tn916 transposon and related Tn916-like elements, frequently carry the ribosomal protection gene *tetM*, which in turn has facilitated the spread of *tetM* among many bacterial species (Roberts 2005).

1.8.1 The conjugative transposon Tn916.

Originally Tn916 was identified in *E. faecalis* DS16 and was notable for being the first transposon discovered that could conjugate between cells independent of a plasmid (Franke and Clewell 1981). Tn916 and related Tn916-like elements carry all of the components necessary to conjugate from cell-to-cell and to then subsequently integrate into the host genome (Roberts and Mullany 2009). Most Tn916-like elements carry the *tetM* gene and consequently many VRE and *E. faecalis* strains in hospitals carry *tetM*, with frequencies of the gene as high as 88.9% among sampled isolates (Frazzon, et al. 2009; Leener, et al. 2004; Lopez, et al. 2009; McBride, et al. 2007; Nishimoto, et al. 2005). Tn916-like elements have a very broad host range and are not only found in *Enterococcus* species, but also in many other species, including *Staphylococcus*, *Streptococcus*, *Clostridium*, *Bacillus*, *Escherichia*, *Neisseria*, and *Pseudomonas* (Rice 1998; Roberts and Mullany 2009). Additionally, Tn916 can conjugate between different species in a variety of environments, such as between *E. faecalis* and *Lactococcus lactis* in the gastrointestinal tract of rats, *Bacillus subtilis* and *Bacillus thuringiensis* in sterile soil, or *E. faecalis* and *Butyrivibrio fibrisolvens* in filter mating experiments (Boguslawska, et al. 2009; Haack, et al. 1996; Hespell and Whitehead 1991; Wasels, et al. 2014). In total the Tn916 element has been identified in greater than thirty five distinct bacterial genera and even more individual species (Roberts and Mullany 2011). The promiscuity of Tn916 conjugation has allowed the element to achieve a high frequency among many organisms and highlights the potential of the element to continue spreading tetracycline resistance to bacteria that are currently susceptible.

1.8.2 Genetic structure of Tn916.

Tn916 is an approximately 18 Kb DNA element with 24 predicted open reading frames (ORFs) (Roberts and Mullany 2009). The ORFs on Tn916 are organized in different functional modules. At the 5' end of Tn916 are ORFs 13-24, which all code for predicted conjugation elements (**Figure 1.5A**). Towards the 3' end of Tn916 are ORFs thought to be involved in transcriptional regulation and transposon recombination, including the *xis* and *int* genes, which encode proteins essential for the excision and integration of Tn916 into a new chromosomal location (**Figure 1.5A**). Additionally, accessory genes are usually located closer to 3' end (**Figure 1.5A**). The most common accessory gene on Tn916-like elements is *tetM*, however variants of Tn916 have been found to carry alleles that confer resistance to non-tetracycline antibiotics, including macrolides, lincosamide, streptogramin, and kanamycin (Haack, et al. 1996). In total there are at least twenty-six major variants of Tn916 ranging in size from about 18 to 33 Kb (Roberts and Mullany 2011). The variation in genetic structure and resistance alleles among Tn916-like elements highlights the ability of this class of transposons to evolve and spread resistance to not just tetracyclines, but to other classes of antibiotics as well.

1.8.3 Regulation of *tetM* expression and Tn916 conjugation.

Expression of *tetM* is regulated by a transcriptional attenuation mechanism involving a terminator stem-loop located 36-bp upstream of the *tetM* start codon (Su, et al. 1992). In the presence of tetracycline, the terminator stem-loop, which prevents expression of *tetM* in the absence of tetracycline, is overcome by a poorly characterized mechanism that may involve ribosomal-mediated transcriptional attenuation (Celli and Trieu-Cuot 1998; Su, et al. 1992). Canonically, the mobilization and conjugal-transfer of Tn916 occurs infrequently, ranging from $\sim 10^{-8}$ to $\sim 10^{-5}$ transconjugants per donor cell, and is

increased in the presence of tetracycline (Celli and Trieu-Cuot 1998; Jaworski and Clewell 1994). Leaky transcription of *tetM* allows read-through expression of the downstream excisionase (*xis*) and integrase (*int*) genes (Celli and Trieu-Cuot 1998; Storrs, et al. 1991) (**Figure 1.5B**). When *xis* and *int* are expressed, Tn916 is excised from the chromosome at an increased frequency and forms a covalently closed circular intermediate (Roberts and Mullany 2009). Circularization of excised Tn916 allows for transcription initiated upstream of *tetM* to continue around the circularized element leading to expression of the now downstream Tn916 conjugation factors (**Figure 1.5C**). Once the conjugation elements are expressed then the Tn916 element can be passed to new cells through conjugation. It is unclear if Tn916-like elements can replicate outside of the host chromosome. However Lee *et al.* showed that the conjugative transposon ICEBs1 in *B. subtilis* could undergo autonomous replication, demonstrating that at least some classes of conjugative transposons can undergo replication independently of the chromosome (Lee, et al. 2010).

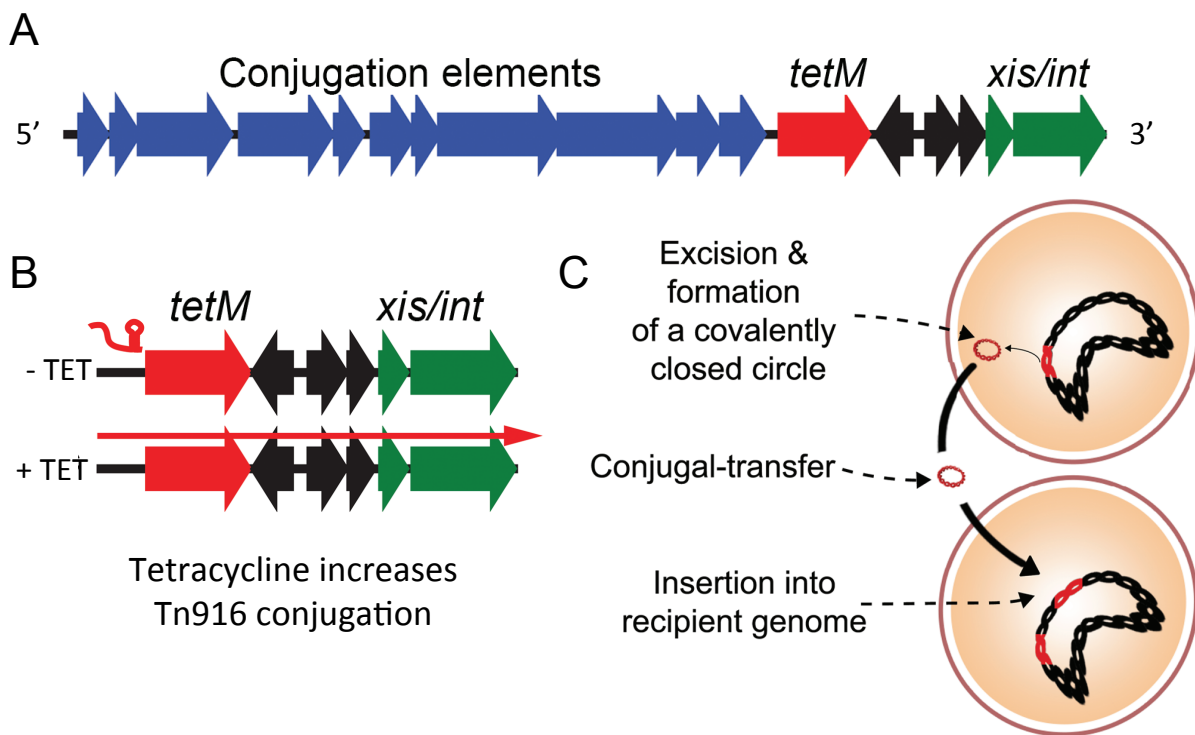


Figure 1.5: A diagram outlining the genetic structure, transcriptional regulation, and movement of the conjugative transposon Tn916. A) Tn916 has twenty-four predicted ORFs. At the 5' end of Tn916 are genes involved in conjugation (blue). Towards the 3' end of Tn916 are the ribosomal protection gene *tetM* (red), several genes predicted to be involved in transcriptional regulation (black), and genes encoding the Tn916 recombinases (green). **B)** The expression of *tetM* is repressed in the absence of tetracycline by a transcription termination mechanism (indicated as the red hairpin) that is relieved when antibiotic is present. In the presence of antibiotic, leaky transcription through *tetM* leads to expression of the downstream excisionase (*xis*) and integrase (*int*) genes. **C)** Upon excision from the genome, Tn916 forms a covalently closed circular intermediate that coordinates excision events with expression of the genes required for conjugation. This figure was adapted with permission from Beabout et al (2015b).

1.9 Experimental evolution.

Observing the natural world has allowed scientists to answer fundamental questions about adaptive evolution. However, certain aspects of evolution can be further explored in a laboratory setting where replicate experiments can be performed under well-controlled conditions. Microbes are excellent model organisms for experimental evolution due to their short generation times and ease to cultivate and store for long periods. Importantly, evolution can be observed over manageable timescales during microbial adaptation experiments allowing researchers to explore a remarkable variety of important evolutionary questions, such as the reproducibility of adaptation (Cooper and Lenski 2010; Korona, et al. 1994), the underlying biophysical basis of fitness (Counago, et al. 2006; Golding and Dean 1998; Pena, et al. 2010; Walkiewicza, et al. 2012), the role of epistasis in adaptation (Burch and Chao 2004; Khan, et al. 2011; Lunzer, et al. 2010), the evolution of cheating and cooperation (Hammerschmidt, et al. 2014; Strassmann and Queller 2011; Strassmann, et al. 2000), and the advantages of sexual reproduction (Azevedo, et al. 2006).

1.9.1 Adaptation techniques of experimental evolution.

There are several different types of adaptation experiments that are commonly implemented by experimental evolutionists, including serial transfer experiments and continuous culture experiments. Serial transfers, or batch culture transfers, typically require growing microbes in flasks or tubes until the population reaches stationary phase and then transferring a portion of the population to fresh media so that the cells can enter a growth phase again. Serial transfer experiments are capable of maintaining a level of genetic diversity while selecting for growth in a particular environment and are relatively simple to execute and maintain for long-term experiments (Barrick and Lenski

2013). However, during serial transfers populations are exposed to varying concentrations of nutrients and enter different growth phases throughout adaptation, which creates a somewhat complex and varying environment. Continuous culture experiments on the other hand expose the cells to a more consistent and less complicated environment, but are more technically challenging to implement as they use bioreactors to constantly maintain the population in a growth phase (Gresham and Dunham 2014). To maintain a continuous culture a constant in flow of media is pumped into a bioreactor to supply the population with fresh nutrients, while at the same time a random collection of media, waste, and cells are removed. Chemostats and turbidostats are two different types of bioreactor setups that are frequently used to maintain continuous cultures. In a chemostat the growth of the population is controlled by the presence of a rate-limiting nutrient in the media. Thus chemostats are ideal for studying the genetic and regulatory dynamics of a population adapting to nutrient deprivation (Ferenci 2007). In a turbidostat the cells are maintained at their fastest growth rate by keeping the population at a constant cell density. This is usually achieved by dynamically altering the in flow of media in response to changes in turbidity. Turbidostats require constant monitoring and therefore are very technically challenging. However, turbidostats have several key advantages: they do not require growth in nutrient-poor conditions and the population is constantly growing at its fastest rate, meaning that many generations can be achieved over a relatively short time and that mutations with a fitness advantage have ample opportunity to emerge and rise in frequency (Beabout, et al. 2015b; Counago, et al. 2006; Hammerstrom, et al. 2015; Miller, et al. 2013).

1.9.2 Advantages of studying antibiotic resistance with experimental evolution.

One approach to identify alleles associated with resistance is to sequence the genome of a resistant clinical isolate and compare it to the genome of a susceptible isolate. While this approach allows for the detection of resistance genes, it does not give insights into which adaptive alleles are most important to conferring resistance and which alleles have secondary roles, such as compensatory or neutral mutations. Combined this means it can be challenging to determine which alleles should be further characterized by time consuming biochemical and biophysical assays. Therefore experimental evolution can be a powerful tool to study resistance because it allows for the reconstruction of adaptive trajectories leading to resistance, which in turn gives insights into which adaptive alleles are more important to resistance. For example, mutations that emerge earlier in adaptation often confer a higher fitness advantage and thus are typically more important to adaptation than subsequent mutations (Barrick, et al. 2009; Elena and Lenski 2003; Gerrish and Lenski 1998). Additionally, experimental evolution allows for important alleles to be identified based on their parallel evolution across replicate populations (Saxer, et al. 2014; Wood, et al. 2005). A gene or pathway is likely important to resistance if it is repeatedly mutated in multiple replicate populations. Ultimately, elucidating the evolutionary dynamics and mechanisms of resistance for a particular antibiotic provides insights that can be applied toward generating strategies to maintain the efficacy of that antibiotic. For example, if mutations up-regulating a signaling pathway were found to play a key role in conferring resistance, designing inhibitors of that pathway might generate an adjuvant drug that would deter the emergence of resistance during antibiotic therapy. Additionally, the adaptive trajectory a pathogen takes to resistance depends greatly on its unique genomic background.

Certain alleles, or combinations of alleles, may be precursors to resistance that allow bacteria to adapt quickly, such as an efflux pump that can confer resistance when mutated or overexpressed. If such alleles were identified, clinicians could sequence a patient's infection to determine if these precursors were present, which could then help the clinician decide which antibiotic or combination of antibiotics would be most likely to avoid resistance (Miller, et al. 2013; Munita, et al. 2014; Munita, et al. 2012).

1.10 Goals of this study.

The main goal of this study was to identify the most important genomic and biochemical changes leading to TGC-resistance in vancomycin resistant *E. faecalis*. Most studies investigating mechanisms of resistance are initiated after resistance to the antibiotic of focus has become widespread. We reasoned that instead, if the most essential adaptive mutations for resistance were identified while the agent still had high efficacy, insights could be gained before resistance became too prevalent to efficiently combat. Therefore, I decided to study resistance to TGC in the hospital-associated pathogen *Enterococcus faecalis*. At the start of these studies TGC remained effective against most enterococci strains since the antibiotic had not yet been widely used; however, there were already several reports of non-susceptibility to TGC in *E. faecalis* isolates (Freitas, et al. 2011; Pillar, et al. 2008; Tsai, et al. 2012). Also, only two cases of infections caused by TGC-resistant *E. faecalis* had been reported in the literature, but both infections were ultimately fatal, underlining the danger of TGC-resistant *E. faecalis* infections (Cordina, et al. 2012; Werner, et al. 2008). Currently, TGC resistant infections are still rare, but more have been reported in the literature (Cattoir, et al. 2014; Fiedler, et al. 2015; Niebel, et al. 2015). As the prevalence of multidrug resistant infections continues to rise,

there will likely be increased usage of TGC, after which an increase in the prevalence of TGC resistance could follow, as has been observed with increased usage of other antibiotics (Cantón and Morosini 2011; Fernández, et al. 2011). By elucidating the molecular mechanisms of resistance against TGC in VRE these insights can now be used before resistance has become widespread. For example, if overexpressing a protein were found to be important to acquiring resistance, perhaps inhibitors of that protein could be generated and used as an adjuvant therapy to avoid resistance during antibiotic treatment.

1.10.1 Summary of approach.

The approach I used to study TGC-resistance in *E. faecalis* is referred to as ‘quantitative experimental evolution’ and uses a combination of experimental evolution and allelic frequency measurements to study adaptation to resistance (**Figure 1.6**). By combining experimental evolution and allelic frequency measurements, I was able to construct the evolutionary trajectories leading to resistance. Then, by applying concepts of evolution to the results of these experiments, the most important proteins and pathways responsible for resistance were identified. Specifically I completed these goals: First, I facilitated adaptation to resistance by using a bioreactor that maintains a population of cells at its fastest growth rate. Then, to understand the evolutionary dynamics of the population I isolated phenotypically unique single end-point colonies for whole genome sequencing and performed deep sequencing on samples of the population as a function of the entire experimental evolution time course. Taken together, these data allowed me to identify the most important adaptive alleles, which I then further characterized by performing physicochemical studies.

1.10.2 Workflow of quantitative experimental evolution.

For the first step of quantitative experimental evolution a large population of cells are continuously maintained in a turbidostat bioreactor at their fastest growth rate for up to a month (**Figure 1.6**). Keeping the cells at their fastest growth rate allows the population to go through many generations, which in turn provides more opportunities for cells with resistance to rise in frequency. During adaptation the antibiotic concentration is increased slowly to reduce the selective pressure of adaptation, which consequently allows the population to remain genetically diverse and polymorphic. If the antibiotic concentration were increased rapidly this would likely lead to the fixation of only a few alleles that could quickly confer resistance, whereas modest increases in antibiotic allow cells in the population to accumulate multiple mutations or more complex mutations, such as large chromosomal rearrangements. Allowing cells to acquire a variety of adaptive alleles subsequently leads to clonal interference and the persistence of diversity within the population. This is advantageous as the more diverse the population, then the more resistance mechanisms can be identified in each experiment. Following the completion of adaptation clones are then randomly isolated from the resistant population and screened for phenotypic diversity to get at their underlying genetic diversity (**Figure 1.6**). Phenotypic assays can include differences in minimal inhibitory concentrations (MICs), growth rates, colony morphologies, propensity to form biofilm and other assays relevant to the specific bacterial species, such as swarming assays for motile bacteria. Once phenotypically diverse clones are identified, whole genome sequencing is used to determine their specific genotypes (**Figure 1.6**). This provides information about which combinations of mutations are present in the genomes of end-point adapted isolates. To construct the adaptive trajectories to resistance, samples of the bioreactor population are collected daily and stored at -80°C with glycerol (**Figure 1.6**). Genomic DNA is then directly extracted from these daily samples without further

outgrowth and used for deep sequencing, which allows for the identification of all alleles and their frequencies in the population (**Figure 1.6**). The daily allelic population measurements reveal when mutations first appeared in the population and what frequency they reached, which in turn indicates the evolutionary success of each mutation. One limitation of the population frequency measurements is they do not reveal the linkages between different alleles, meaning which alleles are found within the same genomes. However, the linkages can be inferred from the end-point clone sequencing, which does provide specific genotypes from the individual clones present at the end of adaptation. Thus by combining the sequencing data from the daily population samples and end-point clones, we can then determine which mutations were most important to resistance (**Figure 1.6**). Once the most important adaptive mutations are identified, appropriate molecular and biophysical assays can be performed to get at the underlying physicochemical basis of resistance. This information can then be applied towards developing strategies to limit the emergence and spread of TGC resistance among VRE.

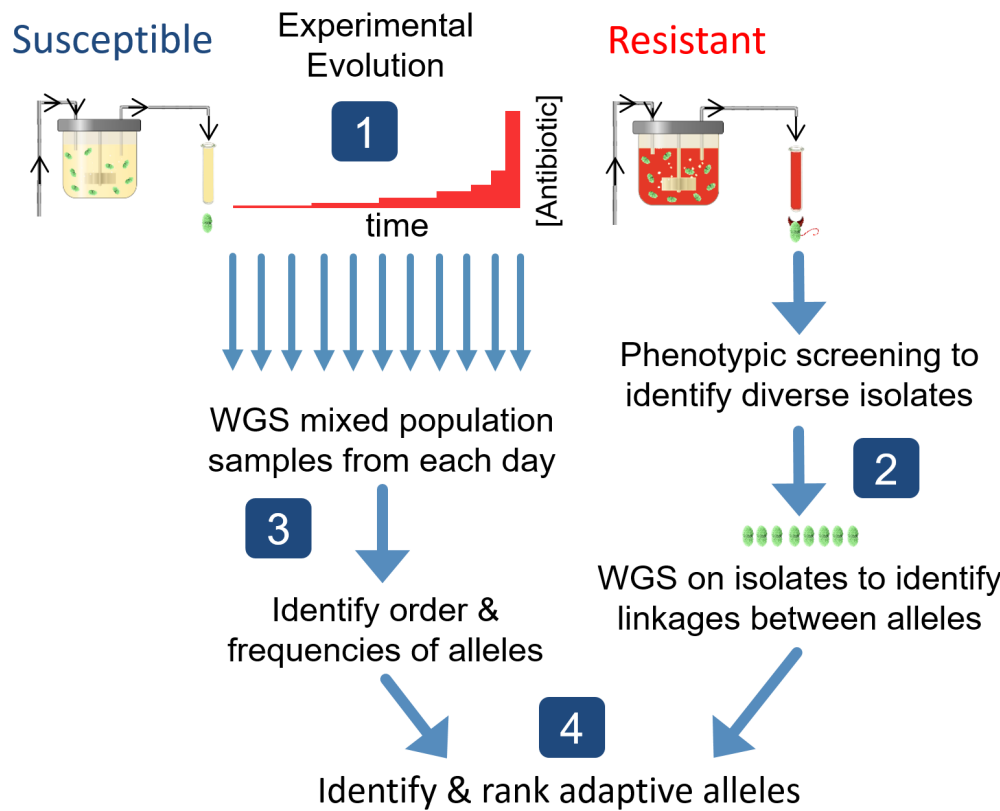


Figure 1.6: Flow chart outlining the steps of quantitative experimental evolution.

Quantitative experimental evolution can be used to identify and rank the importance of resistance alleles. **1)** Adaptation to resistance is facilitated by a turbidostat bioreactor, which is a continuous culture vessel that maintains a population at its fastest growth rate. **2)** Whole genome sequencing (WGS) of phenotypically distinct colonies is then performed to identify resistance alleles and their genomic linkages with other adaptive alleles. **3)** Next, the order mutations appeared within the population and their allelic frequencies are determined by performing deep sequencing on samples of the polymorphic population collected on each day of adaptation. **4)** Combined, concepts of evolution are applied to these data and used to identify the most important adaptive alleles for further analysis and characterization by physiochemical studies.

1.10.3 Relevance of quantitative experimental evolution.

Our lab initially employed quantitative experimental evolution to study resistance to the antibiotic DAP in the clinical *E. faecalis* S613 strain (Miller, et al. 2013). S613 was isolated from a 64-year-old woman who had acquired bacteremia from vancomycin-resistant *E. faecalis* after undergoing intravenous catheterization (Munoz-Price, et al. 2005). After several antibiotic treatments failed to clear the infection, she was switched to DAP. Unfortunately, the infection became resistant to DAP and ultimately proved fatal. S613 was isolated from the patient before DAP treatment, and R712 was isolated from the patient after the infection became DAP-resistant (Munoz-Price, et al. 2005). Our collaborators in the Cesar Arias lab at the University of Texas Health Science Center at Houston (UTHealth) used comparative whole genome sequencing between S613 and R712 to identify clinical DAP resistance alleles (Arias, et al. 2011). Several mutations were identified, but without the evolutionary dynamics leading to resistance it was difficult to determine which mutant alleles were most essential to resistance and which played less significant roles, such as compensatory mutations. Therefore, our lab used quantitative experimental evolution to adapt S613 to DAP resistance in the lab (**Figure 1.6**). Importantly, using this approach we were able to determine that mutation of the LiaFSR membrane-stress response pathway was an essential first step in acquiring DAP-resistance, and that additional mutations emerged later in adaptation, but played smaller roles in conferring resistance (Miller, et al. 2013). It is also significant to note that the predominating mutations identified from quantitative experimental evolution matched those identified by our collaborators in the genome of the clinically resistant R712 isolate (Arias, et al. 2011; Miller, et al. 2013). This finding suggests that although the environment of a bioreactor has significant differences from that of a host organism, clinically relevant mechanisms of resistance can be identified in the lab. While bioreactor-facilitated adaptation *cannot select for virulence or pathogenicity*, the

selective pressure of antibiotic resistance is strong enough that clinically relevant markers of resistance can be identified. In other terms, selection for growth in the presence of an antibiotic is strong enough for similar mechanisms of resistance to emerge across distinctly different environments.

1.10.4 Using quantitative experimental evolution to study tigecycline resistance in VRE.

Since quantitative experimental evolution had successfully identified clinically relevant adaptive trajectories to DAP resistance, I decided to use this approach to elucidate how TGC resistance is acquired in vancomycin resistant *E. faecalis*. I decided to use the S613 *E. faecalis* strain for my experiments because it is a clinical pathogen, but is reasonably well characterized with a sequenced reference genome available. Also, S613 carries the Tn916 conjugative transposon with *tetM* and is therefore tetracycline-resistant, but still susceptible to TGC. Thus, S613 is as a good representation of the background most likely to be observed in a hospital strain of *E. faecalis* and provides the opportunity to study the role of horizontal gene transfer in resistance and the ability of RPPs, such as TetM, to potentially undermine TGC's efficacy (Frazzon, et al. 2009; Leener, et al. 2004; Lopez, et al. 2009; McBride, et al. 2007; Nishimoto, et al. 2005). By using quantitative experimental evolution the most important alleles and molecular mechanisms conferring resistance to TGC in VRE were identified. In the future these insights can now be applied to maintain the efficacy of TGC and combat the rising prevalence and threat of multidrug resistant pathogens.

Chapter 2: Materials and Methods.

Portions of this chapter are reproduced from Beabout, et al. 2015 *Mol Biol Evol* and Beabout, et al. 2015 *Antimicrob Agents Chemother*.

2.1 Bacterial strains and growth conditions.

Clinically isolated strains *E. faecalis* S613 (GCA_000163795.1) (Munoz-Price, et al. 2005), *E. faecalis* R712 (GCA_000163815.1) (Munoz-Price, et al. 2005), *E. faecium* 105 (Munita, et al. 2012), *E. faecium* R499 (GCA_000294875.1) (Diaz, et al. 2014), methicillin-resistant *S. aureus* MRSA131 (GCA_000187145.1), and *A. baumannii* AB210 (GCA_000189655.2) (Hornsey, et al. 2010) and the lab strains *E. faecalis* OG1RF (GCA_000172575.2) and *E. coli* BW25113 (GCA_000750555.1) were used for this study. Enterococcal strains were cultured in 80% Lysogeny Broth and 20% Brain Heart Infusion (LBHI) media at 37°C with or without agitation unless stated otherwise. AB210, MRSA131, and BW25113 were cultured in Lysogeny Broth (LB) on a shaker at 37°C unless stated otherwise.

2.2 Serial transfer adaption of *E. faecalis* S613 to minocycline and tigecycline.

The serial transfer adaptation experiments began with inoculating flasks containing 50 mL of LBHI broth with a single colony of S613. Every 24 hours 500 µL of culture from the flask was transferred to a fresh flask, making a 1/100 dilution of the cultured cells. The drug concentration was increased when the cells were transferred. To determine what

concentration of drug to use for the next transfer, several 1/100 dilutions of the culture were setup in tubes at different concentrations of antibiotic. The next day the tubes were checked to see what concentrations of drug S613 was able to grow to a high cell density in. The highest concentration of drug with visible growth was picked as the next concentration to use in the flask.

2.3 Bioreactor design, setup, and operation.

2.3.1 Overview of bioreactor.

A Sartorius Stedim Biostat Bplus controller and bioreactor (1 L volume) customized for continuous experimental evolution were used for all bioreactor experiments (**Figure 2.1**). Culture conditions within the bioreactor consisted of 300 ml of LBHI media at 37°C with an airflow rate of 0.16–0.2 L/min. To initiate a run, we inoculated the bioreactor with a single colony of *E. faecalis* S613. For both replicate runs, we cultured the population in the bioreactor in the absence of TGC for approximately 48 hr before adding 0.05 µg/ml TGC (approximately half the TGC MIC against S613). Antibiotic was introduced into the bioreactor vessel by supplementing the media inflow tanks with TGC. LBHI media was sterilized in 9 L batches using an Integra Biosciences Mediaclave.

2.3.2 Detection of CO₂ and maintenance of population at a constant cell density.

The population cell density was maintained at a constant optical density (OD) of about OD (600 nm) = 0.6 (~6 x 10⁸ cells/ml). We were unable to directly monitor the optical density within the bioreactor, because biofilm production by *E. faecalis* produced flocculent particulate and coated the optical density probes and all surfaces leading to

interference. Instead, we monitored the metabolism of the population by measuring the outflow of %CO₂ using a Tandem Pro Gas Analyzer (Magellan Instruments, Hagersten, Sweden). When the exhaust %CO₂ of the culture rose, a control loop activated the inflow of fresh media to dilute the culture and maintain a constant population size (**Figure 2.1**). Manual optical density measurements of samples collected from the population outflow were also taken periodically to confirm the culture was at the desired cell density.

2.3.3 Selection regime and increases in antibiotic concentration.

During the experiment, we increased the concentration of TGC in stepwise intervals based upon the next increment of drug concentration that could be tolerated without a marked reduction in growth rate to the new condition. Broth dilution MIC tests were used to determine what concentration of TGC to use for each step in drug concentration. Thus, the entire selection experiment takes place well below the MIC of the population. The advantage of using subinhibitory TGC concentrations during adaptation is that it reduces the selective pressure, which allows for polymorphism to emerge within the population so that more adaptive alleles can be identified.

2.3.4 Collecting samples and sterility checks.

Each day we collected 50 mL samples of the population from a dedicated pump and outflow tubing separate from the waste outflow. We stored the samples at -80°C with 20% glycerol (v/v). We screened the population daily for contamination by streaking a sample of the culture outflow onto non-selective LBHI agar. Colonies on the LBHI plates with morphologies atypical for S613 were transferred to bile esculin agar (BEA), a selective and differential media for enterococci, to determine if the suspicious clones were enterococci.

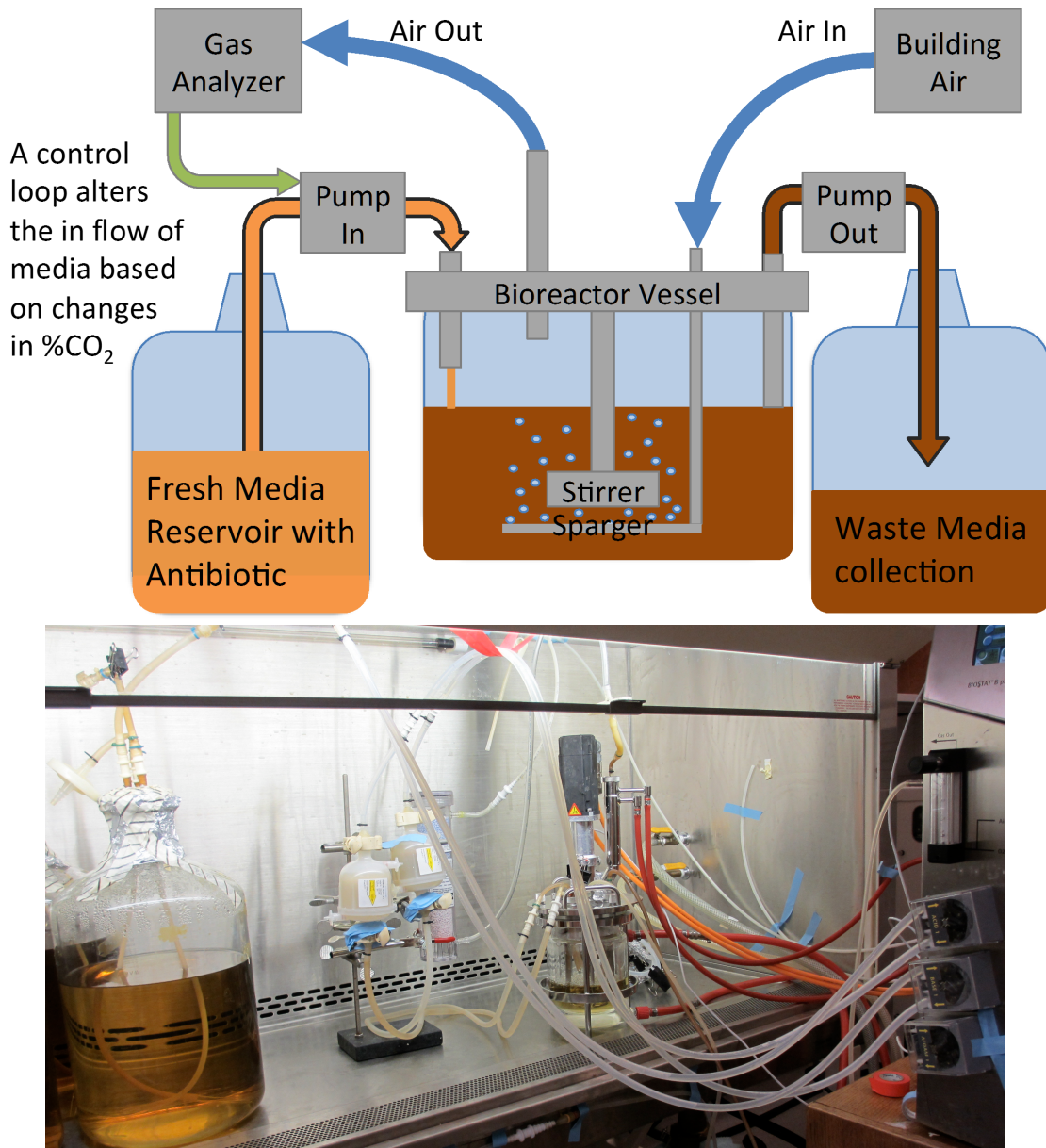


Figure 2.1: The bioreactor setup used for quantitative experimental evolution. A cartoon schematic (above) and photograph (below) of the bioreactor setup used to maintain a continuous culture at its fastest growth rate (turbidostat) during adaptation to TGC resistance. A Sartorius Stedim Biostat Bplus controller and bioreactor were used with modifications. A single colony resuspended in 5 mL of broth was used to inoculate about 300 mL of broth media in a jacketed 1L Sartorius culture vessel. During the adaptation experiment the bioreactor was maintained at a temperature of 37°C and

stirring speed of 100 rpm. The culture was aerated by running building air through the sparger at 0.16–0.2 L/min. A random collection of media, waste, and cells were constantly pumped out of the bioreactor to maintain the culture at a consistent volume. Due to the rapid buildup of biofilm that occurs on probes placed in the vessel, an automated OD probe could not be used to maintain the population at a constant cell density. Instead, the bioreactor exhaust air was sent through drierite, to remove moisture, and then into a Tandem Pro gas analyzer to monitor the level of CO₂ produced by the bacterial culture. As the cell density of the population increased, subsequently more CO₂ was released into the exhaust air. The Sartorius BioPAT® MFCS/win-1 software ran a control loop so that once the %CO₂ exceeded a selected setpoint the inflow of fresh media into the bioreactor was increased to dilute the population and supply the cells with fresh nutrients. Periodically the turbidity of the culture was manually determined by collecting samples of the waste and checking the OD using a McFarland densitometer. The %CO₂ setpoint was then adjusted based on the results of the manual turbidity readings to ensure that the population was at the desired cell density. Combined the MFCS control loop and manual McFarland measurements were used to maintain the population at an OD 600 nm of about 6×10^8 cells/mL. Antibiotic was introduced into the bioreactor by supplementing the fresh media reservoir with antibiotic. Samples of the population for metagenomic analysis were collected from a separate dedicated media outflow during each day of adaptation and stored at -80°C with glycerol.

2.4 Phenotypic characterization of bioreactor end-point strains.

2.4.1 Minimal inhibitory concentrations (MICs) on agar.

LBHI agar plates were made in 150 mm petri dishes and supplemented with 0, 0.25, 0.5, 0.75, 1, 1.25, 1.5, 1.75 or 2 µg/mL TGC. From clonal freezer stocks 94 bioreactor end-point clones and S613 were inoculated into a deep-well plate with 1 mL of LBHI broth in each well and the plate was left overnight at 37°C. To plate the cells, 2 µL of overnight culture from every well was spotted onto each of the agar plates using a multichannel pipette. After 12-16 hours of incubation plates were checked. The lowest drug concentration where the spot of inoculation did not grow was considered the MIC for each isolate. This assay was performed on all 94 isolates taken from the end of the first and second bioreactor runs. An empty well was included as a growth control.

2.4.2 Flocculation assay.

A subset of bioreactor-adapted isolates were selected and grown overnight in 10 mL of LBHI broth media. The next day I removed the cultures from the shaker and let them sit without shaking for 5 minutes so that any floc present would settle. Then I measured the OD₆₀₀ of a sample of broth taken from the top of the culture. Any floc that might be present in the cultures was then broken up by vigorously vortexing the tubes, after which the OD₆₀₀ of the broth off the top of the cultures was measured again. A ratio of OD measurements taken after vortexing and before vortexing, when the cultures were settled, was plotted to compare the differences in flocculation (**Figure 4.2**).

2.4.3 Colony size on chloramphenicol.

I plated some of the end-point adapted isolates onto agar containing a subinhibitory concentration (2 µg/mL) of CL. After 48 hours of incubation I compared the colony sizes

of each isolate to the colony size of the S613 ancestor strain. Some of the isolates produced colonies that were noticeably smaller than S613, while other isolates produced comparatively large colony sizes that were similar to the S613 ancestor. Isolates with a similar colony size to S613 were designated as “large,” while those with a noticeably smaller colony size were designated as “small.” I performed this assay in triplicate to confirm that relative colony sizes were reproducible.

2.5 Preparation of DNA samples for whole genome sequencing.

The individual colonies were selected and grown in 10 mL of LBHI overnight and then pelleted for DNA isolation. Alternatively, for allelic frequency measurements frozen samples of the polymorphic population from each day of adaptation were thawed and immediately pelleted for DNA isolation to avoid any outgrowth. To isolate genomic DNA, we used the UltraClean Microbial DNA Isolation Kit (MoBio), but with an additional lysis step where we added 5 µL of 5 KU/mL mutanolysin and 12.5 µL of 200 mg/mL lysozyme to 300 µL of pelleted cells and incubated the cells at 37°C for 30 minutes. Next, we used the Nextera® XT DNA sample preparation kit from Illumina to generate paired-end libraries. The prepared libraries were sequenced on an Illumina Hi-Seq platform at the Medical College of Wisconsin Human and Molecular Genetics Center and the U.S. Army Edgewood Chemical Biological Center. Clones were sequenced with at least 100-fold coverage (average of 254.5-fold coverage) and the population samples were sequenced with at least 500-fold coverage (average of 818.4-fold coverage).

2.6 Analysis of whole genome sequencing data.

2.6.1 Clonal samples from the end of adaption.

The Illumina reads were aligned to the S613 reference sequence using the open source computational pipeline breseq-0.24rc6 (Deatherage and Barrick 2014). Identified mutations were confirmed using Sanger sequencing (**Table 2.1**). New Tn916 insertions were called in the breseq html output under “Unassigned new junction evidence” and were annotated as junctions between either the 5’ side of the ancestral Tn916 site (NZ_GG739778, position ~132,325) or the 3’ side of the ancestral Tn916 site (NZ_GG739778, position ~150,450) and the position of the new insertion site. To confirm insertions of Tn916 we used primer pairs where one primer complimented either the 5’ or 3’ end of Tn916 and the other primer complimented genomic DNA surrounding the predicted insertion site.

Table 2.1: Primers used for confirmatory Sanger sequencing.

Primer Name	Sequence (5’ – 3’)
rpsJ-F	CAGCGGATAAAATTGTGGAAA
rpsJ-R	AGCGTCAACTGTTTTGGTG
Upstream_tetM-F	TTTCCTGCATCAACATGAGC
Upstream_tetM-R	ACCAAAGCAACGCAGGTATC
ABC_Transporter_1_(msbA)-F	ATTATCGGCGCCTTAATCCT
ABC_Transporter_1_(msbA)-R	GGCAAAGGCATCTTCTCA
ABC_Transporter_2_(Cyto)-F	GCCGAACAAAGCATAAAAGC
ABC_Transporter_2_(Cyto)-R	GACTTGCCGACTGAAAAAGC

2.6.2 Meta-genomic samples from intermediate days of adaptation.

Population samples were also analyzed using breseq, but with the addition of a polymorphism command (-p). The read pile-ups for all mutations within the population

that reached at least 5% frequency during adaptation were manually investigated to exclude predicted mutations that were the result of misalignments. Several clonal samples were run with the polymorphism command to serve as a control: If an allele was called at the same frequency in the population samples and the clonal samples, the allele was excluded, as it was likely an alignment artifact (Saxer, et al. 2014). To visualize the distribution of the different Tn916 insertion sites, all insertion sites were mapped to *E. faecalis* V583 (accession number NC_004668.1) using the BLAST Ring Image Generator (BRIG) (Alikhan, et al. 2011) (**Figure 6.2**). When sequencing mixed populations that contain individuals with varying Tn916 copy number, the measured frequency of any mutation located in Tn916 was an underrepresentation of the frequency of cells with the mutation, because the total number of Tn916 copies exceeded the population size. To correct this issue, these mutations were multiplied by the average Tn916 copy number of the population at each time point (**Figure 5.1A**).

2.6.3 Estimate of average Tn916 copy number in population samples.

To determine the average Tn916 copy number of the population, we used the assembly visualization software Tablet (Milne, et al. 2010) and compared the average sequencing coverage across the ancestral position of the transposon (NZ_GG739778, positions 130,400-155,400) to the average sequencing coverage across a region of the chromosome outside of the transposon (NZ_GG739778, positions 52,500-77,500). This method was validated using sequencing data from individual clones with known Tn916 copy number. For example, one new junction corresponding to a new Tn916 insertion was identified in strain BTR87a. The described method indicated that BTR87a had two copies of Tn916, which is consistent with the strain having the original copy of Tn916 and an additional new copy.

2.7 Quantification of *tetM* gene expression and Tn916 copy number.

2.7.1 Isolation of total RNA and preparation of cDNA for quantification of *tetM* gene expression.

The *E. faecalis* strains (S613, BTR87b, and BTR22) were streaked onto agar plates with LBHI media and placed at 37°C for overnight growth. The following day I selected a single colony off of each plate and inoculated tubes containing 10 mL of LBHI broth. After 24 hours of growth at 37°C I diluted the cultures 100-fold into media supplemented with or without TGC (1 µg/mL TGC for the resistant strains, and 0.0625 µg/mL TGC for the susceptible S613 strain). The diluted cultures were then placed at 37°C until they reached exponential phase ($OD_{600} = 0.3$). Once the cultures reached the correct OD, I spun the cells down at 3,000 rpm for 15 minutes and discarded the supernatant. Three independent cultures for each strain and each test condition were prepared. I resuspended cell pellets in 300 µL of TE buffer. To lyse the cells, they were incubated with 5 µL of 5 U/mL mutanolysin and 12.5 µL of 200 mg/mL lysozyme at 37°C for 30 minutes. To extract total RNA from the lysed cells, I used the RNeasy Kit (Qiagen), and quantified the RNA concentration using a BioTek Synergy microplate reader. For overnight storage, we kept the total RNA in 2 mM EDTA at -80°C. DNA was eliminated from the total RNA using the DNA-free kit (Ambion) and RNA integrity was checked using a standard RNA formaldehyde denaturing gel. I identified intact ribosomal bands (23S and 16S) on the RNA gel. To synthesize cDNA from the total RNA, I used the Reverse Transcriptase Superscript III kit (Invitrogen). Next, a standard Taq PCR reaction was used to check cDNA integrity, and an RNase treatment was used to eliminate RNA.

2.7.2 Isolation of total DNA for quantification of Tn916 copy number.

The *E. faecalis* strains (S613, BTR87b, and BTR22) were grown on LBHI agar plates overnight and a single colony was picked to inoculated tubes containing 10 mL of LBHI broth media supplemented with or without TGC (1 µg/mL TGC for the resistant strains, and 0.0625 µg/mL TGC for the susceptible S613 strain). After overnight growth we used the UltraClean Microbial DNA Isolation Kit (MoBio) with an additional lysis step (as described in Section 2.7.1) to isolate DNA. Primers were designed to amplify the product spanning the new junction created when Tn916 is excised from the chromosome and forms a covalently closed circle. This primer design prevents chromosomal Tn916 from being amplified, so that only excised Tn916 is amplified.

2.7.3 Quantitative real-time PCR.

I setup 25 µL reactions using BR SYBR Green SuperMix (Quanta Biosciences), 200 ng of cDNA or 100 ng of total DNA, and a final primer concentration of 0.4 µM (**Table 2.2**). Reactions were run on a Bio-Rad C1000 Thermal Cycler CFX96 Real-Time System. Reaction protocol was run with an initial denaturation step of 3 min at 95°C, followed by 40 cycles at 95°C for 10s and 55°C for 30s. For quality control, I determined the melting curve for the product of every reaction on each plate. To identify the reaction efficiency of each primer set, S613 genomic DNA was serially diluted five times by a factor of ten and used with each primer set to generate calibration curves. We used the housekeeping gene glutamate dehydrogenase (*gdh*) as a reference gene. Relative gene expression was determined using the Pfaffl method (Pfaffl 2001). Circularized Tn916 copy number was calculated using methods established by Skulj, *et al.* (Skulj, et al. 2008). Error bars represent the 95% confidence interval between three biological samples.

Table 2.2: Primers used for qPCR.

Primer Name	Sequence (5' – 3')
gdh-F	AGCCAAGCAAGAACAGAAAGC
gdh-R	ATTGCGACATTCCCACTACC
tetM-F	TGGGCTTCCATTGGTTATC
tetM-R	AGCAAGCATCCGAAAATCTG
Int-Tn916-F	CAAAATCTAAATCTGGAAGTGTCAA
Int-Tn916-R	CAAGATGATTGTGTTCGGAAGA
Circular-Tn916-F	TGCTCGAAGCCCTTAGAATAA
Circular-Tn916-R	AAATTGAGTGGTTTGACCTTGA

2.8 Conjugation assays.

Overnight cultures of *E. faecalis* donor strains (S613, BTR87a, and BTR22) and the OG1RF recipient strain were diluted 1:10 in Brain Heart Infusion (BHI) and grown for 1h at 37°C. Subsequently, the donor and recipient strains were mixed in a ratio of 1:10 and 10 µL of this mating mixture was spotted on nitrocellulose filters placed on BHI plates for overnight mating at 37°C. Filters were resuspended in 1 mL BHI and the mating mix was serially diluted on BHI plates selective for donors (tetracycline, 10 µg/mL) or transconjugants (rifampicin, 200 µg/mL; fusidic acid, 25 µg/mL; tetracycline, 10 µg/mL). The plasmid transfer frequencies were calculated as the number of transconjugants per donor cell (Chen, et al. 2008). The experiments were done in triplicate. The TGC MICs of the transconjugants were elevated (0.5 µg/mL) compared to the MIC of OG1RF (0.125 µg/mL).

2.9 Competitive Fitness Assay.

I measured the fitness cost of the evolved strains relative to the ancestor by growing them in direct competition (Lenski, et al. 1991). The two competitors were initially grown in LBHI broth separately overnight. The following day, equal volumes of S613 and a BTR strain were diluted together into broth and cultured overnight. In the mixed culture, the initial (time = 0) and final (time = 1 day) cell densities of S613 and the BTR strain were determined by measuring colony-forming units. The plates were replicated onto agar supplemented with TGC to determine the cell density of the BTR strain. The relative fitness (W_{ij}) was then calculated following Lenski (Lenski, et al. 1991). Data was plotted as $W_{ij} - 1$ and the error bars display the 95% confidence interval (**Figure 6.3**). To determine if deletions upstream of *tetM* confer a significant fitness cost, Dr. Gerda Sacher, a faculty fellow in our lab, performed a contrast analysis using JMP Pro, which indicated a significant difference in fitness between BTR0 and the four strains with deletions upstream of *tetM* (BTR22, BTR125, BTR87a, and BTR87b: Planned comparison between $F_{1,27} = 31.2$, $p < 0.0001$). At least four replicate assays were preformed with each strain.

2.10 Measurement of spontaneous mutation rate of S613.

We determined the rate at which S613 spontaneously becomes resistant to the antibiotic DAP. First, a single colony was used to inoculate 5 mL of LBHI broth. After 24 hours of growth, the OD at 600 nm of the culture was measured and 10^8 cells were plated onto 2.0 $\mu\text{g}/\text{mL}$ DAP (S613 DAP MIC = 0.25 $\mu\text{g}/\text{mL}$). Also, dilutions of the culture were plated onto non-selective media. After 48 hours of incubation at 37°C, the colony forming units (CFUs) were determined for the cells plated onto non-selective media and the cells

plated onto media supplemented with 2.0 µg/mL DAP. The number of generations were calculated as binary divisions: Generations = $\log_2(\text{CFUs on non-selective media})$. Then the per genome per generation mutation rates were estimated: Mutation rate = (CFUs on DAP media) / [(CFUs on non-selective media) x (Generations)]. Six replicate assays were performed.

2.11 Long-range PCR.

The Qiagen LongRange PCR Kit was used to amplify an approximately 8 Kb region of DNA. Reactions were setup in 25 µL volumes following the manufacturer's recommendations: 2.5 µL of 10x LongRange PCR Buffer with Mg²⁺, 500 µM of each dNTP, 0.4 µM forward primer, 0.4 µM reverse primer, 0.2 µL LongRange PCR Enzyme Mix, 0.25 µL template DNA, and 18.8 µL of DNase-free water. Reaction thermocycler protocol was run with an initial denaturation step of 3 min at 93°C, followed by 35 cycles at 93°C for 15s, 56°C for 30s, 68°C for 8 min 12s. Primers used are listed in Table 2.3.

Table 2.3: Primers used for long-range PCR.

Primer Name	Sequence (5' – 3')
Tn916-internal	TTGTGATTGCCCTTGTGGTA
Tn916-ancestral_site ^a	GCCAGCAACTGTCTCATTCA
Tn916-yycl ^a	CGGGAAGGTCAACAAAGAAGA
Tn916-O-antigen ligase ^a	TCTTTCCCCTCAACATCTGG
Tn916-intergenic_site_J ^a	ACGGTGTTGCCACTCGTAT

^aPrimer was used with the Tn916-internal primer.

2.12 Creation of Fisher-Muller diagrams outlining models for the role of conjugation during adaptation to TGC resistance.

The shapes and thicknesses of the different genotypes in the Fisher-Muller plots were initially generated using a MatLab program that was generously given to us by Dr. Katya Kosheleva and Dr. Vaughn Cooper. To visually depict the role of conjugation Dr. Vinit Murthy, a professional illustrator (vinit.murthy@the1000words.com), was hired to create the final image (**Figure 6.6**). I came to the conclusion that conjugation played a role in the adaptation of my bioreactor populations using evidence from three different experiments, which are each outlined in the following three subsections. Additionally, these conclusions are discussed further in Chapter 6 Section 6.3.3.

2.12.1 Copies of Tn916 located at the ancestral site lack deletions, while copies of Tn916 at newly acquired sites carry deletions upstream of *tetM*.

First, in my bioreactor end-point strains I determined if the ancestral Tn916 sites were wildtype or if they contained any of the adaptive deletions we identified upstream of *tetM*. Since Next Gen sequencing produces short reads (~100-bp) I could not directly determine the linkages between the deletions and the specific Tn916 insertion site from this data. Therefore I used long range PCR to amplify the ~8 kb of DNA that spans from upstream of *tetM* to the chromosome surrounding a particular insertion site. I then used Sanger sequencing of the region upstream of *tetM* to determine if a deletion was present at that specific site. I found that all strains with multiple insertion sites had the wildtype sequence present at the ancestral site. For three strains (BTR87a, BTR87b, and BTR125a) their secondary insertion sites were confirmed to carry their respective deletions. If the deletions were strictly passed to the different strains through clonal inheritance, than the deletions would most likely have occurred in a copy of Tn916 at the

same insertion site or the ancestral site. Since the 87-bp deletion from Run 1 and the 125-bp deletion from Run 2 were found in distinct genomic locations in different strains from the same run this is more consistent with conjugal-transfer than clonal inheritance.

2.12.2 Identical deletions were identified in different strains despite the fact that deletions of different sizes and locations can confer resistance.

Next, I observed that uniquely sized deletions (22, 37, and 87 from Run 1 and 125-bp from Run 2) were identified in the different replicate runs and that all of these deletions were able to confer resistance. Since the identified deletions were different sizes and occurred in different positions, this indicates that there are several different ways to delete the DNA upstream of *tetM* to achieve resistance. Thus, it is unlikely that an identical deletion of the same size and location occurred *de novo* in different strains from the same run. Rather it is more likely that the mutation first occurred in one strain and then conjugated to a different strain. Thus, these findings are also more consistent with the conclusion that conjugation contributed to the spread of deletions upstream of *tetM* during adaptation to TGC.

2.12.3 The spontaneous mutation rate of S613 is vastly lower than the conjugation of rate of the BTR87a and BTR22 strains.

Finally, I also measured the spontaneous mutation rate of S613 to DAP resistance (5.1×10^{-9} mutations per cell per generation) and found that it was almost 300,000-fold lower than the observed conjugation frequency for BTR87a (1.5×10^{-3} transconjugants per donor cell). Since conjugation of the deletions upstream of *tetM* occurs at a much higher rate than *de novo* mutations, the deletions likely spread to different strains through conjugation rather than independent mutation events.

2.13 Serial transfer adaptation of *Enterococcus faecium*, *Staphylococcus aureus*, *Acinetobacter baumannii* and *Escherichia coli* to tigecycline.

For each strain seven to eleven replicate populations were adapted in parallel to increasing TGC concentrations. At the start of each experiment an individual colony was used to inoculate 10 mL of broth without TGC. After overnight growth, 10 µL of culture was transferred to 10 mL of broth supplemented with a sub-inhibitory concentration of antibiotic (typically 0.5xMIC). To determine the next increase in TGC concentration, 10 µL of the culture was tested for growth against two higher concentrations of TGC (typically 1.25 and 1.5 times the current [TGC]). If the growth at the higher concentration was absent or poor, the populations were transferred to either the current or only 1.25 times the current concentration. Once a specific population achieved growth at a concentration of TGC at least five-fold higher than the starting MIC of the strain, eight colonies were selected from each population and colony PCR was used to amplify *rpsJ* (**Table 2.4**). The PCR product was treated with ExoSap-IT (Affymetrix, USA) and the samples were sequenced by the Sanger method.

Table 2.4: Primers used for *rpsJ* colony PCR and Sanger sequencing.

Primer Name	Sequence (5' – 3')
<i>E. faecium</i> -F	CGTCGGCTAAGAAACGAGAG
<i>E. faecium</i> -R	TAGCCATCCGTTCCATTGT
<i>S. aureus</i> -F	CATTCACCACCGTTCTTATGAC
<i>S. aureus</i> -R	GATTGCGTTGTATCCATCAACTT
<i>A. baumannii</i> -F	GGTTTTCAATTCATCCAGAAATGACAC
<i>A. baumannii</i> -R	CCAACGTTAACACCACCTTGG
<i>E. coli</i> -F	TCTGTGAAGATACTGGGTACATACC
<i>E. coli</i> -R	CAATCGGGAGCTACGTAAGA

2.14 Measuring the growth rate of S613 and BTR0.

The growth curves of S613 and S613(S10^{R53Q-Δ54-57ATHK}) (also referred to as BTR0) at five different concentrations of TGC were evaluated (0, 0.0313, 0.063, 0.125 and 0.25 µg/mL TGC). Triplicate cultures of both strains at each drug concentration were measured in parallel. 100 µL of stationary phase culture was added to 5 mL of LBHI broth and TGC. Cultures were then placed on a shaker at 225 rpm and 37°C. The ODs of the cultures was checked every thirty minutes for twelve hours using a DEN-1 McFarland Densitometer (Grant-Bio). The average of three replicates was plotted with the standard deviation as the error bars (**Figure 7.3**).

2.15 Measuring the affinity of *tetM* leader RNA for tetracycline.

2.15.1 Template DNA for T7 RNA polymerase *in vitro* transcription.

A gene block ordered from Integrated DNA Technologies was used as template DNA for the T7 *in vitro* transcription assays. The sequences of the gene block consisted of the T7 polymerase promoter sequence (5'-TAATACGACTCACTATAGG) followed by two GG, to improve T7 transcription efficiency, and the wildtype sequence for the 5' untranslated region (5' UTR) of *tetM*. Restriction sites were included upstream of the T7 promoter (BamHI) and immediately downstream of the sequence for the 5' UTR of *tetM* (XbaI). The complete gene block sequence from 5' to 3' was:

```

AATCACTAGGATCCCATTCA
ACCGTTCTTATGACTAATACGACTCACTATAGGGATCTATTAAAAGGAGTTAAATAA
TATGCGGCAAGGTATTCTAAATAACTGTCAATTGATAGTGGAACAAATAATTG
GATGTCCTTTTAGGAGGGCTTAGTTTTGTACCCAGTTAAGAACACCTTATCA
TGTGATTCTAAAGTATCCAGAGAATATCTGTATGCTTGTATACCTATGGTTATGCAT
AAAAATCCCGGTGATAAAAGTATTACTGGGATTTATGCCCTTGTTGGTTTT

```

GAATGGAGGAAAATCACTCTAGAGCCAAGTTGATGGATAACGCAATCTG. Once the gene block was received the DNA was resuspended in 50 µL of water, and amplified using a standard Phusion PCR reaction. Phusion reactions were setup in 50 µL volumes: 10 µL of 5x Phusion Buffer, 1 µL of 10 mM dNTPs, 2.5 µL forward primer (5'-GTGATTTCCATTCAAAAAACC), 2.5 µL reverse primer (5'-CATTCAACCACCGTTCTTATGAC), 1 µL template DNA (gene block), 0.5 µL Phusion polymerase, and 32.5 µL of DNase-free water. The reaction thermocycler protocol was run with an initial denaturation step of 30s at 98°C, followed by 25 cycles at 98°C for 10s, and 61°C for 30s, and with a final step of 72°C for 5 min. The complete PCR product was then run on a standard 0.8% agarose gel for 45 min at 100V. To separate the amplified DNA product from the gene block template DNA, the amplified DNA of about 298 bp in size was extracted and purified from the gel using the Zymoclean Gel DNA Recovery Kit. The extracted Phusion PCR product was subsequently further amplified using a Taq PCR. Taq reactions were setup in 50 µL volumes as recommended by the manufacturer: 5 µL of 10x Standard Taq Buffer, 4 µL of 2.5 mM dNTPs, 1 µL forward primer (5'- GTGATTTCCATTCAAAA ACC), 1 µL reverse primer (5'-CATTCAACCACCGTTCTTATGAC), 1 µL template DNA, 0.25 µL Taq polymerase, and 37.75 µL of DNase-free water. The thermocycler protocol was run with an initial denaturation step of 30s at 95°C, followed by 30 cycles at 95°C for 15s, 55°C for 30s, 68°C for 30s and a final extension step of 72°C for 5 min. The Taq PCRs were then directly used as template DNA for the T7 *in vitro* transcription reactions without further purification.

2.15.2 Incorporation of template DNA into pUC19.

To produce larger quantities of template DNA for T7 *in vitro* transcription, the synthetic gene block (described in Section 2.15.1) was integrated into an empty pUC19 vector. Double digestions were performed on the gene block and pUC19 in 25 µL volumes using

2.5 μ L of NEB cutsmart buffer, 0.5 μ L of XbaI, 0.5 μ L of BamHI, and 20 ng/ μ L of either gene block DNA or uncut pCU19. The digestions were incubated at 37°C for one hour.

Next the digested DNA was cleaned using the Zymo DNA Clean and Concentrator kit. A 20 μ L ligation reaction was setup using 50 ng of digested pUC19, 16.67 ng of digested gene block insert, 1 μ L NEB T4 ligase, and 2 μ L of 10x T4 ligase buffer. The ligation reaction was incubated at room temperature for one hour. The ligation was then transformed into Subcloning Efficiency DH5 α competent *E. coli*. Briefly, 3 μ L of ligation was mixed with 50 μ L of competent cells and the mixture was incubated on ice for 30 minutes. The cells were then submerged into a 42°C water bath for 20s and subsequently placed onto ice for 2 minutes. Next, 950 μ L of Super Optimal Broth with Catabolite repression (SOC) was added to the cells and the mixture was placed on a shaker at 37°C and 225 rpm for one hour. Finally, 200 μ L of cells were plated onto LB agar supplemented with 100 μ g/mL ampicillin. The next day colonies were isolated from the plate, grown overnight in LB broth, and then plasmid DNA was isolated using a Zymo classic miniprep kit. The isolated plasmid DNA was Sanger sequenced to verify that the correct insert sequence was present.

2.15.3 T7 RNA polymerase *in vitro* transcription.

The T7 RNA polymerase *in vitro* transcription reactions were setup by Margaret Michnicka in the Dr. Edward Nikonowicz lab at Rice University as previously described (Davlieva, et al. 2014). The buffer conditions used for the T7 transcription reactions were 40 mM Tris, 25 mM MgCl₂, 4 mM DTT, 1 mM spermidine, and 0.1% triton at pH 8. The initial reaction volumes were 40 μ L with 4 mM rNTPs, 10 mM GMP, 5 μ L template DNA and 50 μ g/mL T7 RNA polymerase. After adding the reagents the reactions were briefly vortexed and centrifuged before being placed at 37°C for at least two hours. Later the transcription reactions were setup in larger 450 μ L volumes under the same conditions,

but using 50 µL of template DNA. The RNA was visualized on a 10% denaturing urea polyacrylamide gel or on a 1% bleach agarose gel (Aranda, et al. 2012). The RNA was then cleaned and concentrated using an Amicon 30K centrifugal concentrator as recommended by the manufacturer. The RNA was resuspended in a buffer containing 5 mM MgCl₂, 10 mM KCl, 10 mM KH₂PO₄ at pH 6.5.

2.15.4 Measuring the affinity of *tetM* leader RNA for tetracycline by detection of changes in fluorescence.

To get uniform folding the RNA was heated for one minute at 95°C and then immediately cooled on ice for five minutes. To determine if there is an interaction between tetracycline and the *tetM* leader RNA, samples of the tetracycline and RNA were prepared with a constant concentration of tetracycline, 2 µM, and increasing concentrations of RNA. The fluorescence of the tetracycline alone and in the presence of different RNA concentrations was measured on a Tecan Infinite M1000 microplate reader using an excitation wavelength of 420 nm, emission wavelength of 526 nm, excitation and emission bandwidth of 5nm, gain setting of 190, 50 number of flashes, flash frequency of 400 Hz, integration time of 20 µs, lag and settle time of 0 µs, and Z-position of 2000 µm. The data was plotted as the change in fluorescence, meaning the fluorescence of the tetracycline alone was subtracted from the fluorescence of the solutions with tetracycline and RNA together (**Figure 6.4**).

2.16 Tracking the movement and conjugation of Tn916 in mice gastrointestinal tract.

2.16.1 Animal care and treatment.

Female 6-week-old C57BL/6 mice were purchased from Charles River Laboratories and housed in facilities at Rice University. A total of twenty mice were purchased for four experimental control groups, each group consisting of five mice. After arriving, the mice were given one week to adjust to the facilities and then fed an inoculum of *E. faecalis* cells ($\sim 10^9$ CFUs) in their water once on experimental day 1. Two groups were fed *E. faecalis* S613 (wildtype Tn916) and two groups were fed *E. faecalis* BTR87a (TGC-resistant Tn916). Additionally, one of the S613 groups and one of the BTR87a groups were fed water supplemented with tetracycline daily to achieve a dosage of about 5 mg/kg. Fresh samples of feces from each group were collected every 24 hours for 15 days and stored at -80°C. Mice were euthanized by the administration of isoflurane gas anesthesia by tank induction until recumbent, followed by the administration of CO₂ until death. All work performed with animals was approved by Rice University's Institutional Animal Care and Use Committee (IACUC) under protocol 795406-2.

2.16.2 Determination of CFUs and isolation of bacterial DNA from mouse feces.

For the tested samples about 20 mg of frozen feces was weighed and suspended in 1 mL of 0.9% saline. Serial dilutions of the feces were plated onto four different types of agar: BHI, BHI supplemented with 16 µg/mL tetracycline, Blood and BEA. Plates were incubated at 37°C overnight and then CFUs were counted. To isolate bacterial DNA from the mouse feces, about 50 mg of frozen feces was weighed and immediately processed by the Qiagen QiAamp Stool Mini Kit following the manufacturer's recommendations.

Chapter 3: Bioreactor adaptation of *Enterococcus faecalis* S613 to tigecycline resistance.

Portions of this chapter are reproduced from Beabout, et al. 2015 *Mol Biol Evo*

3.1 Introduction.

As discussed in Chapter 1, quantitative experimental evolution, a pipeline developed by our lab, is a useful approach to studying antibiotic resistance and was successfully employed by Dr. Corwin Miller, a former graduate student in our lab, to identify clinically relevant mechanisms of resistance (Arias, et al. 2011; Miller, et al. 2013). Therefore, I decided to use quantitative experimental evolution to study TGC resistance in *E. faecalis* S613, a vancomycin-resistant hospital strain. The first step of this approach involved using a turbidostat bioreactor to adapt S613 to TGC resistance. Bacterial populations in a turbidostat are usually maintained at a constant cell density by continuously monitoring the culture with an OD probe. However, during Dr. Miller's bioreactor run he discovered that biofilm would buildup on the OD probe within 12 hours of starting his culture, which would render the optics on the probe useless, and therefore he was forced to take manual turbidity readings over the remaining course of his 24 day long experiment (Miller, et al. 2013). Populations growing in the bioreactor require 24 hour monitoring over the course of several continuous weeks and thus manual measurements, while capable of successfully maintaining the turbidity, are tedious and difficult to perform. Therefore, as an alternative approach, we hypothesized that the system could be partly automated by measuring the CO₂ production of the population, which is a proxy for the respiration and metabolism of the growing culture. A postdoctoral researcher in the lab,

Dr. Troy Hammerstrom, and myself worked together to setup and optimize a gas analyzer to assist us with maintaining populations at a constant turbidity in our bioreactor. Once we had optimized the setup, I performed two replicate bioreactor experiments, with the assistance of Dr. Hammerstrom, where *E. faecalis* S613 was adapted from growth at 0.05 µg/mL TGC to a final TGC concentration of 1 µg/mL over the course of 24 or 19 days.

3.2 Advantages of our bioreactor adaptation technique.

While technically very challenging, our semi-batch bioreactor setup provides several advantages over using more traditional techniques, such as serial transfers or chemostats. Unlike a chemostat, which maintains growth rates by limiting an essential nutrient, the population in our bioreactor is kept at its fastest growth rate by adjusting the in-flow of media in response to changes in cell density and respiration. Thus our bioreactor removes the selective pressure of nutrient limitation so that the population adapts mostly to the stress of the antibiotic. Additionally, this means a population would achieve more generations in our bioreactor than it would over the same timespan in a chemostat. This in turn provides more opportunities for successful alleles to rise in frequency over a comparably shorter timespan. Also, in a chemostat the addition of media is continuous, which could potentially bottleneck the population when growth is slowed by the stress of antibiotic. Since the in-flow of media into our bioreactor is dynamically changed in response to the turbidity of the culture, the possibility of bottlenecking the population is greatly reduced.

Unlike batch cultures, the population in our bioreactor does not enter stationary phase and thus a more consistent environment is maintained and experimental runs achieve a

higher number of generations over a relatively shorter timespan. The bioreactor also maintains a continuous culture at a controlled concentration of antibiotic so that the ratio of cells to drug is controlled. TGC is hydrolyzed more rapidly than many antibiotics further diminishing the utility of serial transfer approaches and thus strengthening the need for a continuous culture that supplies the population with fresh antibiotic (Bradford, et al. 2005; Petersen and Bradford 2005). While the technical challenges of this setup limit replication, there are several advantages that allow us to make robust predictions. By using large culture volumes (300 mL) and subinhibitory antibiotic concentrations, we were able to maintain genetically polymorphic populations allowing us to follow multiple adaptive trajectories within an individual population (Beabout, et al. 2015b; Counago, et al. 2006; Hammerstrom, et al. 2015; Miller, et al. 2013). In addition, we have observed similar trajectories across replicate populations indicating that mutations observed in our bioreactor can easily occur and are reasonably reproducible (Beabout, et al. 2015b; Hammerstrom, et al. 2015).

Furthermore, our bioreactor allows for and actually favors the persistence of very long-term biofilms, a trait shown to play an essential role in the pathogenicity of enterococci (**Figure 3.1**). By allowing biofilms to be established on the interior walls of the bioreactor during adaptation we can recapitulate some aspects of the clinical ecologies associated with the development of endocarditis or catheter colonization (Guiton, et al. 2010; Miller, et al. 2013). Overall, this means that the population has a more consistent, controllable and clinically relevant ecology. Thus, by maintaining genetically diverse populations and by comparing the evolutionary outcomes between at least two replicate experiments, using our approach we are able to make robust predictions about what mechanisms might be observed in the clinical setting.

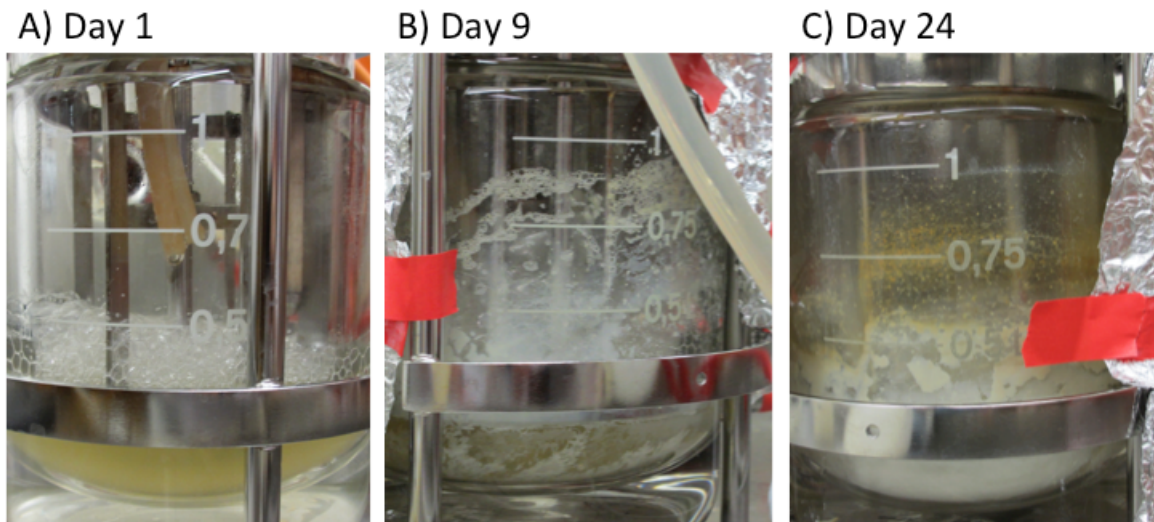


Figure 3.1: Buildup of biofilm on the interior walls of the bioreactor. Pictures of the bioreactor vessel on different days of an experimental run with *E. faecalis* S613. **A)** At the beginning of the experiment on day 1 the culture was turbid, but the vessel had no visible biofilm growing on the interior walls. **B)** Some biofilm began appearing on day 2 and by day 9, about midway through the run, patchy chunks of biofilm were visible on all of the glass and metal surfaces inside of the vessel. **C)** On the final day of adaptation, day 24, the interior walls and surfaces of the vessel were coated in thick layers of biofilm. The ability of biofilm to flourish in the bioreactor is partly due to the selection conditions of the culture: planktonic cells are disadvantaged since they are removed from the culture by the out flow pumps, while biofilm cells are able to persist in the vessel and escape the outflow pump by adhering to surfaces in the vessel. The accumulation of enterococci biofilm on surfaces in hospitals plays an important role in the pathogenicity of the organism (Mohamed and Huang 2007). Therefore the ability of our bioreactor to recapitulate this aspect of enterococci growth is advantageous. I could not sample biofilm during the course of the run, but I was able to collect biofilm samples on the final day of adaptation when the vessel was disassembled.

3.3 Serial transfer adaptation to minocycline and tigecycline.

Before initiating a bioreactor run, I performed preliminary serial transfer experiments in flasks to approximate what TGC concentrations and timeline would be used in the bioreactor. In separate experiments S613 populations were adapted to MIN-resistance and to TGC-resistance. MIN adaptation was preformed first because the drug is similar to TGC, but more affordable. *E. faecalis* are considered resistant to MIN if they have an MIC >16 µg/mL. Over the course of 11 days an S613 population was adapted to grow at 34 µg/mL MIN (**Figure 3.2A**). For TGC the FDA non-susceptibility cutoff is 0.25 µg/mL and the European Committee on Antimicrobial Susceptibility Testing (EUCAST) resistance cutoff is 0.5 µg/mL (Brink, et al. 2010). The starting TGC MIC of S613 was 0.125 µg/mL Over the course of 12 days an S613 population was adapted to growth at 3 µg/mL (**Figure 3.2B**). However, an Etest on the adapted population indicated that the final TGC MIC was 0.5 µg/mL, which indicates TGC resistance, but is less resistant than would be expected considering the final population was growing at 3 µg/mL TGC. Upon further investigation I determined that one possible cause for this discrepancy was the use of oxygenated media for the flask adaptation experiment. Petersen and Bradford showed that when TGC MIC testing was performed in broth media saturated with dissolved oxygen it was two or more dilutions higher than TGC MIC testing performed in broth media supplemented with Oxyrase, an oxygen-reducing catalyst (Petersen and Bradford 2005). This indicates that TGC is susceptible to oxidative degradation and therefore it is imperative to use freshly autoclaved media, which is deoxygenated, when working with TGC. Thus the effective concentration of TGC in my final flask adapted populations was likely lower than 3 µg/mL due to degradation. For following experiments, whenever cells were cultured with TGC I always used freshly autoclaved media or media that had been stored at -80°C to prevent oxygenation.

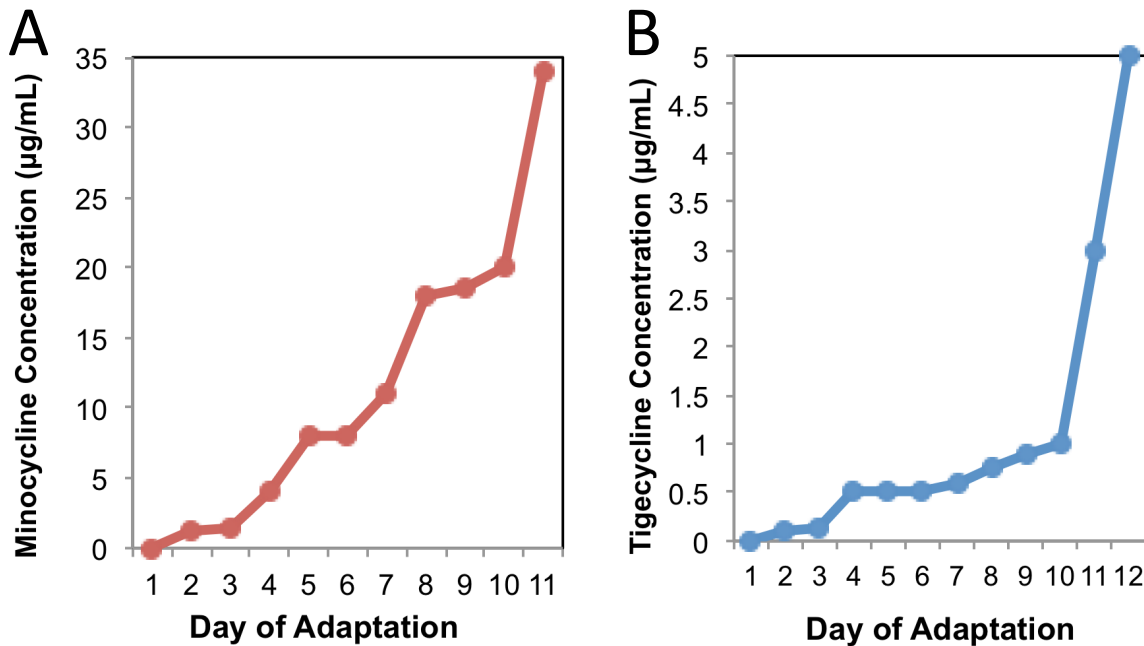


Figure 3.2: Batch culture adaptation of *E. faecalis* S613 to minocycline and TGC.

Preliminary flask adaptation experiments were performed to estimate the drug concentrations and timeline to be used in the bioreactor. **A)** First, a population of S613 was adapted to MIN because of the drugs similarity to TGC. Over the course of 11 days S613 was adapted from growth at 1.25 $\mu\text{g}/\text{mL}$ MIN to growth at a final concentration of 34 $\mu\text{g}/\text{mL}$ MIN. **B)** Next, to get a better estimate of the timeline to be used in the bioreactor, a population of S613 was adapted to growth in increasing concentrations of TGC. The population was adapted from growth at 0.1 $\mu\text{g}/\text{mL}$ TGC to growth at an apparent final concentration of 3 $\mu\text{g}/\text{mL}$ TGC. However, the final flask adapted population had an MIC of only 0.5 $\mu\text{g}/\text{mL}$ TGC. I speculate that the use of oxygenated media during the flask adaptation experiment led to the degradation of TGC, which in turn reduced the selective pressure of the antibiotic during adaptation and resulted in a population that was less resistant than expected. For future experiments I always used deoxygenated media when working with TGC.

3.4 Growth phase and %CO₂ of S613 in the bioreactor.

I performed a preliminary bioreactor run with S613 to determine the relationship between the %CO₂ of the population and the growth phase of S613. A Tandem Pro Gas Analyzer from Magellan Instruments was used to monitor %CO₂ in the exhaust gas from the bioreactor and samples taken from the media outflow were used to measure the turbidity of the population in McFarland (MF) units. For this run I inoculated 300 mL of LBHI broth in the bioreactor the prior evening and left the population to enter stationary phase. The next day I reduced the turbidity by flushing out most of the culture with fresh media. Once the population was at a low turbidity (0.3 MF) I turned off all pumps to stop the inflow of fresh media and began recording the %CO₂ and turbidity of the culture every 30 minutes. For the first hour the turbidity and %CO₂ increased rapidly as the population entered exponential growth phase (**Figure 3.3**). After 1.5 hours the population entered stationary phase when the turbidity reached 4.9 MF (**Figure 3.3**). At the same time the %CO₂ decreased from 0.41% at one hour to 0.34% at 1.5 hours (**Figure 3.3**). As the population remained in stationary phase the %CO₂ continued to decline until it plateaued after 2.5 hours in the range of 0.15-0.20% CO₂ (**Figure 3.3**). This preliminary run shows that as the cell density of the S613 population increases during exponential growth phase, the amount of respiration in the culture also increases, which subsequently results in the release of more and more CO₂. Once the population reaches stationary phase the growth and respiration of the cells decreases, which results in a decline in the release of CO₂. These results also indicate that the %CO₂ of the population needs to be below 0.25-0.30% and that the turbidity of the population needs to be below 4 MF to maintain the culture in exponential growth phase. Additionally, to achieve the fastest growth rate the population should be maintained between about 1-2 MF, which corresponds to early exponential phase.

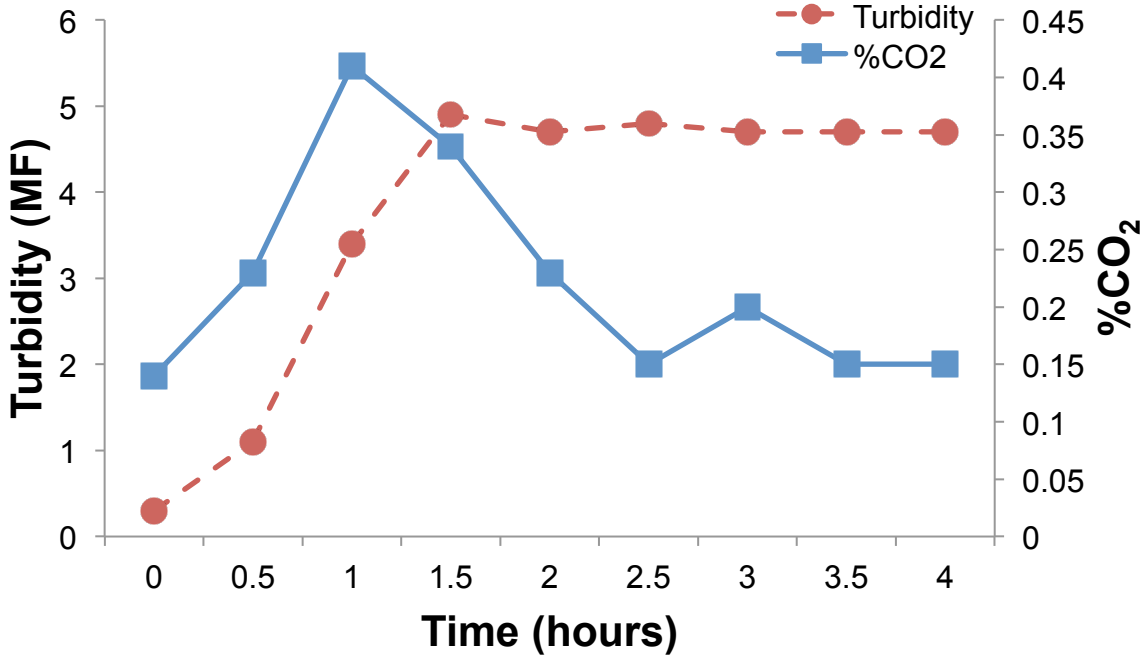


Figure 3.3: Relationship between %CO₂ and the growth phase of S613. A preliminary bioreactor run was performed to determine the relationship between the growth phase of an S613 population and the %CO₂ released into the bioreactor exhaust. The goal was to determine if measuring %CO₂ could be used to estimate the growth phase of S613. Every 30 minutes the turbidity of the bioreactor population was manually measured in McFarland units and the exhaust %CO₂ was recorded. During the first hour as the turbidity of the population increased, the %CO₂ also increased. After 1.5 hours the population entered stationary phase and at the same time the %CO₂ decreased, indicating that the respiration in the population had slowed. Combined, these results indicate that measuring the CO₂ output of the bioreactor can be used to gauge the growth phase of a population of S613 and thus potentially used to help maintain the population at a constant turbidity.

3.5 Using %CO₂ to maintain S613 in exponential growth.

I did another preliminary bioreactor run to test the idea of using CO₂ production and a control loop operated by Sartorius MFCS software to maintain a population of S613 cells in exponential growth phase. I diluted a 300 mL overnight culture in the bioreactor with fresh media to reduce the turbidity to about 0.8 MF. I then measured the %CO₂ and turbidity of the population every 30 min for 7.5 hours (**Figure 3.4**). There were two peristaltic pumps that brought media into the bioreactor vessel. To ensure that the population was continuously supplied with a low level of fresh nutrients, I set one of the media in flow pumps, referred to as 'SUBB', to constantly pump in media at a low flow rate of 10%. After the population grew for 30 min with only the SUBB pump on, I then initiated a control loop to operate the second media in flow pump, which is referred to as 'SUBA' (**Figure 3.4**). The control loop was set to turn the SUBA pump on at 40% in flow rate when the %CO₂ of the population increased passed a setpoint of 0.29% (**Figure 3.4**). About 3 hours into the experiment, when the turbidity rose above 1.9 MF, the %CO₂ also rose above the 0.29% setpoint, which subsequently turned the SUBA pump on and supplied the culture with a high in flow of media (**Figure 3.4**). SUBA was on for about 2 hours until the %CO₂ dropped below the setpoint again, during which the turbidity of the population dropped to 1.2 MF (**Figure 3.4**). When SUBA turned off the turbidity increased back to 1.9 MF and a cycle of SUBA turning on and off began (**Figure 3.4**). During the course of the 7.5-hour run the population was maintained at a turbidity ranging from 1.2-1.9 MF, demonstrating the ability of this setup to maintain S613 in growth phase (**Figure 3.4**). This preliminary run also demonstrated that S613 uses about 0.5 L of LBHI per hour when maintained in early exponential growth phase. I ran several more preliminary runs to optimize the control loop and setpoint conditions.

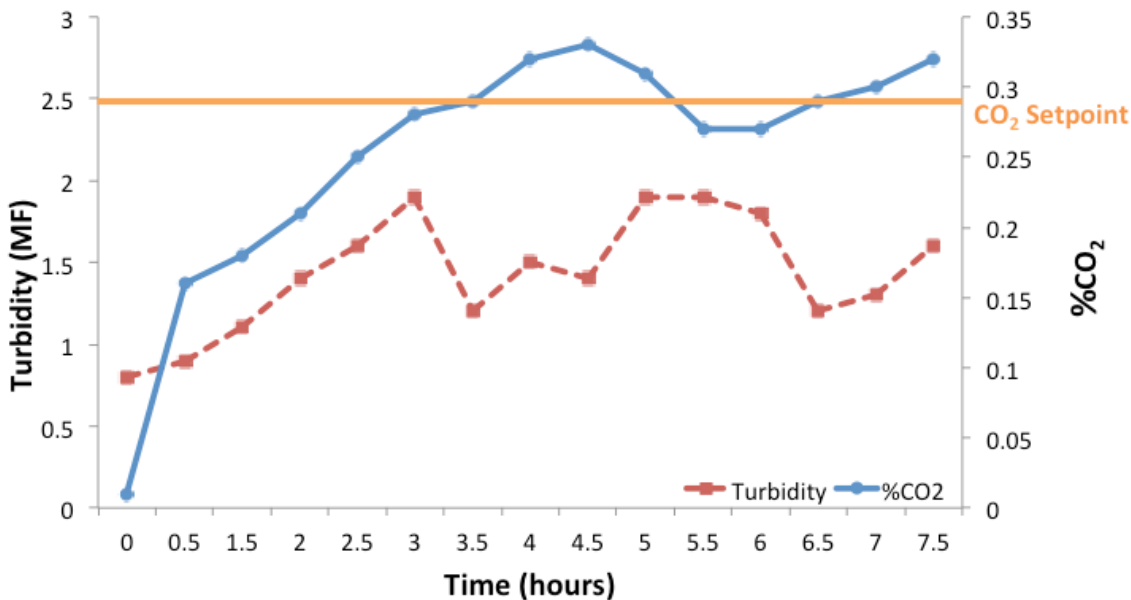


Figure 3.4: Use of a control loop and %CO₂ to maintain a population of S613 in growth phase. Preliminary bioreactor runs were performed to test and optimize the use of a control loop to regulate the in flow of media into the bioreactor and maintain the population at a constant turbidity. The turbidity, in McFarland units, and %CO₂ of a population of S613 cells was monitored in the bioreactor for several hours. After 30 minutes a control loop run by Sartorius MFCS software was initiated to turn on a peristaltic in flow pump when the %CO₂ surpassed a selected setpoint. For this preliminary run a CO₂ setpoint of 0.29% was used (orange). After 3 hours the %CO₂ surpassed the setpoint, which subsequently turned the in flow pump on at a high rate to dilute the population and supply the cells with fresh nutrients. Over the course of seven hours the control loop successfully maintained the population at a turbidity ranging from 1.2-1.9 MF, which corresponds to the turbidity of early exponential growth phase for S613. This preliminary run demonstrates the utility of the %CO₂ and a control loop to help maintain a population of S613 cells at a constant turbidity.

3.6 Bioreactor adaptation of S613 to tigecycline.

Next I performed two replicate bioreactor runs, with the assistance of Dr. Hammerstrom, where S613 was adapted to increasing TGC concentrations in stepwise intervals. During these runs the populations were adapted from 0.05 µg/mL (half the MIC against S613) to a final concentration of 1 µg/mL TGC, well surpassing the EUCAST resistance cutoff of 0.5 µg/mL. Interestingly, during these longer runs the %CO₂ output compared to the turbidity would increase periodically. We attributed this phenomenon to biofilm buildup, as biofilm would produce and release CO₂, but would not increase the planktonic turbidity. Since our goal was to keep the planktonic cells at a constant density, when the %CO₂ rose independently of the turbidity, we would increase the CO₂ setpoint in response to avoid over diluting the planktonic population. During the first bioreactor experiment, referred to as ‘Run 1’, the S613 population was adapted to growth at 1 µg/mL TGC over the course of 24 days (**Figure 3.5A**). At the end of Run 1 the TGC MIC against the adapted population was 1.5 µg/mL TGC, as determined by Etest, and 2.0 µg/mL TGC, as determined by agar dilution. During the course of Run 1 the population used a total of about 420 L of LBHI media (**Figure 3.5A**). To determine the reproducibility of the evolutionary dynamics observed in my initial turbidostat run, I performed a second replicate run, referred to as ‘Run 2’, using the same setup as Run 1. For this replicate bioreactor run a population of S613 cells was adapted to growth at 1 µg/mL TGC over the course of 18.5 days (**Figure 3.5B**). The final TGC MIC of the Run 2 population was 2 µg/mL TGC as determined by agar dilutions. During the course of Run 2 the population used a total of about 287.5 L of LBHI media (**Figure 3.5B**). During both experimental runs the usage of LBHI media per day remained relatively consistent, at about 0.5 L per hour, since the growth rate and cell density of the populations were maintained at fairly constant values throughout adaptation (**Figure 3.5**).

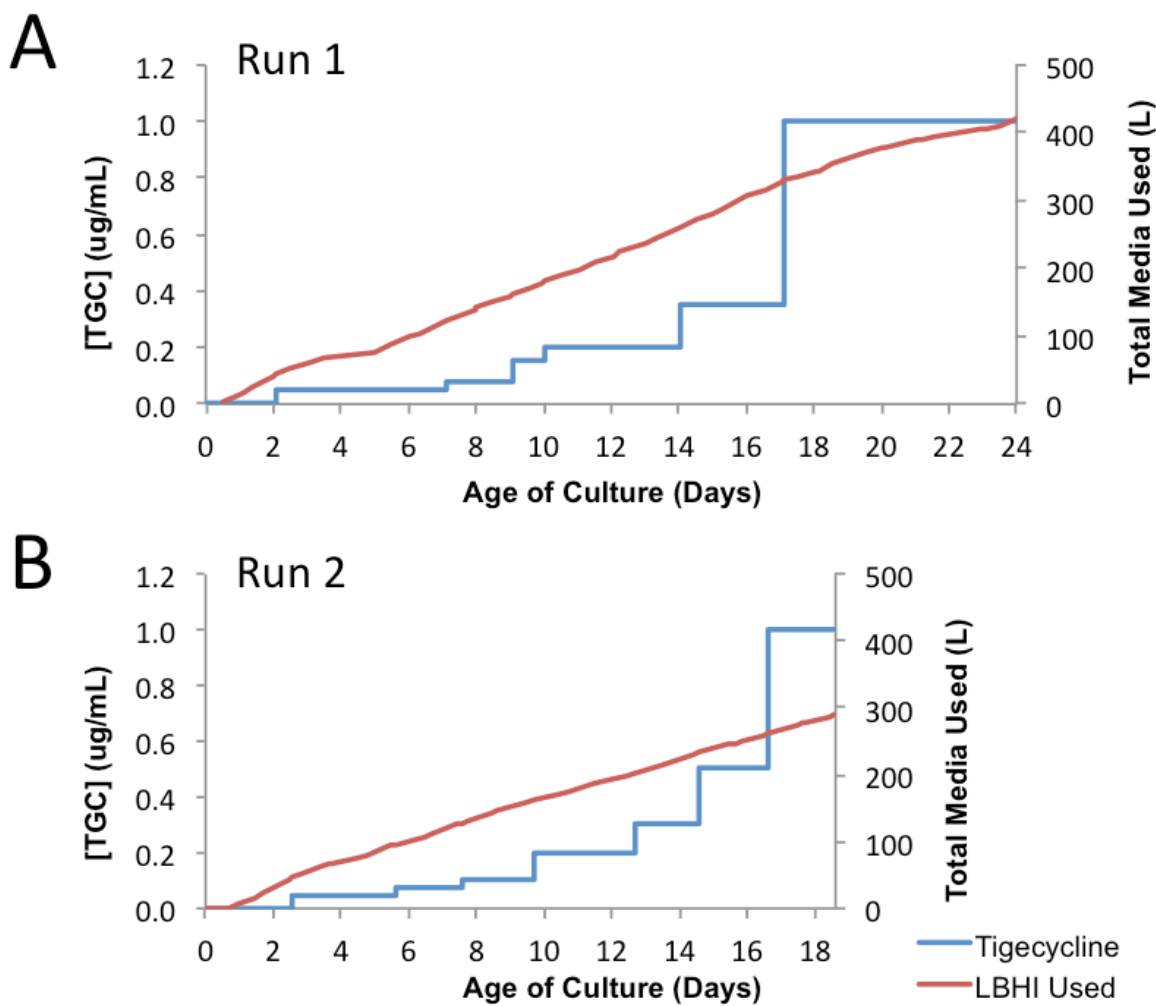


Figure 3.5: The concentrations of TGC and total LBHI media used over the course of two replicate bioreactor runs where S613 populations were adapted to TGC resistance. Two bioreactor runs were performed to adapt populations of S613 from a starting concentration of 0.05 µg/mL TGC to growth at a final concentration of 1 µg/mL TGC. **A)** The first bioreactor run lasted for 24 days (576.5 hours) and **B)** the second bioreactor run latest for 19 days (445.6 hours). By day 14 of both runs the populations were over the FDA non-susceptibility cutoff of 0.25 µg/mL TGC and by day 18 of both runs the populations were over the EUCAST resistance cutoff of 0.5 µg/mL TGC. Both populations had final TGC MICs of 2 µg/mL as determine by agar dilution, indicating that

the populations had reached resistance to TGC. During both runs the TGC concentration was not increased until the population could maintain its current growth rate at the elevated concentration. To accomplish this, samples were collected from the bioreactor and grown in tubes with either the TGC concentration currently in the bioreactor vessel or several higher concentrations of TGC. The growth rates of the samples in the tubes were monitored and once the growth rate of a sample at an elevated TGC concentration was the same as the growth rate of a sample at the TGC concentration currently in the bioreactor, then the population in the bioreactor would be exposed to the higher concentration of TGC. By increasing the TGC concentration in this relatively modest fashion a polymorphic population was maintained. As a result of this selection regime the use of LBHI media remained fairly consistent during the course of both adaptation experiments (about 0.5 L per hour) and thus the slope of the total media used (red) remained fairly linear and consistent during the course of both experiments.

3.7 Discussion.

The interference of biofilm is a common problem encountered when maintaining a turbidostat or continuous culture. Several different approaches have been used by other groups to circumvent biofilm in bioreactors, including switching vessels periodically, adding antibiofilm agents, or using genetically modified strains that are deficient in biofilm formation (Matteau, et al. 2015; Takahashi 2015; Toprak, et al. 2012; Toprak, et al. 2013). Here we demonstrate the utility of using respiration, as determined by measuring CO₂ output, to maintain a bioreactor population. This approach allows us to embrace the growth of biofilm, which is an important virulence trait for many pathogens, while still maintaining a continuous culture at its fastest growth rate. Importantly, in our system we can study any culturable pathogen, including those that produce biofilm and cannot be genetically modified. Additionally, our bioreactor can be run without having to add antibiofilm agents, which complicate the environment of an adaptation experiment, or without periodically having to transfer the culture to new vessels, which is inconvenient and can lead to contamination. In addition to studying S613, we have also successfully used this approach to study TGC resistance in the Gram-negative pathogen *Acinetobacter baumannii* and are currently using this approach to study additional pathogens and antibiotics (Hammerstrom, et al. 2015).

Despite the high efficacy of TGC against *Enterococcus* species, we were able to repeatedly adapt *E. faecalis* S613 to growth in TGC concentrations above the EUCAST resistance cutoff of 0.5 µg/mL TGC using both batch culture and bioreactor adaptation experiments. The ability of *E. faecalis* S613 to adapt rapidly to TGC is consistent with observations of the species ability to adapt to a wide variety of other antibiotics, including ampicillin, vancomycin, DAP and linezolid (Arias and Murray 2009; Arias and Murray

2012; Lins, et al. 2013; Miller, et al. 2013; Rincon, et al. 2014). The high adaptability of pathogens, such as S613, highlights the need to understand how bacteria evolve to the selective pressures of antibiotics.

Chapter 4: Phenotypic characterization of bioreactor end-point adapted populations.

4.1 Introduction.

High concentrations of antibiotic exert strong selective pressures, as bacteria must adapt quickly or perish. Therefore, inhibitory concentrations of antibiotic tend to select for mutations that quickly confer a high degree of resistance. In comparison, lower subinhibitory concentrations of antibiotic confer relatively weaker selective pressures, as cells can continue to grow, albeit at slower rates. Therefore subinhibitory concentrations typically select for bacteria that acquire multiple successive alleles, each mutation conferring a relatively modest level of resistance (Andersson and Hughes 2014). Since alleles conferring modest fitness advantages are slow to outcompete other alleles, this type of weak selection can lead to clonal interference and the persistence of genetic diversity within the population (Lockton, et al. 2008; Sacher, et al. 2014). These dynamics are especially true when bacteria are exposed to bacteriostatic antibiotics, such as tetracycline and TGC, which stall the growth of bacterial cells, but do not directly kill the cells. Therefore, when our lab adapts populations in our bioreactor we reduce the selective pressure of the antibiotic by using subinhibitory concentrations with the goal of maintaining a highly polymorphic population. Since bioreactor runs are technically challenging, it is imperative to identify as many adaptive alleles as possible from each individual run. Additionally, heterogeneity is sometimes observed in clinical infections and is associated with poor outcomes for patients undergoing treatment (Casapao, et al. 2013). Therefore recapitulating these population dynamics in our bioreactor potentially

provides more clinically relevant adaptive trajectories. Importantly, Dr. Corwin Miller previously demonstrated the ability of our bioreactor to maintain genetically diverse populations when using subinhibitory concentrations of antibiotic (Miller, et al. 2013). Therefore, as discussed in Chapter 3, I used subinhibitory concentrations to adapt *E. faecalis* S613 to TGC resistance in our bioreactors. Then to identify the range of genotypes present in the adapted end-point populations, rather than randomly selecting colonies for whole genome sequencing, I performed phenotypic assays, such as MICs, to get at the underlying genetic diversity within the population and increase my chances of sequencing genetically diverse clones. I began with the Run 1 end-point adapted population. First I plated samples of the planktonic and biofilm populations taken from the last day of the Run 1 onto non-selective agar. To survey these end-point populations, I randomly picked a total of 94 colonies, 84 planktonic clones and 10 biofilm clones. I then performed phenotypic assays on these selected colonies to get at their undelying gentic diversity.

4.2 Phenotypic characterization of Run 1 bioreactor isolates.

4.2.1 High-throughput MIC testing on agar.

The Run 1 end-point population had a TGC MIC of 2 µg/mL; however, I reasoned that individual clones within the population would likely have more diverse MICs. Therefore, the first phenotypic assay I performed was to determine the TGC MIC against each of the 94 individual isolates from the end of Run 1 using a simplified version of the agar dilution technique (Chapter 2 Section 2.4.1). Agar plates supplemented with 0, 0.25, 0.5, 0.75, 1, 1.25, 1.5, 1.75 and 2 µg/mL TGC were used. Four replicates of this assay were performed and the average of the replicates was taken (**Figure 4.1**). Indeed, variations

in the MICs of the different isolates were observed, highlighting the diversity present within the population (**Figure 4.1**). Many of the adapted clones had a TGC MIC near 2 µg/mL TGC, similar to the population, however some isolates had lower MICs, such as planktonic 74 and biofilm 08. Planktonic 53 and 57 had the lowest MICs, which were below 1 µg/mL TGC. To simplify the data the clones were categorized into three groups based on their MICs: High (MIC > 1.5 µg/mL), Medium (1.5 µg/mL ≥ MIC > 1.0 µg/mL) and Low (1.0 µg/mL ≥ MIC) (**Figure 4.1**).

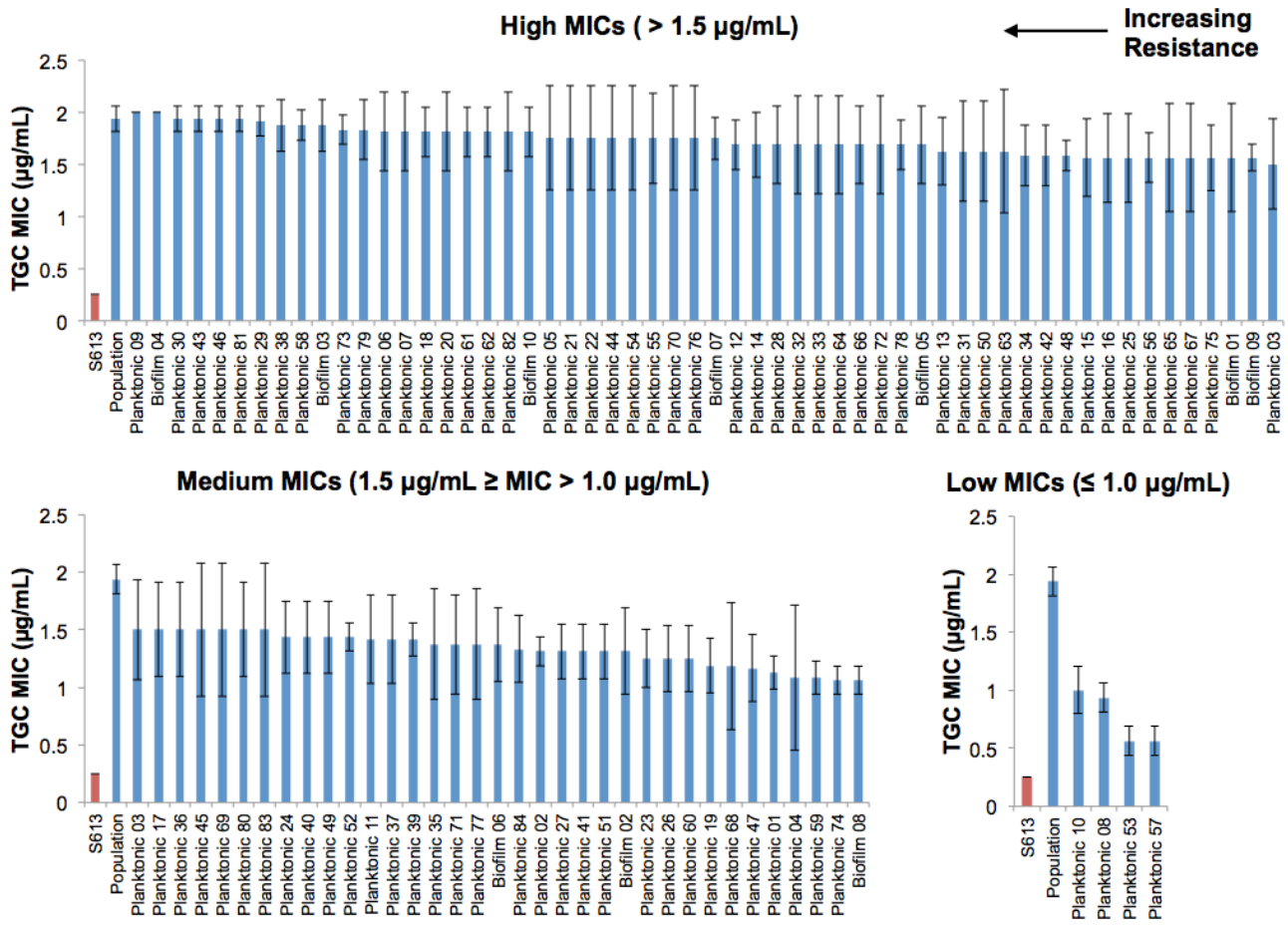


Figure 4.1: TGC MICs against 94 clones selected from the Run 1 end-point

adapted population. The TGC MICs of 84 planktonic and 10 biofilm clones isolated from the end of Run 1 were measured using agar dilutions as described in Chapter 2 Section 2.4.1. The S613 ancestor (red) and end-point population were also assayed. TGC MICs were arranged from highest to lowest and then grouped into one of three categories: High ($\text{MIC} > 1.5 \mu\text{g/mL}$), Medium ($1.5 \mu\text{g/mL} \geq \text{MIC} > 1.0 \mu\text{g/mL}$) and Low ($1.0 \mu\text{g/mL} \geq \text{MIC}$). Most clones were categorized as having a high MIC that was close to the population MIC of $2 \mu\text{g/mL}$. Some clones had distinguishably lower MICs than the population, however all of the end-point clones were more resistant than S613. For each clone the average MIC of four replicates was plotted with the error bars displaying the standard deviation.

4.2.2 Flocculation phenotype.

Of the 24 clones isolated from the end of Run 1, I selected 25 that fell into different TGC MIC categories to be further characterized. For these 25 clones I evaluated a phenotype I observed when culturing some of the isolates in liquid media. Under these conditions many of the clones aggressively formed suspended aggregates, or floc. In comparison, S613 did not flocculate and instead produced planktonic cells. To evaluate this phenotype, first I tested its stability by culturing S613 and 3 of the flocculating clones in tubes without antibiotic. Daily 100-fold dilutions of the cultures were transferred to fresh tubes. After seven days of transfers all 3 of the end-point isolates still produced excessive floc, while S613 continued to grow planktonic cells. Since the flocculation phenotype was reasonably stable I decided to further quantify this phenotype in the 25 selected end-point clones. To do this I simply grew each clone overnight in broth on a shaker. The next day I removed the tubes and let them sit on the lab bench undisturbed for 5 minutes. During this time any floc present in the cultures would settle to the bottom of the tubes (**Figure 4.2A**). Next I measured the OD (600 nm) of a sample taken off of the top of each settled tube. Cultures with a lot of floc would have low ODs, since most cells were clumped at the bottom of the tube. Conversely, cultures lacking floc would have high ODs, since cells were planktonic and would not settle. Next I would vortex the tubes until any floc present had gone into solution and measure ODs off of the top again. Once the cultures were vortexed any floc that was broken up would remain in solution and not clump again. Thus by measuring the ODs after vortexing I determined how many total cells were present in the culture. By taking a ratio of the OD after vortexing over the OD before vortexing I could gauge the degree of flocculation in each culture (**Figure 4.2B**). To summarize this phenotype, the clones were categorized into different groups: High propensity to flocculate (OD ratio > 3.5), Medium propensity to flocculate (3.5 > OD ratio > 2) and Low propensity to flocculate (OD ratio < 2) (**Figure 4.2B**).

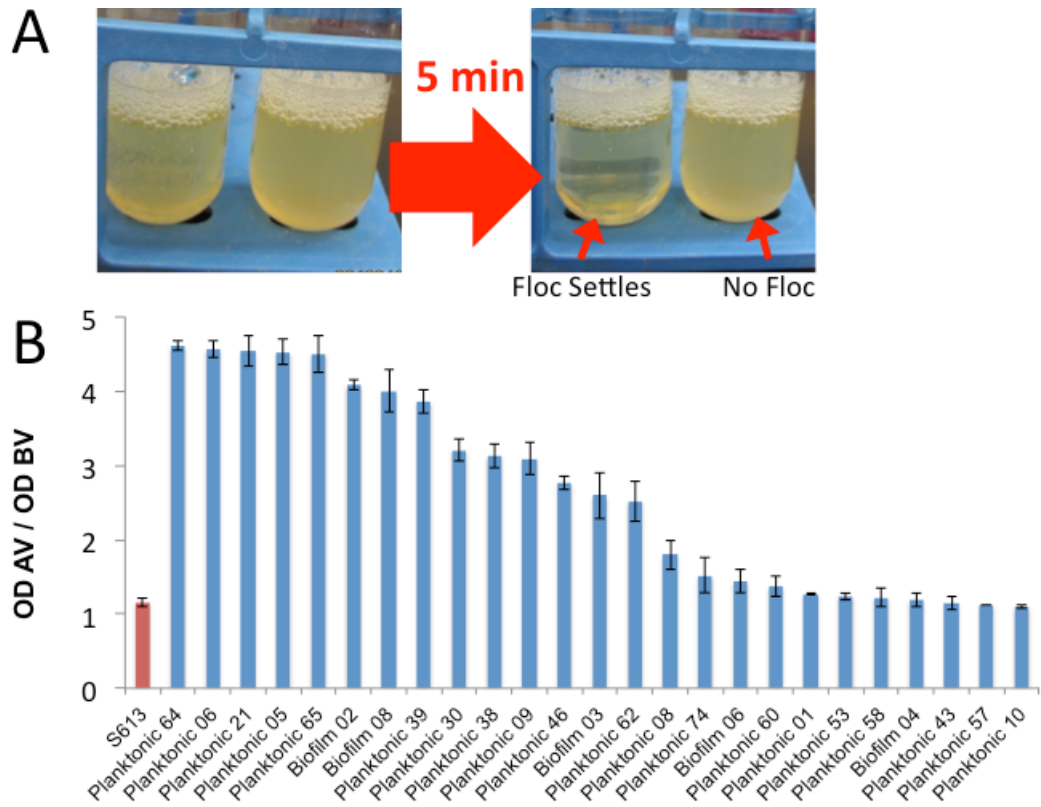


Figure 4.2: Comparison of the propensity of 25 Run 1 end-point clones to flocculate. Some Run 1 end-point adapted clones had a strong propensity to flocculate. A) When overnight cultures were left undisturbed for several minutes floc present would settle to the bottom of the tube, while planktonic cells would remain in suspension. B) The flocculation of 25 Run 1 end-point clones was evaluated. For each clone the ratio of the culture's OD After Vortexing (AV) (when all cells were suspended in solution) over the culture's OD Before Vortexing (BV) (when flocculating cells were absent due to settling) were determined. The larger the ratio, the more floc the clone produced. The S613 ancestor (red) produced less floc than 13 of the adapted isolates. Clones were grouped into three categories: High propensity to flocculate (OD ratio > 3.5), Medium propensity to flocculate (3.5 > OD ratio > 2) and Low propensity to flocculate (OD ratio < 2). Three replicate flocculation assays were performed for each clone and the error bars show the standard deviation between the replicates. Interestingly, increased flocculation was not associated with increased resistance (see Figure 4.4 for comparisons).

4.2.3 Colony sizes on chloramphenicol.

Based on the results of the TGC MIC and flocculation assays I selected fourteen of the Run 1 end-point isolates for further phenotypic characterization. In some cases when bacteria acquire a mutation conferring resistance to an antibiotic, their susceptibility profile to other antibiotics will also change: they may gain cross-resistance to another antibiotic or become susceptible to an antibiotic they were previously resistant to. Therefore, I decided to screen the 14 selected isolates for their ability to grow in the presence of an antibiotic that is distinct from TGC. I used a readily available antibiotic, chloramphenicol (CL), which is a translation inhibitor, but binds to the ribosome at a distinctly different site from tetracycline (Wilson 2014). I reasoned that if any of the Run 1 end-point clones carried diverse alleles conferring TGC resistance, their ability to grow in the presence of CL might be affected differently. I performed a simple assay to test the ability of the clones to grow in the presence of CL: I diluted overnight cultures of the clones and plated them onto agar supplemented with 2 µg/mL CL, then the next day I looked for obvious differences in colony sizes. I compared the colony sizes of each isolate to the colony size of the S613 ancestor strain. Some of the clones produced colonies that were noticeably smaller than S613, while others produced comparatively large colonies that were similar to S613 (**Figure 4.3**). Isolates with similar colony sizes as S613 were designated as ‘large,’ while isolates with noticeably smaller colony sizes were designated as ‘small’ (**Figure 4.3**). The clones were plated onto agar with CL at least three times to confirm that the colony size phenotype occurred reproducibly. Also, when plated onto agar lacking CL, the 14 selected Run 1 end-point adapted clones all had similar colony sizes to the S613 ancestor, indicating that CL is required to observe the smaller colony size phenotype.

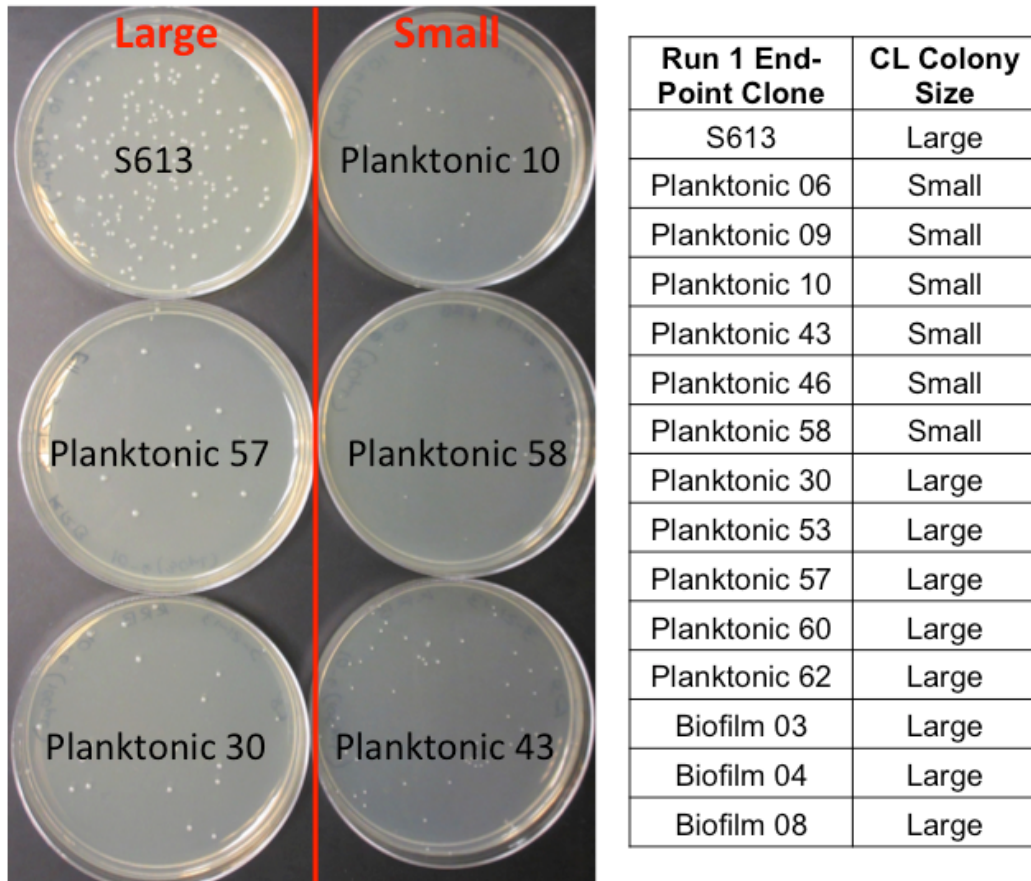
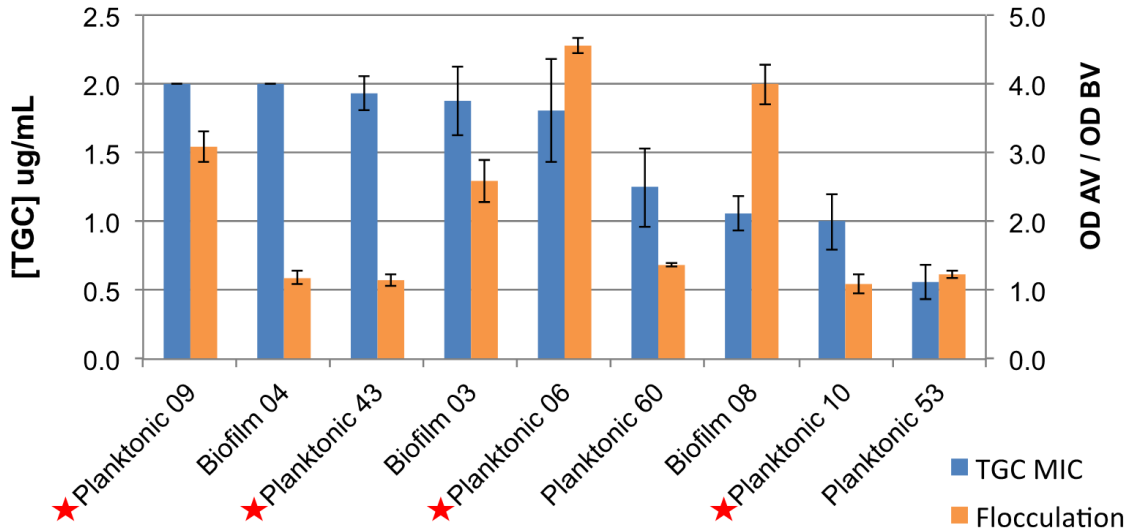


Figure 4.3: Colony sizes of 14 Run 1 end-point adapted clones on agar plates with $2 \mu\text{g/mL CL}$. Pictured on the left are several examples of the different colony sizes observed when the end-point clones were plated on agar with $2 \mu\text{g/mL CL}$. Some clones had large colony sizes, similar to S613, including planktonic 57 and 30, while other clones had noticeably smaller colony sizes, such as planktonic 10, 58 and 43. The table on the right lists all 14 of the end-point isolates that were assayed and whether or not they had a relatively small or large colony size when plated on CL. There were three independent trials performed with each of the fourteen assayed isolates to confirm that the phenotype was reproducible. When plated on agar without CL, all of the end-point adapted isolates had colony sizes similar to S613, indicating that CL is necessary for the small colony size phenotype.

4.2.4 Selection of Run 1 isolates for whole genome sequencing.

The objective of performing these phenotypic screens was to select as many Run 1 end-point clones as possible with distinctly different genotypes for whole genome sequencing. By identifying many different genotypes from the end of adaptation, I can subsequently learn as much as possible about the range of alleles present in the population and their genomic linkages to each other. Therefore, based on the results of these three phenotypic screening assays (TGC MICs, flocculation, and colony sizes on CL), I selected 9 isolates that were distinct from each other and represented different combinations of phenotypes for whole genome sequencing (**Figure 4.4**). For example, both biofilm 04 and planktonic 43 have high TGC MICs and a low propensity to flocculate, however they have different colony sizes on CL. Additionally, the more common a particular phenotype was, then the more clones I selected with that particular phenotype. For example, most of the 9 selected clones had high TGC MICs, which paralleled the observation that most of the 94 randomly selected clones also had high TGC MICs (**Figure 4.4**). However, it is important to note that since the 9 selected clones were not chosen randomly, these clones are not a true representation of the frequencies of any phenotypes or genotypes present within the population. Rather, the allelic frequencies within the population were determined by performing deep sequencing on direct samples of the population (see Chapter 5). Additionally, since my objective was to sequence as many distinctly different clones as possible, I also intentionally chose isolates with rare phenotypes. For example, I selected two clones with low TGC MICs, despite the fact that low MICs were very rare among the Run 1 end-point clones, with only 4 out of 94 clones having an MIC equal to or below 1 µg/mL TGC (**Figures 4.1 & 4.4**). I extracted genomic DNA from the 9 selected Run 1 end-point clones, prepared sequencing libraries using Illumina's Nextera® XT kit and then sent the samples to the University of Wisconsin-Madison core sequencing facilities.



Run 1 Clone	TGC MIC	Flocculation	Colony size on CL
Planktonic 09	High	Medium	Small
Biofilm 04	High	Low	Large
Planktonic 43	High	Low	Small
Biofilm 03	High	Medium	Large
Planktonic 06	High	High	Small
Planktonic 60	Medium	Low	Large
Biofilm 08	Medium	High	Large
Planktonic 10	Low	Low	Small
Planktonic 53	Low	Low	Large

Figure 4.4: Summary of Run 1 end-point adapted isolates selected for whole genome sequencing. On top is a graph showing the TGC MICs (blue) and propensity to flocculate (orange) of the 9 Run 1 end-point clones that were selected for whole genome sequencing. A red star was placed next to the name of clones that produced small colonies on agar with CL. The propensity of the clones to flocculate was plotted as OD After Vortexing (AV) over OD Before Vortexing (BV). The clones were arranged left to right from highest MIC to lowest MIC (most resistant to least resistant). On bottom is a table summarizing the results of all three phenotypic assays for each of the 9 selected Run 1 end-point clones. Each selected end-point clone had a unique combination of phenotypes and was distinct from the other eight selected clones. Interestingly, no correlation was observed between how resistant a clone was and the other two assayed

phenotypes. For example, both biofilm 04 and planktonic 06 were highly resistant to TGC, but planktonic 06 had a high flocculation phenotype and small colony size on CL, while biofilm 04 had a low flocculation phenotype and a large colony size on CL. The two clones with a low level of resistance (planktonic 10 and planktonic 53) both had a low propensity to flocculate. However, since there were only two clones with low MICs it is unclear if low resistance is correlated with low flocculation. Additionally, some of the highly resistant clones also had a low propensity to flocculate, such as biofilm 04 and planktonic 43, suggesting that flocculation and resistance were not correlated.

4.3 Phenotypic characterization of bioreactor Run 2 isolates.

Once I had completed bioreactor Run 2, to select clones for whole genome sequencing I plated dilutions of the end-point planktonic and biofilm populations onto non-selective agar and randomly picked 94 colonies, as I had done with Run 1. This time I selected 58 colonies from the planktonic population and 36 colonies from the biofilm population. Based on the whole genome sequencing of the Run 1 clones (see Chapter 5), it was clear that the most successful phenotypic assay for identifying genomic diversity was the TGC MIC testing. Therefore, to select diverse clones from the end of Run 2, the only phenotypic assay I performed was to measure the TGC MICs. I used the same modified agar dilution protocol that was used for the Run 1 clones, except with the inclusion of a 4 µg/mL TGC plate, since some of the Run 2 clones had MICs above 2 µg/mL. Using this approach I was able to identify variations in the TGC MICs among the different clones, highlighting the diversity within the Run 2 bioreactor population (**Figure 4.5**). Similar to Run 1 many of the clones isolated from the end of Run 2 had high MICs, with planktonic 16 having the highest MIC at 4 µg/mL TGC (**Figure 4.5**). Interestingly, there were also end-point clones with very low MICs, including Biofilm 17, 21 and 22, which all had MICs that were indistinguishable from S613 (**Figure 4.5**). Similar to Run 1, the Run 2 clones were categorized into three different groups depending on their MICs: High (MIC > 2 µg/mL TGC), Medium (2 µg/mL TGC > MIC > 1 µg/mL TGC) and Low (1 µg/mL TGC ≥ MIC) (**Figure 4.5**). From these clones a total of 5 were selected for whole genome sequencing; 2 clones with high MICs (planktonic 05 and 16), 2 clones with medium MICs (biofilm 29 and planktonic 38), and 1 clone with a low MIC (biofilm 30) (**Figure 5.4**). Next I extracted genomic DNA from the five selected Run 2 clones, prepared sequencing libraries using Illumina's Nextera® XT kit and then sent the libraries to the US Army Edgewood Chemical Biological Center for whole genome sequencing.

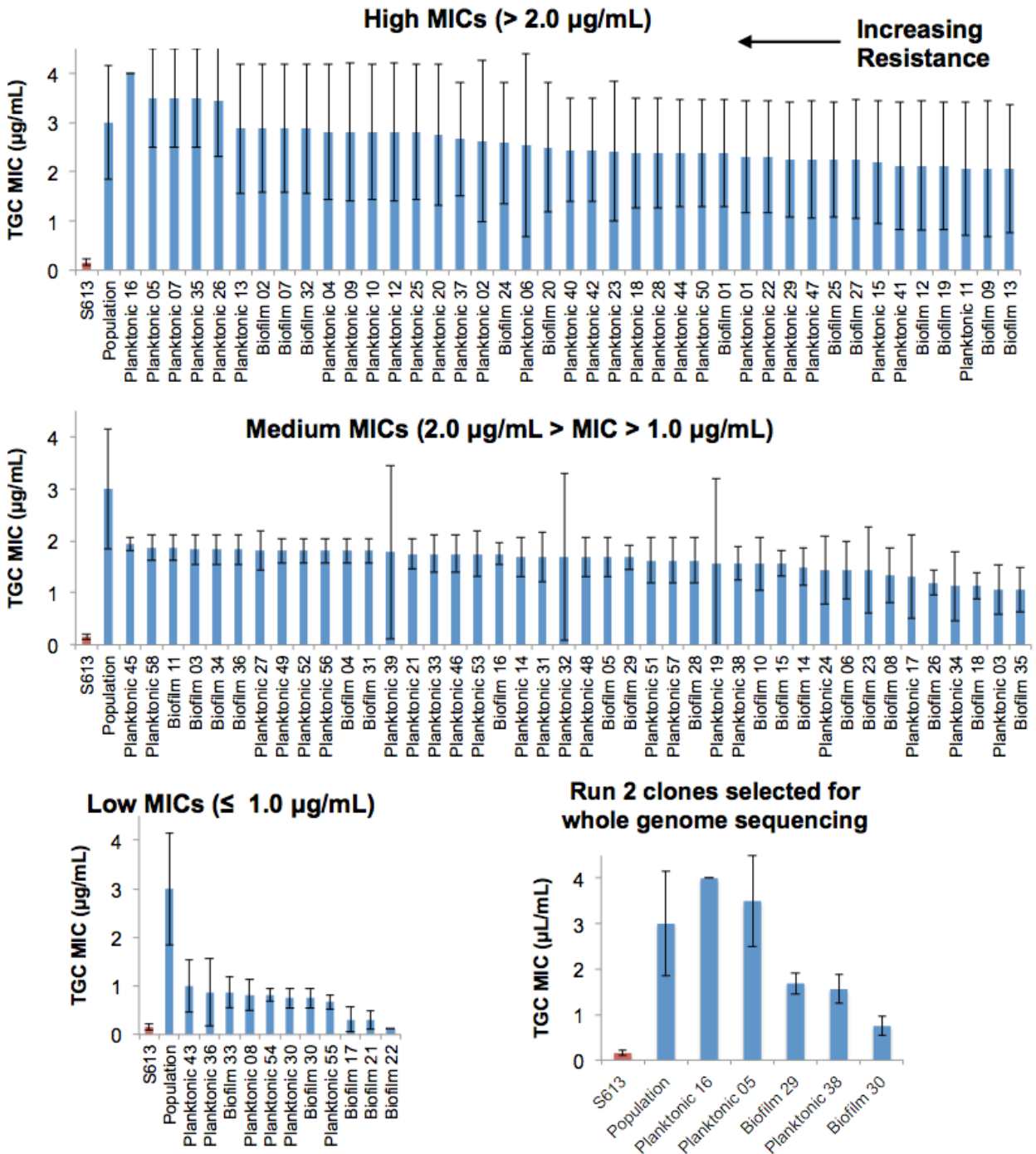


Figure 4.5: TGC MICs against 94 clones selected from the Run 2 end-point

adapted population. The TGC MICs of 58 planktonic and 36 biofilm clones isolated from the end of Run 2 were measured using agar dilutions as described in Chapter 2 Section 2.4.1. The S613 ancestor (red) and Run 2 end-point population were also assayed. The TGC MICs were arranged with left to right showing highest to lowest

MICs. The MICs were also grouped into one of three categories: High ($\text{MIC} > 2 \mu\text{g/mL}$), Medium ($2 \mu\text{g/mL} > \text{MIC} > 1 \mu\text{g/mL}$) and Low ($1.0 \mu\text{g/mL} \geq \text{MIC}$). Similar to Run 1, most of the Run 2 clones were categorized as having a high MIC that was close to the Run 2 population MIC of $3 \mu\text{g/mL}$ (note that the Run 2 end-point population MIC was $2 \mu\text{g/mL}$ when determined using the Clinical Laboratory Standards Institute (CLSI) agar dilution method and $3 \mu\text{g/mL}$ when using the agar dilution method described in Chapter 2 Section 2.4.1). Some clones had distinguishably lower MICs than the population, with several having MICs that were similar to S613, including biofilm 17, 21 and 22. For each clone the average MIC of four replicates was plotted with the error bars displaying the standard deviation.

4.4 Discussion.

The planktonic cells and biofilm were surveyed from the end of each run, yet interestingly none of the assayed phenotypes were specific to either the planktonic or biofilm populations. For example, despite the similarities between floc and biofilm, most clones that flocculated were isolated from the planktonic population, while some of the biofilm clones did not flocculate (**Figure 4.2**). Additionally, both the biofilm and planktonic clones from Run 1 and Run 2 displayed a range of MICs, with some biofilm and planktonic clones having relatively high levels of resistance and others having relatively low levels of resistance (**Figures 4.1 & 4.5**). The lack of a clear association between phenotype and the isolation source of a clone was recaptured in the genomic data, as identical genotypes were found in biofilm and planktonic clones (**Table 5.1**). It is possible that no specific genetic mutation lead to biofilm, but rather transcriptional, regulatory, epigenetic or signaling changes that determined if a cell formed biofilm or remained planktonic.

Among the Run 2 end-point clones, there were 3 biofilm isolates with extremely low TGC MICs that were indistinguishable from the MIC of S613 (**Figure 4.5**). Biofilms are known to protect cells from hostile environments, and it is possible that these clones were able to survive in the bioreactor, despite their low MICs, due to the protective properties of the biofilm (Costerton, et al. 1999). Interestingly, unlike Run 2, all of the Run 1 biofilm isolates had MICs well above S613 (**Figures 4.1**). However since only 10 clones were screened from the Run 1 biofilm, compared to 36 from the Run 2 biofilm, it is possible that such clones were present in the Run 1 biofilm, but not enough were screened to identify this rare phenotype (**Figures 4.1**). Alternatively, the Run 1 population was exposed to the highest TGC concentration (1 µg/mL) for nearly seven days, whereas the

Run 2 population was only exposed to 1 µg/mL TGC for only two days (**Figure 3.5**). Since TGC is bacteriostatic, cells with lower MICs might have been able to persist at 1 µg/mL TGC for two days, but not for seven. Thus the Run 1 population could have lost all cells with such low MICs during the last stage of adaption and this in turn could explain why I did not isolate any clones with this phenotype.

As expected I was able to detect phenotypic diversity among clones isolated from the bioreactor end-point populations. Additionally, the results of the whole genome sequencing of the end point clones, which are discussed in Chapter 5, did indeed reveal genetic diversity among the clones. However, interestingly no correlation was observed between the flocculation or CL colony size phenotypes and the genotypes of clones. For example, Biofilm 03 and Planktonic 43 had identical genotypes despite having strikingly different propensities to flocculate and different colony sizes on CL (**Figures 4.4 & Table 5.1**). Again, it is likely that transcriptional, regulatory, epigenetic or signaling differences resulted in these phenotypes, rather than genetic mutations. These results highlight the importance of considering the role of non-genomic changes in adaption to antibiotic resistance. It would be interesting to monitor transcriptional changes and quorum signaling within the bioreactor during the course of adaption. However, assaying these aspects of the population in addition to maintaining the technical complexity of bioreactor would be challenging.

It is important to note that differences in TGC MICs were indeed related to different genotypes. For example, among the Run 1 isolates Planktonic 09 (High MIC), Planktonic 60 (Medium MIC) and Planktonic 53 (Low MIC) all had different genotypes (**Figure 4.4 & Table 5.1**). Similarly, for Run 2 Planktonic 16 (High MIC), Biofilm 29 (Medium MIC) and Biofilm 30 (low MIC) all had different genotypes (**Figure 4.5 & Table 5.1**). Perhaps

these results are not surprising, as TGC was the selective force during adaptation. Ultimately, the phenotypic screening did allow me to successfully identify a wide range of genotypes, including rare genotypes that were only present at no more than 0.8% frequency within the Run 1 population (**Tables 5.1 & 5.2**). Thus, the phenotypic screening was successfully able to capture the genetic diversity of the adapted populations.

Chapter 5: Identification of the most important alleles leading to TGC resistance in *E. faecalis*.

This chapter was reproduced with permission from Beabout, et al. 2015 *Mol Biol Evol*

5.1 Introduction.

I performed whole genome sequencing on the fourteen phenotypically distinct clones that were isolated from the end of Run 1 and Run 2 to survey adaptive alleles within the population and to provide information about the genomic linkages between different alleles (see Chapter 4 for summary of phenotypes). A total of seven distinct genotypes, or strains, were identified among the fourteen isolates (**Table 5.1**). These distinct strains were referred to as the ‘Bioreactor-adapted TGC Resistant’ (BTR) strains (**Table 5.1**). In addition to sequencing the genomes of phenotypically diverse clones, I also performed deep sequencing on samples of the population during each day of adaptation.

Population samples were directly collected from the bioreactor outflow on every day of both experimental runs. Genomic DNA was isolated from these polymorphic samples without further outgrowth and then whole genome sequencing, with at least 500-fold coverage, was performed on each population sample. This allowed me to determine the allelic frequencies of all mutations that reached at least 5% frequency on one or more days of adaptation to understand the evolutionary dynamics of the populations (**Table 5.2 & Figure 5.1**). Overall, I identified 24 mutations from my metagenomic population and isolate sequencing (**Tables 5.1 & 5.2**). However, only two candidate loci appeared to be tightly linked to resistance, based on their evolutionary dynamics and repeated evolution (**Figure 5.1**).

Table 5.1: Genotypes of bioreactor-adapted TGC resistant (BTR) clonal strains isolated from the end of adaptation

Run	Strain ^a	MIC _{TGC} ^b (µg/mL)	Deletions in 5'UTR of <i>tetM</i>	New Tn916 Insertion Sites ^c	Clones ^d
N/A	S613	0.125	None	None	N/A
1	BTR87a	2.0	Δ87-bp, 51-bp upstream <i>tetM</i>	<i>yycl</i>	P06, B08
1	BTR87b	2.0	Δ87-bp, 51-bp upstream <i>tetM</i>	Intergenic site J	P09
1	BTR22	2.0	Δ22-bp, 231-bp upstream <i>tetM</i>	None	B03, P43, B04
1	BTR37	1.0	Δ37-bp, 98-bp upstream <i>tetM</i>	<i>yycl</i> , Sulfatase, Intergenic sites C, D, H, and I	P60, P10
1	BTR0	0.5	None	None	P53
2	BTR125a	2.0	Δ125-bp, 36-bp upstream <i>tetM</i>	O-antigen ligase ^e	P16
2	BTR125b	2.0	Δ125-bp, 36-bp upstream <i>tetM</i>	None	P05, B29, P38
2	BTR0	0.5	None	None	B30

^aAll BTR strains have the S10^{R53Q-Δ54-58KTHK} allele.

^bTGC MICs were measured using the agar dilution technique following CLSI protocols.

^cAll strains retained the ancestral insertion of Tn916. Strains with multiple copies of Tn916 retained the wildtype sequence at the ancestral site.

^dPlanktonic (P) and biofilm (B) clones that were sequenced with the corresponding genotype (see Chapter 4 for more information).

^eThis copy of Tn916 has an insertion of the IS204 transposon downstream of *tetM*.

Table 5.2: List of all mutations identified from Run 1 and 2 that reached ≥ 5% within the population, or were identified in sequenced isolates from the end of adaptation.

Run	Mutation	Annotation	Coding Change	Locus Tag ^a	Contig	Position	Highest Freq.
1	Δ12-bp	Ribosomal S10 protein	R53Q-Δ54-57ATHK	1375	763	35,999	99.9%
1	Δ87-bp	Intergenic (51-bp upstream of <i>tetM</i>)	N/A	N/A	778	138,433	90.6%
1	G→A	Serine/threonine protein kinase PrkC, regulator of stationary phase	A196V	2283	801	27,053	16.1%
1	G→T	N-acetylmuramoyl-L-alanine amidase family 4	E57*	2682	810	168,069	15.6%
1	Δ71-bp	Intergenic	N/A	N/A	775	6,290	14.6%
1	C→A	Cobalt ABC Transporter	G212V	187	730	27,780	6.3%
1	Δ37-bp	Intergenic (98-bp upstream of <i>tetM</i>)	N/A	N/A	778	138,480	4.2%
1	Δ22-bp	Intergenic (231-bp upstream of <i>tetM</i>)	N/A	N/A	778	138,613	0.8%
2	Δ12-bp	Ribosomal S10 protein	R53Q-Δ54-57ATHK	1375	763	35,999	94.7%
2	Δ125-bp	Intergenic (36-bp upstream of <i>tetM</i>)	N/A	N/A	778	138,448	94.5%
2	T→A	ABC Transporter 1	T278S	2766	810	260,239	23.6%
2	G→C	ABC Transporter 2	G73A	1948	785	39,763	21.8%
2	T→C	Type 1 restriction modification system, specificity subunit S	L187L	1696	778	18,115	14.0%
2	T→C	Type 1 restriction modification system, specificity subunit S	L187F	1696	778	18,117	13.7%
2	C→A	Transcriptional regulator, Cro/CI family	S49Y	971	749	98,114	12.8%
2	G→A	Intergenic	N/A	N/A	739	26,573	9.6%
2	G→A	O-succinylbenzoic acid-CoA Ligase	A409A	2055	787	9,405	9.5%

Run	Mutation	Annotation	Coding Change	Locus Tag ^a	Contig	Position	Highest Freq.
2	G→T	Cell division trigger factor	E60*	2468	809	107,415	9.5%
2	C→G	Hypothetical Protein	G293R	842	746	25,723	8.4%
2	C→A	Hypothetical Protein	W295L	842	746	25,716	8.1%
2	C→A	Intergenic	N/A	N/A	720	3,617	7.9%
2	Δ12-bp	Ribosomal S10 protein	Δ52-55VRAT	1375	763	35,994	7.3%
2	G→A	Type 1 restriction modification system, specificity subunit S	K195K	1696	778	18,141	6.3%
2	A→T	Zn-dependent hydrolase (Beta-lactamase superfamily)	L55F	963	749	92,039	5.7%
2	A→T	Type 1 restriction modification system, specificity subunit S	T181T	1696	778	18,099	5.4%
2	1,505 Kb insertion	Transposase IS204 insertion into Tn916	N/A	733	778	135,277	0.3%

^aLocus tags were obtained from *E. faecalis* S613 file annotated by PATRIC (<http://www.patricbrc.org>)

5.2 Deletion of regulatory elements upstream of *tetM*.

An essential step in adaptation to TGC resistance under these selection conditions is the acquisition of a deletion in the 5' UTR of *tetM*. Expression of *tetM* is regulated by a transcriptional attenuation mechanism involving a terminator stem-loop located 36-bp upstream of the *tetM* start codon (Su, et al. 1992). In the presence of tetracycline, the terminator stem-loop, which prevents expression of *tetM* in the absence of tetracycline, is overcome by a poorly characterized mechanism that may involve ribosomal-mediated transcriptional attenuation (Su, et al. 1992). An 87-bp deletion located 51-bp upstream of the *tetM* start codon exceeded 90% frequency by the end of the first experimental run (**Figure 5.1A**). Additionally, a 125-bp deletion located 36-bp upstream of the *tetM* start codon exceeded 94% frequency by the end of the second experimental run (**Figure 5.1A**). Both the 87-bp and 125-bp deletions eliminate the terminator stem-loop sequence located in the 5' UTR of *tetM* showing that deleting this region plays an important role in adapting to TGC (**Figure 5B**). Interestingly, McAleese et al. identified an 87-bp deletion located 54-bp upstream of the *tetM* start codon in a *Staphylococcus aureus* strain that was adapted to TGC (McAleese, et al. 2005). This demonstrates that eliminating the terminator stem-loop in the 5' UTR of *tetM* plays a role in TGC resistance for species other than enterococci. I also identified deletions in the 5' UTR of *tetM* that do not eliminate the terminator stem-loop. While these deletions did not surpass 5% frequency during adaptation, they were identified in strains at the end of adaptation and included a 22-bp and 37-bp deletion located 231-bp and 98-bp upstream of the *tetM* start codon, respectively (**Figure 5B & Tables 5.1 & 5.2**). Thus, while the deletions observed in *E. faecalis* and *S. aureus* are of varying sizes, there is a consistent observation of deletions upstream of *tetM* among successful trajectories leading to TGC resistance. The effect of the different deletions on the regulation of *tetM* is discussed in Chapter 6 Section 6.2.

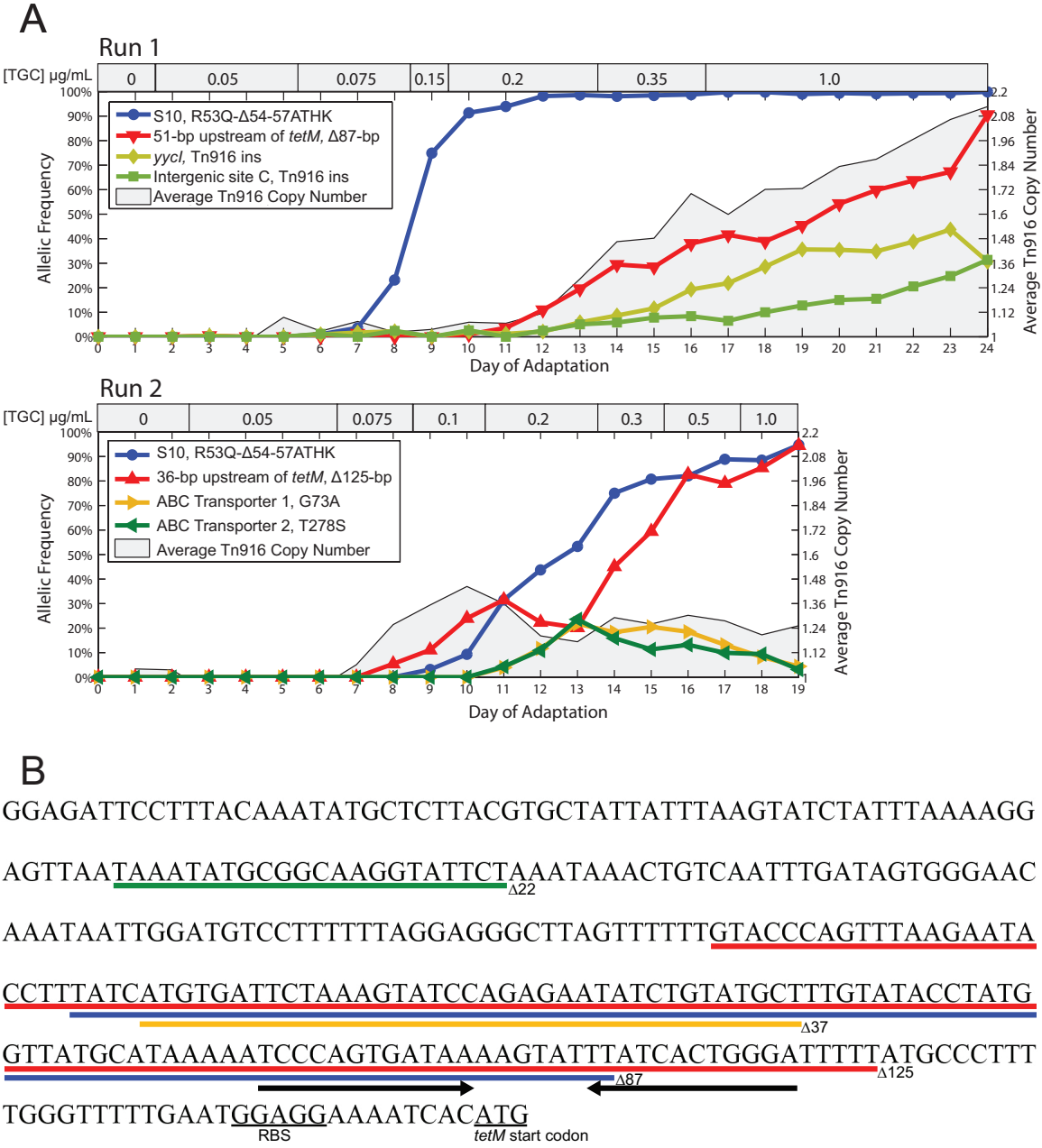


Figure 5.1: Experimental evolution of pathogenic *E. faecalis* to TGC shows that deletion of *tetM* regulatory elements and mutation of the ribosomal protein S10 provides the successful evolutionary trajectories to TGC resistance. A) Deep sequencing was performed on samples of the polymorphic populations collected on each day of adaptation. These population metagenomic data were then used to determine daily allelic frequencies during each bioreactor experiment. This method

detects alleles that reached at least 5% during adaption, however for clarity only alleles that reached at least 20% were plotted. Mutations at two loci were successful in both experimental runs; deletions that eliminate a regulatory element in the 5' UTR of *tetM* (red) and a 12-bp deletion in the ribosomal S10 protein ($S10^{R53Q-\Delta 54-57ATHK}$) (blue). Additionally, during the first experimental run there were two specific insertions of Tn916 that exceeded 20% by the end of adaptation (of 44 insertions that exceeded 1%). The new insertions of Tn916 occurred within the *yycl* gene (light green) and an intergenic site (green). These two sites were not observed during the second run and thus may have hitchhiked with the 87-bp deletion in the 5' UTR of *tetM*. The average Tn916 copy number of the population was determined by sequencing coverage. S613 has one chromosomal copy of Tn916, but after undergoing TGC selection the average cell within the population had 2.13 and 1.25 copies by the end of the first and second run, respectively. **B)** Diagram showing the sequence of the 5' UTR of *tetM* and the deletions identified in this region during adaptation to TGC. Deletions are shown as colored lines and the terminator stem-loop is indicated with black arrows beneath the sequence. An 87-bp (blue) and 125-bp (red) deletion remove the terminator stem loop and were highly successful during adaptation, while a 37-bp (orange) and 22-bp (green) deletion leave the stem-loop intact and were only detected at low frequencies during adaptation but still conferred increased resistance presumably by removal of as yet uncharacterized regulatory sequences.

5.3 Mutation of the S10 protein may remodel the ribosome rendering TGC less effective.

Another important allele was a 12-bp deletion in the ribosomal S10 gene (*rpsJ*) that reached fixation or near fixation by the end of both adaptation experiments (**Figure 5.1A**). This mutation resulted in the complete deletion of three codons (A54, T55, and H56) and the fusion of two codons (R53 and K57) to make a glutamine at position 53 ($S10^{R53Q-\Delta 54-57ATHK}$) and thereby restore the reading frame necessary for production of this essential protein. The altered amino acids are located on an extended loop of S10 that interacts with the sequences of 16S rRNA that make up the TGC binding pocket (**Figure 5.2**). We speculate that changes to S10 may simply decrease TGC affinity for the ribosome by subtle alterations of the RNA structure near to the binding site (see Chapter 8 Section 8.2.4 and Appendix C for further discussion of this hypothesis). Similar mutations have been identified in other species, which suggests that S10 may be a target of selection across species (Cattoir, et al. 2014; Villa, et al. 2014). This is further supported by my finding that TGC resistant strains with only the S10 allele were isolated independently from the end of both experiments and had an intermediate MIC of 0.5 µg/mL (**Table 5.1**).

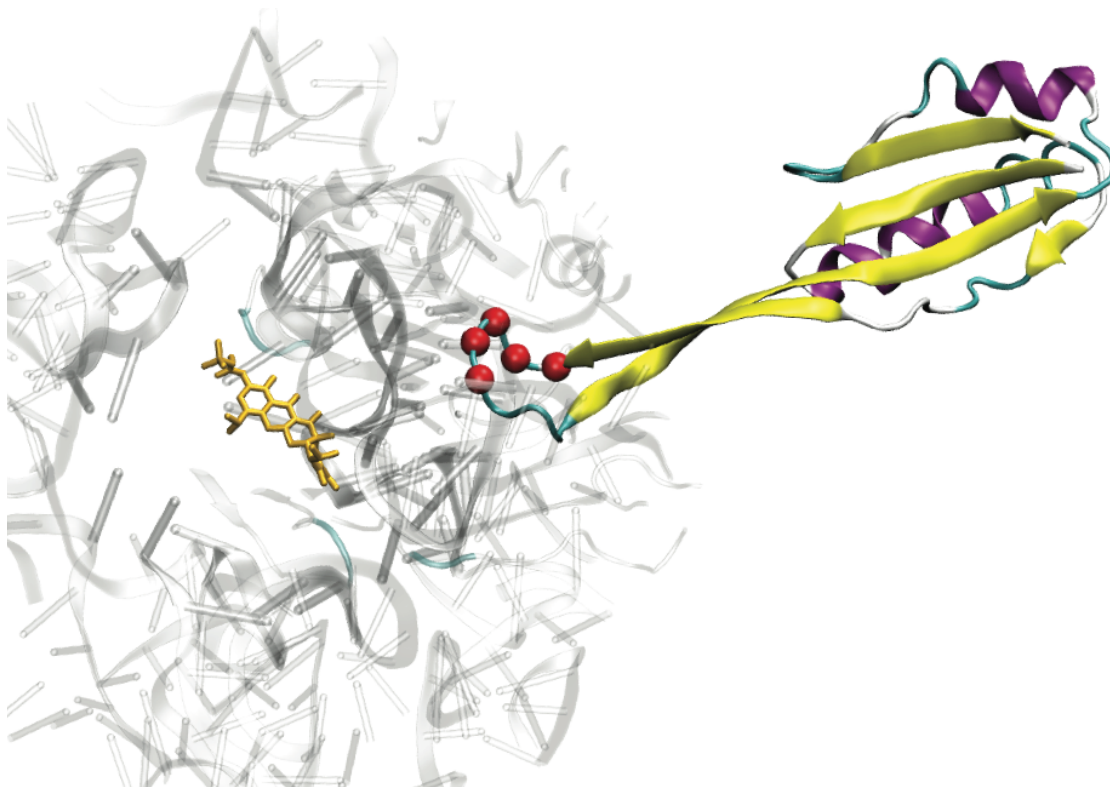


Figure 5.2: Deletion in S10 may decrease the binding affinity of TGC by remodeling the ribosome. The position of the S10 mutations ($S10^{R53Q-\Delta 54-57ATHK}$) within the context of the ribosome suggests that it may indirectly alter TGC binding. The co-structure of the *Thermus thermophiles* 70S ribosome with TGC (yellow sticks) is shown (PDB 4G5T). For clarity, only S10 and the structures proximal to the TGC binding pocket are shown. The mutated residues are located at the tip of a loop (residues 53-61) and are highlighted by red spheres at the carbon alpha position. The S10 loop does not directly contact TGC but instead interacts with several portions of the 16S rRNA (grey) that comprise the TGC binding pocket (Jenner, et al. 2013).

5.4 Mutations in hypothetical ATP-binding cassette-type transporters.

During the second run two different nonsynonymous point mutations occurred in separate hypothetical ATP-binding cassette (ABC) transporters, referred to as ABC transporters 1 and 2, and surpassed 20% frequency on day thirteen of Run 2 (**Figure 5.1A & Table 5.2**). ABC transporter 1 has 29.9% sequence identity with the Gram-negative lipid A export protein MsbA. Interestingly, the *msbA* gene has been implicated in multidrug resistance and was mutated in an *Acinetobacter baumannii* strain that was adapted to TGC using serial transfers (Chen, et al. 2014; King and Sharom 2012). ABC transporter 2 has 19.6% sequence identity with CcmA, a component of the cytochrome c assembly CcmAB (Cook and Poole 2000). CcmA has never been identified to play a role in drug resistance; however, related types of ABC transporters have been implicated in resistance (Cook and Poole 2000). While interesting alleles, the mutations in ABC transporters 1 and 2 began to decline at 0.3 µg/mL TGC (day 14) and dropped to a low frequency by the end of adaptation, suggesting that these mutations are not successful at higher concentrations of TGC (**Figure 5.1A**). In addition, I did not isolate a clone from the end of adaption with a mutation in either ABC transporter 1 or 2, which is consistent with the low frequencies of these alleles on the last day of the second run (**Figure 5.1A**). I was able to isolate a clone that carries both ABC transporter mutations by randomly selecting colonies from day thirteen of the second run and Sanger sequencing the two transporter genes. It is interesting to note that since the frequencies of the two alleles rise and fall together in the population they may be linked (**Figure 5.1A**). This is supported by the identification of both alleles in the same clone and suggests that together they could have an epistatic advantage.

5.5 Discussion.

As discussed in Chapter 1, a successful preemption strategy to limit the spread of multidrug resistance requires two fundamental insights: 1) How *will* a pathogen become resistant to a specific class of antibiotics? and 2) What are the target proteins or biochemical pathways for intervention? TGC is an important drug of last resort for treating VRE infections and at the start of these studies little was known about the mechanisms of TGC resistance in VRE, making it an ideal target for preemptive studies. Since Dr. Corwin Miller demonstrated the ability of quantitative experimental evolution to identify clinically relevant mechanisms of resistance (Miller, et al. 2013), I employed this same approach to predict how resistance to TGC will occur in vancomycin-resistant *E. faecalis*.

Here I have shown that mutations at two loci are essential for *E. faecalis* S613 to adapt to growth in TGC: the upstream regulatory region of *tetM* and the gene that encodes the ribosomal S10 protein. Importantly, several studies have confirmed that these loci are indeed important to TGC resistance in clinical isolates of enterococci. Two different research groups found mutations on the extended loop of S10 in TGC-resistant clinical isolates of *Enterococcus faecium* (Cattoir, et al. 2014; Niebel, et al. 2015). Interestingly, Niebel *et al.* identified a 16-bp deletion in S10 that removes five amino acids (Δ IRATH52-56) and is similar to the S10^{R53Q-Δ54-57ATHK} allele identified in my BTR strains (**Table 5.1 & Figures 5.1 & 5.2**) (Niebel, et al. 2015). Additionally, Fiedler *et al.* confirmed my findings that mutations associated with *tetM* play an important role in TGC-resistance, as their group identified several clinical TGC-resistant *E. faecium* isolates with increased *tetM* copy numbers, which I discuss more in Chapter 8 (Fiedler, et al. 2015). While not all enterococci carry the *tetM* allele, *tetM* has been found at high frequency among hospital isolates and therefore has a strong potential to undermine the

efficacy of TGC (Frazzon, et al. 2009; Leener, et al. 2004; Lopez, et al. 2009; McBride, et al. 2007; Nishimoto, et al. 2005). By identifying these essential loci I have provided an important first step towards taking a preemptive strategy to maintain the efficacy of TGC against VRE.

Chapter 6: The role of *tetM* overexpression and Tn916 conjugation in adaptation of S613 to TGC resistance.

This chapter was reproduced with permission from Beabout, et al. 2015 *Mol Biol Evol*

6.1 Introduction.

As discussed in Chapter 1, by identifying the mechanisms of TGC resistance while the antibiotic still has high therapeutic efficacy, we can gain important insights that can be used to deter the rise and spread of resistance. For example, a molecule that inhibits a specific mechanism of resistance could be developed and administered as a codrug to extend the effectiveness of the antibiotic. This codrug concept has been successfully used in the case of Augmentin®, which is a combination of amoxicillin and the β-lactamase inhibitor clavulanic acid (Brogden, et al. 1981). Clavulanic acid renders resistant cells susceptible to amoxicillin, which in turn expands the efficacy and clinical success of amoxicillin (Todd and Benfield 1990). Furthermore, as multi-drug resistant pathogens spread, a broader understanding for how antibiotic use shapes evolutionary trajectories would inform both utilization of antibiotics and open opportunities for the development of new therapies that would anticipate future resistance mechanisms and preempt them. Therefore by identifying the most important mutations leading to TGC resistance in VRE, we have taken the first step towards achieving this ambition of preempting resistance. Exploring the molecular and biochemical mechanisms through which these mutations confer resistance and the effect of these mutations on the fitness

of the bacteria will build upon these results. In this chapter I demonstrate that deletions in the 5' UTR of *tetM* deregulate the expression of *tetM*, which in turn confers the cells with TGC resistance. Additionally, since *tetM* is located on the conjugative transposon Tn916, I explore the role of horizontal gene transfer in the adaptation of S613 to TGC resistance and show that deletions in the 5' UTR of *tetM* lead to a dramatic increase in the mobilization and conjugation of Tn916 in the adapting bioreactor populations.

6.2 Constitutive overexpression of *tetM* leads to TGC resistance.

Since the deletions upstream of *tetM* are located in a region involved in transcriptional regulation of *tetM*, I hypothesized that they caused an increase in *tetM* expression (**Figures 5.1B & 6.1**). I used quantitative real-time PCR (qPCR) to measure the relative expression of *tetM* for BTR87b (an isolate that has the 87-bp deletion that exceeded 90% in the first experiment) and BTR22 (an isolate that has the much less common 22-bp deletion in the first experiment) compared to the ancestral S613 strain in both the absence and presence of TGC (**Table 5.1**). Both BTR87b and BTR22 strains had a greater than 10-fold increase in *tetM* expression in the presence of TGC regardless of which underlying deletion was present (**Figure 6.1A**). The two BTR strains also had a greater than 18-fold increase in *tetM* expression relative to S613 in the absence of antibiotic, showing that *tetM* overexpression is now constitutive in these strains (**Figure 6.1A**). These results demonstrate that deletions upstream of *tetM*, including the 22-bp deletion, which does not eliminate the terminator stem-loop, lead to a constitutive overexpression of *tetM*. Cells carrying the *tetM* gene with the canonical 5' UTR sequence remain highly susceptible to TGC, despite being resistant to other tetracyclines (see Chapter 1 Section 1.7) (Connell, et al. 2003; Donhofer, et al. 2012;

Jenner, et al. 2013). Under typical *tetM* expression levels, it is likely that the high binding affinity of TGC for the ribosome prevents TetM from displacing TGC. However, in cells with deletions in the 5' UTR of *tetM* the resulting increase in *tetM* expression and subsequent increase in TetM protein concentration likely allows the protein to outcompete the high binding affinity of TGC to the ribosome. These data demonstrate that a simple change in *tetM* expression can lead to TGC resistance in the future.

6.3 Rampant genetic recombination evolves in the S613 bioreactor populations during TGC selection.

6.3.1 Constitutive overexpression of TetM leads to hyperconjugation of Tn916.

Canonically, the mobilization and conjugal-transfer of Tn916 occurs infrequently, ranging from $\sim 10^{-8}$ to $\sim 10^{-5}$ transconjugants per donor cell, and is increased in the presence of tetracycline (Celli and Trieu-Cuot 1998; Jaworski and Clewell 1994). Leaky transcription of *tetM* allows read-through expression of the downstream excisionase (*xis*) and integrase (*int*) genes (Celli and Trieu-Cuot 1998; Storrs, et al. 1991) (Figure 1.5). When *xis* and *int* are expressed, Tn916 is excised from the chromosome at an increased frequency and forms a covalently closed circular intermediate (Roberts and Mullany 2009). Circularization of excised Tn916 allows for transcription initiated upstream of *tetM* to continue around the circularized element leading to expression of the Tn916 conjugation factors (Figure 1.5). Expression of the conjugation elements then leads to increased conjugal-transfer of Tn916.

Since BTR87b and BTR22 constitutively overexpress *tetM* (**Figure 6.1A**), I hypothesized that the expression of the downstream *xis* and *int* genes would also be elevated in these strains via leaky *tetM* expression. I used qPCR to show that the evolved BTR strains had increased *int* expression relative to S613 (**Figure 6.1B**). When grown without TGC, BTR87b and BTR22 had an approximately 3-fold and 1.5-fold increase in *int* expression compared to S613, respectively (**Figure 6.1B**). When cultured with TGC, the expression of *int* for BTR87b was elevated to an 11-fold increase over S613 (**Figure 6.1B**). In contrast, *int* expression in BTR22 was insensitive to TGC suggesting that the position of this more rare deletion event outside the well conserved regulatory stem-loop structure may be mechanistically distinct from the much more common deletion of the regions containing the stem-loop (**Figure 6.1B**). Although their expression patterns varied, both BTR87b and BTR22 had elevated *int* expression over S613, which is consistent with increased transcriptional read-through of *tetM*.

Since the expression of *int* is increased in the BTR strains, I reasoned that the excision rate of Tn916 was likely also increased. To determine if Tn916 is excising at a higher rate in the BTR strains than in S613, I performed qPCR on total DNA using primers that amplified the new junction of circularized Tn916. In the absence of antibiotic, the number of cells with excised Tn916 was greatly increased among the BTR strains when compared to S613 (**Figure 6.1C**). In the absence of drug, approximately 1 in 120,000 S613 cells had an excised copy of Tn916, whereas nearly 1 in 50 cells and 1 in 150 cells had an excised copy of Tn916 for BTR87b and BTR22, respectively (**Figure 6.1C**). These data show that Tn916 excised at an 800- to 2400-fold higher frequency than S613 even in the absence of antibiotic. Interestingly, when S613 and BTR87b were cultured in the presence of TGC, the frequency of cells with an excised copy of Tn916 increased for both strains with approximately 1 in 16,000 cells for S613 to an astonishingly high 1 in 4

cells for BTR87b (**Figure 6.1C**). In contrast, the addition of TGC had no measureable impact on the excised Tn916 copy number of BTR22 (**Figure 6.1C**). This pattern is consistent with the expression of *int* in BTR22, where the addition of TGC did not further elevate expression (**Figure 6.1C**). My data show that the excision of Tn916 is responsive to TGC in S613 and BTR87b, but not in BTR22. Despite the differences, both BTR strains had a highly elevated copy number for excised Tn916 when compared to S613 (**Figure 6.1C**). Additionally, the excised circular transposons were so frequent within the adapting populations, that they could be detected readily in the media outflow of the bioreactors using PCR.

Since the rate of Tn916 excision was elevated in the BTR strains, I hypothesized that the conjugation frequency of Tn916 might also be increased. To test this hypothesis Dr. Minny Bhatty, a postdoctoral research in Dr. Peter Christie's lab at the University of Texas Health Science Center at Houston, conducted conjugation assays in the absence of antibiotic using the *E. faecalis* lab strain OG1RF as a recipient. Transconjugants were not recovered when S613 was the donor; however, conjugation occurred at high frequencies when BTR strains were used as donors, with a rate of 1.5×10^{-3} and 7.0×10^{-5} transconjugants per donor cell for BTR87a and BTR22, respectively (**Figure 6.1D**). Dr. Bhatty's data show that the mutations in the 5' UTR of *tetM* result in a hyperconjugative phenotype leading to increased transfer of Tn916.

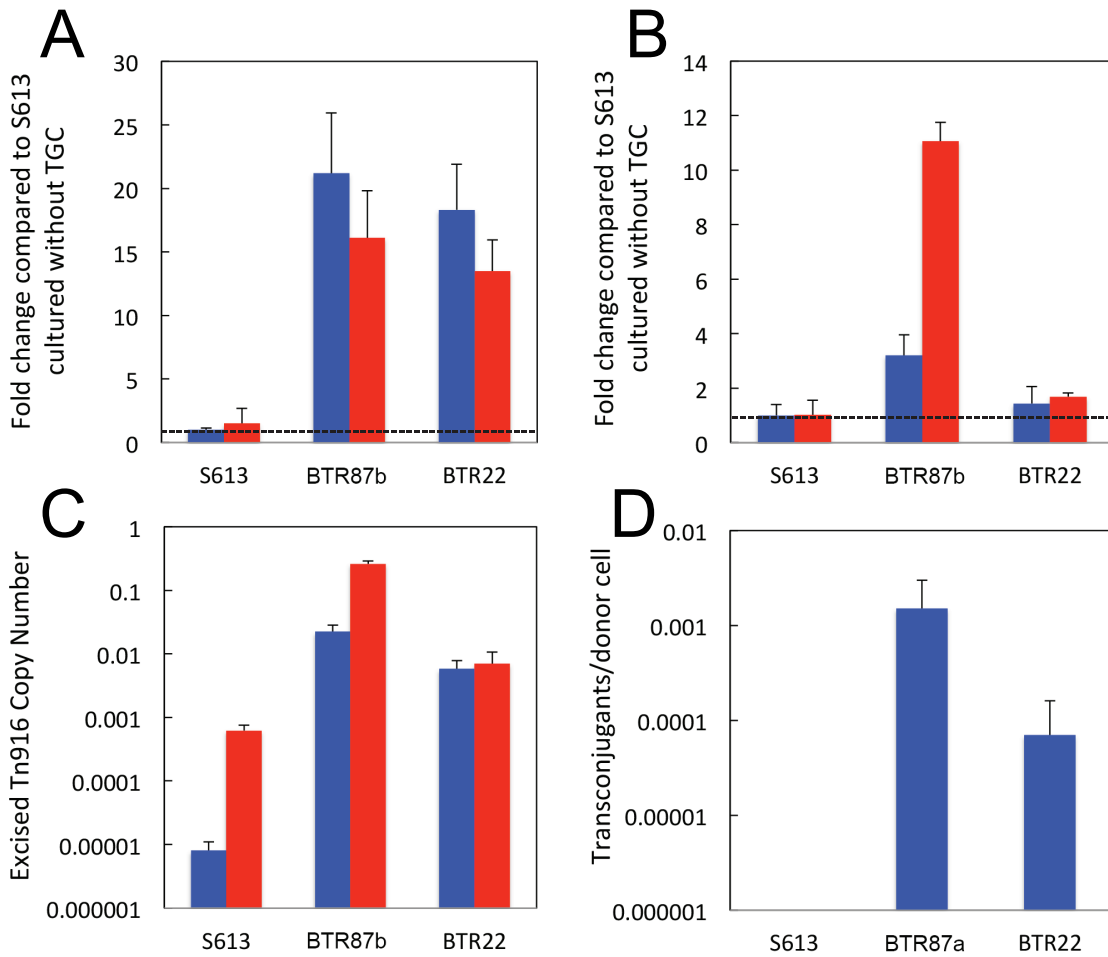


Figure 6.1: Deletions upstream of *tetM* increase *tetM* expression and Tn916 conjugation. We used a combination of qPCR and conjugation assays to determine the effects of deletions in the 5' UTR of *tetM* on *tetM* expression and Tn916 conjugation. **A)** Using qPCR, I measured the expression of *tetM* in S613 and two end-point strains, BTR87b (87-bp deletion in the 5' UTR of *tetM*) and BTR22 (22-bp deletion in the 5' UTR of *tetM*). The relative expression of *tetM* in both BTR strains was increased by more than 10-fold over S613 in both the presence (red) and absence (blue) of TGC. **B)** Since transcriptional read-through of *tetM* is leaky, I also measured the relative expression of the downstream *int* gene. The expression of *int* in the absence of TGC was elevated for both BTR87b (3-fold) and BTR22 (1.5-fold) compared to S613. The expression of *int*

was also elevated in the presence of TGC for BTR87b (11-fold) and BTR22 (1.6-fold) **C)** I used qPCR and primers that amplify the new junction associated with excised and circularized Tn916 to quantify the excised copy number of Tn916 in S613 and the BTR strains. The number of cells with excised Tn916 increases from approximately 1 in 120,000 cells for S613, to about 1 in 150 cells for BTR22 and over 1 in 4 cells for BTR87b cultured with TGC. Error bars for all qPCR data show the 95% confidence interval between three biological replicates. **D)** Conjugation assays were performed by Dr. Bhatty in triplicate using *E. faecalis* OG1RF as a recipient and S613, BTR87a, and BTR22 as donors. No conjugation was detected when S613 was used as a donor, while BTR87a and BTR22 produced conjugation frequencies of 1.5×10^{-3} and 7.0×10^{-5} transconjugants per donor cells, respectively.

6.3.2 Increased chromosomal copy number of Tn916.

Many cells acquired additional copies of the Tn916 element that carries *tetM*. The increase in Tn916 copy number is consistent with the high conjugation frequencies of the BTR strains. Initially, S613 had a single copy of Tn916, but by the end of adaptation the average cell within the population had 2.13 and 1.25 copies of Tn916 as determined by sequencing coverage in Run 1 and Run 2, respectively (**Figure 5.1A**). Although the population at the end of Run 1 had an average of 2.1 copies of Tn916, one strain, BTR37, had seven copies of Tn916 and provides a striking example of the potential for expansion of the Tn916 copy number during selection (**Table 5.1**). New Tn916 insertion sites appeared frequently during Run 1 and Run 2, with 28 and 22 different distinct insertion sites, respectively (**Figure 6.2 & Table 6.1**). While most of the new insertions sites did not reach a high frequency within the bioreactor populations, there were two insertions during Run 1 that achieved a greater than 20% frequency: an insertion into the *ycyI* gene and an intergenic site (referred to as intergenic site C) (**Figure 5.1A & Table 6.1**). Interestingly, the combined frequencies of the *ycyI* and intergenic site C insertions are approximately equal to the frequency of the 87-bp deletion throughout adaptation (**Figure 5.1A**). This indicates that the two most frequent insertions could account for the majority of the cells with the 87-bp deletion during Run 1. While the specific insertion sites could have polar effects that provide fitness advantages, I did not detect an insertion in intergenic site C during Run 2, even at very low frequencies (1%). Also, while an insertion into *ycyI* was detected during Run 2, it did not surpass 5% and dropped below the detectable range by end of the run. It is likely that acquisition of a second copy of Tn916 with the 87-bp deletion was more important than the location of the insertion. I observed that specific insertion sites did not achieve reproducible success across both runs, and the identification of 44 distinct sites is more consistent with a model in which acquiring additional copies of Tn916 is more advantageous than a specific insertion site.

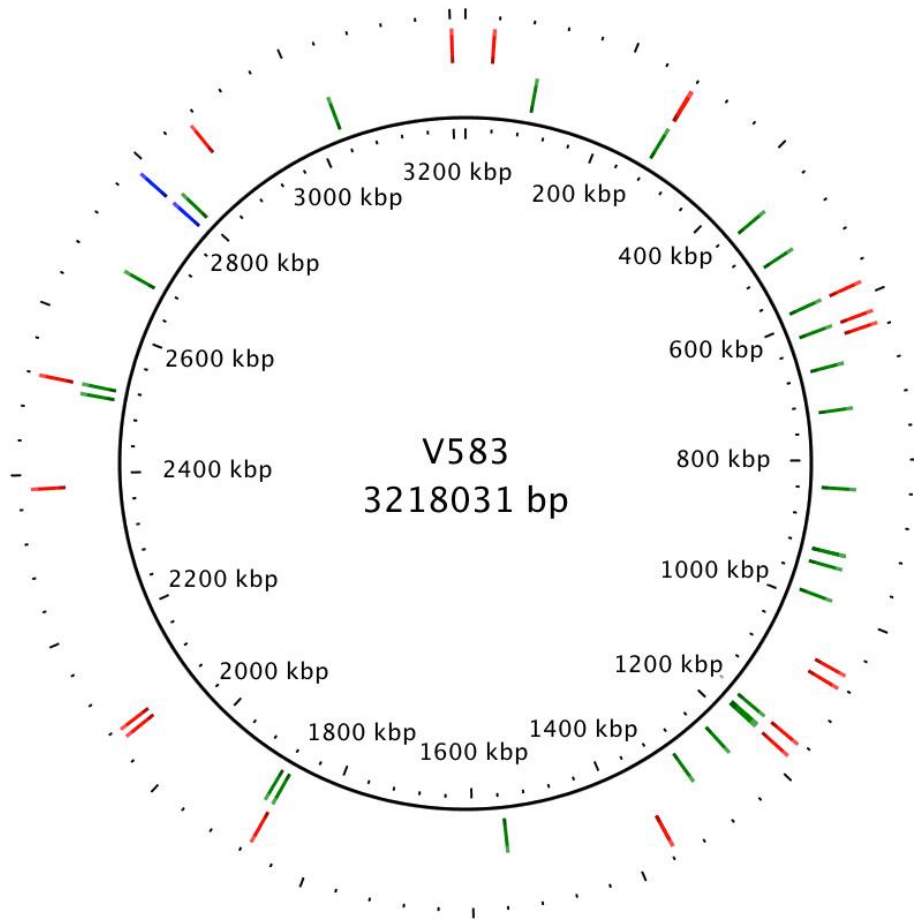


Figure 6.2: New Tn916 insertions emerged frequently in response to TGC selection. Every new Tn916 insertion site that appeared during adaptation in both populations above 1% frequency was mapped to the closed *E. faecalis* V583 genome. 28 new insertion sites were identified from experimental Run 1 (green) and 22 (red) from experimental Run 2. Several insertion sites occurred in regions of S613 absent from V583, including three sites during Run 1 and two during Run 2 (**Table 6.1**). Blue shows the original position of Tn916, which remained at 100% during both adaptation experiments. Only five insertion sites occurred in identical locations between the two experimental runs for a total of 44 unique sites. The identification of many unique insertion sites is consistent with a model where the conjugal-transfer of Tn916 facilitated the rapid spread of TGC resistance among the adapting populations.

Table 6.1: List of new Tn916 insertion sites identified in the population samples from Run 1 and 2

Run	Gene/Intergenic	Locus Tag ^a	Contig	Position	V583 Position
1	Intergenic A	N/A	779	30,972	94,670
1	Intergenic B	N/A	736	10,002	279,291
1	Phage integrase	2328	805	15,959	445,762
1	Intergenic C	N/A	790	3,755	N/A
1	Intergenic D	N/A	809	14,067	583,591
1	Intergenic E	N/A	809	53,587	620,190
1	Intergenic F	N/A	809	85,011	671,283
1	Hypothetical protein	824	746	2,478	731,474
1	Hypothetical protein	2012	785	106,463	838,940
1	Hypothetical protein	1928	785	19,546	927,138
1	Hypothetical protein	1925	785	18,134	927,572
1	Intergenic G	N/A	785	258	945,668
1	Intergenic H	N/A	751	12,994	988,626
1	<i>yycl</i>	962	749	91,333	1,163,977
1	Intergenic I	N/A	749	111,477	1,177,993
1	Intergenic J	N/A	749	116,915	1,181,679
1	Intergenic K	N/A	749	165,449	1,230,204
1	Intergenic L	N/A	749	225,810	1,290,431
1	Intergenic M	N/A	810	184,830	1,553,323
1	Intergenic N	N/A	772	23,123	1,872,853
1	Sulfatase	1580	772	34,410	1,884,260
1	ABC transport system	344	731	101,448	2,505,586
1	Intergenic O	N/A	731	95,161	2,518,299
1	Intergenic P	N/A	730	29,285	2,676,464
1	Intergenic Q	N/A	778	116,150	2,803,049
1	Intergenic R	N/A	819	185	3,034,032
1	Hypothetical protein	17	718	10,283	N/A
1	Intergenic S	N/A	798	129	507,055
2	Intergenic T	N/A	728	32,518	34,623
2	Intergenic U	N/A	736	9,904	279,392
2	<i>ktrB</i>	509	736	8,652	280,644
2	Intergenic V	N/A	809	14,067	583,591
2	Intergenic W	N/A	809	53,577	620,190
2	<i>pqqE</i>	2435	809	72,216	635,312
2	Hypothetical protein	792	744	5,603	1,065,869

Run	Gene/Intergenic	Locus Tag^a	Contig	Position	V583 Position
2	Hypothetical protein	983	749	12,899	1,082,887
2	<i>yycl</i>	962	749	91,343	1,163,977
2	Intergenic X	N/A	749	116,913	1,181,679
2	Intergenic Y	N/A	749	282,540	1,354,664
2	Intergenic Z	N/A	768	16,604	1,354,692
2	Intergenic AA	N/A	772	23,115	1,872,853
2	Intergenic BB	N/A	724	3,871	2,066,469
2	O-antigen ligase	75	724	15,092	2,077,034
2	Intergenic CC	N/A	742	161,863	2,382,841
2	Intergenic DD	N/A	731	95,162	2,518,299
2	Transcriptional regulator	1712	778	38,085	2,868,762
2	Intergenic EE	N/A	765	13,722	3,201,504
2	Intergenic FF	N/A	817	1,263	N/A
2	Intergenic GG	N/A	817	1,280	N/A

^aLocus tags were obtained from *E. faecalis* S613 file annotated by PATRIC
(<http://www.patricbrc.org>)

6.3.3 Hyperconjugation of Tn916 contributed to a rapid spread of resistance within adapting populations.

Since deletions leading to *tetM* overexpression also lead to Tn916 hyperconjugation, I wanted to know if horizontal gene transfer contributed to the spread of resistance within the populations during adaptation. At the end of Run 1 strains with different Tn916 insertions, but with the same 87-bp deletion in the 5' UTR of *tetM* (BTR87a and BTR87b) could be isolated readily (**Table 5.1**). Likewise in Run 2 strains with different Tn916 insertions, but with the same 125-bp deletion in the 5' UTR of *tetM* (BTR125a and BTR125b) were also observed (**Table 5.1**). If the deletions were passed to the different strains through clonal inheritance, then the adaptive Tn916 allele would most likely be at the same insertion site. Alternatively, if the deletions were acquired through conjugation, then the unique Tn916 alleles would likely be in copies of Tn916 at different chromosomal sites. To determine the linkages between the deletions in the 5' UTR of *tetM* and the specific Tn916 insertion site, I used long range PCR to amplify the ~ 8 kb of DNA that spans from upstream of *tetM* to the chromosome surrounding a particular insertion site. I then used Sanger sequencing of the region upstream of *tetM* to determine if a deletion was present at that specific site. I found that all clones with multiple insertion sites had the wildtype sequence present at the ancestral site and new and distinct sites of integration for the additional copies of Tn916 (**Table 5.1**). For three strains (BTR87a, BTR87b, and BTR125a) their secondary insertion sites were confirmed to carry their respective deletions. Thus BTR87a and BTR87b from Run 1 carry the 87-bp deletion at different chromosomal locations: an insertion into *ycf1* for BTR87a and an insertion into intergenic site J for BTR87b (**Table 5.1**). BTR125a and BTR125b from Run 2 carry the 125-bp deletion at different chromosomal locations: an insertion into a hypothetical O-antigen ligase for BTR125a and the copy of Tn916 at the ancestral site

for BTR125b (**Table 5.1**). The observation that the same deletions occur in copies of Tn916 at divergent chromosomal locations between strains is consistent with the role of conjugation in contributing to the rapid spread of *tetM* overexpressing alleles during TGC selection.

It is also possible that different strains acquired the same deletions as *de novo* mutations to copies of Tn916 at different insertion sites, rather than through conjugal-transfer of a copy of Tn916 carrying the deletion. To determine whether conjugation or *de novo* mutations were more likely to have resulted in the observed genotypes, I measured the spontaneous mutation rate of S613 to DAP resistance (5.1×10^{-9} mutations per cell per generation) and found that it was almost 300,000-fold lower than the newly observed conjugation frequency for BTR87a (**Figure 6.1D**). DAP resistance can be achieved by a single point mutation or by small insertions and deletions of three nucleotides (Arias, et al. 2011; Miller, et al. 2013). Larger deletions, such as the 87-bp and 125-bp deletions that eliminate the terminator stem-loop upstream of *tetM*, usually occur at a lower frequency than small deletions (Lee, et al. 2012). Thus the measured mutation rate likely overestimates the frequency at which deletions of the terminator stem-loop occur and suggests that these alleles most likely reached high frequencies by conjugation, rather than through multiple spontaneous and identical mutation events leading to deletions of the upstream regulatory regions. Furthermore, since replicate experiments consistently identified uniquely sized deletions (22, 37, 87 and 125-bp) the finding of identical deletions in copies of Tn916 at distinct chromosomal locations is more consistent with conjugal-transfer than the occurrence of *de novo* mutations (**Figure 5.1B**). Additionally, during Run 1 the 87-bp deletion surpassed 90% frequency, while the 22-bp deletion never surpassed 1% frequency within the population (**Figure 5.1A & Table 5.2**). The conjugation frequency of BTR87a is 21-fold higher than BTR22, which likely facilitated

the rapid spread of the 87-bp deletion over the 22-bp deletion (**Figure 6.1D**). Again, this is consistent with conjugation-mediated horizontal gene transfer. Therefore, conjugation contributing to the spread of alleles overexpressing *tetM* is the most parsimonious model consistent with the observed evolutionary trajectories.

6.4 Fitness cost associated with TGC resistance.

TetM has significant homology with elongation factor EF-G and dislodges tetracycline from the ribosome by occupying the binding site of EF-G on the ribosome (Connell, et al. 2003). While freeing the ribosome of antibiotic, TetM also stalls translation until TetM hydrolyzes GTP and dissociates from the ribosome, which might subsequently reduce the fitness of the cell by slowing the production of proteins. In the absence of antibiotics, production of *tetM* is thus likely to be disadvantageous. In addition, the hyperconjugative phenotype and increased Tn916 copy number that is associated with *tetM* overexpression could also impose an additional fitness cost to the cells. Therefore, we hypothesized that BTR strains with deletions in the 5' UTR of *tetM* have a higher fitness cost in the absence of antibiotic than the S10^{R53Q-Δ54-57ATHK} allele alone. This is consistent with our observation that the S10^{R53Q-Δ54-57ATHK} allele reached fixation first in both experiments despite appearing after the 125-bp deletion in the second experiment (**Figure 5.1A**). To test this hypothesis, I performed competitive fitness assays between the BTR strains and the ancestral strain S613 in the absence of antibiotics (**Figure 6.3**). As shown in Figure 6.3, the deregulation of *tetM*, increased Tn916 copy number, and highly parasexual Tn916 phenotype can impose a 14-44% fitness cost in the absence of antibiotic, while the fitness of the adaptive mutation to S10 alone was indistinguishable from S613 based on the 95% confidence interval. The low cost of the S10 mutation is

consistent with its early appearance and evolutionary success in both trials. Like many costly resistance mechanisms, regulation of *tetM* provides the best fitness benefit to the cell by allowing selective expression of these costly gene products only in the presence of antibiotic challenge (Lenski, et al. 1994; Nguyen, et al. 1989). To become resistant to TGC a much higher concentration of TetM is required and this leads to deregulation, which consequently also imposes an additional fitness cost to the cell in the absence of antibiotic selection. Thus, like many multidrug resistant pathogens, the TGC adapted strains are likely to be poorly adapted in the absence of antibiotic, but have success in environments of strong and continuing antibiotic selection such as hospital environments. Additionally, these results suggest that fluctuating exposure to TGC, rather than continuous high levels of TGC, might reduce the occurrence of TGC resistance.

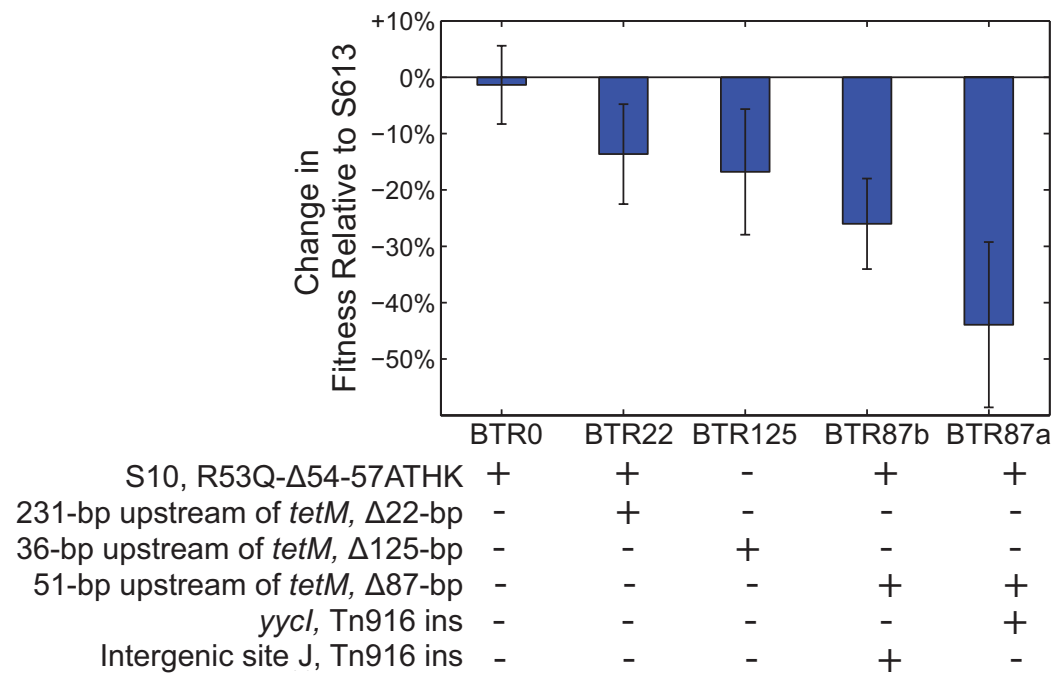


Figure 6.3: Fitness cost associated with *tetM* overexpression and increased Tn916

copy number. Competitive fitness assays were performed as described in Chapter 2 Section 2.9 between BTR strains with a deletion in the 5' UTR of *tetM* and the ancestral S613 strain in the absence of antibiotic. Error bars show the 95% confidence interval between at least four replicate assays. The fitness cost of the S10^{R53Q-Δ54-57ATHK} allele alone (BTR0) is indistinguishable from zero, whereas a fitness cost of BTR strains with deletions upstream of *tetM* was readily detected and was as high as 44% in BTR87a.

6.5 The expression of *tetM* might be regulated by a novel tetracycline-binding riboswitch.

To date, *tetM* regulation remains poorly characterized, but a transcriptional-mediated mechanism involving the ribosome has been proposed (Celli and Trieu-Cuot 1998; Su, et al. 1992). This proposed mechanism only requires the 112-bps that are immediately upstream of the *tetM* start codon (Su, et al. 1992). However, BTR22 has a deletion located 231-bp upstream of *tetM* that leads to constitutive overexpression of *tetM*, despite being more than 100-bps away from where the proposed ribosomal-mediated regulation occurs (**Figures 5.1B & 6.1A**). This suggests that the mechanism of *tetM* regulation differs from the previously proposed mechanism and involves more of the upstream 5' UTR of *tetM*. Additionally, Yao and Lu showed that *tetM* expression does not increase in response to non-tetracycline translation inhibitors, which conflicts with the previously proposed ribosomal-mediated mechanism, but that *tetM* expression does increase in the presence of spermine, a molecule that can stabilize the secondary structures of RNAs (Yao and Lu 2014). Therefore, I hypothesize that a tetracycline-binding riboswitch is present in the *tetM* leader RNA and regulates *tetM* expression, rather than a ribosomal-mediated mechanism. While tetracycline riboswitches have never been identified in wild strains of bacteria, an engineered tetracycline-binding riboswitch has been generated, demonstrating that such a riboswitch is possible (Wunnicke, et al. 2011).

To test my hypothesis I performed several preliminary experiments where I used the natural fluorescence properties of tetracycline. For these experiments I looked for changes in tetracycline fluorescence in response to the presence of increasing concentrations of *tetM* leader RNA. If tetracycline interacts with the *tetM* leader RNA,

then the addition of the RNA to a tetracycline solution might lead to an increase or decrease in fluorescence compared to tetracycline alone. Indeed, for these preliminary experiments I was able to detect increasing fluorescence as I added increasing concentrations of *tetM* leader RNA to a 2 µM tetracycline solution (**Figure 6.4A**). While these data indicate that tetracycline and the *tetM* leader RNA interact with each other, they do not reveal if this interaction is specific or if tetracycline would interact with any structured RNA. Therefore, next I repeated the same experiment, however instead of *tetM* leader RNA I added increasing concentrations of *Bacillus subtilis* *glyQS* T-Box RNA, which is a well-characterized riboswitch (**Figure 6.4B**). In this case no appreciable change in fluorescence was detected (**Figure 6.4B**). Since the T-box riboswitch was a highly structured RNA, but unrelated to the *tetM* leader RNA, these results suggest that the interaction between tetracycline and the *tetM* leader RNA might be specific. Furthermore, I setup several solutions with tetracycline and tRNAs, which also did not show any appreciable changes in fluorescence compared to tetracycline alone, further supporting my hypothesis that the interaction between tetracycline and the *tetM* leader is specific (data not shown). While these preliminary results are promising, further work is needed to confirm this hypothesis, such as detecting the saturation point of the tetracycline-*tetM* leader RNA interaction, demonstrating the biological relevance of this interaction, and determining the structure of the *tetM* leader RNA. The discovery of a riboswitch regulating *tetM* expression would be significant since this regulatory region not only controls *tetM* expression, but also the movement and mobilization of Tn916 (**Figure 1.5**). Therefore, if a tetracycline-binding riboswitch were indeed present upstream of *tetM*, then this would be the first example of a riboswitch that regulates both antibiotic resistance and the transmission of antibiotic resistance by controlling the movement of a mobile element.

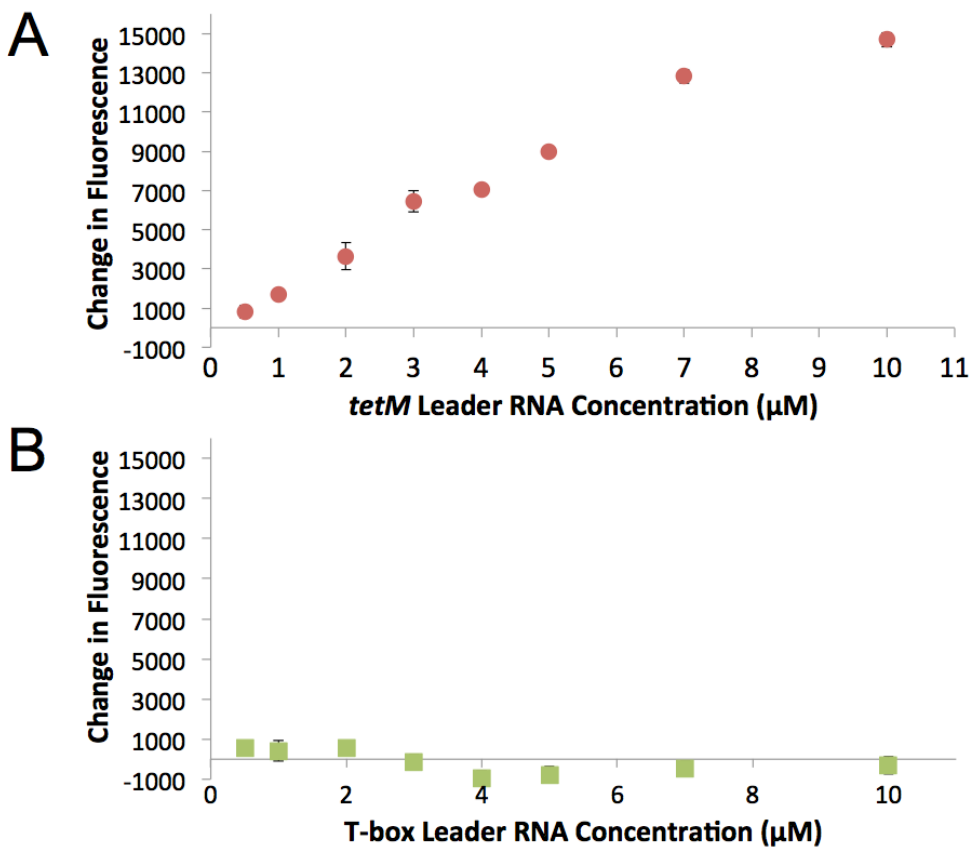


Figure 6.4: Preliminary binding studies investigating a potential tetracycline-binding riboswitch in the *tetM* leader RNA. The natural fluorescence properties of tetracycline were used to determine if tetracycline binds the *tetM* leader RNA. **A)** Fluorescence measurements were taken of samples with 2 μM tetracycline and increasing concentrations of *tetM* leader RNA. The fluorescence values of the tetracycline-RNA solutions minus tetracycline alone were plotted. Increasing fluorescence was observed with increasing *tetM* leader RNA concentrations. Complete saturation was not reached, however the affinity of the interaction appears to be in the μM range, which is consistent with a biological role. **B)** The same experiment was performed, but with increasing concentrations of a known T-box riboswitch to serve as a control. The increasing concentrations of T-box leader RNA had no appreciable affect on the fluorescence of 2 μM tetracycline, indicating that the interaction between tetracycline and the *tetM* leader RNA is specific.

6.6 Movement of hyperconjugative Tn916 in mice intestinal flora.

The Tn916 variants with deletions in the 5' UTR of *tetM* had remarkably increased conjugation rates over the wildtype Tn916 when measured *in vitro* using filter mating experiments (**Figure 6.1D**). Tn916, and related Tn916-like elements, are highly promiscuous conjugative elements that have been major contributors to the spread of tetracycline resistance among pathogens including *Enterococcus*, *Staphylococcus*, *Streptococcus*, *Clostridium*, *Bacillus*, *Escherichia*, *Neisseria*, and *Pseudomonas* (Rice 1998; Roberts and Mullany 2009). Thus, the hyperconjugative variants of Tn916 could potentially lead to the rapid spread of TGC resistance among many species of pathogen. However, it is unclear how promiscuous the TGC-resistant variants are within the gastrointestinal tract of humans or mammals, which are the natural environments of enterococci. To explore this question I performed preliminary experiments where I evaluated the conjugation of bacteria carrying the TGC-resistant Tn916 in the gastrointestinal tracts of mice. Mice were used as a model organism since they have complex and diverse microbial communities, similar to humans, and *E. faecalis* is a natural part of the mouse gastrointestinal flora (Gu, et al. 2013; Hufeldt, et al. 2010; Nguyen, et al. 2015). Specifically the C57BL/6 mouse strain was used because this strain has a well-characterized microbiome and has been used for *in vivo* conjugation studies previously with different species of bacteria (García-Quintanilla, et al. 2008; Gu, et al. 2013; Hufeldt, et al. 2010).

I fed different groups of mice a high inoculum of BTR87a cells (hyperconjugative Tn916), or *E. faecalis* S613 cells (wildtype Tn916) (**Figure 6.5A**). Some of the mice were also fed water supplemented with tetracycline for 15 days, as outlined in Figure 6.5A, to simulate the presence of antibiotic found in a hospital setting. Then I collected feces

from the mice daily and plated dilutions of the feces onto both non-selective and tetracycline-containing plates to determine how many CFUs were present (**Figure 6.5A**). On day 1, before feeding the mice any bacteria, no CFUs were detected on the tetracycline plates, indicating that tetracycline resistant bacteria were either absent or extremely rare within the mouse feces ($< 2 \times 10^6$ CFUs per gram of feces) (**Figure 6.5B**). The next day, which corresponded to 24 hours after being fed the bacterial strains, elevated CFUs in the feces were detected on both the non-selective agar and the tetracycline agar plates, confirming that the mice had received a high does of viable *E. faecalis* (**Figure 6.5B**). However, surprisingly the tetracycline-resistant CFUs per gram of feces quickly began dropping and by day 3 of the experiment were hardly detectable despite the mice still being fed tetracycline (**Figure 6.5B**). These results indicate that the S613 and BTR87a strains were not able to establish in the flora of the mice despite the selective pressure of tetracycline.

I also extracted microbial genomic DNA from the mice fecal samples to monitor the movement of Tn916 using molecular techniques. With PCR I was able to detect *tetM* in the feces collected on day 2 from all four experimental groups. However, by as early as day 5 and 3, I could no longer detect *tetM* in the feces from the mice fed or not fed tetracycline, respectively. Similar to the CFU results, these data further indicate that the S613 and BTR87a strains did not establish in the flora of the mice. Interestingly, Gilmore *et al.* found that the native human gut flora actively kills clinical *E. faecalis* V583 cells (Gilmore, et al. 2015). Therefore, incompatibility with the native mouse flora is one possible reason the *E. faecalis* S613 and BTR87a strains were not able to colonize the mice gastrointestinal tracts. Additionally, the antibiotic concentration may not have been high enough to select for colonization of the *E. faecalis* strains. Future experiments are needed to explore these possibilities.

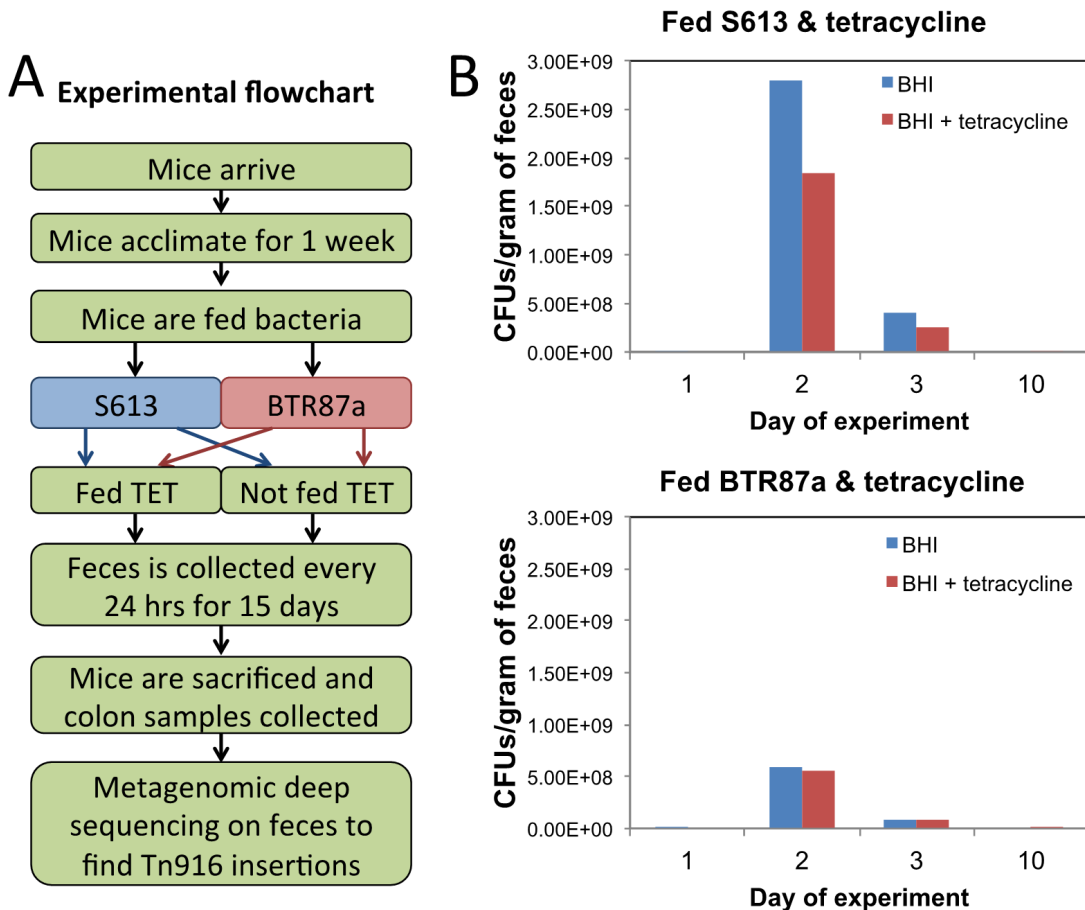


Figure 6.5: Preliminary experiments evaluating the movement of a TGC-resistant hyperconjugative variant of Tn916 in mouse gastrointestinal flora. A) Flowchart

outlining the preliminary experimental workflow. First the mice arrived at the facilities and were given one week to acclimate. Next the mice were fed an inoculum of *E. faecalis* cells (10^9 CFUs) in their water on experimental day 1. Two groups of mice were fed *E. faecalis* S613 (wildtype Tn916) and two groups of mice were fed *E. faecalis* BTR87a (TGC-resistant hyperconjugative Tn916). Additionally, one of the S613 groups and BTR87a groups were fed water supplemented with tetracycline (TET) daily. Thus in total there were four experimental groups: fed S613 with or without tetracycline and fed BTR87a with or without tetracycline. Starting on day 1 samples of feces from each of the four groups was collected daily. Portions of the fecal samples collected from the mice

were suspended in saline and plated onto non-selective BHI agar (total CFUs) and tetracycline supplemented BHI agar (Tn916 carrying CFUs). Microbial DNA was extracted from the fecal samples to analyze the movement of Tn916 using molecular techniques. **B)** I determined the number of CFUs present in the fecal samples collected from the two experimental groups that were fed tetracycline. Plotted are the results from experimental days 1, 2, 3 and 10. On day 1, before the mice were fed any bacteria, both groups had $\sim 2 \times 10^6$ CFUs per gram of feces on non-selective BHI agar and no CFUs on tetracycline-supplemented agar. This indicates that tetracycline-resistant bacteria were not detectable in the feces before the mice were fed the strains. On day 2, twenty-four hours after being fed S613 or BTR87a, the CFUs per gram of feces dramatically increased for the two groups on both BHI agar and BHI agar supplemented with tetracycline. This indicates that the mice did indeed receive a high inoculum of tetracycline-resistant enterococci cells. However, as early as day 3 the CFUs per gram of feces began dropping dramatically and by day 10 the CFUs were close to the pre-inoculation levels. These results indicate that the S613 and BTR87a cells did not effectively colonize the mice gastrointestinal tracts despite the selective pressure of tetracycline. The CFUs present in the feces of the mice not fed tetracycline have yet to be determined.

6.7 Discussion.

Using quantitative experimental evolution, I have identified mechanisms of resistance that are likely to occur in the clinic. I showed that the adaptive alleles arising in response to TGC selection occur in the 5' UTR of *tetM* and result in increased expression of *tetM*. In addition, mutations impacting the regulation of *tetM* also resulted in an increase in the excision of Tn916 via leaky transcriptional read-through to the downstream *xis* and *int*. The high rate of excision leads to the constitutive conjugation of Tn916, which likely contributed to rapid spread of the resistance allele throughout the population during adaptation. This represents the first example of mutations that simultaneously confer resistance to an antibiotic and lead to constant conjugal-transfer of the resistance allele. In our bioreactors the rampant parasexual population dynamics allowed for Tn916 to increase in copy number and jump into the genomes of the entire population (**Figure 6.6**). While an interesting observation, the hyperconjugation of Tn916 is worrisome as it suggests that TGC resistance could spread rapidly among not just *E. faecalis*, but other pathogens as well. Tn916, and related Tn916-like elements, have been identified in a wide-range of species and undergo conjugal-transfer between species (Boguslawska, et al. 2009; Haack, et al. 1996; Hespell and Whitehead 1991; Wasels, et al. 2014). In addition, some Tn916-like elements carry alleles that confer resistance to non-tetracycline antibiotics, indicating that this hyperconjugation mechanism could potentially play a role in spreading resistance to other antibiotics (Haack, et al. 1996). Furthermore, the Tn916 conjugation proteins can mobilize other elements, such as non-conjugal plasmids, which suggests that hyper-conjugative Tn916 could potentially facilitate the spread of markers located outside of Tn916 (Naglich and Andrews Jr 1988). These findings show how the rapid spread of resistance among enterococci, and likely other pathogens, can be achieved readily by the release of antibiotics into an environment.

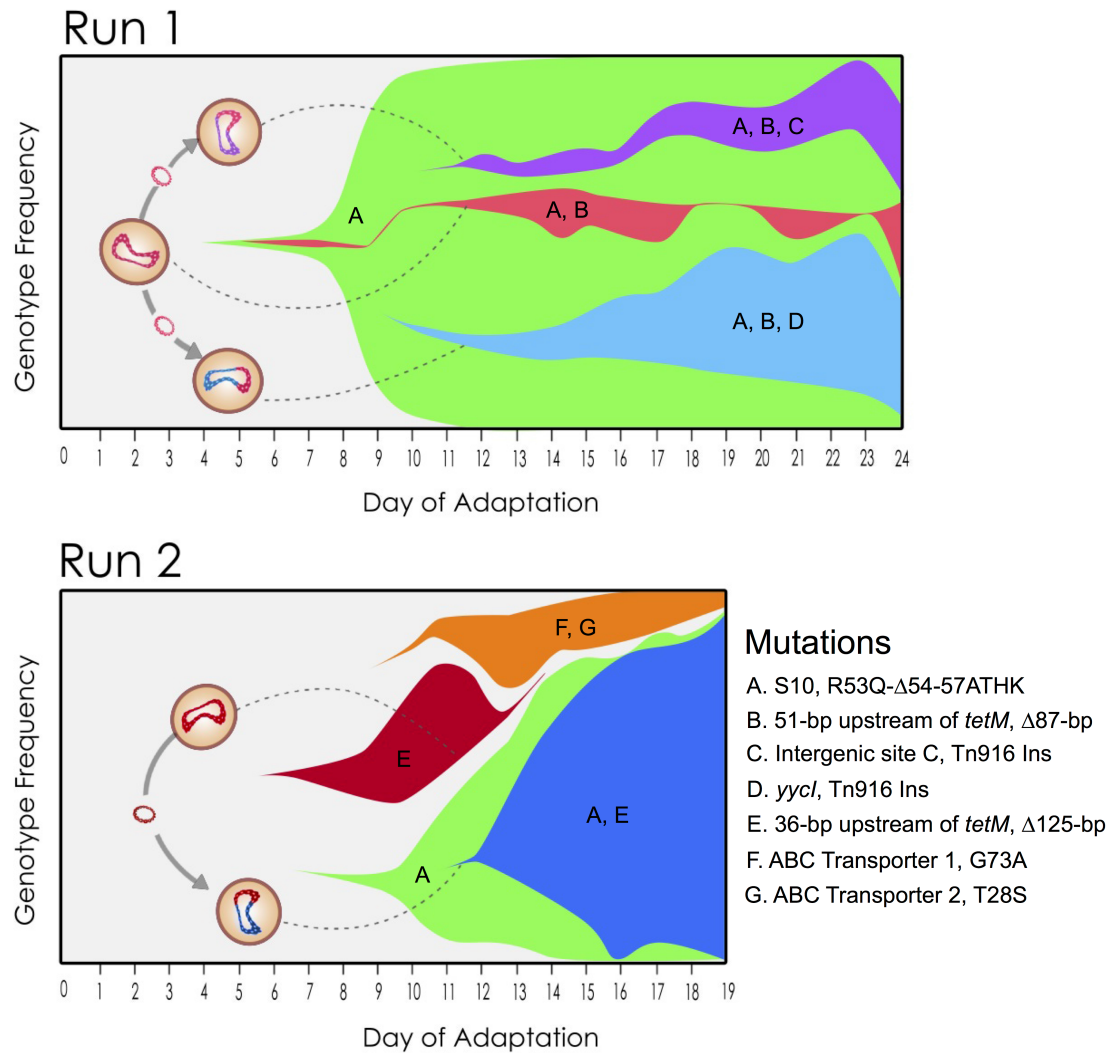


Figure 6.6: Tigecycline selection converts the population to a rampant parasexual phenotype. Fisher-Muller diagrams outlining models for the role of conjugation during adaptation to TGC resistance. These plots show the simplest adaptive trajectories consistent with the deep sequencing of the populations as a function of time and the genome sequencing of isolates from the end of adaptation. Dashed lines indicate the hypothesized conjugation incidences when a copy of Tn916 with a deletion was likely transferred to a genome carrying the S10^{R53Q- Δ 54-57ATHK} allele, thus creating successful genotypes.

Chapter 7: The role of S10 mutations in tigecycline resistance across many different species.

This chapter is reproduced from Beabout, et al. 2015 *Antimicrob Agents Chemother*.

7.1 Introduction.

There have been a few reports, including one from our group, suggesting that mutations in *rpsJ*, the gene that encodes the ribosomal S10 protein, may confer reduced susceptibility to TGC, often in conjunction with other resistance alleles. Interestingly, these reports included both Gram-positive and -negative pathogens suggesting that mutations to *rpsJ* may provide a general mechanism for reduced TGC susceptibility. Due to the emergence of *rpsJ* mutations in response to TGC exposure among a variety of Gram-positive and -negative species, we hypothesized that *rpsJ* is a general target of TGC resistance across many species. To explore this hypothesis, we selected several Gram-positive and -negative strains and used experimental evolution to adapt the populations *in vitro* to TGC. We used Sanger sequencing of the *rpsJ* gene of individual clones isolated from the evolved populations to evaluate the frequency and position of TGC associated S10 mutations within the three-dimensional structure of the ribosome. We determined that 35 out of 47 replicate populations had clones with a mutation in *rpsJ*, showing that mutations in *rpsJ* commonly occur in response to TGC exposure.

7.2 Flask adaptation of *Enterococcus faecium*, *Staphylococcus aureus*, *Acinetobacter baumannii* and *Escherichia coli* to tigecycline.

To determine whether acquisition of mutations in *rpsJ* in response to *in vitro* exposure to TGC occurs broadly in Gram-positive and -negative species, we used experimental evolution to select for populations with reduced TGC susceptibility. Sanger sequencing of *rpsJ* was then used to identify the variety and frequency of adaptive mutations. In each experiment at least eight colonies were selected from each replicate population. Within *rpsJ*, mutations were only identified in a small loop of the S10 protein comprised of residues 53-60. Remarkably, of the 47 replicate populations across four species and five strains, 22 had at least one clone with a mutation at position 57 suggesting this position within S10 is strongly selected for adaptation to TGC (**Figures 7.1 & 7.2**).

7.3 Identification of S10 alleles in tigecycline adapted strains.

7.3.1 Adaptation of *E. faecium* R499 to tigecycline.

Rotation graduate student Bárbara de Freitas Magalhães adapted ten populations of *E. faecium* R499 with a starting MIC of 0.0313 µg/mL TGC to growth at a final concentration of 0.18 µg/mL TGC over the course of thirty days. All colonies selected from six different populations were found to have a D60Y mutation in S10 (**Figure 7.1**). Interestingly, all colonies from one population had a twelve-nucleotide deletion in *rpsJ* ($S10^{R53Q-\Delta 54-57ATHK}$) that is identical to a deletion I identified in strains of *E. faecalis* S613 that were adapted to TGC resistance using the bioreactor (**Table 5.1, Figure 7.1**) (Beabout, et al. 2015b). The net effect of the deletion is to remove residues 54-57 but

restore the reading frame of the S10 protein and change arginine-53 to glutamine. TetM is a ribosomal protection protein that dislodges tetracyclines from the ribosome and is one of the most common tetracycline-resistance mechanism found among enterococci (Lopez, et al. 2009). Interestingly, I showed that overexpression of *tetM* or amplification of gene copy number can produce TGC resistance in *E. faecalis* during experimental evolution (see Chapter 6) (Beabout, et al. 2015b). Using PCR we established that *E. faecium* R499 does not carry the *tetM* tetracycline resistance gene. Additionally, MIC testing confirmed that R499 is susceptible to tetracycline (MIC = 0.25 µg/mL) and no genes with sequence homology to *tetM* were identified in the R499 reference sequence (GCA_000294875.1).

7.3.2 Adaptation of *E. faecium* 105 to tigecycline.

To determine if *rpsJ* mutations arise during TGC exposure when TetM is present we selected a strain of *E. faecium* with *tetM*. Lab member and graduate student Amy Prater identified the presence of *tetM* using PCR and confirmed that *E. faecium* 105 is resistant to tetracycline (MIC = 64 µg/mL). Ms. Prater adapted seven populations of *E. faecium* 105 with a starting TGC MIC of 0.0313 µg/mL to growth at a final concentration of 0.18 µg/mL TGC over the course of eighteen days. Colonies isolated from six of the seven populations had a mutation in *rpsJ*, which demonstrates that *rpsJ* mutations can arise in *E. faecium* strains that carry *tetM* (**Figure 7.1**). All colonies selected from one population retained the ancestral *rpsJ* sequence.

7.3.3 Adaptation of *S. aureus* MRSA131 to tigecycline.

Ms. Prater also adapted eleven populations of *S. aureus* MRSA131 with a starting MIC of 0.5 µg/mL TGC to growth at a final concentration of 11.2 µg/mL TGC over the course

of seventeen days. Among the sampled colonies amino acid K57 of S10 was the most frequently mutated position (**Figure 7.1**). The second most frequently mutated position was D60 of S10 (**Figure 7.1**). Interestingly, two populations had colonies with a double mutation in S10 (**Figure 7.1**).

7.3.4 Adaptation of *A. baumannii* AB210 to tigecycline.

Rotation graduate student Thomas Clements adapted ten populations of *A. baumannii* AB210 with a starting MIC of 0.5 µg/mL TGC to growth at 19 µg/mL TGC over the course of fifteen days. Two of the ten populations had colonies with S10 mutations (**Figure 7.1**). All colonies selected from one population carried a V57L allele, and all colonies from another population carried a V57I mutation (**Figure 7.1**) suggesting that all cells in these two populations had acquired an adaptive mutation to S10. Interestingly, in another study from our lab the V57L and V57I alleles were also identified in *A. baumannii* AB210 clones that were adapted to TGC resistance using our bioreactor (**Figure 7.1**) (Hammerstrom, et al. 2015). Colonies selected from the remaining populations retained the ancestral *rpsJ* sequence.

7.3.5 Adaptation of *E. coli* BW25113 to tigecycline.

Lab member and graduate student Anisha Perez adapted nine populations of *E. coli* BW25113 with a starting MIC of 1 µg/mL TGC to growth at a final concentration of 5.6 µg/mL TGC over the course of 24 days. All colonies selected from two populations had a V57L mutation and all colonies sampled from another population had a V57D mutation (**Figure 7.1**). Colonies selected from the remaining populations retained the ancestral *rpsJ* sequence.

Figure 7.1: S10 mutations identified in strains that underwent TGC exposure.

Species and Strain	S10 Protein Sequences (residues 53-60) ¹								Independent Populations with mutation ²
	I	S	P	H	V	N	K	D	
<i>E. coli</i> BW25113					I				2 of 9
					D				1 of 9
									6 of 9
<i>A. baumannii</i> AB210	T	S	P	H	V	N	K	D	1 of 10
					L				1 of 10
					I				8 of 10
<i>K. pneumoniae</i> KP4-R	I	S	P	H	V	N	K	D	Previous study (Villa, et al. 2014) <i>in vivo</i> mutant
					L				
<i>S. aureus</i> MRSA131	R	A	V	H	K	Y	K	D	5 of 11
					M				4 of 11
					E				3 of 11
						M			1 of 11
						F			1 of 11
						Q	F		1 of 11
							M		1 of 11
							S		1 of 11
<i>E. faecalis</i> S613	R	A	T	H	K	Y	K	D	Previous study (Beabout, et al. 2015b)
	Q	Δ	Δ	Δ	Δ				
<i>E. faecium</i> 105	R	A	T	H	K	Y	K	D	2 of 7
		E	A						1 of 7
				R	N				1 of 7
					E				1 of 7
					R				1 of 7
							Y		1 of 7
						S			1 of 7
									1 of 7
<i>E. faecium</i> R499	R	A	T	H	K	Y	K	D	6 of 10
	Q	Δ	Δ	Δ	Δ				1 of 10
					E				1 of 10
					R	D			1 of 10
						D			1 of 10
						S			1 of 10
<i>E. faecium</i> Aus004	R	A	T	H	K	Y	K	D	Previous study (Cattoir, et al. 2014)
							Y		1 of 1
<i>E. faecium</i> HM1070	R	A	T	H	K	Y	K	D	Previous study (Cattoir, et al. 2014)
							Y		2 of 2
<i>E. faecium</i> EF16	R	A	T	H	K	Y	K	D	Previous study (Cattoir, et al. 2014) <i>in vivo</i> mutant
					E				

¹Δ indicates a deleted residue. ²Eight colonies were sampled from each population. For some populations multiple types of *rpsJ* mutations were identified between different clones, and therefore the number of observations among the different mutations is sometimes greater than the total number of populations.

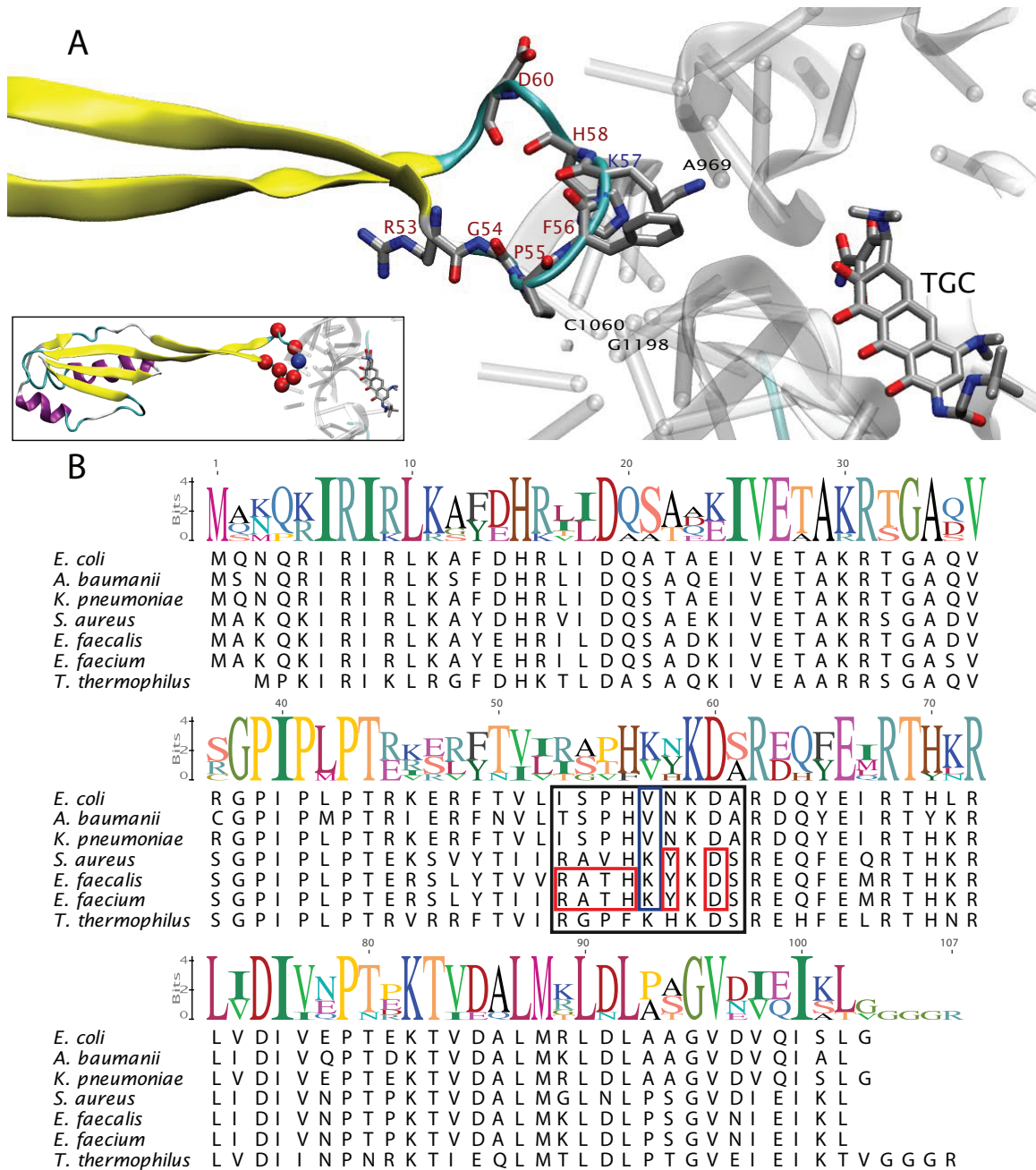


Figure 7.2: TGC selects for mutations on a loop of S10 that is in close proximity to the 16S rRNA that composes the TGC binding pocket. **A)** An image of the crystal structure of TGC bound to the *Thermus thermophilus* ribosome (PDB 4G5T) (Jenner, et al. 2013). Labeled amino acids indicate positions on the loop of S10 where mutations were identified in Gram-positive species (red) or both Gram-positive and -negative species (blue). For clarity, the amino acid numbering corresponds to the respective

positions of the residues in the *E. coli* S10 sequence and only rRNA structure (gray) proximal to the loop is shown. The small insert shows the entire structure of S10 with colored spheres at the α -carbon of residues where mutations were identified in Gram-positive (red) or both Gram-positive and -negative (blue). **B)** An alignment of the *T. thermophilus* S10 sequence and the susceptible S10 sequences for species where mutations in S10 have been identified in response to TGC adaptation. The sequence logo shows the S10 consensus sequence. The black box outlines the residues that compose the loop structure (53 – 61). The blue and red boxes outline the residues where mutations were identified in Gram-positive species (red) or both Gram-positive and -negative species (blue).

7.4 Validation of S10 mutation in conferring resistance.

While the data presented in Figure 7.1 and by Cattoir *et al.* and Villa *et al.* shows a correlation between mutations in *rpsJ* and reduced TGC susceptibility, there has been no direct confirmation that mutations to *rpsJ* alone are able to significantly decrease susceptibility (Cattoir, et al. 2014; Villa, et al. 2014). To confirm the causal link between adaptive mutations in *rpsJ* to reduced TGC susceptibility, I used whole genome sequencing to isolate a strain of *E. faecalis* S613 that contained only a mutation to *rpsJ* (**Table 5.1**) (Beabout, et al. 2015b). Using comparative whole genome sequencing between S613 and clones isolated from an adapted bioreactor population I identified a strain with a single mutation to *rpsJ*, hereafter referred to as S613(S10^{R53Q-Δ54-57ATHK}) (also known as BTR0 in Table 5.1). I used the agar-dilution technique to measure the MICs of TGC, tetracycline (TET), minocycline (MIN) and daptomycin (DAP) against S613 and S613(S10^{R53Q-Δ54-57ATHK}) (**Table 7.1**). The TGC MIC against S613(S10^{R53Q-Δ54-57ATHK}) was 4-fold higher than S613 (**Table 7.1**). Importantly, the TGC MIC against S613(S10^{R53Q-Δ54-57ATHK}) was greater than the FDA non-susceptibility breakpoint (>0.25 µg/mL TGC) and equal to the EUCAST resistance breakpoint ($\geq 0.5 \mu\text{g/mL}$ TGC) (**Table 7.1**). S613(S10^{R53Q-Δ54-57ATHK}) also had higher MICs than S613 for TET and MIN, suggesting that mutation of S10 confers resistance to multiple classes of tetracyclines (**Table 7.1**).

Table 7.1: MICs against four *E. faecalis* strains determined by CLSI agar dilution method.

	TGC	MIN	TET	DAP
OG1RF	0.125	2	4	0.5
R712	0.125	8	32	8
S613	0.125	8	32	0.5
S613(S10^{R53Q-Δ54-57ATHK})	0.5	16	64	0.5

7.5 Mutations to S10 did not alter growth rates in the absence of antibiotic suggesting a low fitness cost.

To further characterize the impact of the $S10^{R53Q-\Delta54-57ATHK}$ allele on growth in the presence of TGC, I evaluated the growth rates of S613 and S613($S10^{R53Q-\Delta54-57ATHK}$) in the presence of different TGC concentrations (0, 0.031, 0.063, 0.125, and 0.25 µg/mL) (**Figure 7.3**). In the absence of antibiotic S613($S10^{R53Q-\Delta54-57ATHK}$) and S613 had similar growth rates, suggesting that the $S10^{R53Q-\Delta54-57ATHK}$ allele does not confer a serious fitness cost (**Figure 7.3A**). In the presence of TGC, S613($S10^{R53Q-\Delta54-57ATHK}$) was able to grow better than S613 (**Figure 7.3B-E**). At 0.125 and 0.25 µg/mL TGC no growth was detected for S613, while S613($S10^{R53Q-\Delta54-57ATHK}$) achieved a high level of growth (**Figure 7.3D-E**). These data demonstrate that mutations in *rpsJ* can increase resistance above the clinical breakpoints and suggests that such mutations would be persistent in the absence of antibiotic, as the $S10^{R53Q-\Delta54-57ATHK}$ allele does not burden the growth rate of the cell under non-selective conditions. These results are also consistent with the fitness assays in Figure 6.3, which showed that the S613($S10^{R53Q-\Delta54-57ATHK}$) strain (also known as BTR0) had a low fitness cost compared to the susceptible S613 strain.

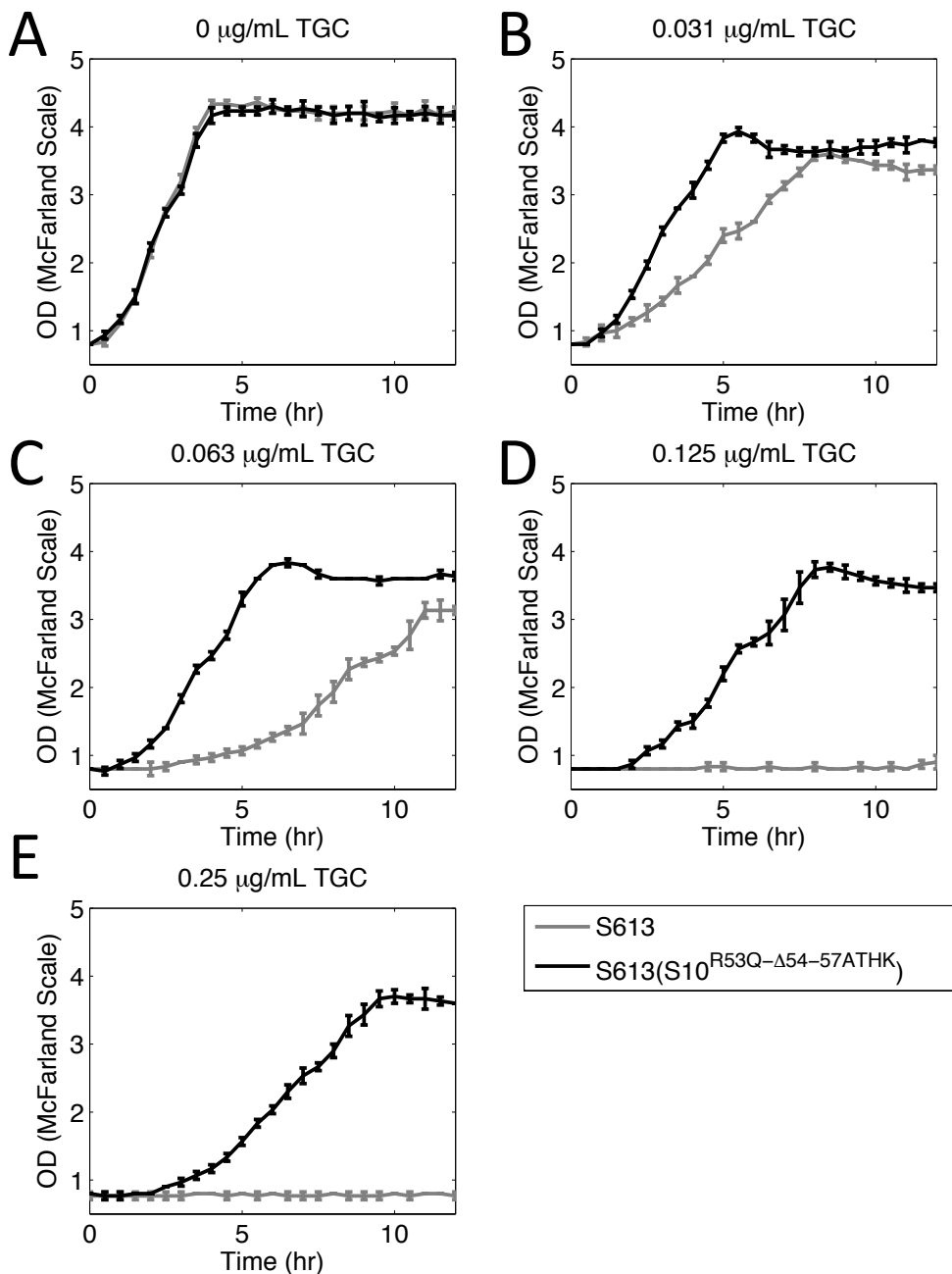


Figure 7.3. The S10^{R53Q-Δ54-57ATHK} mutation in *E. faecalis* confers improved growth in the presence of TGC. The growth of S613 and S613(S10^{R53Q-Δ54-57ATHK}) were measured for twelve hours at **A)** 0 µg/mL TGC, **B)** 0.031 µg/mL TGC, **C)** 0.063 µg/mL TGC, **D)** 0.125 µg/mL TGC and **E)** 0.25 µg/mL TGC. The average of three replicates performed in parallel was plotted with the standard deviation as the error bars.

7.6 Discussion.

Using *in vitro* experimental evolution, the species included in this study were all adapted to growth in TGC concentrations well above their respective resistance or non-susceptibility cutoffs. We have demonstrated that changes in *rpsJ* alone are able to confer increased resistance to TGC in *E. faecalis*. Additionally, we report the first identification of *rpsJ* mutations associated with decreased TGC susceptibility in *S. aureus*, *A. baumannii* and *E. coli* and expanded spectrum of novel *rpsJ* mutations in *E. faecium*. Including previous studies, mutations in *rpsJ* have been identified in a total of six different species after undergoing TGC adaptation; three Gram-negative (*E. coli*, *A. baumannii*, and *K. pneumonia*) and three Gram-positive (*S. aureus*, *E. faecalis*, and *E. faecium*) (Figure 7.1) (Cattoir, et al. 2014; Villa, et al. 2014). Comparable mutations in S10 have also been found in tetracycline resistant *Bacillus subtilis* (Akanuma, et al. 2013), *Neisseria gonorrhoeae* (Hu, et al. 2005) and *S. aureus* (Wozniak, et al. 2012). Combined, these data strongly suggest that the ribosomal S10 protein is a general target for decreased TGC susceptibility across many species of bacteria.

Lab members Anisha Perez and Troy Hammerstrom made several unsuccessful attempts to perform allelic replacement of resistance associated *rpsJ* alleles into the susceptible ancestral strains of *E. coli* BW25113 and *A. baumannii* AB210, respectively. In addition, Cattoir *et al.* report that attempts to perform allelic replacement at this locus in *E. faecium* Aus0004 also failed (Cattoir, et al. 2014). This could be due to the essential role of S10 in translation and transcription; S10 is both a component of the 30S ribosomal subunit and an important transcription factor involved in lambda N-mediated antitermination (Squires and Zaporojets 2000). Therefore, even though the S10 alleles impose a low fitness cost, the transient interference with this locus during allelic

replacement might have a negative effect on lambda N-mediated antitermination and translation. In the absence of successful allelic replacement I tested the effect of *rpsJ* mutations directly using an evolved strain with only a single mutation in *rpsJ*, as determined by whole genome sequencing, and showed that it had an elevated MIC of 0.5 µg/mL TGC compared to 0.125 µg/mL TGC for the susceptible ancestral strain (Beabout, et al. 2015b). This shows that a mutation to S10 alone can reduce susceptibility to TGC. In addition, the high reproducibility of mutant S10 alleles across strains and replicate populations in response to TGC exposure suggests strongly that these mutations commonly play a role in conferring reduced susceptibility to TGC. Overall, we passaged four species (five strains) against TGC and identified mutations to *rpsJ* in 35 of 47 populations and observed six cases where different *rpsJ* mutants were isolated from a single population (**Figure 7.1**).

Importantly, all of the identified mutations have occurred on the tip of an extended loop of the S10 protein that is in close proximity to the 16S rRNA TGC binding site (**Figure 7.2**) (Jenner, et al. 2013). The S10 protein does not appear to make any direct contacts to the TGC binding pocket, as none of the atoms are close enough to make either van der Waals contacts or hydrogen bonds. S10 does contact the 16S rRNA that comprises part of the TGC binding pocket. Thus, altering the structure of the S10 loop likely affects the conformation or conformational dynamics of the 16S rRNA, which in turn could reduce the binding affinity of TGC for the ribosome. Alternatively, the adaptive mutations to S10 that reduce TGC susceptibility might favor tRNA entry and binding to the ribosome, reducing the translational inhibition produced by TGC. In either model mutations to *rpsJ* that reduce TGC effectiveness appear to be broadly observed in both Gram-positive and -negative organisms suggesting it is a general target for the evolutionary selection of mutations leading to reduced TGC susceptibility.

Amino acid position 57 of S10 was a commonly mutated site among both Gram-positive and -negative species after undergoing TGC exposure (**Figure 7.1**). Interestingly, in the Gram-negative species, V57 usually mutated to either a leucine or an isoleucine, with the exception of one population of *E. coli* BW25113 where a S10^{V57D} allele was observed. In contrast, the mutations affecting K57 of the Gram-positive species showed greater variability with no clear pattern (**Figure 7.1**). Also, in the Gram-negative species, the identified S10 mutations all affected position 57, whereas the Gram-positive species displayed more genetic flexibility with the identification of different mutations at the very tip of the extended loop (positions 53-60) (**Figure 7.1**). Particularly, in the Gram-positive species, D60 of S10 was frequently mutated to a tyrosine. In this study the S10^{D60Y} allele was independently isolated from ten different populations and the same allele was also identified in a previous study where *E. faecium* was also adapted *in vitro* to TGC (Cattoir, et al. 2014) (**Figure 7.1**). Together, these data suggest that mutations at position 57 of S10 in both Gram-negative and -positive species and for S10^{D60Y} in Gram-positive species are important to reduced TGC susceptibility.

TGC maintains high efficacy against strains that carry the tetracycline resistance determinant and ribosomal protection protein TetM. However overexpression of *tetM* has been linked to TGC resistance in *E. faecalis* (see Chapter 6) (Beabout, et al. 2015b). Therefore, we adapted two strains of *E. faecium* to TGC: one that carries *tetM* (*E. faecium* 105) and one without *tetM* (*E. faecium* R499). Both *E. faecium* strains had the same MIC before adaptation (0.0313 µg/mL TGC), but the strain that lacked *tetM* required 12 additional passages over the *tetM* carrying strain to reach growth at 0.18 µg/mL TGC. This observation suggests that the presence of *tetM* could play a potentiating role in the adaptation of *E. faecium* to TGC non-susceptibility.

Importantly, here we present novel data showing that mutation of *rpsJ* alone can confer non-susceptibility to TGC and that *rpsJ* mutations in *S. aureus*, *A. baumannii* and *E. coli* emerge repeatedly after exposure to TGC. Additionally, we report an expanded spectrum of novel *rpsJ* mutations in *E. faecium* exposed to TGC. The emergence of these alleles in a diverse range of species strongly suggests that mutation of *rpsJ* is a general strategy to achieve decreased susceptibility to TGC. Previous studies identified mutations affecting the loop of S10 in *E. faecium* and *K. pneumoniae* that developed non-susceptibility to TGC in patients undergoing TGC therapy, which highlights the relevance of these mutations to the clinical setting (Cattoir, et al. 2014; Villa, et al. 2014). My observation that the growth rates of *E. faecalis* S613(S10^{R53Q-Δ54-57ATHK}) are comparable to the original susceptible strain in the absence of antibiotic suggests that there is little fitness cost incurred by this adaptive mutation to the organism and that this would be a stable and persistent allele within the population once established. Therefore, we propose that the identification of *rpsJ* mutations could potentially serve as a useful marker for detecting TGC non-susceptibility in a variety of pathogens.

Chapter 8: Discussion, conclusions, and future work.

8.1 Discussion and conclusions.

I used quantitative experimental evolution to identify the most important alleles necessary for VRE to adapt to TGC resistance. At the start of these studies no candidate alleles or loci for TGC resistance had been identified in enterococci. Here I found that mutations at two loci were essential for acquiring TGC resistance in VRE, including deletions in the 5' UTR of *tetM*, that increase *tetM* expression, and mutation of the ribosomal S10 protein (Beabout, et al. 2015a; Beabout, et al. 2015b). Importantly, several studies have identified similar mutations in clinical isolates that became resistant in patients, demonstrating the ability of our experimental pipeline to accurately predict relevant resistance mechanisms (Cattoir, et al. 2014; Fiedler, et al. 2015; Niebel, et al. 2015). By elucidating the most important alleles for VRE to acquire resistance to TGC, I have gained insights that can be used to take a preemptive approach to limiting and avoiding resistance. For example, if an inhibitor of *tetM* expression or the TetM protein were developed, such an inhibitor could be administered to a patient undergoing TGC therapy to reduce the chances of resistance from emerging during treatment.

Here I found that increased levels of TetM conferred a high level of TGC resistance in enterococci. Deletions upstream of *tetM* that led to constitutive overexpression of *tetM* were very successful in both of my replicate bioreactor populations (**Figures 5.1 & 6.1**). Additionally, many of the strains isolated from the end of my bioreactor runs had

increased chromosomal copies of the Tn916, including BTR37, which had seven copies of Tn916 and thus seven copies of *tetM* (**Table 5.1**). Consistent with these results, Fiedler, *et al.* found that clinical VRE isolates with resistance to TGC had increased copy numbers of a plasmid that carried *tetM* and *tetL* and that as the VRE cells lost copies of this plasmid they became increasingly susceptible to TGC (Fiedler, *et al.* 2015). Their group also showed that *tetM* or *tetL* were able to confer resistance to TGC when overexpressed in *Listeria monocytogenes* (Fiedler, *et al.* 2015). These results further support the significance of *tetM* in conferring resistance to TGC. Additionally, they expand on my results by showing that other tetracycline-resistance alleles, in this case the tetracycline-efflux pump *tetL*, are capable of conferring resistance to TGC when more copies of the gene are acquired (Fiedler, *et al.* 2015). While not all enterococci harbor a tetracycline-resistance determinant, the vast majority of clinical isolates do, with a high percentage of isolates specifically carrying the *tetM* allele. For example, among twenty-eight clinical TGC-resistant enterococci that were surveyed by Fiedler *et al.*, all carried the *tetM* allele and ten also carried *tetL* (Fiedler, *et al.* 2015). Combined, these results support our hypothesis that despite the high efficacy of TGC, the ubiquitous nature of tetracycline-resistance alleles could undermine the antibiotics long-term usefulness.

In this thesis I also showed that mutations in the *rpsJ* gene, which encodes for the ribosomal S10 protein, play an important role in achieving TGC resistance in enterococci and a variety of Gram-positive and Gram-negative species (**Figure 7.1**). More recently, several studies have identified mutations in the ribosomal S10 protein among clinical isolates with decreased susceptibility to TGC. Niebel *et al.* sequenced the genomes of different TGC-resistant VRE isolates and identified three distinct S10 alleles, including A54E-H57R, ΔI52-Y58H, and a deletion of five amino acids (ΔIRATH52-56) (Niebel, *et*

al. 2015). Fiedler, *et al.* sequenced *rpsJ* in twenty-one clinical TGC-resistant *E. faecium* isolates and found that eight had a K57E mutation in S10, which is one of the alleles observed in our flask adapted *E. faecium* populations (**Figure 7.1**) (Fiedler, et al. 2015). Li, *et al.* sequenced the genome of a clinical TGC-resistant *E. coli* and found a V57L mutation in S10 that was associated with a low fitness cost, similar to the low fitness cost of the S10^{R53Q-Δ54-57ATHK} allele identified in my *E. faecalis* bioreactor strains (**Figures 6.3 & 7.3**) (Li, et al. 2016). Using serial transfer experiments Lupien, *et al.* adapted *Streptococcus pneumoniae* strains to TGC and identified the presence of S10 alleles in the adapted populations (Lupien, et al. 2015). To date *S. pneumoniae* is the fifth bacterial species and fourth Gram-positive species found to acquire S10 mutations in response to TGC selection (**Figure 7.1**). Importantly, these S10 mutations all occurred on the same extended loop that was mutated in my bioreactor and flask adapted populations and provide extended spectrum of TGC-associated S10 alleles to those already described in Figure 7.1. Combined, these results strengthen our conclusion that S10 is an important TGC-resistance locus across many species of pathogens. I predict that with time and more usage of TGC, S10 mutations will be discovered in even more bacterial species.

The results of this study also stress the importance of considering the specific genotype of an infection before administering an antibiotic treatment. For example, a VRE infection might be TGC susceptible, but if it harbors a tetracycline-resistance allele, such as *tetM*, it might adapt rapidly to resistance, especially if that allele is located on a mobile or conjugative element. Additionally, if an infection is susceptible to TGC, but is caused by bacteria with a mutation on the extended loop of S10, then the infectious bacteria may have previously been exposed to TGC and may adapt relatively quickly to TGC resistance. Under such conditions, an alternative therapy or combination of therapies might be more successful in treating the infections. Thus by considering the specific

genotype of an infection, clinicians could perhaps devise treatment plans that are more likely to be successful and less likely to lead to resistance.

Using a combination of subinhibitory concentrations of TGC and a bioreactor setup that maintains a large population of bacteria at their fastest growth rate, I was able to maintain a polymorphic population during adaptation to TGC. I then successfully used phenotypic screens to identify the underlying diversity within the population (see Chapter 4). While I did indeed detect genetic diversity among the bioreactor end-point isolates, it is interesting to note that my populations were comparatively less diverse than those from other studies in our lab that were conducted using the same approach (Hammerstrom, et al. 2015; Miller, et al. 2013). Dr. Hammerstrom used quantitative experimental evolution to study TGC resistance in the Gram-negative pathogen *Acinetobacter baumannii* (see Appendix A). During these studies the *A. baumannii* populations became hypermutators resulting in individual clones with as many as 415 mutations (Hammerstrom, et al. 2015). *A. baumannii* has a relatively high propensity to become a hypermutator, which can lead to an incredible level of genetic diversity. Thus differences between species likely plays an important role in the level of diversity observed. However, it is also interesting to note that Dr. Miller used the same *E. faecalis* S613 strain to study resistance to DAP, but still observed more diversity in his population than in my TGC adapted populations (Miller, et al. 2013). Therefore it is also important to consider the specific antibiotic being studied when evaluating the diversity achieved during adaptation. In my experiments TGC selection resulted in a unique hyperconjugative phenotype, which led to a remarkably high rate of horizontal gene transfer. It has been shown that horizontal gene transfer can reduce the diversity within adapting microbial populations, as the transfer of beneficial alleles disrupts clonal interference (Cooper 2007). Rather than competing with each other, cells within the

population can exchange genetic information, which allows for beneficial mutations to spread rapidly through the population. Similarly, the hyperconjugative Tn916 lead to the rapid spread of resistance among my adapting bioreactor populations, resulting in a comparatively less diverse population (**Figure 6.6**). Nonetheless, twenty-four distinct alleles were identified in my bioreactor populations, providing a broad array of TGC resistance alleles (**Table 5.2**).

8.2 Future work.

8.2.1 Does a tetracycline-binding riboswitch regulate *tetM* expression?

If the transcriptional regulatory mechanism upstream of *tetM* were well characterized, perhaps an inhibitor of *tetM* expression could be developed. This would not only deter the emergence of resistance, but also deter the spread of resistance through Tn916-facilitated conjugation. Thus, it is worthwhile to explore my hypothesis of a tetracycline-riboswitch regulating the expression of *tetM* as described in Chapter 6 Section 6.5. In these studies I presented preliminary data suggesting that tetracycline binds the *tetM* leader RNA in a specific manner (**Figure 6.4**). However, it has previously been hypothesized that *tetM* expression is instead regulated by a ribosomal-mediated mechanism (Su, et al. 1992). Therefore to determine if this tetracycline-RNA interaction is biologically relevant, it would be necessary to show that transcriptional read-through past the terminator stem-loop of the *tetM* leader RNA could be achieved more readily by the addition of tetracycline to an *in vitro* transcription reaction lacking ribosomes. If increased transcriptional read-through occurred under such conditions it would demonstrate that only the transcription machinery and tetracycline were necessary to achieve regulation of *tetM* expression, which in turn would strongly suggest that a

tetracycline-binding riboswitch regulates *tetM* expression. X-ray crystallography studies could then be used to determine the secondary structure of the *tetM* leader RNA both unbound and bound to tetracycline. If the structures of the mutant TGC-resistant *tetM* leader RNAs were also determined, insights could be gained into how these deletions deregulate and lead to constitutive overexpression of *tetM*. Additionally, it would be interesting to determine if different tetracycline derivatives bind to the riboswitch. For example, perhaps TGC has a relatively low affinity for the riboswitch and this prevents the activation of *tetM* expression in the presence of TGC, while other tetracycline derivatives, such as MIN, bind with a relatively high affinity. Verifying and elucidating the structure of a tetracycline-binding riboswitch upstream of *tetM* would provide the first example of a riboswitch that regulates not only resistance to an important class of antibiotics, but also the dissemination of resistance by regulating the conjugation of Tn916.

8.2.2 How readily could hyperconjugative Tn916 spread TGC-resistance inside the gastrointestinal tract of animals or within the hospital setting?

Here we showed that the conjugation frequencies of the TGC-resistant Tn916 variants were highly increased over wildtype Tn916 (**Figure 6.1D**). However, the question of how frequently these TGC-resistant Tn916 variants would conjugate within the gastrointestinal flora of animals, which is the natural environment of *Enterococcus* species, is still unanswered. Understanding these dynamics would in turn provide insights into how TGC resistance might spread through the hospital setting, as bacteria in the human intestinal tract are often reservoirs for antibiotic resistance alleles (Salyers, et al. 2004). Therefore I performed preliminary experiments to evaluate the ability of hyperconjugative Tn916 to move between bacterial species inside the gastrointestinal

tract of mice (see Chapter 6 Section 6.6). However, during these experiments the *E. faecalis* strains S613 (wildtype Tn916) and BTR87a (TGC-resistant hyperconjugative Tn916) were not able to effectively colonize the mice, even when the mice were being fed a high dose of tetracycline (**Figure 6.5**). It is possible that the high fitness cost of *tetM* overexpression and Tn916 hyperconjugation could limit the ability of the TGC-resistant Tn916 to establish within the complex and densely populated microbiota of the mice (**Figure 6.3**). However, since it is well known that Tn916 has disseminated wildly between many bacterial species, it is likely that higher concentrations of antibiotic are needed to select for conjugation of Tn916 within the mice. Future experiments to explore these possibilities would help to characterize the ability of hyperconjugative Tn916 to spread TGC resistance.

8.2.3 How stable are the *tetM* overexpressing and hyperconjugative alleles?

The hyperconjugative variants of Tn916 impose a high fitness cost on the *E. faecalis* cells (**Figure 5.3**). Due to the elevated mobility of these elements and their fitness cost, it seems likely that the hyperconjugative variants of Tn916 would quickly be lost in the absence of TGC and lack long-term stability within the host genome. However, it has been shown that Tn916 and other mobile genetic elements often impose a fitness cost on the host cell, but that this cost can be quickly mitigated over several generations of growth (Starikova, et al. 2013). Therefore, it is possible that the *E. faecalis* cells might be able to compensate for the high fitness cost of the hyperconjugative Tn916. To gain an idea of the stability of these TGC-resistant Tn916 variants, I performed daily serial transfers of two different bioreactor strains, BTR22 and BTR87a, in broth media lacking antibiotic for twenty-one days. Remarkably, after completing the transfers three of three replicate BTR22 populations and two of three replicate BTR87a populations retained their high level of resistance and their copy of Tn916 with a deletion upstream of *tetM*.

These results suggest that the hyperconjugative Tn916 variants are surprisingly stable within the *E. faecalis* host genome despite their high cost. However more work is needed to fully characterize this stability. For example, it was unclear if the cells were able to compensate for the cost of the mutant Tn916, or if the mutant Tn916 persisted despite its high cost. Additionally, it has been shown that the stability of tetracycline-resistance genes is partially dependent on the particular growth conditions, such as rich media versus minimal media (Rysz, et al. 2013). Thus it would be worthwhile to evaluate the stability of hyperconjugative Tn916 under various growth conditions. Ultimately, further characterization of the stability of these elements would provide insights into how persistent TGC-resistance might be in the hospital setting.

8.2.4 Do the S10 mutations reduce the affinity of TGC for the ribosome?

In the studies presented here mutations in the ribosomal S10 protein clustered to the tip of an extended loop on S10 that does not directly interact with TGC, but does interact with the 16S rRNA that composes the binding site of TGC (**Figures 5.2, 7.1 & 7.2**). Our group, as well as other groups, have hypothesized that these S10 alleles reduce the affinity of TGC for the ribosome by altering the confirmation of the 16S rRNA, which in turn allows for translation to continue in the presence of the antibiotic (Beabout, et al. 2015a; Cattoir, et al. 2014; Villa, et al. 2014). I attempted to evaluate this hypothesis with *in vitro* transcription and translation assays that compared the ability of ribosomes extracted from S613 (wildtype S10) and BTR0 ($S10^{R53Q-\Delta 54-57ATHK}$) to translate YFP in the presence and absence of TGC (see Appendix C). If my hypothesis were correct, then the translation efficiency of BTR0 ribosomes would remain higher than the ancestral S613 ribosomes in the presence of TGC. However, I was unable to isolate functional ribosomes from S613 and BTR0 using a published protocol for generating ribosomal

extracts from *Staphylococcus aureus* (Murray, et al. 2001). Typically *in vitro* transcription and translation assays are performed using *E. coli* ribosomes. Therefore repeating these experiments with *E. coli* ribosomal extracts might be more successful. Precisely defining the molecular and biochemical mechanism behind the ability of the S10 mutations to confer resistance would provide a greater context for understanding this important TGC allele.

8.2.5 Is there synergistic epistasis between the S10 and *tetM* alleles?

Determining if epistasis exists between any of the TGC resistance alleles would increase our understanding of the evolutionary dynamics leading to resistance. During both bioreactor runs the S10^{R53Q-Δ54-57ATHK} mutation rose in frequency faster than deletions upstream of *tetM*, which is in part due to the low fitness cost of the S10 allele (**Figures 5.1A & 6.3**). However, if the S10^{R53Q-Δ54-57ATHK} allele does reduce the binding affinity of TGC for the ribosome, then there could be synergist epistasis between the S10 and *tetM* overexpression mutations. This is because presumably it would be easier for TetM to dislodge TGC from the ribosome if TGC were bound to the ribosome with a lower affinity. Several biophysical studies have suggested that TetM is ineffective against TGC because of the high binding affinity of TGC for the ribosome and the inability of TetM to access essential nucleotides on the 16S rRNA when TGC is bound (Donhofer, et al. 2012; Jenner, et al. 2013). Thus perhaps only when the interaction between TGC and the ribosome is reduced by mutation of S10 can *tetM* overexpression confer a significant level of resistance. If this is true, then the reason the S10^{R53Q-Δ54-57ATHK} allele reached a high frequency first within my bioreactor populations was likely in part because *tetM* overexpression was most effective in cells that had already acquired the S10 mutation. To test this hypothesis I would need to generate an S613 derivative with only a *tetM* overexpression mutation and compare the fitness of this derivative to the fitness of the

BTR0 ($S10^{R53Q-\Delta 54-57ATHK}$ allele only) and appropriate double mutant ($S10^{R53Q-\Delta 54-57ATHK}$ and $tetM$ overexpression allele). Due to the limited genetic techniques available in *Enterococcus* species, such a derivative might be difficult to obtain. However, these experiments would determine if mutation of S10 is a necessary precursor to acquiring a higher level of resistance by $tetM$ overexpression, which would subsequently be useful for predicting how resistance might arise in infections exposed to TGC.

8.2.6 What alternative alleles play a role in TGC resistance?

While $tetM$ is extremely common among clinical enterococci isolates, it would be beneficial to explore the potential for alternative alleles to play a role in adaptation to TGC resistance. Furthermore, if an inhibitor of $tetM$ expression or the TetM protein were developed, then it would be especially useful to know what alternative alleles might arise when VRE are exposed to TGC. This question could be explored by looking at the adaptation of an enterococci strain lacking $tetM$ to TGC resistance. One possibility is that the two ABC transporter alleles that achieved some success during Run 2 would play a more significant role (**Figure 5.1A**). Alternatively, completely novel mutations may arise and facilitate adaptation to TGC. Additionally, it would be useful to know if tetracycline-resistance alleles other than $tetM$ are likely to play a role in adaptation to TGC. This could be quickly surveyed by taking different enterococci strains, each with a unique tetracycline-resistance determinant, and performing serial transfer experiments to adapt the strains to TGC. Sequencing of the respective tetracycline-resistance determinants would reveal if regulatory or nonsynonymous mutations affecting these genes emerged during adaption. These experiments would determine the potential of a wide-range of tetracycline-resistance determinants to confer resistance to TGC and would possibly provide more candidate loci for clinicians to sequence in their patient's enterococci infections.

8.2.7 Application of quantitative experimental evolution to study more pathogens and antibiotics.

To date, the work presented here is one of three examples from our lab where quantitative experimental evolution was used to successfully recapitulate or predict clinically relevant adaptive trajectories to resistance. Previously, Miller *et al.* adapted *E. faecalis* S613 to DAP resistance and identified changes in LiaFSR, a three-component membrane-stress response pathway, which paralleled mutations observed by our collaborators in clinical isolates (Arias, et al. 2011; Miller, et al. 2013). Hammerstrom *et al.* adapted *A. baumannii* to TGC resistance and identified mutations leading to over production of AdeABC, a multidrug efflux pump, which also paralleled mutations seen in clinical isolates of *A. baumannii* (see Appendix A) (Hammerstrom, et al. 2015; Hornsey, et al. 2010). Combined, our three studies strongly demonstrate the usefulness of quantitative experimental evolution in predicting, verifying, and further characterizing resistance mechanisms in relevant pathogens. Therefore, it is worthwhile to apply this approach to different combinations of antibiotics and pathogenic species to further our understanding of antibiotic resistance and combat the rising threat of resistance.

References.

- Akanuma G, Suzuki S, Yano K, Nanamiya H, Natori Y, Namba E, Watanabe K, Tagami K, Takeda T, Iizuka Y, Kobayashi A, Ishizuka M, Yoshikawa H, Kawamura F. (2013). Single mutations introduced in the essential ribosomal proteins L3 and S10 cause a sporulation defect in *Bacillus subtilis*. *The Journal of General and Applied Microbiology*. 59: 105-117. doi: 10.2323/jgam.59.105
- Alikhan NF, Petty NK, Ben Zakour NL, Beatson SA. (2011). BLAST Ring Image Generator (BRIG): simple prokaryote genome comparisons. *BMC Genomics*. 12: 402. doi: 10.1186/1471-2164-12-402
- Aminov RI, Chee-Sanford JC, Garrigues N, Teferedegne B, Krapac IJ, White BA, Mackie RI. (2002). Development, Validation, and Application of PCR Primers for Detection of Tetracycline Efflux Genes of Gram-Negative Bacteria. *Applied and Environmental Microbiology*. 68: 1786-1793. doi: 10.1128/aem.68.4.1786-1793.2002
- Andersson DI, Hughes D. (2010). Antibiotic resistance and its cost: is it possible to reverse resistance? *Nat Rev Micro*. 8: 260-271.
- Andersson DI, Hughes D. (2014). Microbiological effects of sublethal levels of antibiotics. *Nat Rev Micro*. 12: 465-478. doi: 10.1038/nrmicro3270
- Aranda PS, LaJoie DM, Jorcyk CL. (2012). Bleach Gel: A Simple Agarose Gel for Analyzing RNA Quality. *Electrophoresis*. 33: 366-369. doi: 10.1002/elps.201100335
- Arias CA, Murray BE. (2009). Antibiotic-Resistant Bugs in the 21st Century — A Clinical Super-Challenge. *New England Journal of Medicine*. 360: 439-443. doi: doi:10.1056/NEJMp0804651
- Arias CA, Murray BE. (2012). The rise of the *Enterococcus*: beyond vancomycin resistance. *Nat Rev Microbiol*. 10: 266-278. doi: 10.1038/nrmicro2761
- Arias CA, Panesso D, McGrath DM, Qin X, Mojica MF, Miller C, Diaz L, Tran TT, Rincon S, Barbu EM, Reyes J, Roh JH, Lobos E, Sodergren E, Pasqualini R, Arap W, Quinn JP, Shamoo Y, Murray BE, Weinstock GM. (2011). Genetic Basis for In Vivo Daptomycin Resistance in Enterococci. *New England Journal of Medicine*. 365: 892-900. doi: doi:10.1056/NEJMoa1011138
- Azevedo RBR, Lohaus R, Srinivasan S, Dang KK, Burch CL. (2006). Sexual reproduction selects for robustness and negative epistasis in artificial gene networks. *Nature*. 440: 87-90.
- Barrick JE, Lenski RE. (2013). Genome dynamics during experimental evolution. *Nat Rev Genet*. 14: 827-839. doi: 10.1038/nrg3564
- Barrick JE, Yu DS, Yoon SH, Jeong H, Oh TK, Schneider D, Lenski RE, Kim JF. (2009). Genome evolution and adaptation in a long-term experiment with *Escherichia coli*. *Nature*. 461: 1243-1247. doi: 10.1038/nature08480

- Bauer G, Berens C, Projan SJ, Hillen W. (2004). Comparison of tetracycline and tigecycline binding to ribosomes mapped by dimethylsulphate and drug-directed Fe²⁺ cleavage of 16S rRNA. *J Antimicrob Chemother.* 53: 592-599. doi: 10.1093/jac/dkh125
- Beabout K, Hammerstrom TG, Perez AM, Magalhães BF, Prater AG, Clements TP, Arias CA, Saxon G, Shamoo Y. (2015a). The Ribosomal S10 Protein Is a General Target for Decreased Tigecycline Susceptibility. *Antimicrobial Agents and Chemotherapy.* 59: 5561-5566. doi: 10.1128/aac.00547-15
- Beabout K, Hammerstrom TG, Wang TT, Bhatty M, Christie PJ, Saxon G, Shamoo Y. (2015b). Rampant Parasexuality Evolves in a Hospital Pathogen during Antibiotic Selection. *Molecular Biology and Evolution.* 32: 2585-2597. doi: 10.1093/molbev/msv133
- Bergeron J, Ammirati M, Danley D, James L, Norcia M, Retsema J, Strick CA, Su WG, Sutcliffe J, Wondrack L. (1996). Glycylcyclines bind to the high-affinity tetracycline ribosomal binding site and evade Tet(M)- and Tet(O)-mediated ribosomal protection. *Antimicrobial Agents and Chemotherapy.* 40: 2226-2228.
- Boguslawska J, Zycka-Krzesinska J, Wilcks A, Bardowski J. (2009). Intra- and Interspecies Conjugal Transfer of Tn916-Like Elements from *Lactococcus lactis* In Vitro and In Vivo. *Applied and Environmental Microbiology.* 75: 6352-6360. doi: 10.1128/aem.00470-09
- Bradford PA, Petersen PJ, Young M, Jones CH, Tischler M, O'Connell J. (2005). Tigecycline MIC testing by broth dilution requires use of fresh medium or addition of the biocatalytic oxygen-reducing reagent oxyrase to standardize the test method. *Antimicrob Agents Chemother.* 49: 3903-3909. doi: 10.1128/aac.49.9.3903-3909.2005
- Brink AJ, Bizos D, Boffard KD, Feldman C, Grolman DC, Pretorius J, Richards GA, Senekal M, Steyn E, Welkovic N. (2010). Guideline: appropriate use of tigecycline. *SAMJ: South African Medical Journal.* 100: 388-394.
- Brodersen DE, Clemons Jr WM, Carter AP, Morgan-Warren RJ, Wimberly BT, Ramakrishnan V. (2000). The Structural Basis for the Action of the Antibiotics Tetracycline, Pactamycin, and Hygromycin B on the 30S Ribosomal Subunit. *Cell.* 103: 1143-1154.
- Brogden RN, Carmine A, Heel RC, Morley PA, Speight TM, Avery GS. (1981). Amoxycillin/Clavulanic Acid: A Review of its Antibacterial Activity, Pharmacokinetics and Therapeutic Use. *Drugs.* 22: 337-362. doi: 10.2165/00003495-198122050-00001
- Burch CL, Chao L. (2004). Epistasis and its relationship to canalization in the RNA virus phi 6. *Genetics.* 167: 559-567. doi: 10.1534/genetics.103.021196
- Burdett V. (1996). Tet(M)-promoted release of tetracycline from ribosomes is GTP dependent. *J Bacteriol.* 178: 3246-3251.
- Cantón R, Morosini M-I. (2011). Emergence and spread of antibiotic resistance following exposure to antibiotics. *FEMS Microbiol Rev.* 35: 977-991. doi: 10.1111/j.1574-6976.2011.00295.x

- Casapao AM, Leonard SN, Davis SL, Lodise TP, Patel N, Goff DA, LaPlante KL, Potoski BA, Rybak MJ. (2013). Clinical Outcomes in Patients with Heterogeneous Vancomycin-Intermediate *Staphylococcus aureus* Bloodstream Infection. *Antimicrobial Agents and Chemotherapy*. 57: 4252-4259. doi: 10.1128/aac.00380-13
- Cattoir V, Isnard C, Cosquer T, Odhiambo A, Bucquet F, Guerin F, Giard JC. (2014). Genomic analysis of reduced susceptibility to tigecycline in *Enterococcus faecium*. *Antimicrob Agents Chemother*. doi: 10.1128/aac.04174-14
- CDC. (2013). Antibiotic Resistance Threat Report. In. <http://www.cdc.gov/drugresistance/threat-report-2013/>.
- CDC. (2011). Antimicrobial Resistance Posing Growing Health Threat [Press Release]. In. http://www.cdc.gov/media/releases/2011/p0407_antimicrobialresistance.html.
- CDDEP. (2010). Vancomycin-Resistant *Enterococcus faecalis*: *E. faecalis* resistance is low, but steadily increasing. In. http://cddep.org/projects/resistance_map/vancomycin_resistant_enterococcus_faecalis_sthash.xH44TvB6.dpbs.
- Celli J, Trieu-Cuot P. (1998). Circularization of Tn916 is required for expression of the transposon-encoded transfer functions: characterization of long tetracycline-inducible transcripts reading through the attachment site. *Mol Microbiol*. 28: 103-117. doi: 10.1046/j.1365-2958.1998.00778.x
- Chang Q, Wang W, Regev-Yochay G, Lipsitch M, Hanage WP. (2015). Antibiotics in agriculture and the risk to human health: how worried should we be? *Evolutionary Applications*. 8: 240-247. doi: 10.1111/eva.12185
- Chen Q, Li X, Zhou H, Jiang Y, Chen Y, Hua X, Yu Y. (2014). Decreased susceptibility to tigecycline in *Acinetobacter baumannii* mediated by a mutation in *trm* encoding SAM-dependent methyltransferase. *Journal of Antimicrobial Chemotherapy*. 69: 72-76. doi: 10.1093/jac/dkt319
- Chen Y, Zhang X, Manias D, Yeo HJ, Dunny GM, Christie PJ. (2008). *Enterococcus faecalis* PcfC, a spatially localized substrate receptor for type IV secretion of the pCF10 transfer intermediate. *J Bacteriol*. 190: 3632-3645. doi: 10.1128/jb.01999-07
- Chopra I. (2001). Glycylcyclines: third-generation tetracycline antibiotics. *Current Opinion in Pharmacology*. 1: 464-469.
- Chopra I, Roberts M. (2001). Tetracycline Antibiotics: Mode of Action, Applications, Molecular Biology, and Epidemiology of Bacterial Resistance. *Microbiology and Molecular Biology Reviews*. 65: 232-260. doi: 10.1128/mmbr.65.2.232-260.2001
- Collignon P. (2012). The Importance of a One Health Approach to Preventing the Development and Spread of Antibiotic Resistance. *Curr Top Microbiol Immunol*. doi: 10.1007/82_2012_224

- Collins AS. (2008). Preventing Health Care–Associated Infections. In: RG H, editor. An Evidence-Based Handbook for Nurses. Rockville, MD: Agency for Healthcare Research and Quality (US).
- Connell SR, Tracz DM, Nierhaus KH, Taylor DE. (2003). Ribosomal Protection Proteins and Their Mechanism of Tetracycline Resistance. *Antimicrobial Agents and Chemotherapy*. 47: 3675-3681. doi: 10.1128/aac.47.12.3675-3681.2003
- Cook GM, Poole RK. (2000). Oxidase and periplasmic cytochrome assembly in *Escherichia coli* K-12: CydDC and CcmAB are not required for haem–membrane association. *Microbiology*. 146: 527-536.
- Cooper TF. (2007). Recombination Speeds Adaptation by Reducing Competition between Beneficial Mutations in Populations of *Escherichia coli*. *PloS Biol.* 5: e225. doi: 10.1371/journal.pbio.0050225
- Cooper TF, Lenski RE. (2010). Experimental evolution with *E. coli* in diverse resource environments. I. Fluctuating environments promote divergence of replicate populations. *BMC Evolutionary Biology*. 10: 1-10. doi: 10.1186/1471-2148-10-11
- Cordina C, Hill R, Deshpande A, Hood J, Inkster T. (2012). Tigecycline-resistant *Enterococcus faecalis* associated with omeprazole use in a surgical patient. *J Antimicrob Chemother*. 67: 1806-1807. doi: 10.1093/jac/dks122
- Cosgrove SE. (2006). The Relationship between Antimicrobial Resistance and Patient Outcomes: Mortality, Length of Hospital Stay, and Health Care Costs. *Clinical Infectious Diseases*. 42: S82-S89. doi: 10.1086/499406
- Costerton JW, Stewart PS, Greenberg EP. (1999). Bacterial Biofilms: A Common Cause of Persistent Infections. *Science*. 284: 1318-1322. doi: 10.1126/science.284.5418.1318
- Counago R, Chen S, Shamoo Y. (2006). In vivo molecular evolution reveals biophysical origins of organismal fitness. *Mol Cell*. 22: 441-449. doi: 10.1016/j.molcel.2006.04.012
- Coyne S, Courvalin P, Perichon B. (2011). Efflux-mediated antibiotic resistance in *Acinetobacter* spp. *Antimicrob Agents Chemother*. 55: 947-953. doi: 10.1128/AAC.01388-10
- Davlieva M, Donarski J, Wang J, Shamoo Y, Nikonowicz EP. (2014). Structure Analysis of free and bound states of an RNA Aptamer Against Ribosomal Protein S8 from *Bacillus anthracis*. *Nucl. Acids Res.* In press.
- Deatherage D, Barrick J. (2014). Identification of Mutations in Laboratory-Evolved Microbes from Next-Generation Sequencing Data Using breseq. In: Sun L, Shou W, editors. Engineering and Analyzing Multicellular Systems: Springer New York. p. 165-188.
- Diaz L, Tran TT, Munita JM, Miller WR, Rincon S, Carvajal LP, Wollam A, Reyes J, Panesso D, Rojas NL, Shamoo Y, Murray BE, Weinstock GM, Arias CA. (2014). Whole-Genome Analyses of *Enterococcus faecium* Isolates with Diverse Daptomycin MICs. *Antimicrobial Agents and Chemotherapy*. 58: 4527-4534. doi: 10.1128/aac.02686-14

- Donhofer A, Franckenberg S, Wickles S, Berninghausen O, Beckmann R, Wilson DN. (2012). Structural basis for TetM-mediated tetracycline resistance. *Proc Natl Acad Sci U S A.* 109: 16900-16905. doi: 10.1073/pnas.1208037109
- Elena SF, Lenski RE. (2003). Evolution experiments with microorganisms: the dynamics and genetic bases of adaptation. *Nat Rev Genet.* 4: 457-469. doi: 10.1038/nrg1088
- Eliopoulos GM, Eliopoulos GM, Roberts MC. (2003). Tetracycline Therapy: Update. *Clinical Infectious Diseases.* 36: 462-467. doi: 10.1086/367622
- Ferenci T. (2007). Bacterial Physiology, Regulation and Mutational Adaptation in a Chemostat Environment. In: Robert KP, editor. *Advances in Microbial Physiology:* Academic Press. p. 169-315.
- Fernández L, Breidenstein EBM, Hancock REW. (2011). Creeping baselines and adaptive resistance to antibiotics. *Drug Resistance Updates.* 14: 1-21.
- Fiedler S, Bender JK, Klare I, Halbedel S, Grohmann E, Szewzyk U, Werner G. (2015). Tigecycline resistance in clinical isolates of *Enterococcus faecium* is mediated by an upregulation of plasmid-encoded tetracycline determinants *tet(L)* and *tet(M)*. *Journal of Antimicrobial Chemotherapy.* doi: 10.1093/jac/dkv420
- Foster KR, Grundmann H. (2006). Do We Need to Put Society First? The Potential for Tragedy in Antimicrobial Resistance. *PLoS Med.* 3: e29. doi: 10.1371/journal.pmed.0030029
- Franke AE, Clewell DB. (1981). Evidence for a chromosome-borne resistance transposon (Tn916) in *Streptococcus faecalis* that is capable of "conjugal" transfer in the absence of a conjugative plasmid. *J Bacteriol.* 145: 494-502.
- Frazzon APG, Gama BA, Hermes V, Bierhals CG, Pereira RI, Guedes AG, d'Azevedo PA, Frazzon J. (2009). Prevalence of antimicrobial resistance and molecular characterization of tetracycline resistance mediated by *tet(M)* and *tet(L)* genes in *Enterococcus* spp. isolated from food in Southern Brazil. *World Journal of Microbiology and Biotechnology.* 26: 365-370. doi: 10.1007/s11274-009-0160-x
- Freitas AR, Novais C, Correia R, Monteiro M, Coque TM, Peixe L. (2011). Non-susceptibility to tigecycline in enterococci from hospitalised patients, food products and community sources. *Int J Antimicrob Agents.* 38: 174-176. doi: 10.1016/j.ijantimicag.2011.04.014
- García-Quintanilla M, Ramos-Morales F, Casadesús J. (2008). Conjugal Transfer of the *Salmonella enterica* Virulence Plasmid in the Mouse Intestine. *J Bacteriol.* 190: 1922-1927. doi: 10.1128/jb.01626-07
- Gerrish PJ, Lenski RE. (1998). The fate of competing beneficial mutations in an asexual population. *Genetica.* 102: 127-144. doi: 10.1023/a:1017067816551
- Gerrits MM, de Zoete MR, Arents NLA, Kuipers EJ, Kusters JG. (2002). 16S rRNA Mutation-Mediated Tetracycline Resistance in *Helicobacter pylori*. *Antimicrobial Agents and Chemotherapy.* 46: 2996-3000. doi: 10.1128/aac.46.9.2996-3000.2002

- Gilmore MS, Rauch M, Ramsey MM, Himes PR, Varahan S, Manson JM, Lebreton F, Hancock LE. (2015). Pheromone killing of multidrug-resistant *Enterococcus faecalis* V583 by native commensal strains. *Proc Natl Acad Sci U S A.* 112: 7273-7278. doi: 10.1073/pnas.1500553112
- Golding GB, Dean AM. (1998). The structural basis of molecular adaptation. *Molecular Biology and Evolution.* 15: 355-369.
- Gould IM. (2015). Benefits of antimicrobial stewardship in hospitals: Evidence from a recent Cochrane review. *Journal of Microbiology, Immunology and Infection.* 48: S24. doi: 10.1016/j.jmii.2015.02.193
- Grenier D, Huot M-P, Mayrand D. (2000). Iron-Chelating Activity of Tetracyclines and Its Impact on the Susceptibility of *Actinobacillus actinomycetemcomitans* to These Antibiotics. *Antimicrobial Agents and Chemotherapy.* 44: 763-766. doi: 10.1128/aac.44.3.763-766.2000
- Gresham D, Dunham MJ. (2014). The enduring utility of continuous culturing in experimental evolution. *Genomics.* 104: 399-405.
- Gu S, Chen D, Zhang J-N, Lv X, Wang K, Duan L-P, Nie Y, Wu X-L. (2013). Bacterial Community Mapping of the Mouse Gastrointestinal Tract. *PLoS One.* 8: e74957. doi: 10.1371/journal.pone.0074957
- Guiton PS, Hung CS, Hancock LE, Caparon MG, Hultgren SJ. (2010). *Enterococcal* biofilm formation and virulence in an optimized murine model of foreign body-associated urinary tract infections. *Infect Immun.* 78: 4166-4175. doi: 10.1128/IAI.00711-10
- Haack BJ, Andrews RE, Loynachan TE. (1996). Tn916-mediated genetic exchange in soil. *Soil Biology and Biochemistry.* 28: 765-771.
- Hammerschmidt K, Rose CJ, Kerr B, Rainey PB. (2014). Life cycles, fitness decoupling and the evolution of multicellularity. *Nature.* 515: 75-79. doi: 10.1038/nature13884
- Hammerstrom TG, Beabout K, Clements TP, Saxer G, Shamoo Y. (2015). *Acinetobacter baumannii* Repeatedly Evolves a Hypermutator Phenotype in Response to Tigecycline That Effectively Surveys Evolutionary Trajectories to Resistance. *PLoS One.* 10: e0140489. doi: 10.1371/journal.pone.0140489
- Hellweger FL. (2013). *Escherichia coli* adapts to tetracycline resistance plasmid (pBR322) by mutating endogenous potassium transport: *in silico* hypothesis testing. *FEMS Microbiology Ecology.* 83: 622-631. doi: 10.1111/1574-6941.12019
- Hespell RB, Whitehead TR. (1991). Conjugal transfer of Tn916, Tn916 delta E, and pAM beta 1 from *Enterococcus faecalis* to *Butyrivibrio fibrisolvens* strains. *Applied and Environmental Microbiology.* 57: 2703-2709.
- Hong H, Jung J, Park W. (2014). Plasmid-Encoded Tetracycline Efflux Pump Protein Alters Bacterial Stress Responses and Ecological Fitness of *Acinetobacter oleivorans*. *PLoS One.* 9: e107716. doi: 10.1371/journal.pone.0107716

- Hornsey M, Ellington MJ, Doumith M, Thomas CP, Gordon NC, Wareham DW, Quinn J, Lolans K, Livermore DM, Woodford N. (2010). AdeABC-mediated efflux and tigecycline MICs for epidemic clones of *Acinetobacter baumannii*. *Journal of Antimicrobial Chemotherapy*. doi: 10.1093/jac/dkq218
- Hu M, Nandi S, Davies C, Nicholas RA. (2005). High-level chromosomally mediated tetracycline resistance in *Neisseria gonorrhoeae* results from a point mutation in the *rpsJ* gene encoding ribosomal protein S10 in combination with the *mtrR* and *penB* resistance determinants. *Antimicrob Agents Chemother*. 49: 4327-4334. doi: 10.1128/aac.49.10.4327-4334.2005
- Hufeldt MR, Nielsen DS, Vogensen FK, Midtvedt T, Hansen AK. (2010). Variation in the Gut Microbiota of Laboratory Mice Is Related to Both Genetic and Environmental Factors. *Comparative Medicine*. 60: 336-342.
- Huttner B, Jones M, Rubin MA, Neuhauser MM, Gundlapalli A, Samore M. (2012). Drugs of Last Resort? The Use of Polymyxins and Tigecycline at US Veterans Affairs Medical Centers, 2005-2010. *PLoS One*. 7: e36649. doi: 10.1371/journal.pone.0036649
- Ippolito JA, Kanyo ZF, Wang D, Franceschi FJ, Moore PB, Steitz TA, Duffy EM. (2008). Crystal Structure of the Oxazolidinone Antibiotic Linezolid Bound to the 50S Ribosomal Subunit. *Journal of Medicinal Chemistry*. 51: 3353-3356. doi: 10.1021/jm800379d
- Jaworski DD, Clewell DB. (1994). Evidence that coupling sequences play a frequency-determining role in conjugative transposition of Tn916 in *Enterococcus faecalis*. *J Bacteriol*. 176: 3328-3335.
- Jenner L, Starosta AL, Terry DS, Mikolajka A, Filonava L, Yusupov M, Blanchard SC, Wilson DN, Yusupova G. (2013). Structural basis for potent inhibitory activity of the antibiotic tigecycline during protein synthesis. *Proc Natl Acad Sci U S A*. 110: 3812-3816. doi: 10.1073/pnas.1216691110
- Kahrstrom CT. (2013). Entering a post-antibiotic era? *Nat Rev Micro*. 11: 146-146.
- Kaki R, Elligsen M, Walker S, Simor A, Palmay L, Daneman N. (2011). Impact of antimicrobial stewardship in critical care: a systematic review. *Journal of Antimicrobial Chemotherapy*. 66: 1223-1230. doi: 10.1093/jac/dkr137
- Keeney D, Ruzin A, McAleese F, Murphy E, Bradford PA. (2008). MarA-mediated overexpression of the AcrAB efflux pump results in decreased susceptibility to tigecycline in *Escherichia coli*. *J Antimicrob Chemother*. 61: 46-53. doi: 10.1093/jac/dkm397
- Khan AI, Dinh DM, Schneider D, Lenski RE, Cooper TF. (2011). Negative Epistasis Between Beneficial Mutations in an Evolving Bacterial Population. *Science*. 332: 1193-1196. doi: 10.1126/science.1203801
- King G, Sharom FJ. (2012). Proteins that bind and move lipids: MsbA and NPC1. *Critical Reviews in Biochemistry and Molecular Biology*. 47: 75-95. doi: 10.3109/10409238.2011.636505

- Korona R, Nakatsu CH, Forney LJ, Lenski RE. (1994). Evidence for multiple adaptive peaks from populations of bacteria evolving in a structured habitat. *Proc Natl Acad Sci USA*. 91. doi: 10.1073/pnas.91.19.9037
- Laxminarayan R, Chaudhury RR. (2016). Antibiotic Resistance in India: Drivers and Opportunities for Action. *PLoS Med.* 13: e1001974. doi: 10.1371/journal.pmed.1001974
- Lee CA, Babic A, Grossman AD. (2010). Autonomous plasmid-like replication of a conjugative transposon. *Mol Microbiol.* 75: 268-279. doi: 10.1111/j.1365-2958.2009.06985.x
- Lee H, Popodi E, Tang H, Foster PL. (2012). Rate and molecular spectrum of spontaneous mutations in the bacterium *Escherichia coli* as determined by whole-genome sequencing. *Proceedings of the National Academy of Sciences*. 109: E2774–E2783. doi: 10.1073/pnas.1210309109
- Leener ED, Martel A, Decostere A, Haesebrouck F. (2004). Distribution of the *erm(B)* Gene, Tetracycline Resistance Genes, and Tn1545-like Transposons in Macrolide- and Lincosamide-Resistant Enterococci from Pigs and Humans. *Microbial Drug Resistance*. 10: 341-345.
- Lenski RE, Rose MR, Simpson SC, Tadler SC. (1991). Long-Term Experimental Evolution in *Escherichia coli*. I. Adaptation and Divergence after 2000 Generations. *The American Naturalist*. 138: 1315-1341.
- Lenski RE, Souza V, Duong LP, Phan QG, Nguyen TNM, Bertrand KP. (1994). Epistatic effects of promoter and repressor functions of the Tn10 tetracycline-resistance operon on the fitness of *Escherichia coli*. *Molecular Ecology*. 3: 127-135. doi: 10.1111/j.1365-294X.1994.tb00113.x
- Li W, Atkinson GC, Thakor NS, Allas Ü, Lu C-c, Chan K-Y, Tenson T, Schulten K, Wilson KS, Hauryliuk V, Frank J. (2013). Mechanism of tetracycline resistance by ribosomal protection protein Tet(O). *Nat Commun.* 4: 1477.
- Li X, Mu X, Yang Y, Hua X, Yang Q, Wang N, Du X, Ruan Z, Shen X, Yu Y. (2016). Rapid emergence of high-level tigecycline resistance in *Escherichia coli* strains harbouring blaNDM-5 *in vivo*. *Int J Antimicrob Agents*. 47: 324-327.
- Linkevicius M, Sandegren L, Andersson DI. (2015). Potential of Tetracycline Resistance Proteins To Evolve Tigecycline Resistance. *Antimicrob Agents Chemother*. 60: 789-796. doi: 10.1128/aac.02465-15
- Lins RX, de Oliveira Andrade A, Hirata Junior R, Wilson MJ, Lewis MA, Williams DW, Fidel RA. (2013). Antimicrobial resistance and virulence traits of *Enterococcus faecalis* from primary endodontic infections. *J Dent.* 41: 779-786. doi: 10.1016/j.jdent.2013.07.004
- Livermore DM. (2005). Tigecycline: what is it, and where should it be used? *J Antimicrob Chemother*. 56: 611-614. doi: 10.1093/jac/dki291

Lockton S, Ross-Ibarra J, Gaut BS. (2008). Demography and weak selection drive patterns of transposable element diversity in natural populations of *Arabidopsis lyrata*. *Proceedings of the National Academy of Sciences*. 105: 13965-13970. doi: 10.1073/pnas.0804671105

Lopez M, 'bal JCH, Maldonado A, Saavedra G, Baquero F, Silva J, Torres C, Campo Rd. (2009). Clonal dissemination of *Enterococcus faecalis* ST201 and *Enterococcus faecium* CC17-ST64 containing Tn5382-vanB2 among 16 hospitals in Chile. *Clin Microbiol Infect.* 586–588.

Lunzer M, Golding GB, Dean AM. (2010). Pervasive cryptic epistasis in molecular evolution. *PLoS Genet.* 6: e1001162. doi: 10.1371/journal.pgen.1001162

Lupien A, Gingras H, Leprohon P, Ouellette M. (2015). Induced tigecycline resistance in *Streptococcus pneumoniae* mutants reveals mutations in ribosomal proteins and rRNA. *Journal of Antimicrobial Chemotherapy*. doi: 10.1093/jac/dkv211

Marcel JP, Alfa M, Baquero F, Etienne J, Goossens H, Harbarth S, Hryniewicz W, Jarvis W, Kaku M, Leclercq R, Levy S, Mazel D, Nercelles P, Perl T, Pittet D, Vandebroucke-Grauls C, Woodford N, Jarlier V. (2008). Healthcare-associated infections: think globally, act locally. *Clinical Microbiology and Infection.* 14: 895-907. doi: 10.1111/j.1469-0691.2008.02074.x

Markham PN, Neyfakh AA. (2001). Efflux-mediated drug resistance in Gram-positive bacteria. *Current Opinion in Microbiology.* 4: 509-514.

Matteau D, Baby V, Pelletier S, Rodrigue S. (2015). A Small-Volume, Low-Cost, and Versatile Continuous Culture Device. *PLoS One.* 10: e0133384. doi: 10.1371/journal.pone.0133384

McAleese F, Petersen P, Ruzin A, Dunman PM, Murphy E, Projan SJ, Bradford PA. (2005). A novel MATE family efflux pump contributes to the reduced susceptibility of laboratory-derived *Staphylococcus aureus* mutants to tigecycline. *Antimicrob Agents Chemother.* 49: 1865-1871. doi: 10.1128/AAC.49.5.1865-1871.2005

McBride SM, Fischetti VA, LeBlanc DJ, Moellering RC, Jr., Gilmore MS. (2007). Genetic Diversity among *Enterococcus faecalis*. *PLoS One.* 2: e582. doi: 10.1371/journal.pone.0000582

Miller C, Kong J, Tran TT, Arias CA, Saxer G, Shamoo Y. (2013). Adaptation of *Enterococcus faecalis* to daptomycin reveals an ordered progression to resistance. *Antimicrob Agents Chemother.* 57: 5373-5383. doi: 10.1128/AAC.01473-13

Milne I, Bayer M, Cardle L, Shaw P, Stephen G, Wright F, Marshall D. (2010). Tablet--next generation sequence assembly visualization. *Bioinformatics.* 26: 401-402. doi: 10.1093/bioinformatics/btp666

Mohamed JA, Huang DB. (2007). Biofilm formation by enterococci. *Journal of Medical Microbiology.* 56: 1581-1588. doi: doi:10.1099/jmm.0.47331-0

- Munita JM, Mishra NN, Alvarez D, Tran TT, Diaz L, Panesso D, Reyes J, Murray BE, Adachi JA, Bayer AS, Arias CA. (2014). Failure of High-Dose Daptomycin for Bacteremia Caused by Daptomycin-Susceptible *Enterococcus faecium* Harboring LiaSR Substitutions. *Clinical Infectious Diseases*. 59: 1277-1280. doi: 10.1093/cid/ciu642
- Munita JM, Panesso D, Diaz L, Tran TT, Reyes J, Wanger A, Murray BE, Arias CA. (2012). Correlation between Mutations in *liaFSR* of *Enterococcus faecium* and MIC of Daptomycin: Revisiting Daptomycin Breakpoints. *Antimicrobial Agents and Chemotherapy*. 56: 4354-4359. doi: 10.1128/AAC.00509-12
- Munoz-Price LS, Lolans K, Quinn JP. (2005). Emergence of Resistance to Daptomycin during Treatment of Vancomycin-Resistant *Enterococcus faecalis* Infection. *Clinical Infectious Diseases*. 41: 565-566. doi: 10.1086/432121
- Murray RW, Melchior EP, Hagadorn JC, Marotti KR. (2001). *Staphylococcus aureus* Cell Extract Transcription-Translation Assay: Firefly Luciferase Reporter System for Evaluating Protein Translation Inhibitors. *Antimicrobial Agents and Chemotherapy*. 45: 1900-1904. doi: 10.1128/aac.45.6.1900-1904.2001
- Nagaraj M, Chakraborty A, Srinivas BN. (2015). A Study on the Dispensing Pattern of Over the Counter Drugs in Retail Pharmacies in Sarjapur Area, East Bangalore. *Journal of Clinical and Diagnostic Research : JCDR*. 9: FC11-FC13. doi: 10.7860/JCDR/2015/12940.6119
- Naglich JG, Andrews Jr RE. (1988). Tn916-dependent conjugal transfer of PC194 and PUB110 from *Bacillus subtilis* into *Bacillus thuringiensis* subsp. *israelensis*. *Plasmid*. 20: 113-126.
- Nguyen TLA, Vieira-Silva S, Liston A, Raes J. (2015). How informative is the mouse for human gut microbiota research? *Disease Models and Mechanisms*. 8: 1-16. doi: 10.1242/dmm.017400
- Nguyen TN, Phan QG, Duong LP, Bertrand KP, Lenski RE. (1989). Effects of carriage and expression of the Tn10 tetracycline-resistance operon on the fitness of *Escherichia coli* K12. *Molecular Biology and Evolution*. 6: 213-225.
- Niebel M, Quick J, Prieto AMG, Hill RLR, Pike R, Huber D, David M, Hornsey M, Wareham D, Oppenheim B, Woodford N, van Schaik W, Loman N. (2015). Deletions in a ribosomal protein-coding gene are associated with tigecycline resistance in *Enterococcus faecium*. *Int J Antimicrob Agents*. 46: 572-575.
- Nishimoto Y, Kobayashi N, Alam MM, Ishino M, Uehara N, Watanabe N. (2005). Analysis of the Prevalence of Tetracycline Resistance Genes in Clinical Isolates of *Enterococcus faecalis* and *Enterococcus faecium* in a Japanese Hospital. *Microbial Drug Resistance*. 11.
- Noguchi N, Emura A, Sasatsu M, Kono M. (1994). Expression in *Escherichia coli* of a TetK determinant from *Staphylococcus aureus*. *Biol Pharm Bull*. 17: 352-355.

- Nonaka L, Connell SR, Taylor DE. (2005). 16S rRNA Mutations That Confer Tetracycline Resistance in *Helicobacter pylori* Decrease Drug Binding in *Escherichia coli* Ribosomes. *J Bacteriol.* 187: 3708-3712. doi: 10.1128/jb.187.11.3708-3712.2005
- Olson MW, Ruzin A, Feyfant E, Rush TS, 3rd, O'Connell J, Bradford PA. (2006). Functional, biophysical, and structural bases for antibacterial activity of tigecycline. *Antimicrob Agents Chemother.* 50: 2156-2166. doi: 10.1128/AAC.01499-05
- Outterson K, Powers JH, Daniel GW, McClellan MB. (2015). Repairing The Broken Market For Antibiotic Innovation. *Health Affairs.* 34: 277-285. doi: 10.1377/hlthaff.2014.1003
- Pena MI, Davlieva M, Bennett MR, Olson JS, Shamoo Y. (2010). Evolutionary fates within a microbial population highlight an essential role for protein folding during natural selection. *Mol Syst Biol.* 6: 387. doi: 10.1038/msb.2010.43
- Petersen PJ, Bradford PA. (2005). Effect of Medium Age and Supplementation with the Biocatalytic Oxygen-Reducing Reagent Oxyrase on In Vitro Activities of Tigecycline against Recent Clinical Isolates. *Antimicrobial Agents and Chemotherapy.* 49: 3910-3918. doi: 10.1128/AAC.49.9.3910-3918.2005
- Pfaffl MW. (2001). A new mathematical model for relative quantification in real-time RT-PCR. *Nucleic Acids Res.* 29: e45.
- Pillar CM, Draghi DC, Dowzicky MJ, Sahm DF. (2008). In Vitro Activity of Tigecycline against Gram-Positive and Gram-Negative Pathogens as Evaluated by Broth Microdilution and Etest. *J Clin Microbiol.* 46: 2862-2867. doi: 10.1128/jcm.00637-08
- Pioletti M, Schluenzen F, Harms J, Zarivach R, Glühmann M, Avila H, Bashan A, Bartels H, Auerbach T, Jacobi C, Hartsch T, Yonath A, Franceschi F. (2001). Crystal structures of complexes of the small ribosomal subunit with tetracycline, edeine and IF3. *The EMBO Journal.* 20: 1829-1839. doi: 10.1093/emboj/20.8.1829
- Poole K. (2005). Efflux-mediated antimicrobial resistance. *Journal of Antimicrobial Chemotherapy.* 56: 20-51. doi: 10.1093/jac/dki171
- Reynolds PE. (1989). Structure, biochemistry and mechanism of action of glycopeptide antibiotics. *European Journal of Clinical Microbiology and Infectious Diseases.* 8: 943-950. doi: 10.1007/bf01967563
- Rice LB. (2008). Federal funding for the study of antimicrobial resistance in nosocomial pathogens: no ESKAPE. *J Infect Dis.* 197: 1079-1081. doi: 10.1086/533452
- Rice LB. (1998). Tn916 Family Conjugative Transposons and Dissemination of Antimicrobial Resistance Determinants. *Antimicrob. Agents Chemother.* 42: 1871-1877.
- Rincon S, Panesso D, Diaz L, Carvajal LP, Reyes J, Munita JM, Arias CA. (2014). Resistance to "last resort" antibiotics in Gram-positive cocci: The post-vancomycin era. *Biomedica.* 34 Suppl 1: 191-208. doi: 10.1590/s0120-41572014000500022

- Roberts AP, Mullany P. (2009). A modular master on the move: the Tn916 family of mobile genetic elements. *Trends Microbiol.* 17: 251-258. doi: 10.1016/j.tim.2009.03.002
- Roberts AP, Mullany P. (2011). Tn916-like genetic elements: a diverse group of modular mobile elements conferring antibiotic resistance. *FEMS Microbiol Rev.* 35: 856-871. doi: 10.1111/j.1574-6976.2011.00283.x
- Roberts MC. (1994). Epidemiology of tetracycline-resistance determinants. *Trends Microbiol.* 2: 353-357.
- Roberts MC. (2005). Update on acquired tetracycline resistance genes. *FEMS Microbiol Lett.* 245: 195-203. doi: 10.1016/j.femsle.2005.02.034
- Ross JI, Eady EA, Cove JH, Cunliffe WJ. (1998). 16S rRNA Mutation Associated with Tetracycline Resistance in a Gram-Positive Bacterium. *Antimicrobial Agents and Chemotherapy.* 42: 1702-1705.
- Rysz M, Mansfield WR, Fortner JD, Alvarez PJJ. (2013). Tetracycline Resistance Gene Maintenance under Varying Bacterial Growth Rate, Substrate and Oxygen Availability, and Tetracycline Concentration. *Environmental Science & Technology.* 47: 6995-7001. doi: 10.1021/es3035329
- Sahu R, Walker LA, Tekwani BL. (2014). In vitro and in vivo anti-malarial activity of tigecycline, a glycylcycline antibiotic, in combination with chloroquine. *Malaria Journal.* 13: 1-7. doi: 10.1186/1475-2875-13-414
- Salyers AA, Gupta A, Wang Y. (2004). Human intestinal bacteria as reservoirs for antibiotic resistance genes. *Trends Microbiol.* 12: 412-416.
- Sanchez-Pescador R, Brown JT, Roberts M, Urdea MS. (1988). Homology of the TetM with translational elongation factors: implications for potential modes of *tetM*-conferred tetracycline resistance. *Nucleic Acids Res.* 16: 1218.
- Sapunaric FM, Levy SB. (2005). Substitutions in the interdomain loop of the Tn10 TetA efflux transporter alter tetracycline resistance and substrate specificity. *Microbiology.* 151: 2315-2322. doi: doi:10.1099/mic.0.27997-0
- Saxer G, Krepps MD, Merkley ED, Ansong C, Deatherage Kaiser BL, Valovska M-T, Ristic N, Yeh PT, Prakash VP, Leiser OP, Nakhlé L, Gibbons HS, Kreuzer HW, Shamoo Y. (2014). Mutations in Global Regulators Lead to Metabolic Selection during Adaptation to Complex Environments. *PLoS Genet.* 10: e1004872. doi: 10.1371/journal.pgen.1004872
- Seigal A, Mira P, Sturmels B, Barlow M. (2016). Does Antibiotic Resistance Evolve in Hospitals? *arXiv.* doi: arxiv.org/abs/1605.03660v2
- Skulj M, Okrslar V, Jalen S, Jevsevar S, Slanc P, Strukelj B, Menart V. (2008). Improved determination of plasmid copy number using quantitative real-time PCR for monitoring fermentation processes. *Microbial Cell Factories.* 7: 6.

Speer BS, Shoemaker NB, Salyers AA. (1992). Bacterial resistance to tetracycline: mechanisms, transfer, and clinical significance. *Clinical Microbiology Reviews*. 5: 387–399.

Spellberg B, Srinivasan A, Chambers HF. (2016). New societal approaches to empowering antibiotic stewardship. *JAMA*. 315: 1229-1230. doi: 10.1001/jama.2016.1346

Squires CL, Zaporojets D. (2000). Proteins shared by the transcription and translation machines. *Annual Review of Microbiology*. 54: 775-798. doi: doi:10.1146/annurev.micro.54.1.775

Starikova I, Al-Haroni M, Werner G, Roberts AP, Sørum V, Nielsen KM, Johnsen PJ. (2013). Fitness costs of various mobile genetic elements in *Enterococcus faecium* and *Enterococcus faecalis*. *Journal of Antimicrobial Chemotherapy*. 68: 2755-2765. doi: 10.1093/jac/dkt270

Storrs MJ, Poyart-Salmeron C, Trieu-Cuot P, Courvalin P. (1991). Conjugative transposition of Tn916 requires the excisive and integrative activities of the transposon-encoded integrase. *J Bacteriol*. 173: 4347-4352.

Strassmann JE, Queller DC. (2011). Evolution of cooperation and control of cheating in a social microbe. *Proc Natl Acad Sci U S A*. 108 Suppl 2: 10855-10862. doi: 10.1073/pnas.1102451108

Strassmann JE, Zhu Y, Queller DC. (2000). Altruism and social cheating in the social amoeba *Dictyostelium discoideum*. *Nature*. 408: 965-967.

Su YA, He P, Clewell DB. (1992). Characterization of the *tet(M)* determinant of Tn916: evidence for regulation by transcription attenuation. *Antimicrobial Agents and Chemotherapy*. 36: 769-778. doi: 10.1128/aac.36.4.769

Sun J, Deng Z, Yan A. (2014). Bacterial multidrug efflux pumps: Mechanisms, physiology and pharmacological exploitations. *Biochemical and Biophysical Research Communications*. 453: 254-267.

Takahashi CN (2015). A Platform for Microbial Evolution and Characterization. [Ph.D. Thesis]. [<https://digital.lib.washington.edu/researchworks/handle/1773/35185?show=full>]: University of Washington.

Todd PA, Benfield P. (1990). Amoxicillin/Clavulanic Acid. *Drugs*. 39: 264-307. doi: 10.2165/00003495-199039020-00008

Toprak E, Veres A, Michel JB, Chait R, Hartl DL, Kishony R. (2012). Evolutionary paths to antibiotic resistance under dynamically sustained drug selection. *Nat Genet*. 44: 101-105. doi: 10.1038/ng.1034

Toprak E, Veres A, Yildiz S, Pedraza JM, Chait R, Paulsson J, Kishony R. (2013). Building a Morbidostat: An automated continuous-culture device for studying bacterial drug resistance under dynamically sustained drug inhibition. *Nature protocols*. 8: 555-567. doi: 10.1038/nprot.nprot.2013.021

Tran TT, Panesso D, Mishra NN, Mileykovskaya E, Guan Z, Munita JM, Reyes J, Diaz L, Weinstock GM, Murray BE, Shamoo Y, Dowhan W, Bayer AS, Arias CA. (2013).

Daptomycin-Resistant *Enterococcus faecalis* Diverts the Antibiotic Molecule from the Division Septum and Remodels Cell Membrane Phospholipids. *MBio*. 4: e00281-00213. doi: 10.1128/mBio.00281-13

Trieber CA, Taylor DE. (2002). Mutations in the 16S rRNA Genes of *Helicobacter pylori* Mediate Resistance to Tetracycline. *J Bacteriol*. 184: 2131-2140. doi: 10.1128/jb.184.8.2131-2140.2002

Tsai HY, Liao CH, Chen YH, Lu PL, Huang CH, Lu CT, Chuang YC, Tsao SM, Chen YS, Liu YC, Chen WY, Jang TN, Lin HC, Chen CM, Shi ZY, Pan SC, Yang JL, Kung HC, Liu CE, Cheng YJ, Liu JW, Sun W, Wang LS, Ko WC, Yu KW, Chiang PC, Lee MH, Lee CM, Hsu GJ, Hsueh PR. (2012). Trends in susceptibility of vancomycin-resistant *Enterococcus faecium* to tigecycline, daptomycin, and linezolid and molecular epidemiology of the isolates: results from the Tigecycline In Vitro Surveillance in Taiwan (TIST) study, 2006 to 2010. *Antimicrob Agents Chemother*. 56: 3402-3405. doi: 10.1128/AAC.00533-12

Ventola CL. (2015). The Antibiotic Resistance Crisis: Part 1: Causes and Threats. *Pharmacy and Therapeutics*. 40: 277-283.

Villa L, Feudi C, Fortini D, Garcia-Fernandez A, Carattoli A. (2014). Genomics of KPC-producing *Klebsiella pneumoniae* sequence type 512 clone highlights the role of RamR and ribosomal S10 protein mutations in conferring tigecycline resistance. *Antimicrob Agents Chemother*. 58: 1707-1712. doi: 10.1128/AAC.01803-13

Walkiewicza K, Cardenas ASB, Sun C, Bacorn C, Saxon G, Shamoo Y. (2012). Small changes in enzyme function can lead to surprisingly large fitness effects during adaptive evolution of antibiotic resistance. *PNAS*. 109: 21408-21413. doi: 10.1073/pnas.1209335110

Wasels F, Monot M, Spigaglia P, Barbanti F, Ma L, Bouchier C, Dupuy B, Mastrantonio P. (2014). Inter- and Intraspecies Transfer of a *Clostridium difficile* Conjugative Transposon Conferring Resistance to MLSB. *Microbial Drug Resistance*. 20: 555-560. doi: 10.1089/mdr.2014.0015

Werner G, Gfrorer S, Fleige C, Witte W, Klare I. (2008). Tigecycline-resistant *Enterococcus faecalis* strain isolated from a German intensive care unit patient. *J Antimicrob Chemother*. 61: 1182-1183. doi: 10.1093/jac/dkn065

Wilson DN. (2014). Ribosome-targeting antibiotics and mechanisms of bacterial resistance. *Nat Rev Micro*. 12: 35-48. doi: 10.1038/nrmicro3155

Wood TE, Burke JM, Rieseberg LH. (2005). Parallel genotypic adaptation: when evolution repeats itself. *Genetica*. 123: 157-170. doi: 10.1007/s10709-003-2738-9

Wozniak M, Tiuryn J, Wong L. (2012). An approach to identifying drug resistance associated mutations in bacterial strains. *BMC Genomics*. 13 Suppl 7: S23. doi: 10.1186/1471-2164-13-S7-S23

Wunnicke D, Strohbach D, Weigand JE, Appel B, Feresin E, Suess B, Müller S, Steinhoff H-J. (2011). Ligand-induced conformational capture of a synthetic tetracycline riboswitch revealed by pulse EPR. *RNA*. 17: 182-188. doi: 10.1261/rna.2222811

Yang W, Moore IF, Koteva KP, Bareich DC, Hughes DW, Wright GD. (2004). TetX Is a Flavin-dependent Monooxygenase Conferring Resistance to Tetracycline Antibiotics. *Journal of Biological Chemistry*. 279: 52346-52352. doi: 10.1074/jbc.M409573200

Yao X, Lu C-D. (2014). Characterization of *Staphylococcus aureus* Responses to Spermine Stress. *Curr Microbiol*. 69: 394-403. doi: 10.1007/s00284-014-0603-y

Appendix A: Bioreactor adaptation of a hypermutator *Acinetobacter baumannii* to tigecycline resistance.

This appendix is reproduced in part from (Hammerstrom, et al. 2015).

Copyright 2015 by Hammerstrom *et al.*

<http://journals.plos.org/plosone/article?id=10.1371/journal.pone.0140489>.

Used under Creative Commons Attribution 4.0 International license:

<http://creativecommons.org/licenses/by/4.0/>.

A.1 My contribution to this work.

Continuous monitoring and maintenance for up to a month is required to adapt bacterial populations to antibiotic resistance in our bioreactor. Therefore to keep up with the high workload and technical demands of this setup, we often operate the bioreactor in teams. Multiple researchers work together to maintain the bioreactor, troubleshoot problems as they arise, and make important experimental decisions, such as when to increase the antibiotic concentration. As described in Chapter 3 of this thesis, Dr. Troy Hammerstrom, a postdoctoral researcher in our lab, was an important contributor to the adaption of *E. faecalis* S613 to TGC resistance in our bioreactor. Likewise, Dr. Hammerstrom took the lead studying TGC resistance in the Gram-negative pathogen *A. baumannii* AB210M, however I played an important role helping to adapt AB201M to TGC resistance in our bioreactor. Some of the major findings from this work are described here.

A.2 Introduction.

One frequent outcome of selection in both patients undergoing antibiotic therapies and *in vitro* laboratory evolution is the generation of hypermutators. These hypermutators often have 10-100 fold higher mutation rates than their ancestors and can provide a significant adaptive advantage over slower evolving strains. Hypermutators in clinical settings have been observed in many species including *Pseudomonas aeruginosa*, *Escherichia coli*, *Salmonella enterica*, and *Neisseria meningitidis* (reviewed in (Chopra, et al. 2003)). While hypermutator strains confer a significant adaptive advantage in the short run, they also burden the organism with a plethora of mutations most of which are non-adaptive and may reduce overall fitness to a range of environmental conditions (Arjan G., et al. 1999; Barrick, et al. 2009; Denamur and Matic 2006; Giraud, et al. 2001). In bacteremia or other infections of niche environments within a patient, the short-term adaptive benefits of a hypermutator phenotype can prove very advantageous as the role of purifying selection is diminished under such strong selection for a single adaptive phenotype (e.g. resistance).

In this report, we studied the evolution of a hypermutator strain of *Acinetobacter baumannii* AB210 during antibiotic selection to the frontline antibiotic TGC. As a hospital-acquired pathogen, *A. baumannii* causes 12,000 infections per year in the United States in critically ill patients (CDC 2013). Strains of *A. baumannii* have rapidly acquired antibiotic resistance via upregulation of efflux pumps and horizontal gene transfer which have severely decreased the efficacy of most antibiotics including TGC (Gordon and Wareham 2010). TGC-susceptible *A. baumannii* AB210 was isolated originally from an intra-abdominal infection. After one week of TGC therapy, AB211 was isolated and identified as a TGC-resistant, hypermutator strain. A large deletion in

AB211 truncated *mutS*, which encodes an essential protein of the DNA mismatch repair pathway (reviewed in (Li 2008)) leading to a hypermutator phenotype (Miller 1996).

One prominent mechanism for TGC resistance is overexpression of the resistance-nodule-diffusion family of efflux pumps (RND pumps). There are three RND pumps in *A. baumannii*, AdeABC, AdeFGH, and AdeJK, which are controlled by the transcriptional regulators AdeRS, AdeL, and AdeN, respectively. Mutations in AdeRS, AdeL, and AdeN lead to increased expression of the RND pumps and cause decreased susceptibility to several classes of antibiotics (Coyne, et al. 2011; Coyne, et al. 2010; Magnet, et al. 2001; Marchand, et al. 2004; Rosenfeld, et al. 2012; Yoon, et al. 2016). For example, comparative genomic sequencing of AB210 and AB211 revealed a mutation in *adeS* that increased expression of AdeABC thus conferring TGC resistance (Hornsey, et al. 2010; Hornsey, et al. 2011).

To identify genes associated with TGC resistance as well as their relative importance, we cultured *A. baumannii* AB210M, a derivative of AB210, to achieve high levels of TGC resistance. We used a selection and cultivation scheme that favors the formation of strongly polymorphic populations and biofilms in a novel bioreactor configuration under well-controlled parameters such as drug concentration, metabolic respiration rate, and the maintenance of non-limiting nutrient concentrations. Using our bioreactor system, we were able to recapitulate the evolution of the hypermutator phenotype in two separate populations of AB210M and then deconstruct the tremendous number of evolutionary trajectories leading to high levels of TGC resistance. We observed thousands of mutations of varying types and classes and then identified a subset of those most likely to be involved with resistance. By surveying samples of the adapting population on each day of the trial, we were able to determine the order and frequency of adaptive alleles

and thus gain insights into the relative importance of each. One interesting aspect of the evolution of a hypermutator population is the extent to which they saturate the genome with mutations and provide a rich and comprehensive exploration of the available evolutionary trajectories leading to a new phenotype, in this case TGC resistance. While it is challenging to analyze and comprehensively validate this wealth of mutational data, we are able to identify clinically relevant pathways as well as discover several new pathways that may contribute to emerging TGC resistance in *A. baumannii* and potentially other Gram-negative pathogens like *Klebsiella pneumoniae* and *E. coli*.

A.3 Materials and Methods.

A.3.1 Bacterial strains and culturing conditions.

A. baumannii strains AB210M and AB211 were obtained from Dr. Michael Hornsey at Queen Mary's University London. *A. baumannii* were cultured in Luria Broth (LB) or Mueller Hinton Broth supplemented with 20 mg/ml CaCl₂ and 10 mg/ml MgCl₂ (MHBI) at 37°C. *E. coli* strain DH5α was used for cloning purposes and was cultured in LB at 37°C. When needed, 50 µg/ml kanamycin (KAN) was added to the medium. TGC was prepared fresh or frozen at -20° C and added to medium freshly prepared or medium frozen at -80° C to prevent aeration.

A.3.2 Adaptation of AB210M to TGC in a bioreactor using metabolic control.

AB210M was adapted to TGC resistance using the same protocols as described in Chapter 2 Section 2.3 with several minor differences. For the first three days of each trial, the populations were cultured without TGC to provide an opportunity for the cells to adapt to the bioreactor and establish biofilms. To begin the selection, 0.1 µg/ml TGC

(less than half the MIC of AB210M) was added to the culture medium. Daily, we measured the MIC of the culture and increased the TGC concentration only when the growth rate of the population was not affected by the new drug concentration. For Trial 1, the following drug titration was employed: 0.1, 0.25, 0.4, 0.8, 1.2, 2, 3, 6, 10, and 16 µg/ml TGC. Trial 2 followed a similar titration; however, instead of 6 and 10 µg/ml, we added 5 and 8 µg/ml TGC.

A.3.3 Whole genome sequencing and analysis.

The whole genome sequencing analysis of end-point clones and metagenomic population samples were performed using the same protocols as described in Chapter 2 Section 2.6. The AB210M reference sequence was constructed by modifying the AB210 genome (NCBI accession #AEOX00000000, see S1 Text). The AB210M genome consists of 72 contiguous sequences (contigs) containing 4.06 Mb. The AB210M reference genome was deposited into NCBI as LAPU00000000 and genes are numbered WM39_00005 – WM39_19210. All clonal samples and mixed populations were aligned to the AB210M reference genome using breseq v.024rc7 (Deatherage and Barrick 2014).

A.3.4 Statistical Analysis of mutated genes.

The Fisher's Exact Test was used to determine if a gene was mutated more frequently than expected if mutations were distributed randomly. The input for the Fisher's Exact Tests were the number of mutations in the dataset (896 for polymorphic populations and 1712 for isolated clones), genome size (3.98 Gb), number of mutations in that gene and length of the gene. To determine if *p* values were significant, we used a sequential Bonferroni correction for multiple tests. After ranking the *p* values from largest to

smallest, we compared the *p* value to 0.05 divided by the rank of the *p* value. If the *p* value was less than the correction, the result was deemed significant. For the polymorphic populations, which contained 626 mutated genes, 8.04×10^{-5} was the cutoff for significance. The threshold for the isolated clones, which contained 1093 mutated genes, was $< 4.64 \times 10^{-5}$.

A.4 Results.

A.4.1 Adaptation of a clinical *A. baumannii* strain to increasing but subinhibitory concentrations of tigecycline leads to a rapid rise to resistance.

Using our bioreactor setup Dr. Hammerstrom and I gradually evolved *A. baumannii* strain AB210M to TGC resistance over 26 days in two independent experiments (Trial 1 and Trial 2). The final populations were cultured in 16 µg/ml TGC, which was twice the minimal inhibitory concentration (MIC) of AB211, the clinical TGC-resistant isolate, and greater than the clinical breakpoint (>8 µg/ml TGC) (Hornsey, et al. 2010). Each culture contained $\sim 10^{10}$ CFU with ~ 36 generations per day. We noted that biofilm communities were readily visible on the stainless steel and borosilicate glass surfaces within the bioreactor as early as 72 hr after inoculation.

A.4.2 Deletions in the *mutS* locus evolve repeatedly and lead to a hypermutator phenotype.

Hypermutator strains arose rapidly ($>50\%$ of the population on Day 5 in Trial 1) and comprised all but two of the successful evolutionary trajectories. The hypermutator phenotypes were due to ~ 60 kb deletions that began within or included *mutS* and the last

~14kb of contig AEOXM024 and all of contig AEOXM025 (contig names are abbreviated to the last two digits, **Figure A.1**) (Miller 1996). The frequency of the deletion nears fixation (>95%) by Day 10 of Trial 1 and remains at that level through the end of the adaptation. Within individual clones, the exact size of the deletion varied from 56 - 69 kb and included approximately 49 genes depending on the specific event. The movement of an insertion element (IS15 D1, (Labigne-Roussel and Courvalin 1983)) produced this family of *mutS*-associated deletions. Incorporating all the sequencing results from endpoint stains and metagenomic analysis of population samples from both trials, we identified 26 different IS15 D1 insertion sites in the *mutS* region. We found examples where the IS15 D1 element inserted in either orientation into the *mutS* locus to delete *mutS*. Interestingly, a similar deletion was found in the clinical resistant isolate AB211 and produced a hypermutator phenotype in the patient (Hornsey, et al. 2011). However, in the case of AB211, the deletion of *mutS* was not made by IS15 D1 but by an unknown mechanism. The variety and consistency of events leading to the hypermutator phenotype suggests a selective benefit for hypermutators both in clinical and experimental conditions.

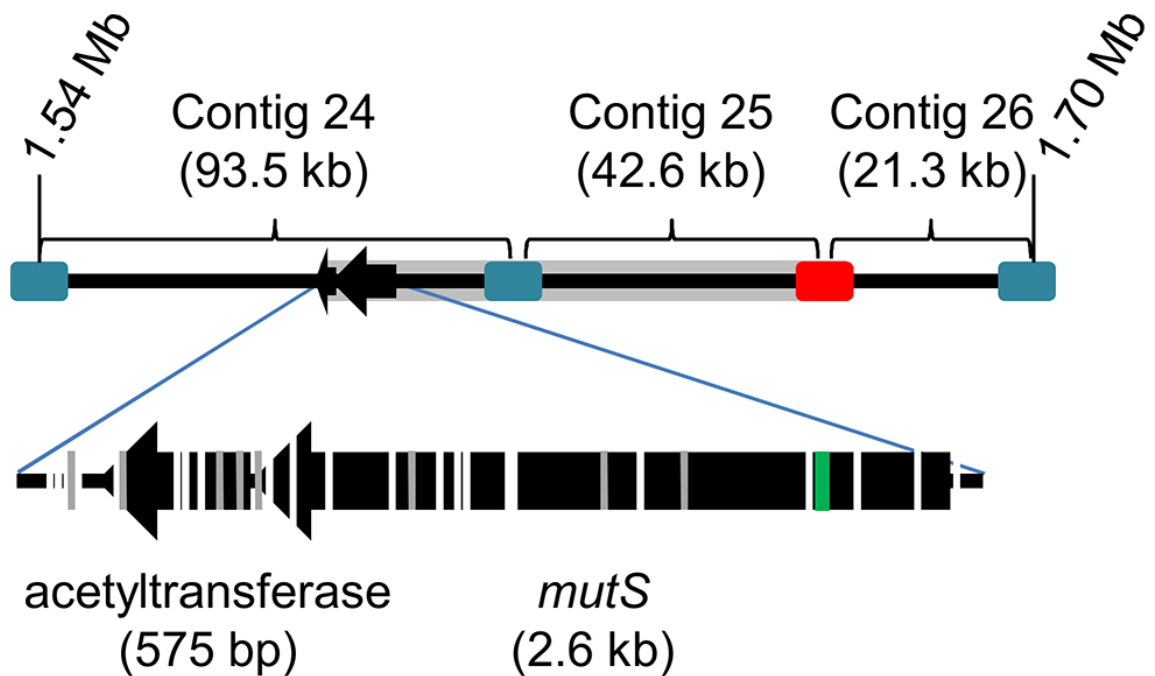


Figure A.1: ~60 kb deletions begin near and extend into *mutS* to confer the hypermutator phenotype. The top line demonstrates contigs 24-26 separated by mobile elements IS *Aba-1* (blue) and IS15 D1 (red) and the deleted region (gray). The genomic position of the region can be compared to Fig. 2C and 4C. In the lower portion of the figure, the *mutS* gene is enlarged to identify IS15 D1 insertion sites. White breaks in *mutS* and the adjacent gene indicate positions where IS15 D1 inserted in one or more polymorphic samples. Gray lines mark where IS15 D1 inserted in the clonal isolates. The deletion in clinical isolate AB211 is indicated (green).

A.4.3 Genomic analysis reveals both expected and novel families of genes associated with TGC resistance.

Analyses of the polymorphic populations and isolates produced a list of 17 genes, including *adeS* that may contribute to TGC resistance. Genes were selected for further analysis if they met at least one of the following criteria: 1) the Fisher Exact Test *p* value was < 0.001 for either the mixed population dataset or the clonal isolates; or 2) the gene contained the same nsSNP during both trials. If a gene can confer TGC resistance via a loss of function or slight change of function, we expect that many different mutations could have that effect, and we would detect the gene via the Fisher Exact Test. On the other hand, if there are relatively few positions in a gene that confer TGC resistance, we expect that the same mutation would be present in both trials. Therefore, we also used the criterion of a gene containing the same nsSNP in both trials.

From the list of 17 genes, we focused on five genes that may confer TGC resistance for further validation: *adeS*, *rpsJ*, *rrf*, *msbA*, and *gna* (**Figure A.2 7**). Four genes (*adeS*, *rrf*, *msbA*, and *gna*) were mutated several times in many clones. In addition, *adeS*, *rrf*, and *msbA* have highly significant *p* values in both the population and clonal samples when the sequential Bonferroni correction was applied. *rpsJ* was the fifth gene, and it was included because it contained identical nsSNPs in both trials and was previously shown to confer resistance to TGC (Cattoir, et al. 2014; Villa, et al. 2014). Lastly, all of the sequenced isolates, including the two strains with only three and six mutations each, contained mutations in at least two of these genes.

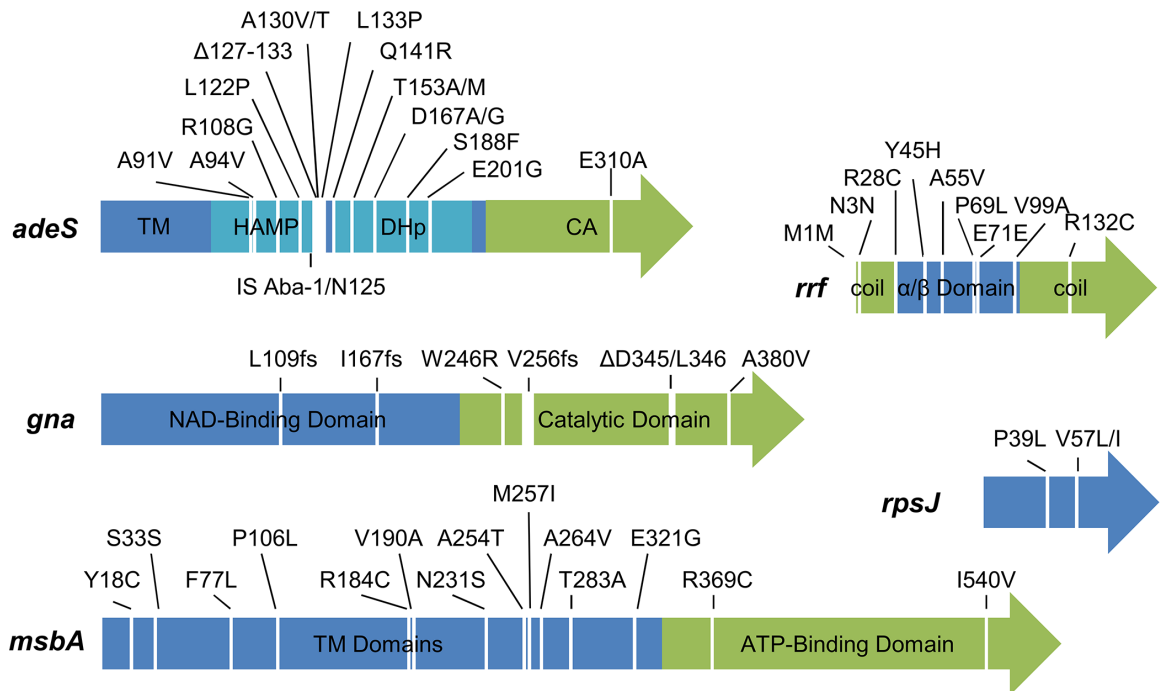


Figure 7: Mutations in genes that may reduce TGC susceptibility. Arrows represent the coding regions. The labels indicate the amino acid changes present in each protein. If a position was mutated to more than one residue, the two amino acids are listed, for example “A130V/T” indicates A130 was mutated to both a valine and threonine. Frameshift mutations are indicated by “fs”. For multi-domain proteins, the predicted domains are represented by different colors. HAMP, histidine kinase, adenyl cyclase, methyl-accepting protein, and phosphatase linker; DHp, dimerization and histidine-containing phosphotransfer domain; CA, catalytic and ATP-binding domain; TM, transmembrane motif.

A.5 Discussion.

Hypermutating strains can arise during adaptation to an environment whether that environment is a human host (Baquero, et al. 2004; Hornsey, et al. 2011; Marvig, et al. 2013) or a laboratory system (Barrick, et al. 2009; Lee, et al. 2012; Sacher, et al. 2014). In this study, we found that, as in the patient, a strain of *A. baumannii* evolved a hypermutator phenotype repeatedly while adapting to the front-line antibiotic TGC. We exploited the wealth of mutations generated by the hypermutator to explore the potential evolutionary trajectories that lead to TGC resistance. Six genes stood apart as the primary or secondary mechanisms to decrease susceptibility to TGC: *adeS*, *gna*, *rpsJ*, *rrf*, and *msbA*. One important aspect of our work is the discovery of new adaptive alleles that can confer high levels of TGC-resistance in conjunction with the previously characterized *adeS* family of mutations.

In complex ecologies where many competing microbial species are present and variable environmental conditions challenge the fitness of an organism, hypermutation will lead to rapid decline in fitness. However, in a sterile site, such as an indwelling medical device or within a wound, hypermutator strains can flourish as strongly adaptive mutations provide higher fitness to an antibiotic than the costs of rapidly accumulating deleterious mutations (Giraud, et al. 2001). This is particularly true over the shorter time scale of a clinical infection or strong selection via antibiotic usage; therefore, it may not be surprising that hypermutator phenotypes have been observed for pathogens including *E. coli*, *P. aeruginosa*, and *S. enterica* causing chronic, persistent infections (Baquero, et al. 2004; Chopra, et al. 2003; Macia, et al. 2005; Marvig, et al. 2013; Oliver and Mena 2010). In addition, *A. baumannii* AB210, the ancestor for our studies, evolved into AB211, a TGC-resistant strain that contained an inactivated *mutS* via a large deletion,

during an intra-abdominal infection in a patient receiving TGC. AB211 harbored several additional mutations including *adeS*^{A94V} resulting in an overexpression of the AdeABC efflux pump likely conferring TGC resistance (Hornsey, et al. 2011).

It is clear from our data and others that the most important adaptive changes to reduce TGC susceptibility occur through mutations in *adeS* that upregulate *adeABC*. All of our successful evolutionary trajectories included at least one mutation that likely increased *adeABC* expression. Mutations to *adeS* that lead to increased expression of *adeABC* have been observed with remarkable consistency in TGC-resistant clinical strains (Hornsey, et al. 2011; Ruzin, et al. 2007; Sun, et al. 2012; Yoon, et al. 2013). In addition, *adeS* knockout strains have shown a decrease in *adeABC* induction and loss of TGC resistance (Sun, et al. 2012). Recently, two groups determined the sequences of *adeS* from different clonal clusters of *A. baumannii* and detected several polymorphic sites and an insertion of IS Aba-1 (Sun, et al. 2012; Yoon, et al. 2013). Previous reports have identified mutations in *adeS* at the same positions as our cultures including A94, IS Aba-1 insertion at N125, A130, D167, T153, and R313 (Hornsey, et al. 2010; Marchand, et al. 2004; Ruzin, et al. 2007; Sun, et al. 2010; Sun, et al. 2012; Yoon, et al. 2013). As shown in Figure A.2, 13 of the 16 *adeS* mutations in our study affected amino acids 91-167 of the 357-residue protein. This region is the junction between the histidine kinase, adenyl cyclase, methyl-accepting protein, and phosphatase linker (HAMP) and dimerization and histidine-containing Phosphotransfer (DHp) domains (Yoon, et al. 2013). Interestingly, the phosphorylated histidine is in the same region at residue 149. As a histidine kinase of a two-component system, AdeS likely autophosphorylates in the presence of an activating signal and then phosphorylates AdeR, the response regulator (Coyne, et al. 2010). The mutations we identified suggest that the AdeS-AdeR phosphor-relay may be deregulated causing constitutive phosphorylation of AdeR.

Though *adeS* is the most important TGC resistance gene, the TGC MIC of T2_H3 $\Delta adeS$ was elevated over the ancestor strain indicating that additional TGC resistance genes are present. This led us to examine further the mutations identified from the bioreactor samples for additional adaptive mutations.

In the present study, over 2500 mutations were present in individual isolates or mixed populations at greater than 5% frequency. These mutations affected 1465, or nearly 40%, of the coding regions in AB210M. Analyzing the mutations found in clones and mixed populations using Fisher's Exact Test and presence of parallel evolved nsSNPs resulted in 17 candidate genes that can contribute to TGC resistance. We further reduced the list of putative TGC resistance genes to genes with the most significant *p* values when applying the sequential Bonferroni correction for multiple tests, which resulted in five genes that had the highest potential to confer TGC resistance.

A.5.1 Candidate TGC genes and proposed mechanisms of action in TGC resistance.

MsbA is an essential ATP-binding cassette transporter (ABC-transporter) (Shilling, et al. 2006). MsbA transports lipid A molecules from the inner leaflet of the inner membrane into the periplasmic side of the inner membrane. MsbA-like proteins in *Lactobacillus lactis* have been shown to confer resistance to antibiotics and toxic compounds (King and Sharom 2012). Interestingly, overproduction of lipid A decreases the transport of antibiotics via MsbA (Reuter, et al. 2003; Woebking, et al. 2005). Chen et al. recently reported a mutation in *msbA* in a TGC-resistant isolate of *A. baumannii* from a serial passage experiment (Chen, et al. 2014). When the authors overexpressed wild-type *msbA* in the mutant background containing *msbA*^{A84V}, the TGC MIC did not change

leading them to conclude that *msbA* was not involved in resistance. Complementing a mutant allele with the native allele *in trans* is effective for loss-of-function mutations; however, the method does not necessarily provide insight into gain-of-function mutations. Since 12 of the 14 mutations in *msbA* from the bioreactor samples were located in the substrate-recognition and transmembrane portion of the protein, we speculate that the mutations broaden the specificity of the pump and facilitate efflux of TGC. Therefore, the *msbA* mutations likely were gain-of-function mutations, and *msbA* should be reexamined as a potential player in TGC resistance. Interestingly, in a different study by our group we identified mutations in a gene with homology to *msbA* in *E. faecalis* strains that were adapted to TGC (see Chapter 5 Section 5.4) (Beabout, et al. 2015b).

S10 is the ribosomal protein closest to the TGC binding pocket and is a general target for TGC resistance (Beabout, et al. 2015a). Previously, researchers have discovered S10 mutations, which confer TGC and tetracycline resistance in *Neisseria gonorrhoeae*, *Enterococcus faecium*, *K. pneumoniae*, *Enterococcus faecalis*, and *E. coli* (see Chapter 7) (Beabout, et al. 2015a; Beabout, et al. 2015b; Cattoir, et al. 2014; Hu, et al. 2005; Villa, et al. 2014). The mutations were located in the same extended loop (amino acids 53–60) as V57L and V57I found in Trials 1 and 2. We hypothesize that mutations in the S10 loop alter the TGC binding pocket of the ribosome resulting in a decrease in TGC affinity for the ribosome.

RRF, with the help of elongation factor Tu, recycles ribosomes by dissociating the large and small subunits after reaching a stop codon or if a ribosome stalls during translation (Vivanco-Dominguez, et al. 2012). Since TGC binds to the A site within the ribosome and prevents elongation of a polypeptide, RRF may play a role in dissociating TGC-

bound ribosomes that appear to be stalled on the mRNA. RRF is an essential protein; therefore, the mutations are not likely to completely disrupt RRF function (Janosi, et al. 1998). However, we predict that the mutations may decrease RRF function. One of the mutations we identified ($\text{RRF}^{\text{R132C}}$) was shown in an earlier study to decrease RRF-dependent disassembly of ribosomes in *E. coli* (Ishino, et al. 2000). In addition, two mutations were present at the beginning of the *rrf* gene that encodes RRF (M1V and N3N) and are likely to decrease translation from the *rrf* mRNA. The M1V mutation is a conversion of an ATG to GTG. GTG is an alternative start codon in *A. baumannii* and is predicted to be used by 172 of the 3741 protein coding genes. If the total amount or activity of RRF is reduced, then ribosomes stalled by TGC may be able to pause until the drug diffuses away from the binding site and proceed with translation rather than be recycled prematurely.

The *gna* gene resides within the K locus, a region encoding extracellular polysaccharide biosynthesis enzymes, which play a role in constructing capsule or lipooligosaccharide (LOS) (Kenyon and Hall 2013). AB210M contains KL7, which is predicted to synthesize legionaminic acid (originally identified in *A. baumannii* strain TCDC-AB0715 (Chen, et al. 2011)). Increased expression of the K locus was recently shown to decrease susceptibility to colistin and other peptide antibiotics (Geisinger and Isberg 2015), and work in *P. aeruginosa* demonstrated that certain polysaccharides can bind antibiotics (Mah, et al. 2003). The *gna* gene is one of 22 genes in this operon and converts UDP-*N*-acetyl-D-glucosamine to UDP-*N*-acetyl-D-glucosaminuronic acid or UDP-*N*-acetyl-D-galactosamine to UDP-*N*-acetyl-D-galactosaminuronic acid (Kenyon and Hall 2013). In the TGC-resistant bioreactor samples, *gna* contains several frameshift mutations likely disrupting its function. Interestingly, seven of the nine mutations in *gna* included repeat elements, such as homopolymer stretches and a 6 bp repeat. With the loss of Gna, the

structure of the capsular polysaccharide or LOS would be modified. We speculate that changes in the extracellular polysaccharides could alter the rate of diffusion of TGC into the cell.

There does not appear to be a strong epistatic link between the TGC resistance genes. All the endpoint clones contained at least one *adeS* mutation, but there were many combinations of mutations in *rpsJ*, *rrf*, *msbA*, and *gna*. For example, strains were detected with a mutation in only one of the five candidate TGC resistance genes (i.e. T1_E12 *msbA*, T2_F9 *rpsJ*, T1_E8 *gna*). Likewise, there were clones with combinations of mutations in only two genes (i.e. T1_F6 *rpsJ* and *msbA*, T2_G7 *rrf* and *msbA*, T2_H3 *rrf* and *gna*, and T2_H4 *msbA* and *gna*). Additional work is needed to determine the contributions of each gene to TGC resistance and the epistatic relationships (if any) between the genes. It is possible that some of the changes correlated with adaptation to TGC may be compensatory for earlier mutations to improve fitness.

The evolutionary dynamics of emergent pathogens provide an interesting contrast to our more classical views of long-term evolution. It is clear from both theory and experimental evolution that hypermutators provide short-term gains but is essentially a dead end as deleterious mutations continue to accumulate. However, during strong selection and over shorter time scales, hypermutators can be highly successful and can lead to patient deaths. In this study we show that under selection to TGC, *A. baumannii* commonly evolves a hypermutator phenotype that illustrated both a common clinical mechanism for genetic adaptation and permitted a comprehensive survey of the successful evolutionary trajectories. We identified known alleles leading to TGC resistance as well as new ones not yet discovered clinically but that may emerge in the near future.

A.6 References.

- Arjan G. J, Visser Md, Zeyl CW, Gerrish PJ, Blanchard JL, Lenski RE. (1999). Diminishing Returns from Mutation Supply Rate in Asexual Populations. *Science*. 283: 404-406. doi: 10.1126/science.283.5400.404
- Baquero M-R, Nilsson AI, del Carmen Turrientes M, Sandvang D, Galán JC, Martínez JL, Frimodt-Møller N, Baquero F, Andersson DI. (2004). Polymorphic Mutation Frequencies in *Escherichia coli*: Emergence of Weak Mutators in Clinical Isolates. *J Bacteriol*. 186: 5538-5542. doi: 10.1128/JB.186.16.5538-5542.2004
- Barrick JE, Yu DS, Yoon SH, Jeong H, Oh TK, Schneider D, Lenski RE, Kim JF. (2009). Genome evolution and adaptation in a long-term experiment with *Escherichia coli*. *Nature*. 461: 1243-1247. doi: 10.1038/nature08480
- Beabout K, Hammerstrom TG, Perez AM, Magalhães BF, Prater AG, Clements TP, Arias CA, Saxon G, Shamoo Y. (2015a). The Ribosomal S10 Protein Is a General Target for Decreased Tigecycline Susceptibility. *Antimicrobial Agents and Chemotherapy*. 59: 5561-5566. doi: 10.1128/aac.00547-15
- Beabout K, Hammerstrom TG, Wang TT, Bhatty M, Christie PJ, Saxon G, Shamoo Y. (2015b). Rampant Parosexuality Evolves in a Hospital Pathogen during Antibiotic Selection. *Molecular Biology and Evolution*. 32: 2585-2597. doi: 10.1093/molbev/msv133
- Cattoir V, Isnard C, Cosquer T, Odhiambo A, Bucquet F, Guerin F, Giard JC. (2014). Genomic analysis of reduced susceptibility to tigecycline in *Enterococcus faecium*. *Antimicrob Agents Chemother*. doi: 10.1128/aac.04174-14
- CDC. (2013). Antibiotic Resistance Threat Report. In. <http://www.cdc.gov/drugresistance/threat-report-2013/>.
- Chen CC, Lin YC, Sheng WH, Chen YC, Chang SC, Hsia KC, Liao MH, Li SY. (2011). Genome sequence of a dominant, multidrug-resistant *Acinetobacter baumannii* strain, TCDC-AB0715. *J Bacteriol*. 193: 2361-2362. doi: 10.1128/jb.00244-11
- Chen Q, Li X, Zhou H, Jiang Y, Chen Y, Hua X, Yu Y. (2014). Decreased susceptibility to tigecycline in *Acinetobacter baumannii* mediated by a mutation in *trm* encoding SAM-dependent methyltransferase. *Journal of Antimicrobial Chemotherapy*. 69: 72-76. doi: 10.1093/jac/dkt319

Chopra I, O'Neill AJ, Miller K. (2003). The role of mutators in the emergence of antibiotic-resistant bacteria. *Drug Resist Updat.* 6: 137-145.

Coyne S, Courvalin P, Perichon B. (2011). Efflux-mediated antibiotic resistance in *Acinetobacter* spp. *Antimicrob Agents Chemother.* 55: 947-953. doi: 10.1128/AAC.01388-10

Coyne S, Rosenfeld N, Lambert T, Courvalin P, Perichon B. (2010). Overexpression of resistance-nodulation-cell division pump AdeFGH confers multidrug resistance in *Acinetobacter baumannii*. *Antimicrob Agents Chemother.* 54: 4389-4393. doi: 10.1128/aac.00155-10

Deatherage D, Barrick J. (2014). Identification of Mutations in Laboratory-Evolved Microbes from Next-Generation Sequencing Data Using breseq. In: Sun L, Shou W, editors. *Engineering and Analyzing Multicellular Systems*: Springer New York. p. 165-188.

Denamur E, Matic I. (2006). Evolution of mutation rates in bacteria. *Mol Microbiol.* 60: 820-827. doi: 10.1111/j.1365-2958.2006.05150.x

Geisinger E, Isberg RR. (2015). Antibiotic modulation of capsular exopolysaccharide and virulence in *Acinetobacter baumannii*. *PLoS Pathog.* 11: e1004691. doi: 10.1371/journal.ppat.1004691

Giraud A, Matic I, Tenaillon O, Clara A, Radman M, Fons M, Taddei F. (2001). Costs and Benefits of High Mutation Rates: Adaptive Evolution of Bacteria in the Mouse Gut. *Science.* 291: 2606-2608. doi: 10.1126/science.1056421

Gordon NC, Wareham DW. (2010). Multidrug-resistant *Acinetobacter baumannii*: mechanisms of virulence and resistance. *Int J Antimicrob Agents.* 35: 219-226. doi: 10.1016/j.ijantimicag.2009.10.024

Hammerstrom TG, Beabout K, Clements TP, Saxon G, Shamoo Y. (2015). *Acinetobacter baumannii* Repeatedly Evolves a Hypermutator Phenotype in Response to Tigecycline That Effectively Surveys Evolutionary Trajectories to Resistance. *PLoS One.* 10: e0140489. doi: 10.1371/journal.pone.0140489

Hornsey M, Ellington MJ, Doumith M, Thomas CP, Gordon NC, Wareham DW, Quinn J, Lolans K, Livermore DM, Woodford N. (2010). AdeABC-mediated efflux and tigecycline MICs for epidemic clones of *Acinetobacter baumannii*. *Journal of Antimicrobial Chemotherapy.* doi: 10.1093/jac/dkq218

Hornsey M, Loman N, Wareham DW, Ellington MJ, Pallen MJ, Turton JF, Underwood A, Gaulton T, Thomas CP, Doumith M, Livermore DM, Woodford N. (2011). Whole-genome comparison of two *Acinetobacter baumannii* isolates from a single patient, where resistance developed during tigecycline therapy. *Journal of Antimicrobial Chemotherapy*. 66: 1499-1503. doi: 10.1093/jac/dkr168

Hu M, Nandi S, Davies C, Nicholas RA. (2005). High-level chromosomally mediated tetracycline resistance in *Neisseria gonorrhoeae* results from a point mutation in the *rpsJ* gene encoding ribosomal protein S10 in combination with the *mtrR* and *penB* resistance determinants. *Antimicrob Agents Chemother*. 49: 4327-4334. doi: 10.1128/aac.49.10.4327-4334.2005

Ishino T, Atarashi K, Uchiyama S, Yamami T, Sahara Y, Yoshida T, Hara H, Yokose K, Kobayashi Y, Nakamura Y. (2000). Interaction of ribosome recycling factor and elongation factor EF-G with *E. coli* ribosomes studied by the surface plasmon resonance technique. *Genes Cells*. 5: 953-963.

Janosi L, Mottagui-Tabar S, Isaksson LA, Sekine Y, Ohtsubo E, Zhang S, Goon S, Nelken S, Shuda M, Kaji A. (1998). Evidence for *in vivo* ribosome recycling, the fourth step in protein biosynthesis. *EMBO J*. 17: 1141-1151. doi: 10.1093/emboj/17.4.1141

Kenyon JJ, Hall RM. (2013). Variation in the complex carbohydrate biosynthesis loci of *Acinetobacter baumannii* genomes. *PLoS One*. 8: e62160. doi: 10.1371/journal.pone.0062160

King G, Sharom FJ. (2012). Proteins that bind and move lipids: MsbA and NPC1. *Critical Reviews in Biochemistry and Molecular Biology*. 47: 75-95. doi: doi:10.3109/10409238.2011.636505

Labigne-Roussel A, Courvalin P. (1983). IS15, a new insertion sequence widely spread in R plasmids of gram-negative bacteria. *Mol Gen Genet*. 189: 102-112.

Lee H, Popodi E, Tang H, Foster PL. (2012). Rate and molecular spectrum of spontaneous mutations in the bacterium *Escherichia coli* as determined by whole-genome sequencing. *Proceedings of the National Academy of Sciences*. 109: E2774-E2783. doi: 10.1073/pnas.1210309109

Li GM. (2008). Mechanisms and functions of DNA mismatch repair. *Cell Res*. 18: 85-98. doi: 10.1038/cr.2007.115

Macia MD, Blanquer D, Togores B, Sauleda J, Perez JL, Oliver A. (2005). Hypermutation is a key factor in development of multiple-antimicrobial resistance in

Pseudomonas aeruginosa strains causing chronic lung infections. *Antimicrob Agents Chemother.* 49: 3382-3386. doi: 10.1128/aac.49.8.3382-3386.2005

Magnet S, Courvalin P, Lambert T. (2001). Resistance-nodulation-cell division-type efflux pump involved in aminoglycoside resistance in *Acinetobacter baumannii* strain BM4454. *Antimicrob Agents Chemother.* 45: 3375-3380. doi: 10.1128/aac.45.12.3375-3380.2001

Mah TF, Pitts B, Pellock B, Walker GC, Stewart PS, O'Toole GA. (2003). A genetic basis for *Pseudomonas aeruginosa* biofilm antibiotic resistance. *Nature.* 426: 306-310. doi: 10.1038/nature02122

Marchand I, Damier-Piolle L, Courvalin P, Lambert T. (2004). Expression of the RND-type efflux pump AdeABC in *Acinetobacter baumannii* is regulated by the AdeRS two-component system. *Antimicrob Agents Chemother.* 48: 3298-3304. doi: 10.1128/aac.48.9.3298-3304.2004

Marvig RL, Johansen HK, Molin S, Jelsbak L. (2013). Genome analysis of a transmissible lineage of *Pseudomonas aeruginosa* reveals pathoadaptive mutations and distinct evolutionary paths of hypermutators. *PLoS Genet.* 9: e1003741. doi: 10.1371/journal.pgen.1003741

Miller JH. (1996). Spontaneous mutators in bacteria: insights into pathways of mutagenesis and repair. *Annu Rev Microbiol.* 50: 625-643. doi: 10.1146/annurev.micro.50.1.625

Oliver A, Mena A. (2010). Bacterial hypermutation in cystic fibrosis, not only for antibiotic resistance. *Clin Microbiol Infect.* 16: 798-808. doi: 10.1111/j.1469-0691.2010.03250.x

Reuter G, Janvilisri T, Venter H, Shahi S, Balakrishnan L, van Veen HW. (2003). The ATP binding cassette multidrug transporter LmrA and lipid transporter MsbA have overlapping substrate specificities. *J Biol Chem.* 278: 35193-35198. doi: 10.1074/jbc.M306226200

Rosenfeld N, Bouchier C, Courvalin P, Perichon B. (2012). Expression of the resistance-nodulation-cell division pump AdeIJK in *Acinetobacter baumannii* is regulated by AdeN, a TetR-type regulator. *Antimicrob Agents Chemother.* 56: 2504-2510. doi: 10.1128/aac.06422-11

Ruzin A, Keeney D, Bradford PA. (2007). AdeABC multidrug efflux pump is associated with decreased susceptibility to tigecycline in *Acinetobacter calcoaceticus-Acinetobacter baumannii* complex. *J Antimicrob Chemother.* 59: 1001-1004. doi: 10.1093/jac/dkm058

Saxer G, Krepps MD, Merkley ED, Ansong C, Deatherage Kaiser BL, Valovska M-T, Ristic N, Yeh PT, Prakash VP, Leiser OP, Nakhleh L, Gibbons HS, Kreuzer HW, Shamoo Y. (2014). Mutations in Global Regulators Lead to Metabolic Selection during Adaptation to Complex Environments. *PLoS Genet.* 10: e1004872. doi: 10.1371/journal.pgen.1004872

Shilling RA, Venter H, Velamakanni S, Bapna A, Woebking B, Shahi S, van Veen HW. (2006). New light on multidrug binding by an ATP-binding-cassette transporter. *Trends Pharmacol Sci.* 27: 195-203. doi: 10.1016/j.tips.2006.02.008

Sun JR, Chan MC, Chang TY, Wang WY, Chiueh TS. (2010). Overexpression of the *adeB* gene in clinical isolates of tigecycline-nonsusceptible *Acinetobacter baumannii* without insertion mutations in *adeRS*. *Antimicrob Agents Chemother.* 54: 4934-4938. doi: 10.1128/aac.00414-10

Sun JR, Perng CL, Chan MC, Morita Y, Lin JC, Su CM, Wang WY, Chang TY, Chiueh TS. (2012). A truncated AdeS kinase protein generated by ISAbal insertion correlates with tigecycline resistance in *Acinetobacter baumannii*. *PLoS One.* 7: e49534. doi: 10.1371/journal.pone.0049534

Villa L, Feudi C, Fortini D, Garcia-Fernandez A, Carattoli A. (2014). Genomics of KPC-producing *Klebsiella pneumoniae* sequence type 512 clone highlights the role of RamR and ribosomal S10 protein mutations in conferring tigecycline resistance. *Antimicrob Agents Chemother.* 58: 1707-1712. doi: 10.1128/AAC.01803-13

Vivanco-Dominguez S, Bueno-Martinez J, Leon-Avila G, Iwakura N, Kaji A, Kaji H, Guarneros G. (2012). Protein synthesis factors (RF1, RF2, RF3, RRF, and tmRNA) and peptidyl-tRNA hydrolase rescue stalled ribosomes at sense codons. *J Mol Biol.* 417: 425-439. doi: 10.1016/j.jmb.2012.02.008

Woebking B, Reuter G, Shilling RA, Velamakanni S, Shahi S, Venter H, Balakrishnan L, van Veen HW. (2005). Drug-lipid A interactions on the *Escherichia coli* ABC transporter MsbA. *J Bacteriol.* 187: 6363-6369. doi: 10.1128/JB.18.6363-6369.2005

Yoon EJ, Balloy V, Fiette L, Chignard M, Courvalin P, Grillot-Courvalin C. (2016). Contribution of the Ade Resistance-Nodulation-Cell Division-Type Efflux Pumps to Fitness and Pathogenesis of *Acinetobacter baumannii*. *MBio.* 7. doi: 10.1128/mBio.00697-16

Yoon EJ, Courvalin P, Grillot-Courvalin C. (2013). RND-type efflux pumps in multidrug-resistant clinical isolates of *Acinetobacter baumannii*: major role for AdeABC overexpression and AdeRS mutations. *Antimicrob Agents Chemother.* 57: 2989-2995. doi: 10.1128/aac.02556-12

Appendix B: Biological evaluations of viridicatumtoxin antibiotic analogues.

This appendix is reproduced in part with permission from (Nicolaou, et al. 2014).

Copyright 2014 American Chemical Society.

B.1 My contribution to this work.

The K.C. Nicolaou lab, a synthetic chemistry lab in the Rice University Department of Chemistry, developed a total synthesis pathway for the tetracycline antibiotics viridicatumtoxin A, viridicatumtoxin B, and several analogues of these antibiotics. Under my guidance and supervision an undergraduate in the lab, Tim Wang, tested the efficacy of these analogues by measuring their MICs against several different species of bacterial pathogens. Under my direction Mr. Wang also performed time-kill assays to determine if the natural compounds and analogues have bacteriostatic or bactericidal activity. The results of this work are described here.

B.2 Introduction.

Within the class of tetracycline antibiotics, viridicatumtoxin B (**1**), viridicatumtoxin A (**2**), (**Figure B.1**) are unique in that they include in their structures a geranyl-derived subunit in the form of a spirobicyclic system (Hutchison, et al. 1973; Zheng, et al. 2008). In contrast to the majority of tetracyclines, these members of the group are also distinguished by their fungal, rather than bacterial, origins. The K.C. Nicolaou lab developed the total synthesis and full structural elucidation of viridicatumtoxin B (**1**) and

several synthetic analogues. Here Mr. Wang and myself investigated the antibacterial properties of viridicatumtoxin B (**1**) and the analogues.

B.3 Materials and Methods.

B.3.1 Bacterial Strains and Growth Media.

Four clinical strains were used for these studies, *E. faecalis* S613, *E. faecium* 105, Methicillin-Resistant *S. aureus* 371 (MRSA 371) and *A. baumannii* AB210. *Enterococcus* strains were cultured in 80% Lysogeny Broth (LB) & 20% Brain Heart Infusion (BHI). MRSA 371 and AB210 were cultured in 100% LB.

B.3.2 Minimal Inhibitory Concentration (MIC) Assays.

Micro-broth MIC assays were performed in triplicate using 96-well plates. Wells were filled with 150 µL of broth media and inoculated with 2 µL of stationary phase culture. The concentration of the test antibiotics increased in 2-fold increments and ranged from 0.25 – 128 µg/mL. Plates were incubated overnight at 37 °C and the MICs were defined as the lowest drug concentration that had no growth after 16 – 24 hours.

B.3.3 Time-Kill Assay.

We performed time-kill assays using *E. faecalis* S613 cultures. Cells were taken at early exponential phase and diluted to 9×10^5 – 1×10^6 CFU/mL. Cells were then treated with 2x the MIC of TGC (**9**), viridicatumtoxin A (**2**), or **V6**. A growth control with no antibiotic was also included and CFUs were determined at 0, 2, 4 and 6 hours after the addition of antibiotic. The time-kill assay was setup in triplicate with error bars displaying the standard deviation.

B.4 Results and Discussion.

B.4.1 Viridicatumtoxin antibiotics and analogues are active against Gram-positive bacterial pathogens.

The K.C. Nicolaou research program was able to access not only (\pm) -viridicatumtoxin B [(\pm) -**1**] but also a number of analogues that are simpler and easier to synthesize for biological evaluation (see **Figure B.1** for structures). Specifically, analogues (\pm) -**V2**, (\pm) -**V3**, (\pm) -**V4**, (\pm) -**V5** and (\pm) -**V6**, were synthesized and, together with (\pm) -**1**, were tested by Mr. Wang and myself against a number of bacterial strains and compared to natural viridicatumtoxin B [$(+)$ -**1**, reported values (Zheng, et al. 2008)], natural viridicatumtoxin A [$(+)$ -**2**, obtained from Professor Yi Tang], minocycline (Minocin., **7**) and TGC (Tygacil., **9**) (see **Figure B.1** for structures).

As shown in Table B.1, all of the viridicatumtoxins and analogues tested exhibited antibacterial efficacy against Gram-positive bacteria [*(E. faecalis* S613, *E. faecium* 501, and methicillin-resistant *Staphylococcus aureus* 371 (MRSA 371)] but were largely inactive against Gram-negative bacteria (i.e., *A. baumannii* AB210). Thus, synthetic viridicatumtoxin B [(\pm) -**1**] exhibited comparable antibacterial properties against these strains (*E. faecalis* S613, *E. faecium* 501, and MRSA 371: MIC = 1, 0.5, and 4 μ g/mL, respectively) to those reported for natural viridicatumtoxin B [$(+)$ -**1**] against similar strains (*E. faecalis* KCTC5191, *E. faecium* KCTC3122, MRSA CCARM3167: MIC = 2, 0.5, and 0.5 μ g/mL, respectively), despite the racemic nature of the former. The potencies of synthetic (\pm) -**1** were also comparable to those reported (Zheng, et al. 2008) for natural viridicatumtoxin A [$(+)$ -**2**] against similar strains (**Table B.1**).

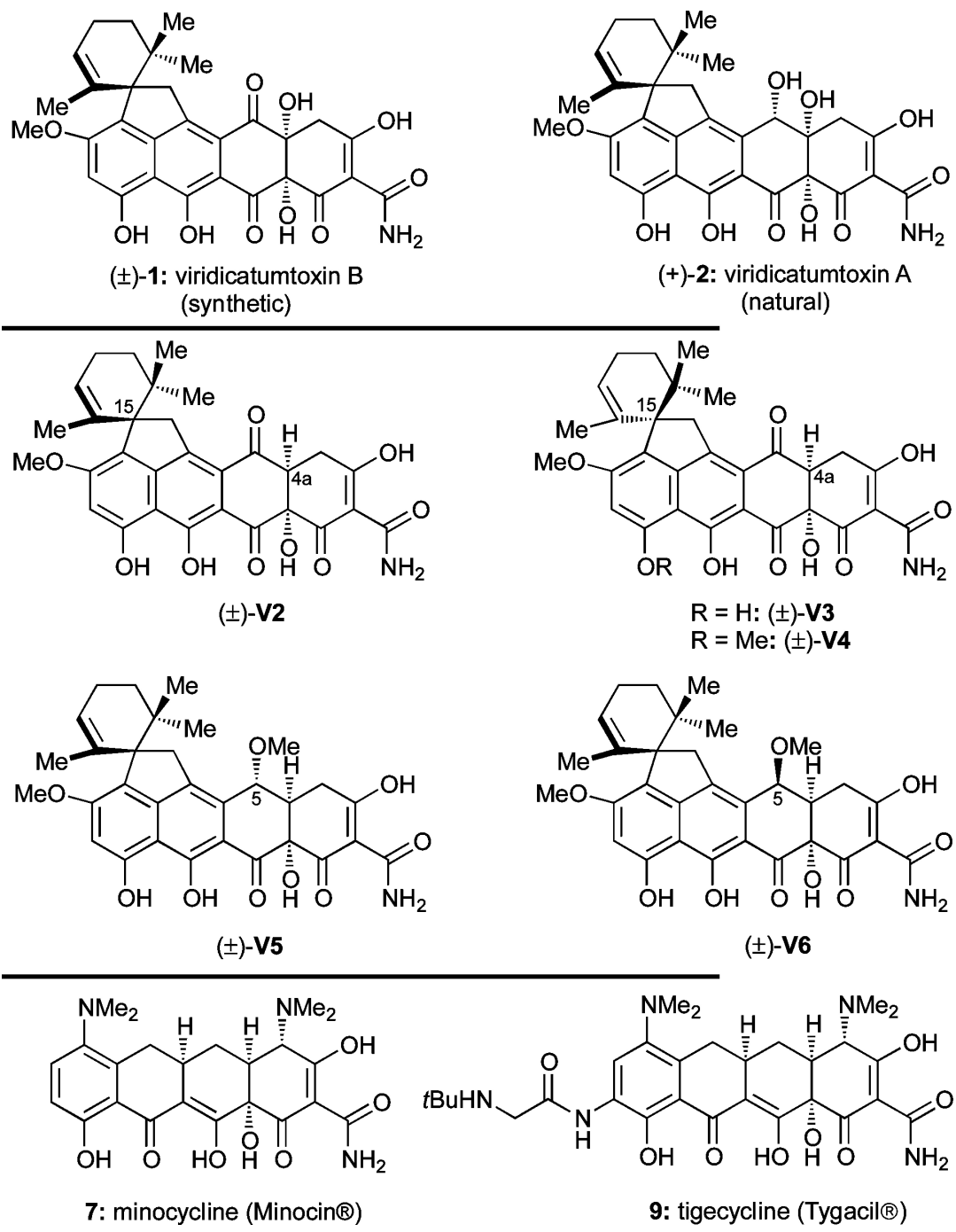


Figure B.1: Molecular structures of viridicatumtoxin antibiotics. Shown are natural viridicatumtoxin A (**2**), synthetic viridicatumtoxin B (**1**), synthesized viridicatumtoxin analogues (**V2–V6**), and tetracycline drugs minocycline (**7**) and TGC (**9**)

B.4.2 Characterization of the relationship between structure and function of viridicatumtoxin analogues.

Viridicatumtoxin analogue (\pm)-**V2**, lacking the C4a hydroxyl group, displayed high potency against the same strains (*E. faecalis* S613: MIC = 0.5 μ g/mL; *E. faecium* 501: MIC = 0.5 μ g/mL; MRSA 371: MIC = 2 μ g/mL) leading to the conclusion that this functionality is not necessary for antibacterial activity in this subclass of tetracyclines. Of note is the loss of considerable potency in going from the natural to the opposite C15 configuration [analogues (\pm)-**V3** and (\pm)-**V4**] as shown in Table B.1. Interestingly, methyl ethers (\pm)-**V5** and (\pm)-**V6**, also lacking the C4a hydroxyl moiety, demonstrated potent antibacterial properties against *E. faecalis* S613 [(\pm)-**V5**: MIC = 1 μ g/mL; (\pm)-**V6**: MIC = 0.5 μ g/mL], *E. faecium* 501 [(\pm)-**V5**: MIC = 1 μ g/mL; (\pm)-**V6**: MIC = 0.5 μ g/mL], and MRSA 371 [(\pm)-**V5**: MIC = 8 μ g/mL; (\pm)-**V6**: MIC = 2 μ g/mL]. These results further support the conclusion that the C4a hydroxyl group of the viridicatumtoxin analogues is not necessary for biological activity (see Table B.1). Finally, despite the previously reported activity of viridicatumtoxins against several Gram-negative bacterial strains by Zheng *et. al.*, our tested compounds were inactive against *A. baumannii* AB210, consistent with previous reports suggesting that the C4-dimethylamino residue is important for imparting the broad-spectrum activity observed for both minocycline (**7**) and TGC (**9**) (Nelson, et al. 2001; Zheng, et al. 2008). Incorporation of such a moiety into the viridicatumtoxin scaffold could expand their antibacterial profile as well as improve their pharmacological properties (Nelson, et al. 2001).

Table B.1. MIC data of compounds against Gram-positive and Gram-negative bacteria and comparison with selected literature data.

entry	Gram-(+)						Gram(-)		
	This study ^a			Reference 1			This study ^a	Reference 1	
	<i>E. faecalis</i> S613	<i>E. faecium</i> 501	MRSA 371	<i>E. faecalis</i> KCTC5191 ^b	<i>E. faecium</i> KCTC3122 ^b	MRSA CCARM3167 ^b	<i>A. baumannii</i> AB210	<i>A. calcoaceticus</i> KCTC2357 ^b	<i>E. coli</i> CCARM1356 ^b
(-)-7	4	4	2	—	—	—	4	—	—
(-)-9	0.5	0.5	1	—	—	—	0.5	—	—
(±)-1	1	0.5	4	2 ^c	0.5 ^c	0.5 ^c	64	1 ^c	>64 ^c
(+)-2 ⁷⁸	1	1	4	4	1	0.25	64	2	>64
(±)-V2	0.5	0.5	2	—	—	—	64	—	—
(±)-V3	4	2	8	—	—	—	64	—	—
(±)-V4	4	4	4	—	—	—	64	—	—
(±)-V5	1	1	8	—	—	—	64	—	—
(±)-V6	0.5	0.5	2	—	—	—	64	—	—

^aMIC assays were run in triplicate; data are given in units of µg/mL; ^bTaken from reference 1 (Zheng, et al. 2008) for comparison; ^cEnantiopure material [(+)-1] isolated from *Penicillium* sp. FR11 was used in reference 1 (Zheng, et al. 2008). ⁷⁸Professor Yi Tang (UCLA) is acknowledged for providing natural viridicatumtoxin A [(+)-2] obtained from *P. aethiopicum*. In this study, that material was used for antibacterial testing.

B.4.3 Viridicatumtoxin analogues display bacteriostatic activity against *E. faecalis* S613.

In preliminary experiments to probe the mode-of-action of viridicatumtoxin analogues, time-kill assays were performed by Mr. Wang to measure the killing of *E. faecalis* S613 by viridicatumtoxin A (**2**) and (\pm)-**V6** alongside tigecycline (**9**). The motivation for this study was previous reports that tetracycline analogues with an aromatic C-ring [e.g., viridicatumtoxin A (**2**) and (\pm)-**V6**] act via a bactericidal mechanism as opposed to a bacteriostatic one (i.e., inhibition of the bacterial ribosome) (Oliva, et al. 1992). Our time-kill assays clearly indicated that both viridicatumtoxin A (**2**) and (\pm)-**V6** act bacteriostatically and not bactericidally based on The Clinical and Laboratory Standards Institute (CLSI) definition that a bactericidal compound is one capable of inducing a ≥ 3 log₁₀ drop in colony-forming units (CFU)/mL (**Figure B.2**). Although (\pm)-**V6** did not meet the criterion for bactericidal activity, the ability of (\pm)-**V6** to kill *E. faecalis* S613 was similar to the clinically used and bacteriostatic antibiotic TGC (**9**). If viridicatumtoxins [i.e., viridicatumtoxin A (**2**) and (\pm)-**V6**] are indeed inhibitors of the bacterial ribosome, as opposed to inhibitors of UPP synthase as suggested by Tomoda and co-workers (Inokoshi, et al. 2013), then based on the structure of TGC (**9**) bound to the *Thermus thermophilus* ribosome, the C4–C7 positions of viridicatumtoxins are likely ideal sites for further modifications, as those positions do not directly interact with the ribosome (Jenner, et al. 2013).

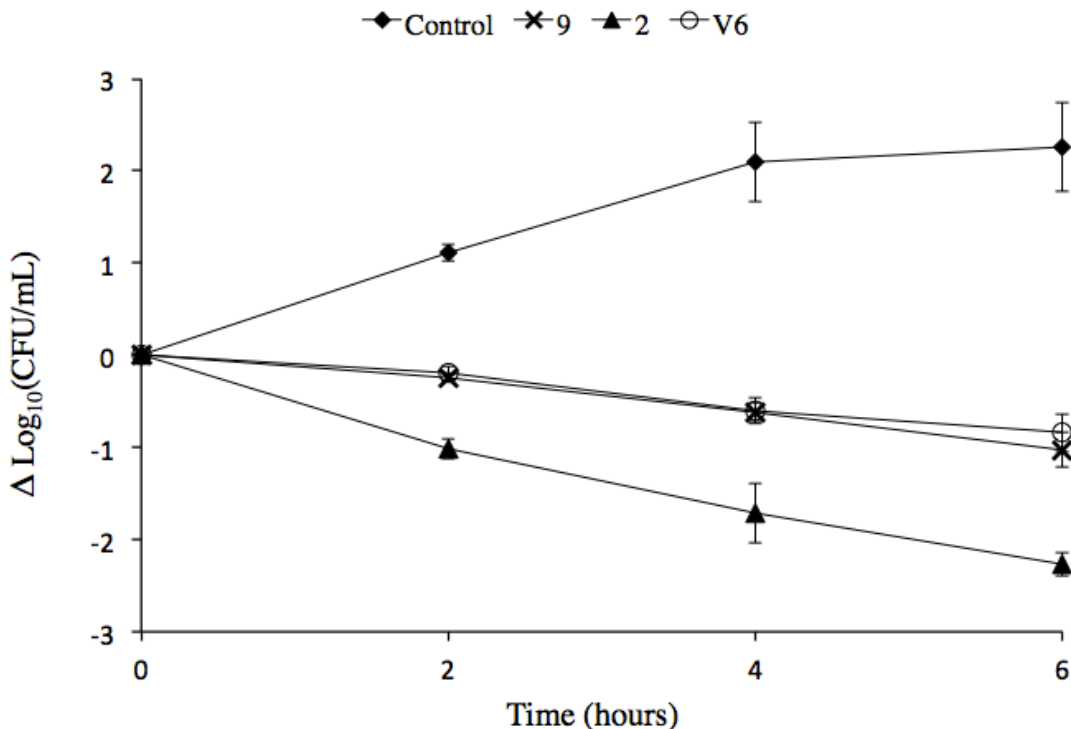


Figure B.2: Viridicatumtoxin analogues display bacteriostatic activity against *E. faecalis* S613. Time-kill assays performed at 2x the MIC against *E. faecalis* S613 show that viridicatumtoxin A (**2**), and analogue -**V6** have bacteriostatic activity, similar to TGC (**9**) which is a known bacteriostatic agent. The time-kill assays were performed in triplicate with error bars displaying the standard deviation.

B.5 References.

- Hutchison RD, Steyn PS, Van Rensburg SJ. (1973). Viridicatumtoxin, a new mycotoxin from *Penicillium viridicatum*. *Toxicology and Applied Pharmacology*. 24: 507 - 509.
- Inokoshi J, Nakamura Y, Hongbin Z, Uchida R, Nonaka K-i, Masuma R, Tomoda H. (2013). Spirohexalines, new inhibitors of bacterial undecaprenyl pyrophosphate synthase, produced by *Penicillium brasiliense* FKI-3368. *Journal of Antibiotics*. 66: 37-41. doi: 10.1038/ja.2012.83
- Jenner L, Starosta AL, Terry DS, Mikolajka A, Filonava L, Yusupov M, Blanchard SC, Wilson DN, Yusupova G. (2013). Structural basis for potent inhibitory activity of the antibiotic tigecycline during protein synthesis. *Proc Natl Acad Sci U S A*. 110: 3812-3816. doi: 10.1073/pnas.1216691110
- Nelson M, Hillen W, Greenwald RA. (2001). Tetracyclines in Biology, Chemistry and Medicine: Birkhäuser Basel.
- Nicolaou KC, Hale CRH, Nilewski C, Ioannidou HA, ElMarrouni A, Nilewski LG, Beabout K, Wang TT, Shamoo Y. (2014). Total Synthesis of Viridicatumtoxin B and Analogues Thereof: Strategy Evolution, Structural Revision, and Biological Evaluation. *Journal of the American Chemical Society*. doi: 10.1021/ja506472u
- Oliva B, Gordon G, McNicholas P, Ellestad G, Chopra I. (1992). Evidence that tetracycline analogs whose primary target is not the bacterial ribosome cause lysis of *Escherichia coli*. *Antimicrobial Agents and Chemotherapy*. 36: 913-919.
- Zheng C-J, Yu H-E, Kim E-H, Kim W-G. (2008). Viridicatumtoxin B, a new anti-MRSA agent from *Penicillium sp* FR11. *Journal of Antibiotics*. 61: 633-637.

Appendix C: Molecular mechanism of S10^{R53Q-Δ54-57ATHK} allele in conferring tigecycline resistance.

C.1 Introduction.

As discussed in Chapters 5 and 7, the S10^{R53Q-Δ54-57ATHK} allele is important to TGC resistance in *Enterococcus* species (Beabout, et al. 2015a; Beabout, et al. 2015b). We hypothesize that the S10^{R53Q-Δ54-57ATHK} allele reduces the affinity of TGC for the ribosome, which then allows translation to continue in the presence of the antibiotic. To evaluate the effect of the S10 allele on the translational efficiency of ribosomes in the presence of TGC, I attempted to use a published protocol by Murray *et al.* for preparing crude cell extracts from Gram-positive organisms in combination with an *in vitro* transcription/translation (*in vitro* T/T) kit produced by Promega (Murray, et al. 2001). An undergraduate student in the lab, Megan McCurry, assisted me with this work. The goal of these experiments was to compare the ability of ribosomes extracted from S613 (wildtype S10) and BTR0 (S10^{R53Q-Δ54-57ATHK}) to translate yellow fluorescent protein (YFP) in the presence and absence of TGC by measuring fluorescence. If our hypothesis were correct, then the translation efficiency of BTR0 ribosomes would remain higher than the ancestral S613 ribosomes in the presence of TGC.

C.2 Materials and Methods.

C.2.1 Template DNA and plasmid isolation.

To serve as template DNA for the *in vitro* T/T assays, a pET28a-sfYFP plasmid was kindly supplied from Matt Bennett's lab (Rice University, BioSciences Department). The plasmid was isolated from *E. coli* Dh10b using the ZR Classic MiniprepTM-Classic Kit (Zymo Research Corp., Irvine, CA). Several plasmid preps were pooled, frozen, and then concentrated using a Speed Vac Concentrator to ~1 µg/µL.

C.2.2 Preparation of S30 Ribosomal Extracts.

Protocols by Murrey *et al.* were followed to prepare the ribosomal extracts. The reagents are listed below in Table C.1 and the specific protocol used is as follows: Add 250 mL of overnight inoculum to 6 L of BHI broth and incubate at 37°C for 4-5 hrs until culture reaches an OD 600 nm between 2 – 4. Pellet the cells at 4°C and 5,000 rpm for 15 min. Wash cell pellets with 500 mL of cold Buffer A at 1M KCl (work in 4°C cold room and resuspend pellets on ice). Pellet the cells at 4°C and 5,000 rpm for 15 min. Wash cells with 250 mL of cold Buffer A at 50 mM KCl (work in 4°C cold room and resuspend pellets on ice). Pellet the cells at 4°C and 5,000 rpm for 15 min and store the pellets at -80°C. The next day thaw the pellets on ice for 30 – 60 min while gently inverting the tubes periodically. Then resuspend slurry up to a final volume of 99 mL of cold Buffer B in the cold room. Add 1.5 mL of lysostaphin stock to the bottom of 3 precooled 35-mL polyallomer SS-34 centrifuge tubes. Then add 33 mL of cell slurry to each of the lysostaphin-containing tubes, cap the tubes, and gently invert them. Incubate slurry at 37°C for 45 – 60 min and invert tubes periodically. Add 150 uL of 0.5 M DTT to each tube and gently invert to mix. Spin cells at 4°C in an SS-34 rotor (16,000 rpm) for 30 min. Next, in the cold room remove and save the supernatant. Add 150 uL of 0.5 M DTT to

the pellet again and spin the pellet under the same conditions (4°C, 16,000 rpm, 30 min with). Pool the supernatants and recentrifuge to remove cellular debris (3,000 G, 15 min at 4°C). Collect the top two-thirds of the supernatant, add 0.25 volume of Preincubation Buffer and incubate mixture at 37°C for 30 min. Dialyze preincubated supernatant overnight at 4°C against 2 L of dialysis buffer with one buffer change. The next day concentrate the dialysate to ~10 mg/mL by covering the dialysis bag containing the extract with precooled polyethylene glycol 8000 powder at 4°C. Aliquot samples, flash freeze and store at -80°C.

Table C.1: S30 Ribosomal Extract Materials and Reagents.

Reagent Name	Composition
Buffer A	10 mM Tris-acetate, pH 8.0, 14 mM Mg-acetate, 1 mM dithiothreitol [DTT] (One stock with 1 M KCl & one stock with 50 mM KCl).
Buffer B	10 mM Tris-acetate, pH 8.0, 20 mM Mg-acetate, 50 mM KCl, 1 mM DTT.
Lysostaphin stock	0.8 mg/mL in Buffer B
Preincubation Buffer	670 mM Tris-acetate, pH 8.0, 20 mM Mg-acetate, 7 mM Na ₃ -phosphoenolpyruvate, 7 mM DTT, 5.5 mM ATP, 70 µM amino acids, complete [Promega], 75 µg of pyruvate kinase [Sigma]/ml
Dialysis Membrane	Spectra-Por 7; molecular weight cutoff, 3,500
Dialysis Buffer	10 mM Tris-acetate, pH 8.0, 14 mM Mg-acetate, 60 mM K-acetate, 1 mM DTT
PEG 8000	Polyethylene glycol 8000 powder

C.2.3 Transcription and Translation Assay

The reagents from the *E. coli* T7S30 Extract System for Circular DNA Kit (Promega Corporation, Madison, WI) were thawed on ice. Reactions were setup in 25 µL volumes as recommended by the manufacturer with plasmid DNA at 1 µg/µL and incubated at 37°C for one hour. The fluorescence was then read in a 96-well plate with black walls using a Synergy 2 microplate reader (BioTeK) with an excitation wavelength of 495 nm, emission wavelength of 526 nm, bottom optics and autoscale gain.

C.3 Discussion and Results.

Before initiating the cell extract protocol, I first established that the *in vitro* T/T Promega kit works with my template DNA. The template DNA consisted of YFP under a T7 promoter on a pET28 vector and was kindly supplied to me by David Shis from Matt Bennett's lab (Rice University, BioSciences Department). I setup *in vitro* T/T reactions in triplicate using the Promega kit *E. coli* extract and measured an inhibition curve for TGC that was similar to a curve published by Olson *et al.*, indicating that the experimental setup works efficiently (**Figure C.1A**) (Olson, et al. 2006). Next, several attempts were made by myself and by my undergraduate student in the lab, Megan McCurry, to prepare extract from *E. faecalis* S613. One issue with the protocol was lysing *E. faecalis* S613. When the cells are lysed the extract should be slightly yellow. To lyse cells the protocol uses an enzyme called lysostaphen (Murray, et al. 2001). When lysostaphen was used on *S. aureus* MRSA131 a clear, viscous, and yellow extract was generated (**Figure C.1B**). However, when lysostaphen was used on *E. faecalis* S613, the resulting extract was cloudy and white (**Figure C.1C**). After several attempts using alternative enzymes, the lysis step was finally improved by passing the *E. faecalis* cells through a French Press five times at 800 psi.

Despite overcoming issues with lysing, we were not able to prepare extracts that produced enough protein to detect significantly over background (**Figure C.1D**). Ms. McCurry and I tried numerous additional troubleshooting steps, including using alternative reporter proteins (GFP and mCherry), using the same strain of *S. aureus* that was used in the published protocol (*S. aureus* SA113), using different volumes of extract in the *in vitro* T/T reactions (**Figure C.1E**), performing every step of the protocol in a 4°C cold room when possible, concentrating the extract more or less, using freshly

purchased reagents for the buffers, using extract from various stages of the protocol (i.e., immediately after lysing, before dialysis, ect.), and increasing the incubation time for the *in vitro* T/T assay. We next considered varying the buffer conditions, such as pH and salt concentrations, but felt that there were too many variables to test. We also considered an alternative protocol by Maguire, *et al.* where ribosomes are extracted on a column using SulfoLink coupling resin (Maguire, et al. 2008). However, to use pure ribosomes for *in vitro* T/T, the other translation factors (elongation factors, initiation factors, ect.) need to be added to the reactions, and these factors are not available to be purchased for *E. faecalis*. Since our lab does not specialize in ribosomal extraction protocols, we felt it was pertinent to focus future efforts on different experiments.

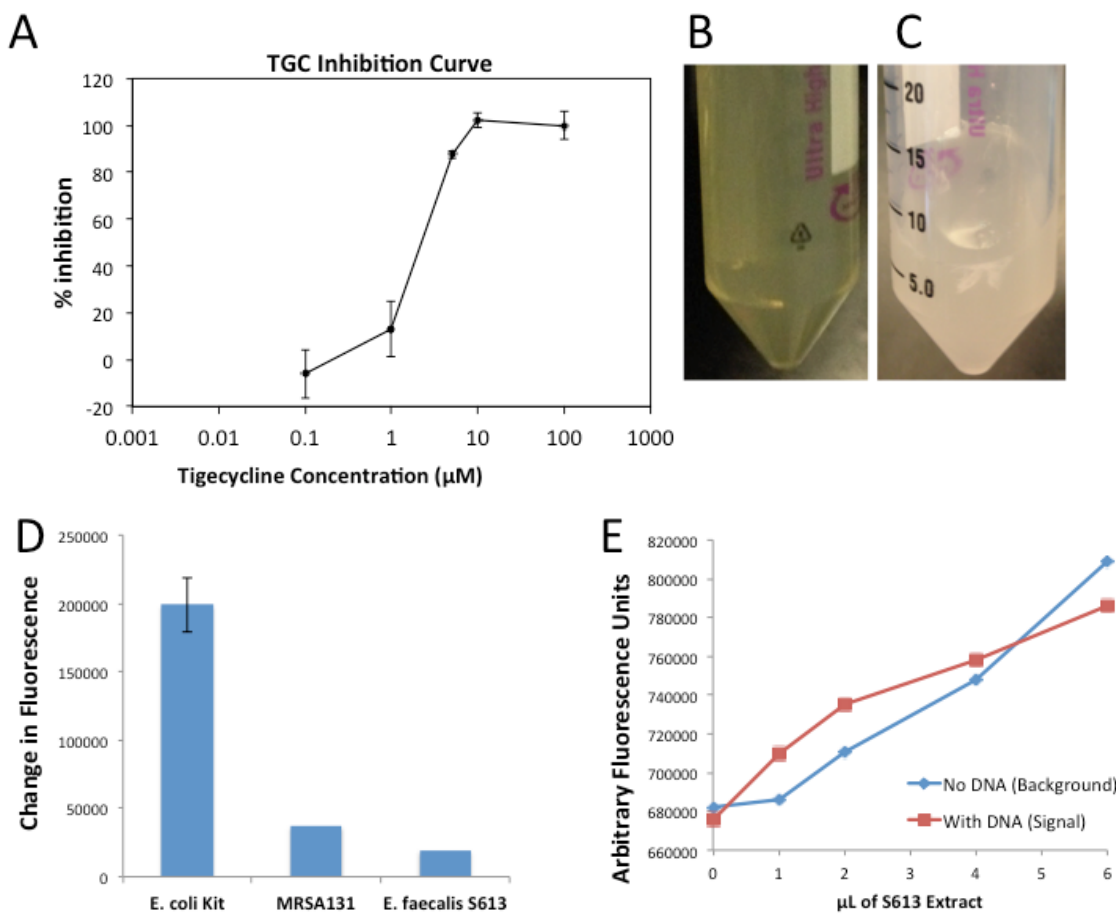


Figure C.1: Attempts at preparing ribosomal extracts from S613 using a protocol developed by Murray, et al. **A)** Results of *in vitro* T/T reactions using YFP as a reporter protein and the Promega *in vitro* T/T kit *E. coli* extract. TGC displayed an expected inhibition curve, which demonstrates that the pET28-sfYFP vector is viable as template DNA for the *in vitro* T/T reactions. **B)** *S. aureus* MRSA131 extract after lysing with the enzyme lysostaphen was clear and yellow. **C)** *E. faecalis* S613 extract after lysing with the enzyme lysostaphen was white and cloudy. **D)** Detection of YFP with background fluorescence subtracted from *in vitro* T/T reactions using purchased *E. coli* extract, and extract prepared using the protocol by Murray, et. al. from MRSA131 and S613. The MRSA131 and S613 extracts barely produced any fluorescence compared to the *E. coli* kit. **E)** Detection of YFP (red) over background (blue) with different volumes of S613 extract. Increasing volumes of S613 extract did not improve the signal of the assay.

C.4 References.

- Beabout K, Hammerstrom TG, Perez AM, Magalhães BF, Prater AG, Clements TP, Arias CA, Saxon G, Shamoo Y. (2015a). The Ribosomal S10 Protein Is a General Target for Decreased Tigecycline Susceptibility. *Antimicrobial Agents and Chemotherapy*. 59: 5561-5566. doi: 10.1128/aac.00547-15
- Beabout K, Hammerstrom TG, Wang TT, Bhatty M, Christie PJ, Saxon G, Shamoo Y. (2015b). Rampant Parasexuality Evolves in a Hospital Pathogen during Antibiotic Selection. *Molecular Biology and Evolution*. 32: 2585-2597. doi: 10.1093/molbev/msv133
- Maguire BA, Wondrack LM, Contillo LG, Xu Z. (2008). A novel chromatography system to isolate active ribosomes from pathogenic bacteria. *RNA*. 14: 188-195. doi: 10.1261/rna.692408
- Murray RW, Melchior EP, Hagadorn JC, Marotti KR. (2001). *Staphylococcus aureus* Cell Extract Transcription-Translation Assay: Firefly Luciferase Reporter System for Evaluating Protein Translation Inhibitors. *Antimicrobial Agents and Chemotherapy*. 45: 1900-1904. doi: 10.1128/aac.45.6.1900-1904.2001
- Olson MW, Ruzin A, Feyfant E, Rush TS, 3rd, O'Connell J, Bradford PA. (2006). Functional, biophysical, and structural bases for antibacterial activity of tigecycline. *Antimicrob Agents Chemother*. 50: 2156-2166. doi: 10.1128/AAC.01499-05